

Terrestrial laser scanning for crop monitoring

-

Capturing 3D data of plant height
for estimating biomass at field scale

Inaugural-Dissertation

zur

Erlangung des Doktorgrades

der Mathematisch-Naturwissenschaftlichen Fakultät

der Universität zu Köln

vorgelegt von

Nora Isabelle Tilly

aus Köln

Köln 2015

Berichtersteller: Prof. Dr. Georg Bareth
Prof. Dr. Olaf Bubenzer

Tag der mündlichen Prüfung: 15.01.2016

Abstract

In comparison with other remote sensing methods terrestrial laser scanning (TLS) is quite a young discipline, but the trustworthiness of the laser-based distance measurements offers great potential for accurate surveying. TLS allows non-experts, outside the traditional surveying disciplines, to rapidly acquire 3D data of high density. Generally, this acquisition of accurate geoinformation is increasingly desired in various fields, however this study focuses on the application of TLS for crop monitoring in an agricultural context.

The increasing cost and efficiency pressure on agriculture induced the emergence of site-specific crop management, which requires a comprehensive knowledge about the plant development. An important parameter to evaluate this development or rather the actual plant status is the amount of plant biomass, which is however directly only determinable with destructive sampling. With the aim of avoiding destructive measurements, interest is increasingly directed towards non-contact remote sensing surveys. Nowadays, different approaches address biomass estimations based on other parameters, such as vegetation indices (VIs) from spectral data or plant height. A main benefit of all remote sensing approaches is that plant parameters are obtained without disturbing the plant growth by the taking of measurements. Since the plants are not taken it is in an economic and ecologic way feasible to perform several measurements across a field and across the growing season. Hence, the change of spatial and temporal patterns can be monitored.

This study applies TLS for objectively measuring and monitoring plant height as estimator for biomass at field scale. Although the application of the here introduced approach is generally conceivable for a variety of crops, the focus of this study was narrowed to cereals as most important group of crops regarding world nutrition. Three examples of this group were chosen, namely paddy rice, maize, and barley.

In the course of this work, 35 TLS field campaigns were carried out at three sites over four growing seasons to achieve a comprehensive data set. In each campaign a 3D point cloud, covering the surface of the field, was obtained and interpolated to a crop surface model (CSM) in the post-processing. A CSM represents the crop canopy in a very high spatial resolution on a specific date. By subtracting a digital terrain model (DTM) of the bare ground from each CSM, plant heights were calculated pixel-wise. Extensive manual measurements aligned well with the TLS data and demonstrated the main benefit of CSMs: the highly detailed acquisition of the entire crop surface.

In a further step, the plant height data were used to estimate biomass with empirically developed biomass regression models (BRMs). Validation analyses against destructive measurements were carried out to confirm the results. Moreover, the spatial and temporal transferability of crop-specific BRMs was shown with the multi-site and multi-annual studies. In one of the case studies, the estimations from plant height and six VIs were compared and the benefit of fusing both parameters was investigated. The analyses were based on the TLS-derived CSMs and spectral data measured with a field spectrometer. From these results the important role of plant height as a robust estimator was shown in contrast to a varying performance of BRMs based on the VIs. A major benefit through the fusion of both parameters in multivariate BRMs could not be concluded in this study. Nevertheless, further research

should address this fusion, with regard to the capability of VIs to assess information about the vegetation cover (plant density, leaf area index) or biochemical and biophysical parameters (nitrogen, chlorophyll, and water content).

In summary, a major advantage of the presented approach is the possibility to rapidly and easily receive 3D data of plant height at field scale, which is a robust estimator for crop biomass. Moreover, the high resolution of the TLS-derived CSMs enables detailed and spatially resolved estimations of biomass. Even though several issues have to be solved before practical applications in conventional agriculture are possible, approaches based on laser scanning offer great potential for crop monitoring.

Zusammenfassung

Im Vergleich zu anderen Methoden der Fernerkundung ist Terrestrisches Laser Scanning (TLS) noch eine recht junge Disziplin, jedoch bietet die Zuverlässigkeit der laserbasierten Abstandsmessungen großes Potenzial für genaue Vermessungen. Außerhalb der traditionellen Vermessungsdisziplinen können somit auch Nicht-Experten 3D Daten mit hoher Messdichte zügig erfassen. Die Erfassung genauer Geoinformationen wird zwar generell in verschiedenen Anwendungsbereichen immer wichtiger, die hier präsentierte Studie richtet sich allerdings speziell auf die Anwendung von TLS zum Monitoring von Feldfrüchten im agrarwissenschaftlichen Bereich.

Der steigende Kosten- und Effizienzdruck in der Landwirtschaft hat zur Entwicklung der standortspezifischen Ackerbewirtschaftung geführt, welche ein umfassendes Wissen über die Pflanzenentwicklung erfordert. Ein wichtiger Parameter, um diese Entwicklung oder genauer gesagt den aktuellen Zustand der Pflanzen zu beurteilen ist die Biomasse, welche direkt nur durch destruktive Probenahme bestimmbar ist. Mit dem Ziel solche destruktiven Messungen zu vermeiden, nimmt das Interesse an berührungslosen Erfassungen mittels Fernerkundung zu. Heutzutage beschäftigen sich verschiedene Ansätze mit der Schätzung von Biomasse auf Grundlage anderer Parameter, wie z.B. Vegetationsindizes (VIs) basierend auf Spektraldaten oder Pflanzenhöhe. Ein großer Vorteil aller Fernerkundungsverfahren ist, dass Parameter erfasst werden, ohne die Pflanzen durch die Durchführung der Messungen zu stören. Da die Pflanzen bei den Messungen nicht entnommen werden ist es darüber hinaus aus ökonomischer und ökologischer Sicht möglich mehrere Messungen über ein Feld und über die Vegetationsperiode verteilt durchzuführen. Dadurch kann die Veränderung räumlicher und zeitlicher Muster beobachtet werden.

Diese Studie verwendet TLS zum objektiven Messen und Beobachten von Pflanzenhöhen als Schätzgröße für Biomasse auf Feldskala. Die Anwendung des hier vorgestellten Ansatzes ist zwar generell für eine Vielzahl von Feldfrüchten vorstellbar, der Fokus dieser Studie richtet sich jedoch auf Getreide, da diese hinsichtlich der Welternährung die größte Rolle spielen. Drei Beispiele wurden dabei ausgewählt, namentlich Paddyreis, Mais und Gerste.

Im Rahmen dieser Arbeit wurden verteilt über fünf Standorte und vier Vegetationsperioden insgesamt 35 TLS Feldkampagnen durchgeführt um einen umfangreichen Datensatz zu erhalten. In jeder Kampagne wurde eine 3D Punktwolke zur Erfassung der Oberfläche des Feldes aufgenommen und in der Nachbearbeitung zu einem Oberflächenmodell der Pflanzendecke (crop surface model, CSM) interpoliert. Ein CSM stellt somit die Pflanzendecke in sehr hoher räumlicher Auflösung zu einem bestimmten Zeitpunkt dar. Durch die Subtraktion eines digitalen Geländemodelles (digital terrain model, DTM) des blanken Bodens vom CSM wurden die Pflanzenhöhen pixelweise berechnet. Umfangreiche manuelle Messungen bestätigten die TLS Daten und zeigten einen der großen Vorteile der CSMs: die sehr detaillierte Erfassung der gesamten Pflanzendecke.

In einem weiteren Schritt wurden die Pflanzenhöhen verwendet, um die Biomasse mit empirisch entwickelten Biomasse-Regressionsmodellen (biomass regression models, BRMs) zu schätzen. Diese Werte wurden zur Prüfung der Ergebnisse gegen destruktive Messungen validiert. Darüber hinaus wurde die räumliche und zeitliche Übertragbarkeit der für die

jeweilige Feldfrucht spezifischen BRMs anhand von Studien über verschiedene Standorte und mehrere Jahre gezeigt. In einem der Fallbeispiele wurden die Schätzungen auf Grundlage der Pflanzenhöhe mit den Schätzungen basierend auf sechs VIs verglichen und der Mehrwert durch eine Kombination beider Parameter untersucht. Die Analysen beruhten dabei auf den aus den TLS Daten abgeleiteten CSMs und Spektraldaten, die mit einem Feldspektrometer erfasst wurden. Die Ergebnisse unterstreichen die große Bedeutung der Pflanzenhöhe als robuste Schätzgröße für Biomasse, während die aus den VIs abgeleiteten BRMs sehr unterschiedliche Ergebnisse lieferten. Ein wesentlicher Vorteil aus der Kombination beider Parameter in multivarianten BRMs konnte in dieser Studie nicht festgestellt werden. Dennoch sollten Ansätze weiter untersucht werden, in denen die Parameter kombiniert werden, da aus VIs Informationen über die Vegetationsdecke (Pflanzendichte, Blattflächenindex) oder über biochemische und biophysikalische Parameter (Stickstoff-, Chlorophyll- und Wassergehalt) abgeleitet werden können.

Zusammengefasst ist einer der größeren Vorteile des vorgestellten Ansatzes die Möglichkeit, schnell und einfach 3D Daten der Pflanzenhöhe auf Feldskala zu erfassen, welche eine robuste Schätzgröße für Biomasse sind. Darüber hinaus ermöglicht die hohe Auflösung der durch TLS gewonnenen CSMs eine detaillierte und räumlich aufgelöste Schätzung der Biomasse. Vor der praktischen Anwendung in der konventionellen Landwirtschaft müssen zwar noch einige Probleme gelöst werden, dennoch bieten auf Laser Scanning beruhende Ansätze großes Potential für das Monitoring des Pflanzenwachstums.

Acknowledgments

This thesis is based on a comprehensive data set, which I have achieved in a great and exciting time accompanied by the help of many nice people. First of all, I am grateful to my supervisor Prof. Dr. Georg Bareth for the education in remote sensing, for giving me the opportunity to do this research, and for his extensive support. I also would like to thank Prof. Dr. Olaf Bubenzer as second examiner of this thesis, as well those who have kindly proofread the manuscript.

I am very grateful to my workmates and all the people who have enriched my life and my learning throughout this time, with special thanks directed to my colleagues of the GIS & RS Group. Worth particular mention are Dr. Dirk Hoffmeister for introducing me to the world of laser scanning and for his helpful advices and my cave mate Helge Aasen for the great working together and valuable discussions, but also for improving the work/life balance. I wish to thank our student assistants most sincerely for their great effort also under at times uncomfortable conditions. Furthermore, I acknowledge Cao Qiang for his selfless support and cultural introduction in Jiansanjiang and Henning Schiedung for his dedication in the laborious work of destructive maize plant sampling. Another thanks goes to the staff of the Campus Klein-Altendorf and the collaborators at the Forschungszentrum Jülich for greatly supporting the measurements related to the barley field experiment.

The campaigns in Jiansanjiang were facilitated by the International Center for Agro-Informatics and Sustainable Development (ICASD), financially supported by the International Bureau of the German Federal Ministry of Education and Research (BMBF, project number 01DO12013) and the German Research Foundation (DFG, project number BA 2062/8-1). For the study in Klein-Altendorf the funding and organization within the CROP.SENSE.net project is acknowledged, which was instituted in context of the Ziel 2-Programm NRW 2007 - 2013 "Regionale Wettbewerbsfähigkeit und Beschäftigung", financially supported by the Ministry for Innovation, Science and Research (MIWF) of the state North Rhine Westphalia (NRW) and European Union Funds for regional development (EFRE) (005-1103-0018).

Finally, my warmest thanks go to my family, especially to my parents Michael and Klaus Tilly for their love and support throughout my life. I also want to thank all my friends for their patience and understanding over the last months. Thanks are owed particularly to Roman Eckhardt. Last but not least, a special cheers to our office mascot, the Hyp-Las unicorn.

Table of contents

ABSTRACT	I
ZUSAMMENFASSUNG	III
ACKNOWLEDGMENTS	V
TABLE OF CONTENTS.....	VI
FIGURES.....	IX
TABLES.....	XII
ABBREVIATIONS.....	XIII
1 INTRODUCTION	1
1.1 Preface.....	1
1.2 Research issue and study aim.....	3
1.3 Outline	5
2 BASICS	7
2.1 Remote sensing	7
2.1.1 <i>Application in agriculture</i>	7
2.1.2 <i>Terrestrial laser scanning</i>	9
2.2 Crops.....	11
2.2.1 <i>Paddy rice</i>	12
2.2.2 <i>Maize</i>	12
2.2.3 <i>Barley</i>	12
2.2.4 <i>Growth and development</i>	13
2.3 Crop monitoring	15
2.3.1 <i>Evolution and existing studies</i>	15
2.3.2 <i>Crop surface model</i>	16
2.3.3 <i>Biomass regression model</i>	17
2.3.4 <i>Scales and dimensions</i>	18
2.4 Study sites.....	19
2.4.1 <i>Jiansanjiang, China</i>	20
2.4.2 <i>Selhausen, Germany</i>	20
2.4.3 <i>Klein-Altendorf, Germany</i>	21
3 MULTITEMPORAL CROP SURFACE MODELS: ACCURATE PLANT HEIGHT MEASUREMENT AND BIOMASS ESTIMATION WITH TERRESTRIAL LASER SCANNING IN PADDY RICE	22
3.1 Introduction.....	23
3.2 Materials and methods.....	25
3.2.1 <i>Study area</i>	25
3.2.1.1 <i>Field experiment</i>	25
3.2.1.2 <i>Farmer's field</i>	26
3.2.2 <i>TLS measurements</i>	26
3.2.3 <i>Manual measurements</i>	29
3.2.4 <i>TLS data processing</i>	30
3.2.5 <i>Spatial analysis</i>	31
3.2.6 <i>Statistical analysis</i>	32
3.2.7 <i>Biomass regression model</i>	32

3.3	Results	33
3.3.1	<i>Spatial analysis</i>	33
3.3.2	<i>Statistical analysis</i>	35
3.3.3	<i>Biomass regression model</i>	36
3.4	Discussion	38
3.5	Conclusion	42
	Acknowledgment	42
	References	43
4	TRANSFERABILITY OF MODELS FOR ESTIMATING PADDY RICE BIOMASS FROM SPATIAL PLANT HEIGHT DATA.....	48
4.1	Introduction.....	48
4.2	Data and methods	50
4.2.1	<i>Study area</i>	50
4.2.2	<i>Field measurements</i>	52
4.2.3	<i>Post-processing of the TLS data</i>	54
4.2.4	<i>Calculation of plant height and visualization as maps of plant height</i>	55
4.2.5	<i>Estimation of biomass</i>	56
4.3	Results	56
4.3.1	<i>Maps of CSM-derived plant height</i>	56
4.3.2	<i>Analysis of plant height data</i>	57
4.3.3	<i>Analysis of estimated biomass</i>	58
4.4	Discussion	61
4.5	Conclusions.....	64
	Acknowledgments.....	65
	References	66
5	TERRESTRIAL LASER SCANNING FOR PLANT HEIGHT MEASUREMENT AND BIOMASS ESTIMATION OF MAIZE.....	71
5.1	Introduction.....	71
5.2	Methods.....	72
5.2.1	<i>Data acquisition</i>	72
5.2.2	<i>Data processing</i>	74
5.3	Results	75
5.3.1	<i>Spatial analysis</i>	75
5.3.2	<i>Statistical analysis</i>	76
5.4	Discussion	78
5.5	Conclusion and outlook	79
	References	80
6	FUSION OF PLANT HEIGHT AND VEGETATION INDICES FOR THE ESTIMATION OF BARLEY BIOMASS.....	82
6.1	Introduction.....	82
6.2	Methods.....	84
6.2.1	<i>Field measurements</i>	84
6.2.1.1	<i>Terrestrial laser scanning</i>	86
6.2.1.2	<i>Field spectrometer measurements</i>	87

6.2.2	Post-processing	88
6.2.2.1	TLS data	88
6.2.2.2	Spectral data.....	88
6.2.3	Biomass regression models	90
6.3	Results	92
6.3.1	Acquired plant parameters.....	92
6.3.2	Biomass estimation	94
6.3.2.1	Bivariate models	96
6.3.2.2	Multivariate models.....	98
6.4	Discussion	99
6.4.1	TLS-derived plant height.....	100
6.4.2	Biomass estimation from plant height	101
6.4.3	Biomass estimation from vegetation indices	102
6.4.4	Biomass estimation with fused models	103
6.5	Conclusion and outlook	105
	Acknowledgments.....	106
	Appendix	107
	References	108
7	DISCUSSION.....	115
7.1	Sensor set-ups and scanning geometries	115
7.2	Platforms	118
7.3	Plant height measurements	120
7.4	Biomass estimations	122
7.5	Future prospects for laser scanning in agriculture	129
8	CONCLUSION.....	134
	REFERENCES.....	136
	APPENDIX A: EIGENANTEIL.....	145
	Kapitel 3	145
	Kapitel 4	145
	Kapitel 5	146
	Kapitel 6	146
	APPENDIX B: ERKLÄRUNG.....	147
	APPENDIX C: CURRICULUM VITAE	148

Figures

Figure 1-1. Patterns of spatial variability. The average yield (2.5 t/ha) and the amount of variation (50% = 1 t/ha; 50% = 4 t/ha) are the same in (A) and (B), but the patterns differ (Whelan and Taylor, 2013).	2
Figure 1-2. Overall workflow and allocation of research papers in the chapters 3 to 6 according to their main focuses.	6
Figure 2-1. Selection of remote sensing methods for the estimation of crop biomass across scales. Content of the studies is summarized to sensor and regarded crop or grassland.	8
Figure 2-2. Principle of time-of-flight measurements with laser ranging, profiling, and scanning systems.	10
Figure 2-3. Worldwide harvested area for the five main cereals. Values according to FAO (2014).	11
Figure 2-4. Growth stages of cereals based on the Feekes scale (Large, 1954).	14
Figure 2-5. Concept of multi-temporal crop surface models. Single plants modified from Large (1954).	17
Figure 2-6. Overview map of all study sites: Jiansanjiang (right); Selhausen and Klein-Altendorf (left).	19
Figure 2-7. Climate diagram for (A) Jiansanjiang, (B) Jülich, and (C) Klein-Altendorf (long-term average), modified from Gnyp (2014), Research Centre Jülich (2015), Uni Bonn (2010b), respectively.	21
Figure 3-1. Location of the study sites in China (modified from Gnyp et al. (2013)).	25
Figure 3-2. Overview of the investigated field experiment from scan position six (Figure 3-3). On the right side the scanner with the tripod mounted on the small trailer can be seen (taken: 04.07.11).	27
Figure 3-3. Experimental design and scan positions of the field experiment. Number in the plot represents: rice variety (1 = Kongyu 131; 2 = Longjing 21); treatment (1 - 9 in Table 3-1); repetition (1 - 3).	28
Figure 3-4. Experimental design and scan positions of the farmer's field.	28
Figure 3-5. General overview of the workflow for the post-processing of the TLS data.	30
Figure 3-6. Corner of the field experiment, showing the least dense vegetation (taken: 21.06.11).	31
Figure 3-7. General concept of crop surface models (CSMs) (Bendig et al., 2013).	32
Figure 3-8. CSM-derived maps of plant height for four selected plots of the field experiment (left: Kongyu 131; right: Longjing 21, marked in Figure 3-3).	33
Figure 3-9. Maps of plant growth for two selected plots of the field experiment, derived from the difference between two consecutive CSMs (left: Kongyu 131; right: Longjing 21, marked in Figure 3-3).	34
Figure 3-10. Difference between the averaged manually measured plant heights and the CSM-derived mean plant heights for each plot for the first campaign of the field experiment.	35
Figure 3-11. Regression of the mean CSM-derived and manually measured plant heights for the field experiment (n = 162) and the intensively investigated units on the farmer's field (n = 72).	36
Figure 3-12. Regression of the mean CSM-derived plant height and dry biomass for the field experiment (n = 90) and the intensively investigated units on the farmer's field (n = 72).	37
Figure 3-13. Theoretical biomass simulated with regression model and the measured values for the intensively investigated units on the farmer's field (each: n = 72).	38

Figure 4-1. Design of the field experiment and scan positions. Three-digit number in the plot represents rice variety (1 = Kongyu 131; 2 = Longjing 21); treatment (1 to 9); and repetition (1 to 3). Modified from Tilly et al. (2014). 51

Figure 4-2. One management unit with very heterogeneous plant growth in village 36. 51

Figure 4-3. Scan positions and bamboo stick positions on the farmer’s fields. 53

Figure 4-4. Small, round reflectors were permanently attached to trees in village 36..... 54

Figure 4-5. Crop surface model (CSM)-derived maps of plant height for two field experiment plots of both years, given with mean plant height per plot. 57

Figure 4-6. Regression of the mean CSM-derived and manually measured plant heights of the field experiment of both years (each n = 162)..... 58

Figure 4-7. Linear (left) and exponential (right) regression between mean CSM-derived plant height and dry biomass for the field experiment of both years (each n = 90); regression equations are given in Table 4-5. Biomass values for the exponential regression are natural log-transformed. 61

Figure 5-1. a) TLS system (marked with arrow) mounted on a cherry picker; b) highly reflective cylinders arranged on ranging pole. 73

Figure 5-2. CSM-derived maps of plant height for the whole maize field on the last campaign date (top) and for the buffer area around sample point 5 on each date (bottom)..... 75

Figure 5-3. CSM-derived maps of plant growth for the whole maize field (at the top between 3rd and 31st of July; at the bottom between the 31st of July and the 24h of September). 76

Figure 5-4. Regression of the mean CSM-derived plant height and the dry biomass (n = 48). 78

Figure 5-5. Regression of the mean CSM-derived and manually measured plant heights (n = 60). 78

Figure 6-1. Instrumental set-up: (A) terrestrial laser scanner Riegl LMS-Z420i; (B) tractor with hydraulic platform; (C) ranging pole with reflective cylinder..... 87

Figure 6-2. Workflow for the calibration and validation of the biomass regression models and distinction of cases for each model. 91

Figure 6-3. Maps of four plots from the last six and five campaigns of 2013 and 2014, respectively. One plot of each N fertilizer level of the barley cultivar Trumpf is shown for each year (∅: Plot mean height). 92

Figure 6-4. Regression of the mean CSM-derived and manual measured plant heights (2012: n = 131; 2013: n = 196; 2014: n = 180). 93

Figure 6-5. Scatterplots of measured vs. estimated dry biomass for one validation data set for NDVI, RGBVI, REIP, and GnyLi (exponential model). Pre-anthesis: crosses and solid green line; whole observed period: circles and dashed black line; 1:1 line: light grey..... 97

Figure 6-6. Scatterplots of measured vs. estimated fresh biomass for one validation data set for NDVI, RGBVI, REIP, and GnyLi (exponential model). Pre-anthesis: crosses and solid green line; whole observed period: circles and dashed black line; 1:1 line: light grey..... 98

Figure 6-7. Scatterplot for one validation data set for the pre-anthesis (green) and for the whole observed period (black) of the bivariate BRM of PH (circles and solid regression line) and multivariate BRM of PH and GnyLi (crosses and dashed regression line) for dry biomass (top) and fresh biomass (bottom) (all exponential models); 1:1 line: light grey. 99

Figure 7-1. Platforms for TLS with the approximate sensor height: (A) Tripod (1.5 m); (B) Tractor-trailer system (3 m); (C) Tractor with hydraulic platform (4 m); (D) Cherry picker (8 m)..... 116

Figure 7-2. Influence of the sensor height and the resulting inclination angle on the incidence angle. This affects which plant parts are ascertainable, which in turn influences the calculated mean plant height. Single plants modified from Large (1954). 117

Figure 7-3. Influence of platform movements during the scans on the calculated maize plant heights. Scans were acquired from the basket of the cherry picker, placed close to the corners of the field.	119
Figure 7-4. Plant heights ascertainable from the TLS-derived point clouds and the manual measurements. The measuring processes influence the calculated mean plant height. Single plants modified from Large (1954).....	120
Figure 7-5. Averaged CSM-derived vs. manually measured plant heights of all campaigns on paddy rice, maize, and barley (left) and of all except maize (right).....	121
Figure 7-6. Mean trend of plant height and dry biomass of barley across the growing season with trend curves as polynomial functions of the 3rd degree.	124
Figure 7-7. Dry biomass accumulation in crop parts. Modified from Fischer (1983).	125
Figure 7-8. Dry biomass map of the paddy rice units in village 36 for the 16.07.2012. Estimated from the CSM-derived plant height with the BRM: $Biomass = 12.37 \cdot \text{plant height} - 273.19$ (Table 4-5).	126
Figure 7-9. Assimilation in ripening cereal. Green color marks active plant parts. Modified from Munzert and Frahm (2005).	128
Figure 7-10. MLS systems for crop monitoring: (A) Phenomobile (Deery et al., 2014); (B) LiDAR sensor, attached to a combined harvester (Lenaerts et al., 2012).....	130
Figure 7-11. Low-altitude airborne platforms: (A) MikroCopter Okto XL with hyperspectral snapshot camera (modified from Aasen et al., 2015); (B) Gyrocopter (Weber et al., 2015).	132

Tables

Table 2-1. Chronological selection of TLS systems with maximal measuring rate (Large and Heritage, 2009; Riegl LMS GmbH, 2015a, 2013).....	10
Table 2-2. Principal growth stages of the BBCH scale and criteria for their subdivision in developmental steps, modified from Meier (2001).....	14
Table 2-3. Equations of the biomass regression models.....	18
Table 3-1. Fertilizer application scheme for both study sites.....	26
Table 3-2. Dates of the scan campaigns and corresponding phenological stages.....	27
Table 3-3. Mean CSM-derived and manually measured plant heights for both fields.....	35
Table 3-4. Mean CSM-derived plant heights and biomass values.....	36
Table 3-5. Biomass values for the overall farmer's field.....	38
Table 4-1. Dates of the terrestrial laser scanning (TLS) campaigns and corresponding phenological stages.....	52
Table 4-2. Mean crop surface model (CSM)-derived and manually measured plant heights of the field experiment (n : number of samples; \bar{X} : mean value; SD: standard deviation; min: minimum; max: maximum).....	58
Table 4-3. Mean CSM-derived plant heights and destructively measured biomass values of all sites (n : number of samples; \bar{X} : mean value; SD: standard deviation; min: minimum; max: maximum).....	59
Table 4-4. Trial biomass regression models (BRMs) and validation of estimated against measured biomass (R^2 : coefficient of determination; d : index of agreement; RMSE: root mean square error).....	60
Table 4-5. Biomass regression models (BRMs), derived from field experiment and validation of estimated against measured biomass for the farmer's fields (R^2 : coefficient of determination; d : index of agreement; RMSE: root mean square error).....	61
Table 5-1. CSM-derived and manually measured plant heights as well as destructively taken biomass, based on the averaged values for the buffer areas (each date $n = 12$).....	77
Table 6-1. Dates of the terrestrial laser scanning (TLS) and spectrometer (S) campaigns listed as day after seeding (DAS). Averaged codes for the developmental steps are given for the dates of manual plant parameter measurements (BBCH). For some dates BBCH codes were not determined (N/A).....	85
Table 6-2. Principal growth stages of the BBCH scale.....	86
Table 6-3. Vegetation indices used in this study.....	90
Table 6-4. Statistics for the plot-wise averaged CSM-derived plant heights and destructively taken biomass for the reduced data sets of 2013 and 2014 (n : number of samples; \bar{X} : mean value; min: minimum; max: maximum; SD: standard deviation).....	94
Table 6-5. Statistics for the model calibration as mean values of the four subset combinations (R^2 : coefficient of determination; SE_E : standard error of the estimate).....	95
Table 6-6. Statistics for the model validation as mean values of the four subset combinations (R^2 : coefficient of determination; RMSE: root mean square error (g/m^2); d : Willmott's index of agreement).....	96
Table 7-1. Advantages and disadvantages of the platforms used for field surveys.....	119
Table 7-2. R^2 values for linear and exponential regression between CSM-derived plant height and dry biomass for the field experiments.....	123

Abbreviations

ALS	Airborne laser scanning
AOI	Area of interest
BBCH	Biologische Bundesanstalt (German Federal Biological Research Centre for Agriculture and Forestry), Bundessortenamt (German Federal Office of Plant Varieties), and Chemical industry
BRM	Biomass regression model
CSM	Crop surface model
d	Willmott's index of agreement
DAS	Day after seeding
DEM	Digital elevation model
DGPS	Differential global positioning system
DSM	Digital surface model
DTM	Digital terrain model
FAO	Food and Agriculture Organization of the United Nations
GNSS	Global navigation satellite systems
ICP	Iterative closest point
IDW	Inverse distance weighting
IMU	Inertial measurement unit
LAI	Leaf area index
LiDAR	Light detection and ranging
MLS	Mobile laser scanning
N	Nitrogen
NDVI	Normalized difference vegetation index
NIR	Near-infrared domain
NNI	Nitrogen nutrition index
NRI	Normalized reflectance index
PA	Precision agriculture
PH	Plant height
PLS	Personal laser scanning
R ²	Coefficient of determination
RDVI	Renormalized difference vegetation index
REIP	Red edge inflection point
RGBVI	Red green blue vegetation index
RMSE	Root mean square error
S	Spectrometer
SAR	Synthetic aperture radar
SE _E	Standard error of the estimate
SWIR	Shortwave infrared domain
TLS	Terrestrial laser scanning
UAV	Unmanned aerial vehicle
VI	Vegetation index
VIS	Visible domain
VISNIR	Visible and near-infrared domain

1 Introduction

1.1 Preface

The rapidly growing world population and the related demand for food security causes challenges for agri-food researchers (Marsden and Morley, 2014). According to the figures of the Food and Agriculture Organization of the United Nations (FAO) the total cereal production increased from ~2.0 to ~2.8 billion tons over the last 20 years (FAO, 2014). In the same period, the worldwide harvested area for cereals stayed almost constant at ~700 million hectares, which underlines the pressure on the efficiency of land use. Moreover, the FAO indicates that within this 20 years the world population rose from ~5.5 billion to ~7.1 billion people, with a supposed rise up to ~8.6 billion within the next 20 years. By the middle of this century already ~10 billion world citizens are expected. This growing population demands a secure food supply, which in turn increases the pressure on the conventional agricultural sector and requires an improvement of management methods (Liaghat and Balasundram, 2010).

Fortunately, an increasing recognition of the interaction between production and consumption and between food security and sustainability is observable in large sections of the population (Marsden and Morley, 2014). Since the 1990's technical management methods and practices which aim at improving the food production emerged and can be summarized under the term precision agriculture (Mulla, 2012). One of the first definitions for precision agriculture came from the US House of Representatives and stated it as "an integrated information- and production-based farming system that is designed to increase long-term, site specific and whole farm production efficiencies, productivity, and profitability while minimizing unintended impacts on wildlife and the environment" (US House of Representatives, 1997). Considering the topic of this thesis, this definition should be narrowed to the term site-specific crop management to differentiate from animal industries or forestry (Whelan and Taylor, 2013). Related approaches address the improvement of farming practices to better suit soil and crop requirements. However, both terms precision agriculture and site-specific crop management are often used synonymously.

Based on these definitions two main aspects in this research field can be derived (Whelan and Taylor, 2013). First, from an economic point of view, improving the productivity of crops, which means the harvested yield, is obviously most important. Second, from an ecological point of view, exhausting or polluting soil, groundwater, and the entire environment through intensive field management needs to be minimized or, even better, avoided.

Generally, a number of natural and human-induced processes are relevant for site-specific crop management and moreover they can show spatial and temporal variations (Oliver, 2013). These changes across time involve differences between the growing seasons, but also within one season. Beside quite stable factors, such as the physical landscape, climate, and biological lifecycle of crops, the efficiency of an agricultural production depends on varying weather conditions and field management practices for example (Atzberger, 2013). Hence, the required frequency of measurements to observe temporal variations depends strongly on the concrete issue. In contrast to these factors which are generally quite uniform across regions, spatial variabilities can be detected between adjacent fields and moreover within one field.

Possible sources are fertilizer residues in the ground, varying water availability, or generally small-scale heterogeneities of soil properties. The importance of detecting in-field variations for site-specific crop management can be demonstrated by the example of Whelan and Taylor (2013), shown in **Figure 1-1**. The average yield and amount of variation are equal in both fields, but the patterns differ. It is obvious that for an acquisition of patterns such as in the right field (**B**), measuring systems with a high in-field resolution are required.

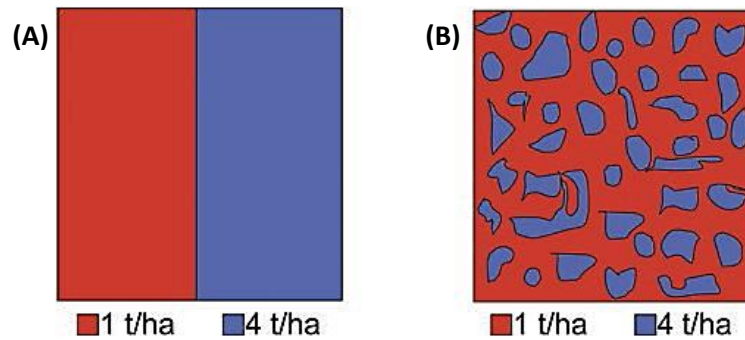


Figure 1-1. Patterns of spatial variability. The average yield (2.5 t/ha) and the amount of variation (50% = 1 t/ha; 50% = 4 t/ha) are the same in (A) and (B), but the patterns differ (Whelan and Taylor, 2013).

Today, sensor-based approaches are already findable for some applications assignable to precision agriculture. Such technologies can support plant protection and site-specific seeding (Auernhammer, 2001) or the detection of foliar diseases (Lee et al., 2010). With the aim of enhancing the yield, precision agriculture is frequently associated with site-specific fertilization (Auernhammer, 2001). Xu et al. (2014), for example, showed that appropriate fertilizer recommendations can increase the grain yield and moreover reduce the nutrient loss and environmental pollution. In this context, biomass estimations are of major interest, since studies show that crop yield is correlated to biomass (Boukerrou and Rasmusson, 1990; Fischer, 1993). This correlation can be quantified by the harvest index, expressing the yield versus total dry biomass (Price and Munns, 2010). Hence, accurately determining biomass can help to forecast yield.

Beyond the yield-correlated amount of biomass at the end of the growing season, the in-season status of the plants is more important. One reason therefore is that adequate conditions during early growing stages could preserve the yield against challenges of later stages, caused by drought stress for example (Bidinger et al., 1977). An essential prerequisite for optimizing plant conditions through adequate field management is to acquire the current state of the crop and monitor changes. A benchmark for quantifying the plant status in-season is the nitrogen nutrition index (NNI), showing the ratio between actual and critical nitrogen (N) content (Lemaire et al., 2008). Since this critical value corresponds to the actual crop biomass, a precise determining of biomass is desirable.

A major difficulty for all biomass-related indices is that a non-destructive determination of biomass is not possible. This is why several approaches focus on its estimations based on other parameters. Remote sensing methods were therefore increasingly applied over the last several decades (Mulla, 2012). Casanova et al. (1998), for example, measured the reflectance on rice plants across the growing season with a hand-held radiometer and attained very good

results for the estimation of biomass at field scale; 97 % of the variance in biomass could be explained by their model. On a far greater observation scale, satellite-based remote sensing enables to capture entire regions in a short time. As shown by Claverie et al. (2012), remote sensing data with a high spatial and temporal resolution, in this case Formosat-2 images, can be used to estimate biomass. Through the daily revisit time of the satellite, the authors obtained a comprehensive data set and well estimated biomass, with a relative error of 28 %. However, a main issue for all approaches based on optical satellites is the dependence on cloud-free conditions. In their first observation year Claverie et al. (2012) obtained only 27 almost cloud-free images from a total number of 51. Active satellite-based remote sensing systems, such as synthetic aperture radar (SAR) sensors, are used to overcome this problem (Koppe et al., 2012; Zhang et al., 2014). Nevertheless, referring to the variability of processes which influence site-specific crop management, the temporal resolution reachable with a satellite-based system always depends on the satellite revisit time, which limits the flexibility of the approach. Regarding the spatial resolution, only recently systems have been developed which allow surveys with a high in-field resolution. One example is WorldView-3 with a pixel size of ~0.3 m (DigitalGlobe, 2014). Between these approaches, which regarded very different observation levels, numerous studies on crop monitoring with different remote sensing sensors are findable across almost all scales.

It can be summarized, that in the field of precision agriculture or rather site-specific crop management, a growing demand arises for approaches on monitoring plant parameters with a spatial in-field resolution. Parameters usable for reliable biomass estimations are thereby of major importance. In general, the required temporal and spatial resolution is very case-specific, but timely flexible systems which allow a high spatial resolution are desirable, since the influencing environmental factors are variable in time and space (Atzberger, 2013). Moreover, they should be as robust as possible against poor weather conditions and ideally almost independent from external factors, such as solar radiation.

1.2 Research issue and study aim

The request for the reliable determination of biomass motivates the overall aim of this study: developing a robust method for the non-destructive estimation of crop biomass at field scale. Looking at the literature, biomass-related parameters, such as plant height, leaf area index (LAI), or crop density are assumed to be suitable estimators. Having regard to ground- or vehicle-based measurements, plant parameters like crop density, LAI, or directly biomass are widely estimated with vegetation indices (VIs) from spectral data (Casanova et al., 1998; Clevers et al., 2008; Gnyp et al., 2014b; Montes et al., 2011; Thenkabail et al., 2000). Therein, the reflectance is often measured with passive sensors, having disadvantages like the dependency on solar radiation and the influence through atmospheric conditions. Since these factors are variable in space and time, a site-specific spectral calibration is required (Adamchuk et al., 2004), which has to be frequently repeated during the measurements (Psomas et al., 2011). This makes surveys quite laborious.

In contrast, an active system like terrestrial laser scanning (TLS) operates with a self-generated signal, making the measurements independent from an external light source (Briese, 2010). In addition, the system is flexible for the application in the field as the scanner can be established on a tripod or small vehicle. The result of a TLS survey is a very dense 3D point cloud, representing the spatial distribution of reflection points in the area of interest (AOI), but measured with one wavelength. This makes a derivation of VIs impossible but enables to easily capture the entire field. Consequently, the question is how to derive plant parameter information from the TLS data?

In this work, the 3D point cloud from each TLS campaign is interpolated to a crop surface model (CSM). CSMs were introduced by Hoffmeister et al. (2010) to represent the entire crop canopy with a very high spatial resolution at a specific date. At each site multi-temporal CSMs are established based on several campaigns. By subtracting a digital terrain model (DTM) of the bare ground from each CSM, plant heights are calculated pixel-wise and stored as raster data sets. These measurements of plant height are then used for estimating biomass. First promising results for the estimation of aboveground biomass were already attained in a feasibility study for sugar beet by Hoffmeister (2014), but regarding world nutrition sugar beet plays a minor role. The most important group of crops are cereals due to their high proportion of carbohydrates (FAO, 1994). In view of the worldwide harvested area the five most important cereals are wheat, maize, paddy rice, barley, and rye, which cover already more than 85 % of the total area. Cereals might be further grouped in three categories by their general appearance and cultivation methods. Except for maize, which is clearly distinguishable through the larger plant height and paddy rice, which is grown on flooded fields, the remaining wheat, barley, and rye share main characteristics like plant heights of ~1 m and the cultivation on regular arable land.

A comprehensive investigation of this novel approach in terms of its usability for monitoring cereals at field scale is targeted in this study. Hence, the main aims are (I) to demonstrate the usability of TLS-derived point clouds for establishing CSMs, (II) to obtain plant height, and (III) to estimate cereal biomass from these plant height data. In four case studies biomass regression models (BRMs) are therefore empirically developed with three cereals as examples, namely paddy rice, maize, and barley. According to the above stated subdivision, all three categories of cereals are covered by these examples. In addition to the bivariate BRMs, a comparison with estimations based on VIs is performed and first steps towards a fusion of both parameters are carried out by establishing multivariate BRMs. The working process can be divided into the following steps:

- I. Execution of field surveys at three sites with different platforms over four years.
- II. Construction of CSMs from each TLS-derived point clouds.
- III. Calculation of plant height.
- IV. Estimation of biomass based on plant height.
- V. Comparison of plant height and VIs as individual estimators and fused in multivariate BRMs for the barley case study.
- VI. Validation of plant height and estimated biomass against comparative data.

Generally, any remote sensing approach can be evaluated by its reachable spatial and temporal resolution (Campbell and Wynne, 2011). Thereby is the detection of spatial patterns limited by the size of the areas which can be separately recorded by the sensor. The repeatability in time strongly depends on the flexibility of the platform. According to these criteria the presented ground-based TLS approach shows promising potential for the acquisition of plant height at field scale. Consequently, the same high spatial resolution can be assumed for spatially resolved biomass estimations across the entire field. The major innovative aspects are in particular the possibility to capture entire fields, the very high spatial resolution, and the flexible usage. Moreover, the survey dates can be quite easily adapted to capture particular steps of the plant development or measurements can be postponed due to poor weather.

1.3 Outline

This chapter 1 should have given a first impression of how important crop monitoring is, in particular the acquisition of biomass-related parameters for site-specific crop management. Within the framework of this study, a comprehensive data set was achieved, allowing to evaluate the potential of TLS-derived 3D data of plant height for estimating biomass at field scale. In the following chapter 2 fundamental basics therefore are given, including a summary about remote sensing, with particular attention on applications in agriculture and a general introduction into TLS. After that, the regarded cereals are briefly portrayed and the general crop development across the growing season is addressed. Then, existing approaches for crop monitoring are presented and the methodology requisite for the case studies is introduced. This involves the construction of CSMs and the development of BRMs. In this context, the attainable scales and dimensions are regarded. Finally, the three case study sites are placed in a geographical context.

The chapters 3 to 6 contain the research papers, presenting the results of the case studies. They are sorted along the overall workflow (**Figure 1-2**). Although, the major steps like the post-processing of the point clouds, the calculation of plant height, and the estimation of biomass are addressed in all papers, they are broadly assigned to the workflow according to their main focuses. First of all, the general concept of obtaining plant height from multi-temporal TLS-derived CSMs is examined in Tilly et al. (2014a; chapter 3) based on surveys on two paddy rice fields of one growing season. Moreover, the potential of CSM-derived plant height for estimating biomass is investigated. Then, in conjunction with these data sets, the measurements of two paddy rice fields from the subsequent growing season are analyzed in Tilly et al. (2015b; chapter 4). The main focus of this study lies on the spatial and temporal transferability of the BRMs. Concerning the data acquisition, the results of measurements on a larger field are shown for a maize field in Tilly et al. (2014b; chapter 5). Furthermore, the applicability of a cherry picker as platform is investigated based on several campaigns in one growing season. In Tilly et al. (2015a; chapter 6) the performances of plant height and VIs as individual estimators are compared and first attempts of improving the BRMs through fusing both parameters are carried out. A barley field experiment was therefore monitored with TLS and with a field spectrometer over three growing seasons.

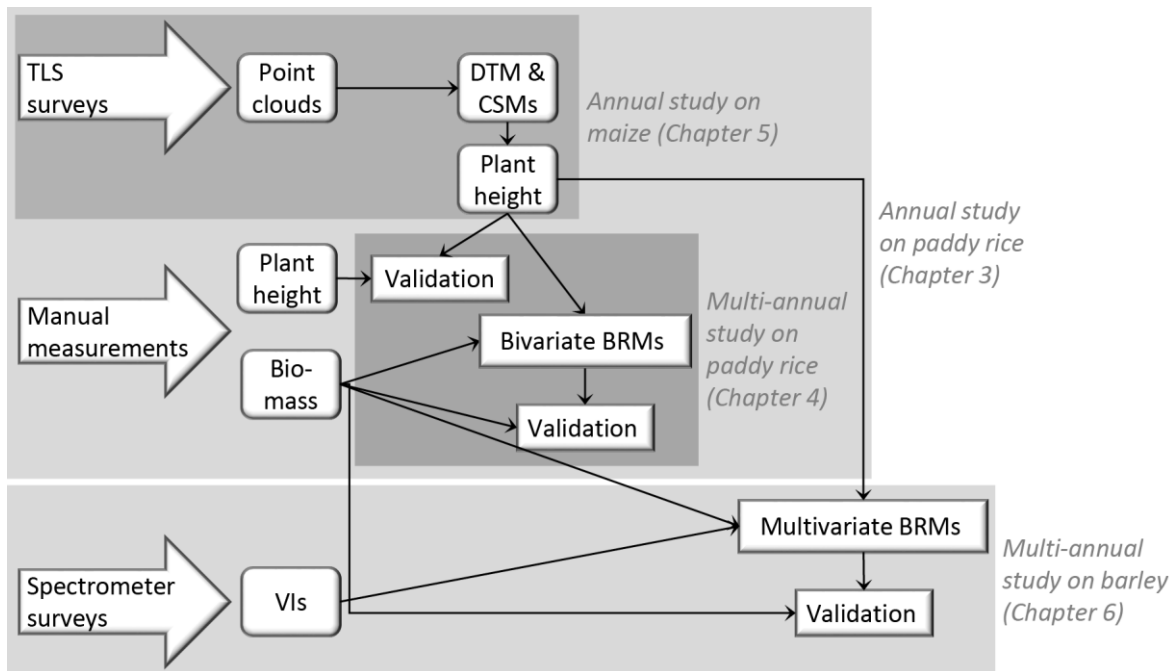


Figure 1-2. Overall workflow and allocation of research papers in the chapters 3 to 6 according to their main focuses.

Based on the results of these case studies chapter 7 gives an overall discussion. In this, firstly some issues related to the field measurements are regarded. Then the reliability and utility of the CSM-derived 3D data of plant height is evaluated and the validity of the biomass estimations is assessed. This also includes an evaluation of the fusion with spectral data. Afterwards, future prospects for laser scanning approaches in agriculture are outlined. Finally, Chapter 8 gives a concluding assessment of the applied methods and achieved results.

2 Basics

2.1 Remote sensing

One of the earliest approaches commonly assigned to remote sensing is the use of balloons for aerial photography in the late 19th century (Lillesand et al., 2004). Enabled through the development of airplanes, the interpretation of aerial photos increased in importance during the world wars (Jensen, 2007). In the late 1950s civilian applications of aerial photography arose as a source of cartographic information (Campbell and Wynne, 2011). From these approaches, the common aspect in definitions of remote sensing can be concluded: sensor-based data acquisition to derive information about an object with a certain distance between sensor and object (Lillesand et al., 2004). Since no clear definition exists how great this distance is, a variety of sensors and platforms, from ground-based over low- and high-altitude airborne to spaceborne systems are currently included under the rubric of remote sensing. The former ones are sometimes referred to as proximal (remote) sensing.

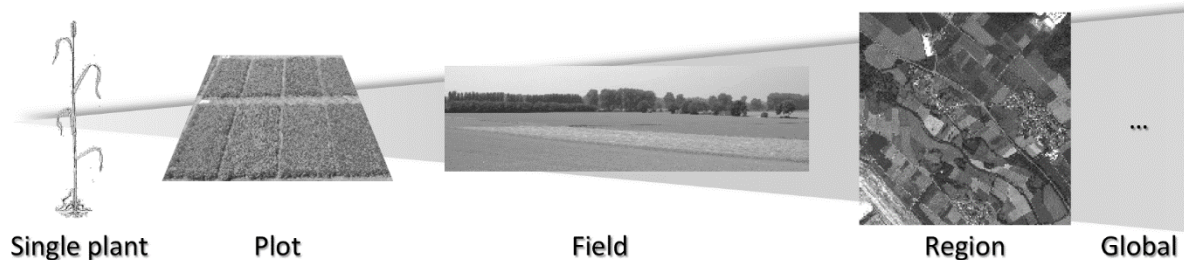
Moreover, remote sensing might not be regarded as an own science, rather it is a tool or technology which is applied in a multitude of scientific disciplines (Löffler, 1985). In this respect - contemporaneously with the development of new sensors from a technical perspective - the application of remote sensing has reached more and more fields of human activity. Only looking at remote sensing of the natural environment, applications range already from the acquisition of data regarding vegetation and water to the assessment of soils, minerals, or geomorphological structures (Jensen, 2007). Extending the application fields to urban areas, further issues are, for example, the detection of city structures, like roads and buildings, detailed monitoring of production facilities, or human-induced changes of the natural environment, such as forest or agricultural land. With regard to the extent of this thesis, the focus of this chapter is narrowed to remote sensing in agricultural applications with different sensors and a more detailed introduction into TLS.

2.1.1 Application in agriculture

Remote sensing methods are widely used in agriculture, as they allow non-contact surveys and thus prevent disturbing the plants by the taking of measurements (Liaghat and Balasundram, 2010). Applied sensors and platforms range across almost all scales, from hand-held and tractor-based sensors to air- and spaceborne systems in micro-level to regional and global surveys, respectively (Allan, 1990). As for any application of remote sensing, major factors for choosing a system are the targeted spatial and temporal resolution. Mulla (2012) prognosticates that, compared to current approaches, future site-specific crop management will claim for greater spatial and temporal resolutions. Atzberger (2013) summarized the current research focuses of such approaches to five main topics: (I) crop yield and biomass, (II) crop nutrient and water stress, (III) infestations of weeds, (IV) insects and plant diseases, and (V) soil properties.

According to this subdivision, the presented study belongs to the first topic and hence the following remarks are limited to applications dealing with crop biomass. **Figure 2-1** lists several remote sensing sensors and platforms, usable for biomass estimations. The selection is based on recent exemplary studies of the last five years and cannot claim to completeness, rather it

should give a general view across methods at different observation scales. It has to be noted that an acquisition at an entire global scale is not very useful for agricultural applications.



Ground-based imagery

Grassland biomass estimation from ground-based imagery (Inoue et al., 2015).

Field spectrometer

Hyperspectral canopy sensing for estimating rice biomass (Gnyp et al., 2014b); Maize biomass determination from measurements with tractor-based spectral reflectance sensor (Montes et al., 2011); Predicting grassland biomass with spectral sensor (Reddersen et al., 2014).

Light curtain

Maize biomass determination from measurements with tractor-based light curtain (Montes et al., 2011).

Ultrasonic sensor

Predicting biomass of grassland from ultrasonic sensor (Reddersen et al., 2014); Use of ultrasonic sensor for estimating biomass of Bermudagrass, alfalfa, and wheat (Pittman et al., 2015).

Terrestrial laser scanning

Measuring crop biomass with laser rangefinder (Ehlert et al., 2009); TLS-based estimation of wheat biomass (Eitel et al., 2014); Estimating biomass of paddy rice with TLS (Tilly et al., 2015b, 2014a) (Chapter 3 & 4).

Low-altitude airborne imagery

Estimating barley biomass from UAV-based RGB imaging (Bendig et al., 2014).

Low-altitude airborne spectral measurements

UAV-based hyperspectral snapshot camera for estimating barley biomass (Aasen et al., 2015); UAV-based spectral camera for biomass estimation of wheat and barley (Honkavaara et al., 2013).

High-altitude airborne laser scanning

Airborne laser scanning for estimating maize biomass (Li et al., 2015).

Satellite-based spectral measurements

Maize and sunflower biomass estimation from Formosat-2 data (Claverie et al., 2012); Estimation of wheat biomass from hyperspectral remote sensing (Koppe et al., 2012); Detection of biomass in maize and soybean from rapid eye data (Kross et al., 2015).

Satellite-based radar measurements

Estimation of wheat biomass from radar remote sensing (Koppe et al., 2012).

Figure 2-1. Selection of remote sensing methods for the estimation of crop biomass across scales. Content of the studies is summarized to sensor and regarded crop or grassland.

This selection of studies demonstrates the general interest in the use of remote sensing methods for estimating biomass. Thereby advantages and disadvantages can be assumed for each system, considering factors like the spatial resolution, the possible temporal frequency of measurements, or the dependency on external sources. In this study, TLS was chosen as

system which allows measurements at field scale in a high spatial resolution. In addition, the ground-based active sensor is fairly flexible and independently usable.

2.1.2 Terrestrial laser scanning

Out of the variety of remote sensing sensors TLS is quite a young discipline. It is assignable to the proximal sensing methods with a short sensor range, compared to satellite-based systems for example. However, in the beginning laser-based measurements were applied with greater distances between sensor and object (Jensen, 2007). The origin of laser-based distance measurements can be dated back to the development of the first optical laser in 1960. Since the 1970s light detection and ranging (LiDAR) systems based on aircrafts, also known as airborne laser scanning (ALS), were used for elevation mapping (Lillesand et al., 2004). In these early stages such measurements were primarily used in traditional engineering surveying, but caused by technical refinements and the development of weather-resistant systems during the late 20th century, laser scanning aroused the interest of environmental scientists (Large and Heritage, 2009). In several cases the application of a plane was however not flexible enough or too expensive and the spatial resolution of ALS was not sufficient. The resulting demand for ground-based systems led to the evolution of TLS.

Only in the late 1990s the first TLS systems have been introduced, but the development of new sensors rapidly increased and their usage is now extended over a wide range of research areas (Large and Heritage, 2009). Applications of TLS range across various fields, such as geomorphology (Schaefer and Inkpen, 2010), geology (Buckley et al., 2008), forestry studies (van Leeuwen et al., 2011), archeology (Lambers et al., 2007), or urban mapping (Kukko et al., 2012). With the main advantage of easily capturing data in a high rate and density, TLS offers opportunities for non-experts, outside traditional surveying disciplines, to acquire 3D spatial information. Nevertheless, a basic understanding of the measuring principle is necessary. This can be exemplified by two simpler versions of laser-based measuring devices, namely laser ranging and laser profiling systems.

The basic principle of so called time-of-flight measurements can be explained with the laser ranger (Petrie and Toth, 2008). Emitted by the ranger, the laser radiation is used to accurately measure the travel time, or time-of-flight, between transmitting a signal and its return to the receiver after reflection on any point of an object, also referred to as reflection point (ranging in **Figure 2-2**). From this time-of-flight, the slant distance or range (R) between the ranger and the reflection point is calculated as half of the entire path, with the speed of light is known to be ~0.3 m/ns:

$$R = \frac{(\text{speed of light} \cdot \text{time of flight})}{2}$$

In environmental science, rather than locating individual reflection points, capturing 2D profiles is desired for detecting terrain features. Similar as ranging systems, laser profiling devices measure the ranges (R) of several reflection points in equidistant steps along a line, but in addition the vertical angles (V) between R and the horizontal are observed (profiling in **Figure 2-2**). The profile is then determined through calculating each horizontal distance (D) and difference in height (ΔH) between the sensor and the reflection points:

$$D = R \cos V \qquad \Delta H = R \sin V$$

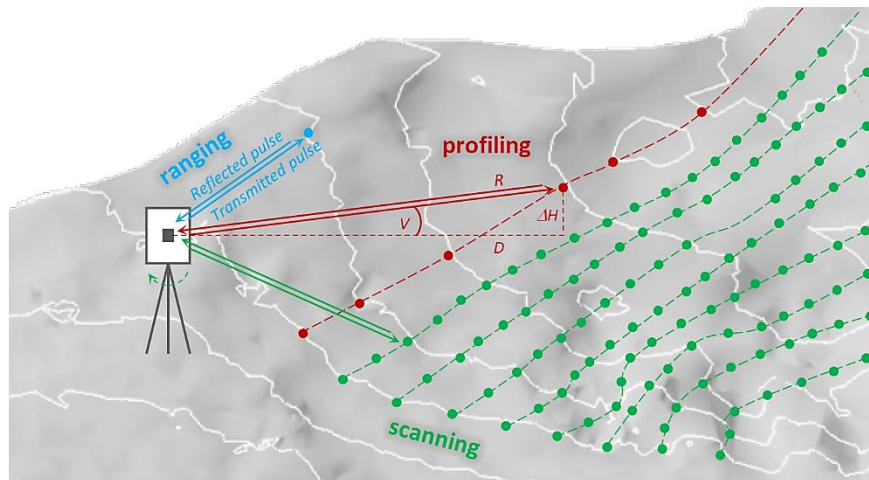


Figure 2-2. Principle of time-of-flight measurements with laser ranging, profiling, and scanning systems.

Through adding a scanning mechanism to the system, such as a rotating mirror or a prism, a laser scanner is attained, which can measure the vertical dimension of a profile along a topographic features in a high detail (Petrie and Toth, 2008). Due to the static position of the terrestrial laser scanner, an additional motion is necessary to attain a horizontal resolution. Usually, a movable component, containing the scanning mechanism is rotated by an engine around the vertical axis, which allows to measure a series of parallel profiles (scanning in **Figure 2-2**). The result of one measurement is then a cluster of reflection points, known as point cloud, containing the x, y, and z coordinates of each point.

In the short history of TLS, the measuring rate of reflection points has rapidly increased with the development of new systems. While the first launched sensor Leica Cyrax 2400 was capable of measuring only 100 point/sec, the sensors used in the case studies of this thesis measure 100 to 1,000 times more points/sec. **Table 2-1** gives an overview about selected systems, whereby the selection is limited to time-of-flight scanners, since only such systems were used in this study. Beyond that, phase scanning systems should be mentioned as available alternatives, which achieve higher measuring rates and a better accuracy, but can only measure in shorter ranges (Beraldin et al., 2010). Their measuring principle differs slightly from time-of-flight scanners. Phase scanners emit the laser beam at alternating frequencies and measure the phase difference between the emitted and reflected signal.

Table 2-1. Chronological selection of TLS systems with maximal measuring rate (Large and Heritage, 2009; Riegl LMS GmbH, 2015a, 2013).

Launch year	Sensor	Maximal measuring rate
1998	Leica Cyrax 2400	100 points/sec
2001	Leica Cyrax 2500	1,000 points/sec
2007	Riegl LMS-Z420i^a	11,000 points/sec
2007	Leica ScanStation 2	50,000 points/sec
2010	Riegl VZ-1000^a	122,000 points/sec
2014	Riegl VZ-2000	400,000 points/sec

^a Sensors used for the case studies.

2.2 Crops

In the framework of this study, time-of-flight scanners are used to monitor crop height across the growing season. According to the definition of the FAO, crops are agricultural products, coming directly from the field without any real processing, except cleaning (FAO, 2011). They might be further subdivided into cereals, pulses, roots and tubers, sugar crops, oil-bearing crops, fiber crops, vegetables, tobacco, fodder crops, fruits and berries, nuts, spices and aromatic herbs, and other crops (coffee, cacao, tea, and hops). In addition, it can be distinguished between temporary crops, being sown and harvested during the same growing season (sometimes more than once per year), and permanent crops, which have not to be replanted after each annual harvest.

The most important group of crops are cereals, as they contribute the most to world nutrition. In general, cereals are annual plants of the gramineous family, characterized by carbohydrate as main nutrient element (FAO, 1994). According to the statistics of the FAO, the five largest cereals alone (wheat, maize, paddy rice, barley, and rye) make up more than 85 % of the total harvested area for cereals (**Figure 2-3**). Based on their general appearance and growing characteristics three categories of cereals might be classified. Most cereals like wheat, barley, and rye reach plant heights of ~1 m and are grown on regular arable land. Exceptions from this are maize due to the larger plant height and paddy rice due to its cultivation on flooded fields. All herein regarded examples (paddy rice, maize, and barley) are cereals and corresponding to this subdivision, they cover all subcategories and are thus regarded as suitable representatives for cereals. However, the broader term crop is preferred in the further course of the work as the presented concept of monitoring is transferable to other groups. Brief characterizations of paddy rice, maize, and barley are given in the following sections, listed in the order of their appearance in the chapters 3 to 6. Afterwards some general characteristics of crop growth and development are given as a basis for the concept of crop monitoring.

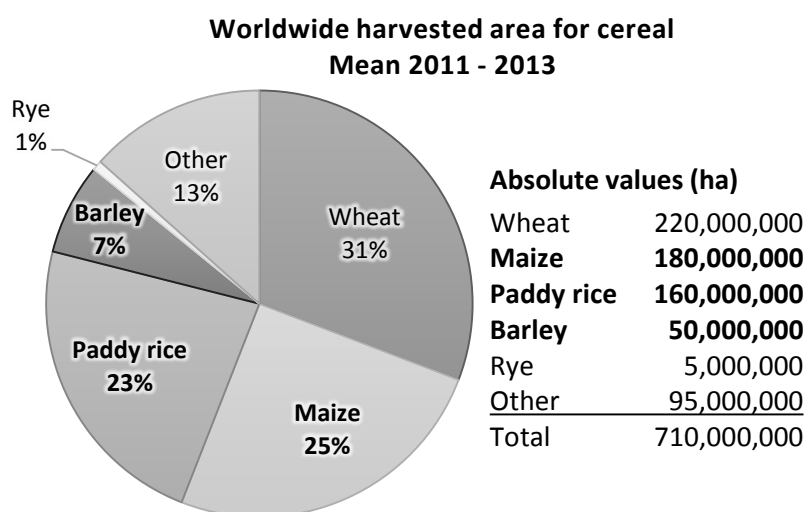


Figure 2-3. Worldwide harvested area for the five main cereals. Values according to FAO (2014).

2.2.1 Paddy rice

Cultivated rice (*Oryza*) is the staple food for two thirds of the world population and the leading food crop in developing countries (Juliano, 2004). It is a cereal grain grass (family *Poaceae*) and although it is an annual species, it may grow more than once per year under reasonable environmental conditions. This quality of growth is influenced by factors like temperature, day length, nutrition, planting density, and humidity (Nemoto et al., 1995). Even though rice was originally a plant of wetlands, some species are cultivated on dry land or in water. It is common practice to flood the paddy rice fields for irrigation and simplifying weed control. The term paddy is the anglicized form of the Malayan word padi, meaning 'of rice straw' (Arendt and Zannini, 2013). Today, the term paddy rice is used for both the water-covered fields and the harvested product.

Historically, the most ancient archaeological findings of rice cultivation were found in the Yangzi delta in China, dating back to 5,000 BC (Arendt and Zannini, 2013). Although with almost 30 %, meaning about 200 Mio tons per year, China still accounts for the largest part of the world rice production, the cultivation of rice is nowadays widely distributed around the world. It is grown in more than 100 countries between 53° N and 40° S and from sea level to altitudes of up to 3,000 m, covering in total about one quarter of the worldwide harvested area for cereals (**Figure 2-3**). Assumable about ~100,000 rice varieties exist, of which only a small number is cultivated (Juliano, 2004).

The appearance of the rice plants is marked by round and hollow stems with flat sessile leaf blades and a terminal panicle (Arendt and Zannini, 2013). Several stems are grouped to hills with fibrous roots at the bottom. Each stem is enveloped by leaf sheath, which continuously merge into the leaf blade. The height of the majority of the rice varieties ranges between 1 and 2 m at their final growth.

2.2.2 Maize

Cultivated maize (*Zea mays* L.), also known as corn, is along with wheat and rice one of the most extensively cultivated cereals (Arendt and Zannini, 2013). It is an important source for a wide range of applications, such as human diet, feeding animals, or production of fuel and fibers. For a long time different theories on the origin of maize existed (Lee, 2004). The widely shared assumption today is that it was domesticated at least 6,700 BC in the highlands of Mexico. Nowadays, cultivated areas are spread worldwide, horizontally between 50° N and 40° S and vertically from the Caribbean islands to 3,400 m above sea level in the Andean mountains. About one quarter of the worldwide harvested area for cereals in more than 160 countries is cultivated with maize (**Figure 2-3**).

Like paddy rice, maize is a cereal grain grass of the family *Poaceae*, sharing characteristics such as conspicuous nodes in the stem and a single leaf at each node, with leaves alternately arranged (Lee, 2004). On the contrary, final plant heights are much larger; typically maize plants reach heights of 2.0 - 3.5 m. Plant height and yield are obviously influenced by environmental factors, irrigation, and fertilization.

2.2.3 Barley

Cultivated barley (*Hordeum vulgare* L.) is one of the most versatile cereal crops (Arendt and Zannini, 2013). It has been one of the most important cereals in ancient times, as it can be

grown under a large range of environmental conditions. Archaeological findings allow to infer that barley was grown in the Near East and North Africa around 8,000 and 6,000 BC, respectively. During the course of time, it was more and more replaced through the increasing use of wheat, rice, and maize. Nowadays, considering the worldwide harvested area for cereals barley only ranks fourth (**Figure 2-3**), but an increasing use is predicted for the future, because unique benefits to human health are assumed (Edney, 2010). The highest prices for barley are achievable when used for malting and brewing, which also supports the promising future for barley, as the worldwide beer consumption is likely to further increase. However, since malting has high quality requirements, today the majority of the produced barley is used to feed animals, where lower quality is sufficient.

Barley is a cereal grain grass of the family *Poaceae*, which is however distinguishable from other species of this family, like wheat, through the ears with long awns, although some awnless types also exist (Kling et al., 2004). Typically plants reach heights of about 1 m. In modern varieties the plant height was reduced and straw strength was increased to enhance the resistance against lodging.

2.2.4 Growth and development

From a general botanic point of view, the changes in plants across the growing season have to be divided in a qualitative and quantitative part (Price and Munns, 2010). While, qualitative changes are related to a plant development, involving changing plants appearance or function, quantitative changes reflect the growth, meaning a rising plant size, linked to an increasing biomass. Obviously, the development and growth cycles interact to a high degree and are furthermore influenced by environmental conditions. In the following, the term growth always implies the associated development of the plants, otherwise it is mentioned separately.

The entire biological lifecycle of any plant can be divided into a reproductive phase, starting with the germination process, and a vegetative phase, marked by plant growth and development such as organ formation. This passes into the reproductive phase for the next generation (Price and Munns, 2010). The growth process of cereals can be broadly summarized to the tillering process after the germination, followed by the stem extension and heading, and finally the ripening as start of the new reproductive phase (Larcher, 2003). An illustration of these stages by Large (1954) is shown in **Figure 2-4**. The stages are based on the Feekes scale, which was developed by Willem Feekes in a pioneering approach of defining growth stages (Feekes, 1941).

Nowadays, various scales exist for describing crop growth across the growing season through the declaration of stages. These scales slightly differ in the definition of each stage and its allocation to either the vegetative or reproductive phase. From this variety, the BBCH scale is used in all case studies of this thesis. The acronym BBCH is derived from the funding organizations: Biologische Bundesanstalt (German Federal Biological Research Centre for Agriculture and Forestry), Bundessortenamt (German Federal Office of Plant Varieties), and Chemical industry. A main benefit of this scale is the fine subdivision of each growth stage in further so called developmental steps. The scale is classified by a two-digit number of which the first decodes the principal growth stage and the second subdivides into the developmental steps. As shown in **Table 2-2**, the scale starts with the early reproductive phase, the

germination, and ends with the senescence, the withering of the plants but start for the reproductive phase of the next generation. It should be mentioned that the vegetative phase is most important for the development of crops and appropriate field management can mainly influence the plant growth during these stages. The application of N fertilizer on barley, for example, should be completed prior to BBCH stage 3 (Munzert and Frahm, 2005). Hence, this phase is mainly in the focus of crop management.

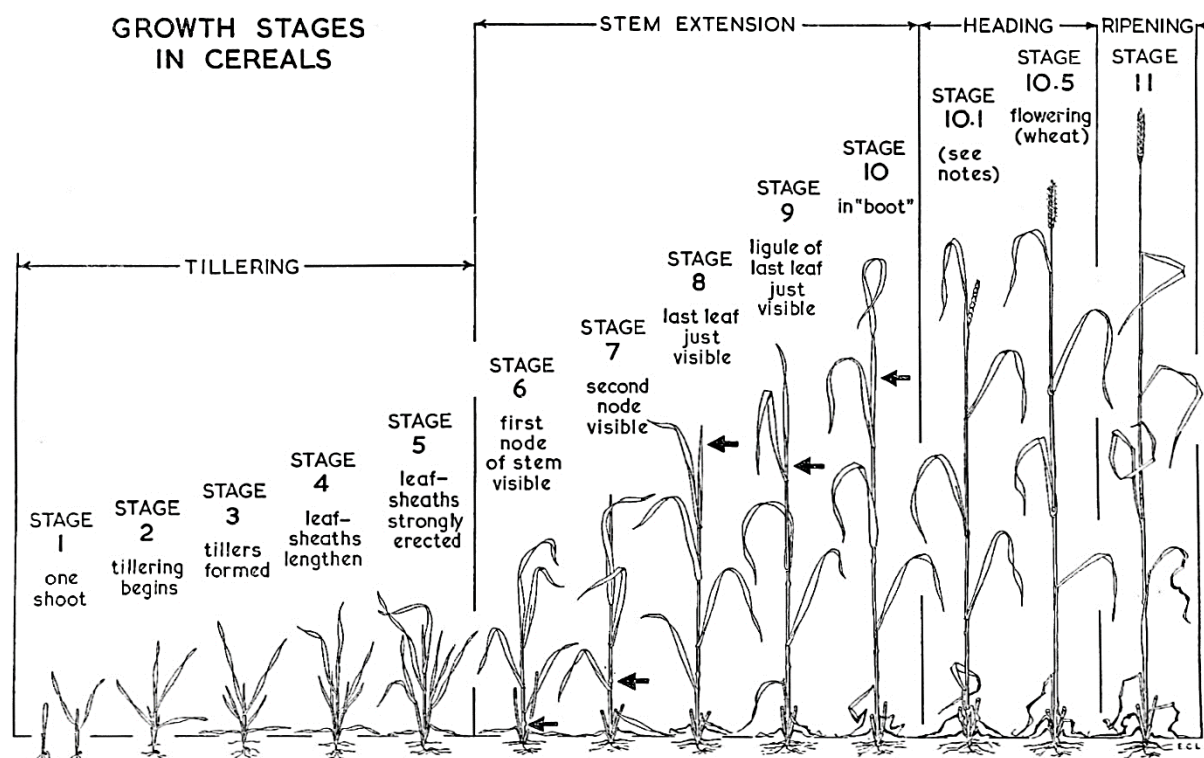


Figure 2-4. Growth stages of cereals based on the Feekes scale (Large, 1954).

Table 2-2. Principal growth stages of the BBCH scale and criteria for their subdivision in developmental steps, modified from Meier (2001).

	Principal growth stage ^a	Code ^b	Subdivision of developmental steps based on:
reproductive phase	0 Germination	00 - 09	Steps of germination and sprouting
	1 Leaf development	10 - 19	Number of true leaves, leaf pairs, or whorls unfolded
	2 Tillering	21 - 29	Number of side shoots and tillers
vegetative phase	3 Stem elongation	31 - 39	Number of detectable nodes and stem length
	4 Booting	40 - 49	Percentage of reached harvestable vegetative plant parts
	5 Inflorescence emergence, heading	51 - 59	Amount of inflorescence emerged
	6 Flowering, anthesis	60 - 69	Percentage of flowers open
start for reproductive phase of next generation	7 Development of fruit	71 - 79	Percentage of fruits have reached final size
	8 Ripening	81 - 89	Steps of ripening or fruit coloration
	9 Senescence	91 - 99	Steps of leaf-falling, withering till harvested product

^a first number of code; ^b entire code to subdivide developmental steps

2.3 Crop monitoring

The plant height of the herein investigated crops is monitored across each respective growing season. Generally, monitoring means to observe the progress of something over a period of time but without any information about how this is done. Hence, crop monitoring can be interpreted as observing plant development during its growth. This is nowadays often associated with sensor-based measurements as part of site-specific field management. However, referring to the non-consideration of the applied method, crop monitoring has a longer history in agriculture than the remote sensing approaches. This evolution and chronological development is shortly addressed in the next section, followed by an introduction of the approach presented in this study and some aspects about scales and dimensions.

2.3.1 Evolution and existing studies

During the pre-industrial times, farmers have cultivated small fields. Since they needed to have a detailed knowledge about their fields or rather the plant development, some kind of human-based crop monitoring was already necessary. However, they had no possibilities to quantify variabilities so far (Whelan and Taylor, 2013). The industrial revolution induced then a mechanization of conventional agriculture during the second half of the 20th century. As a consequence, management practices have widely been applied, in which fields were considered as being uniform over large scales. This allowed the deployment of machines but reduced the flexibility to adapt the field management. A contrary development can be stated for the end of the 20th and beginning of the 21st century. Enabled through further technical refinements, a trend towards site-specific management practices was and is still observable. Nowadays, various approaches address site-specific crop monitoring and management. In particular non-contact surveys, enabled through remote sensing sensors, are in the focus of research (Atzberger, 2013). With regard to the aim of this study, the focus of this section is held on monitoring biomass and plant height with ground- or vehicle-based approaches.

Due to its strong link to yield, biomass is an important plant parameter and approaches as to its estimation and monitoring are widely researched. In early approaches rising plate meters were applied for biomass estimations on grassland (Michell and Large, 1983). A pole is placed perpendicular to the ground, surrounded by a plate which falls down on the grass cover. Through measuring the height, biomass is determined, which depends on the turf density and grass species. Since this method is not well suited for determining biomass of cereals and measurements in larger spatial extents, other non-destructive estimation methods are necessary.

Widespread remote sensing methods for biomass estimations exist and range across almost all scales (**Figure 2-1**). Commonly, measurements of the reflected radiation from plants are used to calculate VIs, which allow the estimation of plant parameters such as plant height, LAI, water content or biomass (Casanova et al., 1998; Clevers et al., 2008; Guyot et al., 1992; Haboudane et al., 2004). An extensive study on different crops and their characteristics across several growth stages was conducted by Thenkabail et al. (2000). They complained about weaknesses of the widely used normalized difference vegetation index (NDVI) and suggested that other combinations of spectral bands are better suited to obtain biophysical

characteristics. Several other studies focused on this establishment of more suitable VIs, such as the four-band VI GnyLi, which was empirically developed for estimating biomass (Gnyp et al., 2014a). In that study, winter wheat fields were monitored with both field spectrometer and satellite images to develop a VI which can be used for multiscale biomass estimations. The reliability of the GnyLi was demonstrated with an averaged R^2 values across all scales of 0.78, on the contrary the NDVI reached only an R^2 values of 0.24.

Despite estimations based on VIs, plant height can be used to estimate biomass. However, unlike VIs, it is not very widely investigated so far. At the field scale, plant height can be measured by different ground-based sensors. Montes et al. (2011) showed the usability of height measurements with a light curtain for estimating maize biomass and reached R^2 values of up to 0.91. With R^2 values between 0.73 - 0.76 the usability of an ultrasonic sensor for measuring sward height as biomass estimator was demonstrated by Reddersen et al. (2014). Continuous monitoring of rice growth with a radar sensor was performed by Kim et al. (2013) and good correlations to plant height (0.88) were achieved. The potential of laser scanning systems was shown by Ehlert et al. (2010) with strong relation between height and crop biomass density of wheat ($R^2 > 0.90$). Moreover, plant heights are measured manually with a ruler or measuring tape, as shown, for example, by Marshall and Thenkabail (2015). They used such manual measurements for improving biomass estimations from spectral measurements. Compared to estimations on spectral data alone, up to 29 % more variance could be explained by the combined models. In contrast to the discrete measurements of ultrasonic sensors or manual measurements, continuous measurements capture the entire crop surface in the considered range, achievable from a TLS-derived point cloud for example. TLS sensors are also known to reach up to sub-centimeter accuracies (Large and Heritage, 2009) and thus they should be regarded as promising systems for exact crop monitoring.

2.3.2 Crop surface model

In this study, 3D point clouds of multi-temporal TLS surveys are used to monitor the crop height across the growing season. Details of the acquisition process and the individual steps of the post-processing are given in the research papers for each case study. Nevertheless, the general methodology as common concept is presented briefly in the following.

The final point cloud of each campaign is interpolated to a crop surface model (CSMs), representing the crop surface with a very high spatial resolution at a specific date (Hoffmeister et al., 2010). Previously, the point clouds are filtered with a scheme for selecting maximum points to detect the crop canopy. Thereby one value remains for each 1 cm by 1 cm cell. By capturing several CSMs across the growing season and an additional digital terrain model (DTM), representing the bare ground of the field at the beginning of the growing season, spatially resolved plant height data are calculated and temporal changes can be monitored (**Figure 2-5**). For example, the plant height values for the first campaign date (t_1) are calculated by subtracting the DTM from CSM_1 . The plant growth, in this context meaning an increase in plant height, is obtained by calculating the difference between the CSMs of two campaigns, e.g. $CSM_2 - CSM_1$. This results in raster data sets with pixel-wise stored plant height or growth.

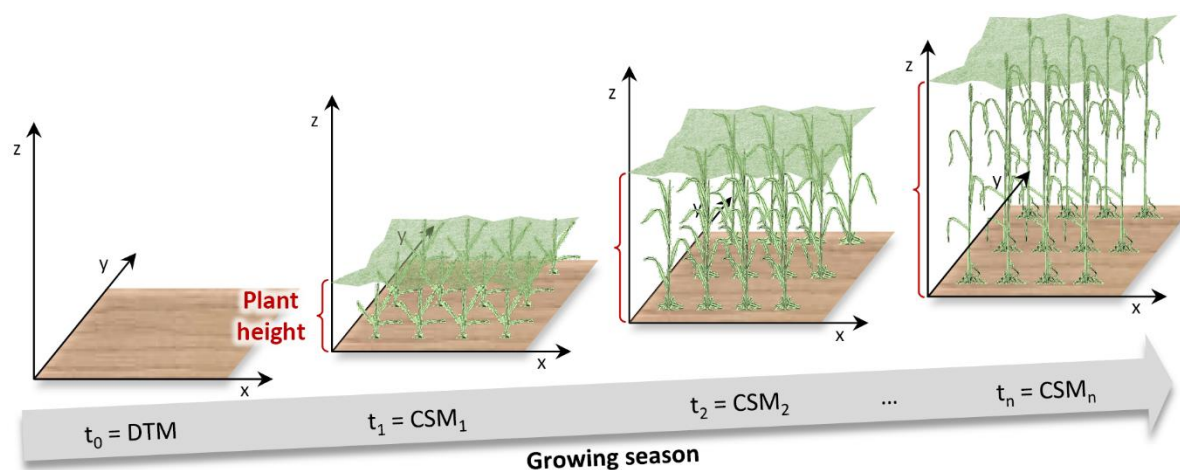


Figure 2-5. Concept of multi-temporal crop surface models. Single plants modified from Large (1954).

2.3.3 Biomass regression model

In the further course of this study, plant height is used to estimate crop biomass. During tillering and in particular during stem extension and elongation (BBCH stages 2 & 3, **Table 2-2**), increasing biomass is mainly related to increasing plant height (**Figure 2-4**). In the case studies (Chapter 3 to 6) biomass regression models (BRMs) are empirically developed to express this relation between TLS-derived plant height and destructively taken biomass for the examples of paddy rice, maize, and barley. In the paddy rice and maize case studies only dry biomass is regarded since this value is important for calculating biomass-related indices, such as the harvest index and the NNI. Additionally, the relation to fresh biomass is investigated in the comprehensive barley case study as this parameter is frequently used in crop growth models. Prior to the establishment of the BRMs, the pixel-wise stored plant height and the biomass values are averaged across equal spatial extents to allow the derivation of model equations.

In a first attempt, increasing plant height and biomass are both expected as being linear during the key vegetative phase. Hence, the simplest approach to express the relation between these parameters is also a linear BRM, according to *equation [1]*, **Table 2-3**. However, during the later stages, in particular after heading (BBCH stage 5, **Table 2-2**), further increasing biomass values can be expected due to the development of ears while the plant height stays almost constant (**Figure 2-4**). Consequently non-linear functions might suit better to the trend between the two parameters across the entire growing season. This is also confirmed in other studies, suggesting that biomass across the season is best estimated with exponential models (Aasen et al., 2014; Thenkabail et al., 2000). Therefore, exponential BRMs are established according to *equation [2]*, **Table 2-3**. For the exponential BRMs, the biomass values are natural log-transformed, which simplifies the calculation (*equation [3]*).

Linear BRMs are established in all case studies as comparable basis. Since the main focus of the first research paper (Chapter 3) lies on the general construction and usability of CSMs, exponential models are not considered yet. Exponential models are also excluded from the maize case study (Chapter 5), since the application of a different platform for measuring the larger maize plants and the larger fields is mainly addressed. The results of linear and exponential BRMs are shown for paddy rice and barley in chapter 4 and 6, respectively. In the

latter chapter, the benefit of fusing plant height with each of six VIs is investigated based on linear (equation [4]) and exponential (equation [5] and [6]) multivariate BRMs (Table 2-3).

Table 2-3. Equations of the biomass regression models.

Linear BRMs		
Bivariate	$Biomass = m \cdot plant\ height + b$	[1]
Multivariate	$Biomass = m \cdot plant\ height + n \cdot VI + b$	[4]
<i>with m and n as slopes and b as intercept.</i>		
Exponential BRMs		
Bivariate	$Biomass = b_0 \cdot e^{b_1 \cdot plant\ height}$	[2]
	$\ln(Biomass) = \ln(b_0) + b_1 \cdot plant\ height$	[3]
Multivariate	$Biomass = b_0 \cdot e^{b_1 \cdot plant\ height + b_2 \cdot VI}$	[5]
	$\ln(Biomass) = \ln(b_0) + b_1 \cdot plant\ height + b_2 \cdot VI$	[6]
<i>with $b_0 - b_2$ as factors and e as base of the natural logarithm.</i>		

2.3.4 Scales and dimensions

For any field survey, a general consideration should be given to the regarded scales and dimensions. As shown in **Figure 2-1**, remote sensing methods for the estimation of crop biomass range across various scales. For site-specific crop management a high in-field spatial resolution is required. The presented TLS approach for measuring plant height aims at the application at field scale, but prior to this, a sufficient knowledge about the development of plant height and biomass across the growing season is necessary. Therefore, two field experiments were monitored, in which several cultivars of one crop were cultivated with different fertilizer treatment in small-scale plots. This execution of experiments at plot level is common practice in crop science, for example, to investigate the performance of newly developed varieties (Kling et al., 2004).

Apart from this, the expected difference between the plots are useful for the monitoring approach to capture different plant conditions at one growing stage. Firstly, a paddy rice experiment was investigated in two growing seasons, where each plot was 10 m by 7 m in size (Chapters 3 and 4). Secondly, a spring barley experiment was surveyed in three growing seasons, where each plot was 7 m by 3 m in size (Chapter 6). The measurements on the paddy rice fields were supplemented by campaigns on two farmer's conventionally managed fields, having a total extent of 500 m by 300 m and 100 m by 80 m. Moreover, a maize field, which was 160 m by 60 m in size was monitored to examine the applicability of the approach at field scale (Chapter 5). The overall intent was to establish BRMs based on comprehensive measurements at plot level and use the models for estimations at field scale.

Furthermore, the dimension of the acquired data has to be regarded. The result of a TLS survey is a 3D point cloud, which is commonly used to generate a DTM (Briese, 2010). In these point clouds more than one height value (z) can be obtained for each 2D location (x, y). Since the representation of a DTM is typically limited to 2.5D, the point clouds need to be converted to data sets where one z value is stored for each 2D location. This involves a loss of information, which however cannot be avoided when using raster data sets. In the here presented crop monitoring approach, it is very likely that several z values with the same x, y coordinates are attained due to the almost vertical plants. Through interpolating the CSMs

from the filtered point clouds, raster data sets with a resolution of 1 cm are generated to store the highest z value per 2D location. As the plant height is then calculated based on the CSMs, the true dimension of these data sets is also 2.5D. However, the term 3D data of plant height is used in the further course of the work, referring to the point cloud as origin and since the term 2.5D is frequently unknown. Previous to the establishment of the BRMs, the pixel-wise stored plant heights are averaged across equal spatial extents, resulting in 1D data. In these data sets one value of plant height is stored per spatial unit for which the x , y coordinates are not considered, such as one field experiment plot. This was necessary to attain a common dimension with the biomass values, which are recorded for these spatial units.

2.4 Study sites

Crop monitoring with TLS was carried out at three sites during the growing seasons of 2011 to 2014, resulting in a total number of 35 field campaigns. The study site locations are marked in **Figure 2-6**. From a geographical point of view, all sites belong to the same ecozone, the temperate midlatitudes, ranging on the west sides of the continents from $40^\circ - 60^\circ$ and at the east sides from $35^\circ - 50^\circ$ (Schultz, 2005), but they differ in their location at the west and east sides of Eurasia. On the east site, paddy rice fields at three sites around the city of Jiansanjiang, Heilongjiang Province were surveyed in China. In Germany, on the west site, fields at two sites were investigated, both located in the federal state of North Rhine-Westphalia. Firstly, a maize field in the village Selhausen, about 40 km west of Cologne and secondly, a barley field in the village Klein-Altendorf, about 20 km southwest of Bonn, were investigated. According to the Köppen-Geiger climate classification the sites in China and Germany are assigned to the temperate climates Cwb and Cfb, respectively (Peel et al., 2007). Hence, they show the same temperature range across the year (hottest month $> 10^\circ\text{C}$ and coldest month $< 18^\circ\text{C}$) with

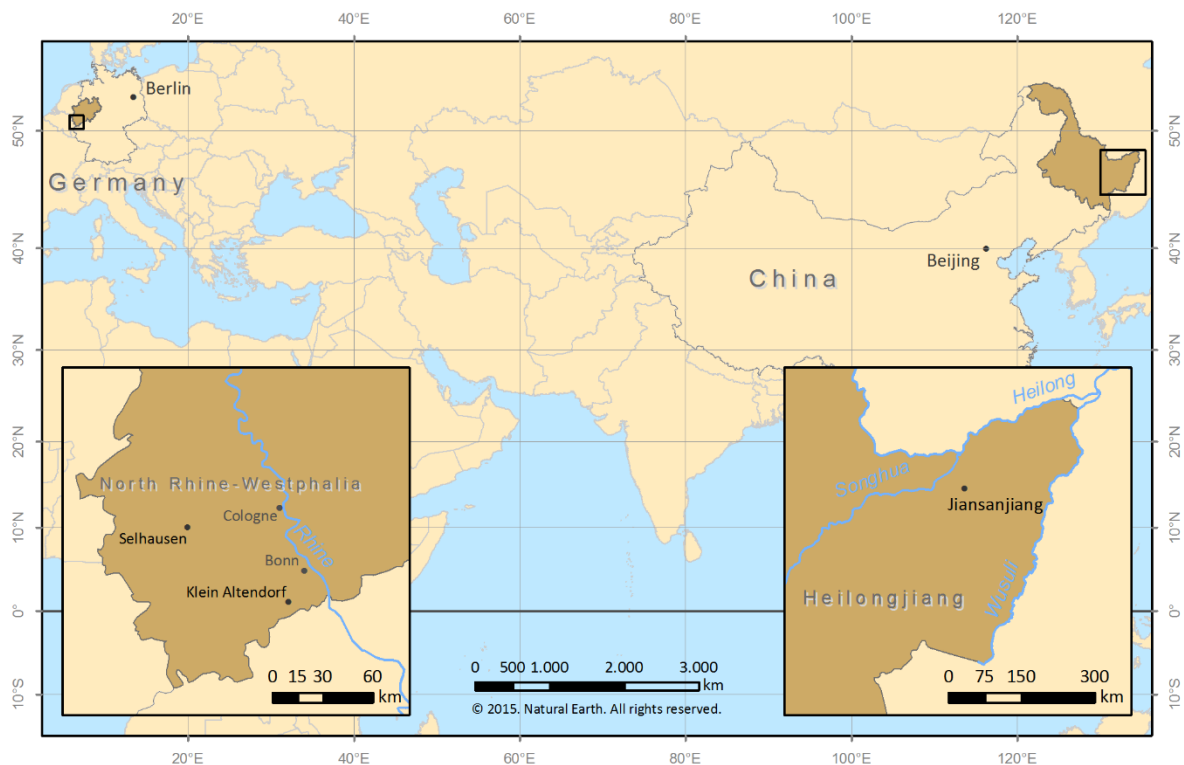


Figure 2-6. Overview map of all study sites: Jiansanjiang (right); Selhausen and Klein-Altendorf (left).

warm summers, but they differ in the characteristic of the winter season. Cwb climates are characterized by dry winters with the precipitation of the driest winter month being lower than 10 % of the precipitation of the wettest summer month. In contrast, no dry season is ascertainable for Cfb climates. In the following all sites are briefly portrayed.

2.4.1 Jiansanjiang, China

The city of Jiansanjiang is located in the province Heilongjiang, Northeast China. The topography of the province is flat and low in altitude, complemented by a few mountain ranges. In the northeasternmost part the Sanjiang Plain is situated, an alluvial plain, mainly deposited by the rivers Heilong, Songhua, and Wusuli. Through the land reclamation since 1950 the low-lying former wetlands are now well suited for agricultural production and the area has become an important basis for agricultural products in China (Gao and Liu, 2011). Underlying soil types of the marshlands as original land cover of the Sanjiang Plain were peat marsh soil, humus marsh soil, mire soil, and meadow marsh soil, but the reclamation induced a soil development. The four main soil types, making up 95 % of the area, are now meadow soil, lessive, swamp soil, and black soil (Liu et al., 2013; Wang et al., 2006).

The climate is marked by the East Asian summer monsoon, resulting in cold and dry winters, but warm and humid summers (Ding and Chan, 2005). The average annual temperature is about 1.4 - 4.3 °C, but an average maximum of 21 - 22 °C is reached in July. Moreover, about 70 % of the annual precipitation of 500 - 650 mm occurs between July and September. Resulting from the climatic conditions, the growing season lasts about 120 - 140 days (Wang and Yang, 2001; Wang et al., 2006). According to the records of the local weather station of Jiansanjiang the annual mean temperature is 3.6 °C with an average yearly precipitation of about 490 mm (Gnyp, 2014); the climate diagram for Jiansanjiang is shown in **Figure 2-7 (A)**.

In Jiansanjiang the Keyansuo experiment station is located, where field management approaches for irrigated rice cultivation are carried out. In each growing season of 2011 and 2012 the same field experiment was investigated at this station. In addition, one nearby farmer's conventionally managed field was monitored each year. Descriptions of the three sites and the field experiment are given in the research papers (Section 3.2.1 and 4.2.1).

2.4.2 Selhausen, Germany

Selhausen is a small village in the district of Düren, about 40 km west of Cologne. The area is part of the lower Rhine basin with a flat or slightly undulated surface, characterized by small valleys of the rivers Rur and Ellbach. The investigated field is situated on the upper terrace of the Rhine/Meuse river system, which consists of Pleistocene sand and gravel sediments (Rudolph et al., 2015). All soils in the area are developed in Quaternary sediments and Cambisols, Luvisols, Planosols, and Stagnosols are the main soil types.

The long-term records of the weather station at the nearby Research Centre Jülich are used to regard the climatic conditions. They show an average annual temperature of 10.0 °C with an average yearly precipitation of about 700 mm (Research Centre Jülich, 2015); the climate diagram for Jülich is shown in **Figure 2-7 (B)**.

At this site a farmer's conventionally managed maize field was monitored across the growing season of 2013. Therefore six TLS campaigns were carried out. More details are given in the research paper (section 5.2.1).

2.4.3 Klein-Altendorf, Germany

The village Klein-Altendorf lies about 20 km southwest of Bonn. Since the area belongs to the main terrace of the southern part of the lower Rhine basin, the ground is almost flat and the clayey silt luvisol is well suited for crop cultivation (Uni Bonn, 2010a). On these nutritious soils in the Rhenish area typically crops like sugar beet, wheat, and barley are cultivated.

The region lies in the warm temperate climate zone, with the mesoclimatic conditions being influenced by the sheltered location of the lower Rhine basin (Uni Bonn, 2010b). Records of the weather station in Klein-Altendorf show an average annual temperature of 9.3 °C and a long-term average yearly precipitation of about 600 mm; **Figure 2-7 (C)** shows the climate diagram for Klein-Altendorf. The growing season comprises about 165 - 170 days.

A field experiment campus, belonging to the Faculty of Agriculture, University of Bonn, is hosted in Klein-Altendorf. Across the growing seasons of 2012 to 2014 a field experiment with different cultivars of spring barley was monitored with several TLS campaigns each year. More details about the experiment are provided in the research paper (section 6.2.1).

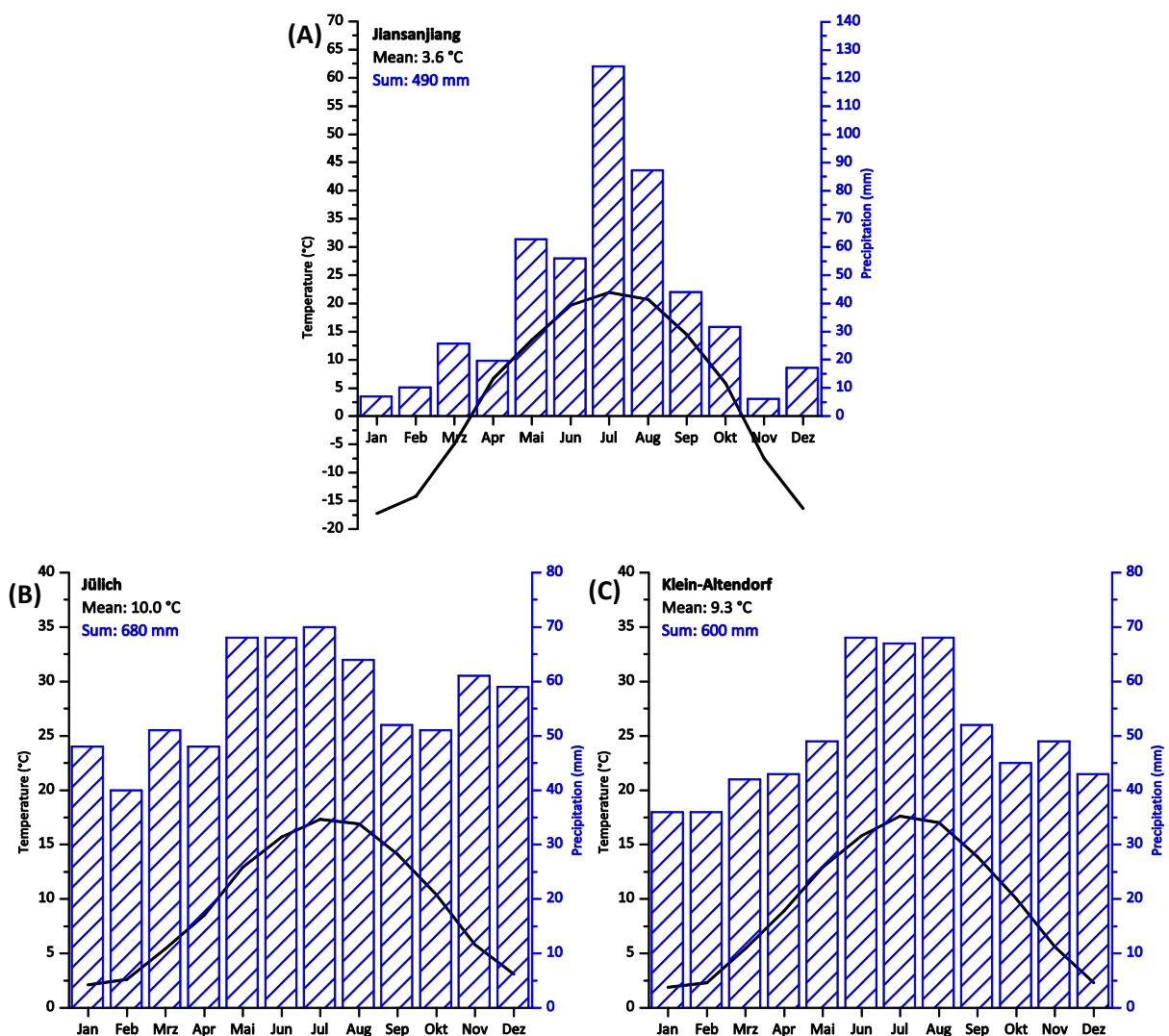


Figure 2-7. Climate diagram for (A) Jiansanjiang, (B) Jülich, and (C) Klein-Altendorf (long-term average), modified from Gnyp (2014), Research Centre Jülich (2015), Uni Bonn (2010b), respectively.

3 Multitemporal crop surface models: accurate plant height measurement and biomass estimation with terrestrial laser scanning in paddy rice

NORA TILLY^{1,3,*}, DIRK HOFFMEISTER^{1,3}, QIANG CAO^{2,3}, SHANYU HUANG^{2,3}, VICTORIA LENZ-WIEDEMANN^{1,3}, YUXIN MIAO^{2,3}, GEORG BARETH^{1,3}

Published in: Journal of Applied Remote Sensing 2014, **8**, 083671-1 -22

DOI: 10.1117/1.JRS.8.083671

Formatting and orthography of the manuscript is adapted to the dissertation style.

¹ Institute of Geography (GIS & Remote Sensing Group), University of Cologne, 50923 Cologne, Germany

² Department of Plant Nutrition, China Agricultural University, 100193 Beijing, China

³ International Center for Agro-Informatics and Sustainable Development (ICASD), www.icasd.org

* Corresponding author: Tel.: +49 221 470 6265, Fax: +49 221 470 8838, Email: nora.tilly@uni-koeln.de

Abstract. Appropriate field management requires methods of measuring plant height with high precision, accuracy, and resolution. Studies show that terrestrial laser scanning (TLS) is suitable for capturing small objects like crops. In this contribution, the results of multi-temporal TLS surveys for monitoring plant height on paddy rice fields in China are presented. Three campaigns were carried out on a field experiment and on a farmer's conventionally managed field. The high density of measurement points allows to establish crop surface models (CSMs) with a resolution of 1 cm, which can be used for deriving plant heights. For both sites, strong correlations (each $R^2 = 0.91$) between TLS-derived and manually measured plant heights confirm the accuracy of the scan data. A biomass regression model was established based on the correlation between plant height and biomass samples from the field experiment ($R^2 = 0.86$). The transferability to the farmer's field was supported with a strong correlation between simulated and measured values ($R^2 = 0.90$). Independent biomass measurements were used for validating the temporal transferability. The study demonstrates the advantages of TLS for deriving plant height, which can be used for modeling biomass. Consequently, laser scanning methods are a promising tool for precision agriculture.

Nontechnical Research Summary. In general, efficiency of crop production is influenced by adequate field management during the growing period. This requires appropriate technical equipment, but even more, knowledge about the nutrient content of plants during cultivation is necessary. Key factors for management decisions are nitrogen content and biomass. Determination of the desired plant parameters and accurate estimation of the actual crop status are in the focus of research. While several non-destructive methods are introduced for monitoring nitrogen status in standing crops, the matter of determining biomass non-destructively is still not solved. Consequently, other plant parameters, like the plant height, are used for biomass estimations. The results of this study show that terrestrial laser scanning can be used for measuring plant height accurate and within-field resolution. Measurements on a field experiment were used for establishing a regression model for the

determination of biomass. The transferability to a larger scale and the temporal transferability were supported with independent measurements on a farmer's conventionally managed field. The developed methods can support the monitoring of paddy rice fields during the growing period for getting detailed spatially and temporally resolved information. Hence, the field management can be optimized for conserving natural and financial resources.

Keywords: terrestrial laser scanning; plant height; growth; biomass; rice; precision agriculture; crop monitoring; field level

3.1 Introduction

The cultivation of rice is increasingly important in consequence of its role as a staple food, in particular for the rapidly growing Asian population. In 2011, about 90 % of the estimated world rice production, about 650 million tons, was produced in Asia (FAO, 2014). Due to a further growing population with a constant or even decreasing cultivation area, a field management aiming at high production and sustainability of natural resources is required. Main goal is to close the gap between potential and current yield in developed and developing countries (van Wart et al., 2013). Therefore, in the context of precision agriculture, accurate crop monitoring should be based on remote and proximal sensing for improving the relation between inputs and outputs (Mulla, 2012).

Rice grain yield for example, is positively correlated to biomass and nitrogen (N) translocation efficiency (Ntanos and Koutroubas, 2002). However, the over-fertilization with N by farmers is a major problem for soil and groundwater. Hence, ways for enhancing the field management are necessary. Overviews about the actual situation and recent trends in China are given by Miao et al. (2011) and Roelcke et al. (2004).

Considering that the biomass production of crops can be described as a function of N content, an optimal fertilization requires the knowledge about the suitable N content of the plants as well as methods of determining the actual N content and the biomass (Devienne-Barret et al., 2000; Lemaire et al., 2005; Mistele and Schmidhalter, 2008). A widely used indicator for quantifying the actual status is the nitrogen nutrition index (NNI), as the ratio between measured and critical N content (Elia and Conversa, 2012; Greenwood et al., 1991; Lemaire et al., 2008). The critical N content is determined by the N dilution curve, which represents the relation between N concentration and biomass.

In order to estimate the values for the calculation of the NNI, the use of non-destructive remote sensing technologies is in the focus of research. Several studies exist using a chlorophyll meter (Huang et al., 2008; Peng et al., 1996), a hand-held spectro-radiometer (Stroppiana et al., 2009; Yi et al., 2007; Yu et al., 2013), or an airborne hyperspectral sensor (Ryu et al., 2011) for determining the N content of rice plants. Moreover, various approaches are presented for assessing the actual biomass. Spaceborne data is commonly used due to the usually wide areal extent of paddy rice fields (Koppe et al., 2012; Lopez-Sanchez et al., 2011; Ribbes and Le Toan, 1999). In addition, satellite remote sensing images enable the estimation of rice yield based on the calculation of vegetation indices (Li et al., 2011; Yang et al., 2011).

A higher spatial and temporal resolution is required for estimating the biomass more precisely and with within-field variability. Few works on the virtual modeling of rice plants in

a high resolution exist (Ding et al., 2011; Watanabe et al., 2005), but the complex plant structure and growing process cause uncertainties about the transferability to the field. Thus, in-situ measurements for biomass estimation are useful. In an early approach, the biomass of rice was predicted from reflectance data, measured with a hand-held radiometer (Casanova et al., 1998). Similar results are reported in Gnyp et al. (2013) and Aasen et al. (2014). In Yao et al. (2012), the authors used an active hand-held optical reflectance sensor for monitoring the rice canopy during the growing period and developed a precise N management strategy. Furthermore, the authors in Confalonieri et al. (2011) emphasized that rice plant height is a key factor for predicting yield potential and established a model for estimating the plant height increase, but methods for accurate in-situ determination are rare.

Besides hyperspectral and optical sensors, the technology of light detection and ranging (LiDAR) became increasingly important in a wide range of research fields, including the acquisition of vegetation parameters. Advantages of airborne and ground-based LiDAR remote sensing for ecosystem studies are highlighted in van Leeuwen et al. (2011) and Lefsky et al. (2002). Tremendous research is conducted in forestry applications (Henning and Radtke, 2006; Hosoi and Omasa, 2006; Hyyppä et al., 2008; Lovell et al., 2011; Omasa et al., 2007; Van der Zande et al., 2006). The main benefits are the fast and accurate data capturing, the high point density data, and therefore the highly realistic representation.

Several crops were already investigated with ground-based LiDAR approaches for various purposes, for example measuring height of perennial grass (Zhang and Grift, 2012) or biomass of grapevine (Keightley and Bawden, 2010), oilseed rape, winter rye, winter wheat, and grassland (Ehlert et al., 2009, 2008). Furthermore, estimating crop density (Hosoi and Omasa, 2009; Saeys et al., 2009), nitrogen status (Eitel et al., 2011), and leaf area index (Gebbers et al., 2011) of wheat, or detecting spatial and temporal changes of different sugar beet cultivars (Hoffmeister et al., 2012) are evaluated. Single plant detection is possible based on analysis of the measured intensity values (Hoffmeister et al., 2012; Höfle, 2014). In Hosoi and Omasa (2012), the authors examined the use of a portable scanner in combination with a mirror for assessing the vertical plant area density in a rice canopy and achieved good results. They used the density values for estimating the dry weight of plant organs (ears, leaves, and stems). As stated in Lumme et al. (2008), terrestrial laser scanning (TLS) is a promising method for estimating the biomass of small grain cereals like barley, oat, and wheat.

In this study, multi-temporal crop surface models (CSMs) were established for determining the plant height from TLS measurements on paddy rice fields at different growing stages. CSMs are introduced in Hoffmeister et al. (2010) for deriving spatial crop growth patterns on field level. Manual measurements were performed for validating the TLS measurements. In addition, the CSMs are used for estimating the actual crop biomass. Therefore, a regression model based on the findings from a field experiment was established. The model was used for estimating the biomass of rice plants on a farmer's field on the base of multi-temporal CSMs.

The presented research is part of the activities of the International Center for Agro-Informatics and Sustainable Development (ICASD). It was founded in 2009 as an open,

One half of the field experiment with a spatial extent of 60 m by 63 m was cultivated with the rice variety Kongyu 131, the other half with Longjing 21. The plants sprout in a greenhouse, were transplanted between the 17th and 20th of May, and harvested on the 20th of September 2011. Nine different treatments were repeated thrice for both rice varieties. Thus, the area was divided into 54 plots, each about 10 m by 7 m in size. As shown in **Table 3-1**, the treatments differ in the amount of applied N fertilizer during the growing period. The amount of fertilizer was predefined for five treatments, whereas the amount for treatment six to nine was adjusted based on in-season N content analysis. The content was approximated based on spectral reflectance measurements, performed with GreenSeeker™ (Ntech Industries, USA) and Crop Circle™ (Holland Scientific, USA) and the actual biomass, which was measured destructively several times within the vegetation period. A detailed description of the experiment design is given in Cao et al. (2013).

Table 3-1. Fertilizer application scheme for both study sites.

Treatment	Base N (kg/ha)	Topdressing 1 (kg/ha)	Topdressing 2 (kg/ha)	Topdressing 3 (kg/ha)	Total N (kg/ha)
Field experiment					
Date	06.05.11	30.05.11	09.-21.07.11	29.07.11	
1	0	0	0	0	0
2	28	14	19.6	8.4	70
3	40	20	28	12	100
4	52	26	36.4	15.6	130
5	64	32	44.8	19.2	160
6 - 8	40	20	N/A ^a	N/A ^a	N/A ^b
9	40 + 55 SCU ^c	0	N/A ^a	0	N/A ^b
Farmer's field					
Date	14.-16.04.11	29.05.11	09.06.11	08.07.11	
	40	12	18	30	100

^a Amount based on N content analysis; ^b Resulting from the calculated amount; ^c Sulphur-coated urea (slow release fertilizer)

3.2.1.2 Farmer's field

The aim of investigating a farmer's conventionally managed field was to provide an independent validation data set and check the transferability of the findings from the field experiment described above. For this purpose, a farmer's field with similar growing pattern but a considerably larger spatial extent of 300 m by 500 m was chosen. The plants also sprout in a greenhouse, were transplanted on the 17th and 18th of May, and harvested between the 25th of September and 10th of October 2011. Unfortunately, it was not possible to find any field with one of the rice varieties investigated at the Keyansuo experiment station, where the farmer would have allowed to enter the rice paddies and to take destructive samplings several times within the growing season. The field was cultivated with the rice variety Kenjiandao 6. The dates of fertilization differ from the field experiment (**Table 3-1**).

3.2.2 TLS measurements

The chosen survey period of late June to July captures the key vegetative stage of the rice plants, when the stem elongation process takes place. Remarkable differences in plant development occur due to the increase of tillers and plant height during this stage. For the monitoring approach, three campaigns were carried out on both fields, which were each time conducted on two consecutive days. The campaign dates are given in **Table 3-2**.

Table 3-2. Dates of the scan campaigns and corresponding phenological stages.

Date	Field	Variety	BBCH-scale ^a
21.06.11	Experiment	Kongyu 131	13
		Longjing 21	13
22.06.11	Farmer's	Kenjiandao 6	13
04.07.11	Experiment	Kongyu 131	13 - 15; 22 - 23
		Longjing 21	13 - 15; 22 - 23
05.07.11	Farmer's	Kenjiandao 6	13;21
18.07.11	Experiment	Kongyu 131	19; 29; 32
		Longjing 21	19; 29; 32
19.07.11	Farmer's	Kenjiandao 6	19; 29; 34

^a multiple values due to several samples

For all field campaigns the terrestrial laser scanner Riegl VZ-1000 (Riegl LMS GmbH, 2013), provided by Five Star Electronic Technologies, located in Beijing, was used. The scanner operates with the time-of-flight technique, where the time between transmitting and receiving a pulsed laser signal is measured. The time is used for calculating the distance between sensor and target. Parallel scan lines are achieved with a rotating multi-facet polygon mirror and the rotation of the scanners head itself, which implies a wide field of view, up to 100° in vertical and 360° in horizontal direction. The infrared laser beam has a high precision of 5 mm and an accuracy of 8 mm. Apart from a measurement rate of up to 122,000 points/sec, long range distance measurements of up to 1,400 m are possible. In addition, the system is capable of an online full-waveform analysis and according echo digitization.

Additionally, a digital camera, Nikon D700, was mounted on the laser scanner. From the recorded RGB photos the point clouds gained from the laser scanner can be colorized, resulting in 3D RGB point clouds and the corresponding surfaces can be textured. The camera was connected via USB interface to the scanner for adjusting the camera settings and ensuring an accurate alignment between the devices. During the acquisition, the whole system was remotely controlled with the RiSCAN Pro Software on a notebook, linked via a LAN connection.

During the campaigns at the field experiment, the scanner was fixed on a tripod which raised the sensor up to 1.5 m above ground. Where possible, a small trailer behind a tractor was used for achieving a greater height of about 3 m (**Figure 3-2**). The study area was scanned from nine scan positions for capturing all fields of the Keyansuo experiment station and minimizing shadowing effects. Although the data from all positions was used for the analysis, four of them were of major importance, as they were located closely to the investigated



Figure 3-2. Overview of the investigated field experiment from scan position six (Figure 3-3). On the right side the scanner with the tripod mounted on the small trailer can be seen (taken: 04.07.11).

N field experiment. Two positions were accomplished without the trailer at the north edge and two positions with the trailer at the south edge of the field. The whole setting is shown in **Figure 3-3**.

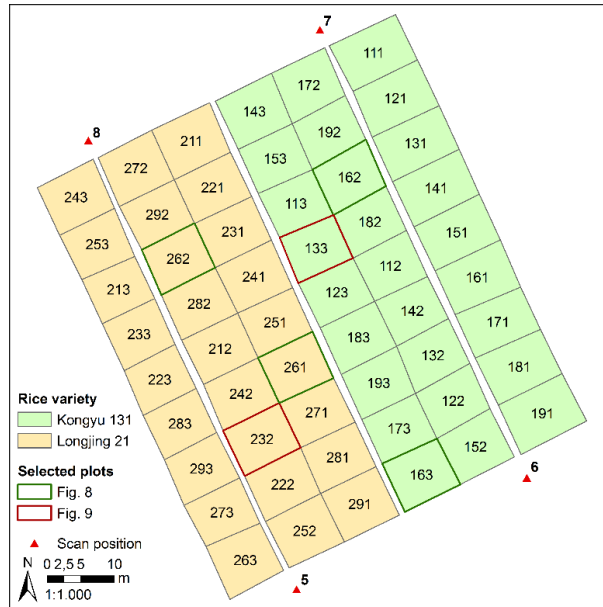


Figure 3-3. Experimental design and scan positions of the field experiment. Number in the plot represents: rice variety (1 = Kongyu 131; 2 = Longjing 21); treatment (1 - 9 in Table 3-1); repetition (1 - 3).

On the farmer's field (**Figure 3-4**) the scanner was also mounted on the tripod. Accordingly, the sensor height was about 1.5 m above ground. Due to a limited access on the small dikes between the plots, it was impossible to use a trailer or to reach any lifted position. The field was scanned from seven scan positions. For this study, the whole field is divided in the overall field and two intensively investigated units (W and E in **Figure 3-4**). In order to get a high

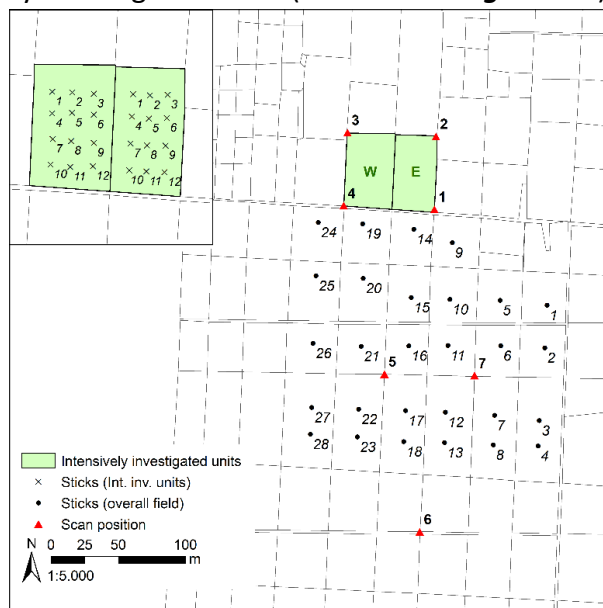


Figure 3-4. Experimental design and scan positions of the farmer's field.

resolution for the latter ones, four scan positions were placed at their corners. Twelve thin, long bamboo sticks per unit were stuck in the ground, placed in an equally spaced grid, which can be detected in the point clouds and located in the field to ensure the spatial linkage to other plant parameter measurements. An additional grid with 28 measurement points represented by bamboo sticks was placed in the overall field.

Common tie points in all scans of each site are required to enable the merging of all scan positions in the post-processing. Therefore, high-reflective cylinders, which can be easily detected by the laser scanner, were fixed on ranging poles built upon the dikes between the fields (Hoffmeister et al., 2010). The reflectors had to be detected from all scan positions for computing the spatial relation between all positions of the scanner and the cylinders. In the first TLS campaigns, the position of each pole was marked in the fields. All scans of each date from a respective field can be merged together by re-establishing the ranging poles for the other campaigns.

3.2.3 Manual measurements

During the whole vegetation period, manual measurements were performed at both sites for monitoring the development of the rice plants. The phenological stage of the plants and more precisely, the steps in the plant development are defined here by the BBCH scale (Meier, 2001). The abbreviation BBCH was derived from Biologische Bundesanstalt (German Federal Biological Research Centre for Agriculture and Forestry), Bundessortenamt (German Federal Office of Plant Varieties), and Chemical industry, who funded the development of the scale. For both sites, the BBCH-values at the campaign dates are given in **Table 3-2**. The similar values confirm the comparable phenological development of the rice plants on the field experiment and the farmer's field.

Corresponding to each TLS campaign, plant heights were manually measured. On the field experiment, eight to ten hills per plot were regarded. Each hill consists of four to six rice plants (Cao et al., 2013). In both intensively investigated units of the farmer's field, the heights of four hills around each bamboo stick were measured.

As mentioned above, destructive biomass sampling was performed several times during the vegetation period at the field experiment. Samples were taken from both varieties for the respective three repetitions of treatment one to five ($n = 30$). Due to the small plot size, it was not feasible to take additional samples corresponding to the TLS campaigns. As the dates of sampling differ from the TLS campaign dates, the biomass values were linear interpolated.

On the farmer's field, the four hills around each bamboo stick in the two intensively investigated units were destructively taken after the TLS measurements for measuring the biomass ($n = 24$). After each campaign, the grid of bamboo sticks was moved for having an undisturbed area around the bamboo sticks for the following campaign. Furthermore, in the overall field destructive samplings were taken around the mentioned 28 bamboo sticks on the 26th of June, as an additional independent validation data set (**Figure 3-4**). For all samplings, the cleaned above ground biomass was dried in a compartment dryer and weighed after dehydrating. The average dry biomass per m^2 was calculated, considering the number of hills per m^2 , which was counted in the field corresponding to each sampling.

3.2.4 TLS data processing

The general workflow for the post-processing of the TLS data is shown in **Figure 3-5**. It consists of the (1) registration and merging of all point clouds, (2) filtering and extraction of the area of interest (AOI), (3) spatial, and (4) statistical analyses, considering the manual measurements.

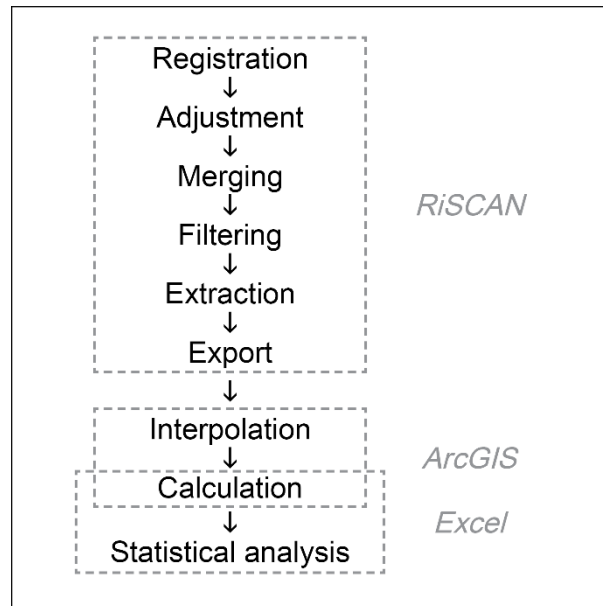


Figure 3-5. General overview of the workflow for the post-processing of the TLS data.

The first steps (1 and 2) were carried out directly in Riegli's software RiSCAN Pro, which was already used for the data acquisition. First of all, the scans from the respective three campaigns were imported into one RiSCAN Pro project. The registration of the scan positions was executed with an indirect registration method, based on the above mentioned high-reflective cylinders acting as tie points. With an automatic algorithm, corresponding tie points between the scan positions can be found. After the registration, the datasets still showed alignment errors, due to non-optimal reflector positioning, imprecise re-establishing of the ranging poles, or instabilities during the measurements. A further adjustment was applied to minimize these errors. RiSCAN Pro offers the Multi Station Adjustment, which is based on the iterative closest point (ICP) algorithm (Besl and McKay, 1992). The position and orientation of each scan position were modified in multiple iterations for getting the best fitting result for all of them.

The point clouds still contained noise, caused by reflections on water in the field or on small particles in the air. Thus, a further filtering based on the reflectance, measured for each point during the data acquisition, was performed. Points under a certain reflectance value, regarded as noise, were removed. As the reflectance value depends on the distance from the sensor to the field as well as other factors, the critical value was slightly different for each scan.

Subsequently, all point clouds of each respective date were merged to one dataset and the AOI was manually extracted. For an easier orientation and the distinction between field and dikes, the point clouds were previously colored from the recorded pictures. The AOI was further separated for each date and plot to have a common spatial base. A filtering scheme

was used for selecting the maximum points and determining the crop surface. Finally, those filtered point clouds were exported as ASCII files for spatial and statistical analyses.

3.2.5 Spatial analysis

ArcGIS Desktop 10 by Esri was used for constructing the crop surface models (CSMs) and following spatial analyses. The exported ASCII files were converted to vector point data and interpolated with the inverse distance weighting (IDW) algorithm for receiving a raster, representing a digital surface model (DSM) with a consistent spatial resolution of 1 cm. IDW is a deterministic, exact interpolation method and retains a measured value at its sample location (Johnston et al., 2001). Hence, the method is suitable for preserving the accuracy of measurements with a high density, like the TLS point clouds.

A common reference surface is required for the calculation of the plant heights. Usually a high-accurate digital elevation model (DEM) is used; achievable from scanning the AOI without any vegetation (Hoffmeister et al., 2010). Since it was not possible to obtain such data in this study, another method was applied: the lowest parts in the point clouds from the first date, accordingly containing the least dense vegetation, were manually selected for interpolating a DEM surface representing the real ground. As it can be seen in **Figure 3-6**, the rice plants were small enough for clearly identifying points on the ground and the water height in the irrigated field was less than 4 cm at this stage. Hence, enough ground points at the edges and around the hills remained for interpolating a DEM.



Figure 3-6. Corner of the field experiment, showing the least dense vegetation (taken: 21.06.11).

Finally, the CSMs, introduced in (Hoffmeister et al., 2010) for plant growth monitoring at field level, were established for each date. The application of CSMs is presented in Hoffmeister et al. (2013). A CSM represents the crop surface with high spatial resolution at one campaign date, gained from the merged and filtered point cloud. As shown in **Figure 3-7** (Bendig et al., 2013), CSMs are used for determining the actual plant height for a given growing stage. Therefore, the DEM from the first acquisition date, representing the ground, is subtracted from the CSM, representing the crop surface. The result is the plant height above ground with the same spatial resolution as the CSMs, which is visualized in maps of plant height. By subtracting a CSM of an earlier date from a CSM of a later date, the plant growth

between the dates can be spatially measured, e.g. CSM_2 minus CSM_1 in **Figure 3-7**. The spatial patterns of the plant growth are visualized in maps of plant growth. In the following, plant growth is always defined as the spatio-temporal difference in height.

Multi-temporal Crop Surface Models

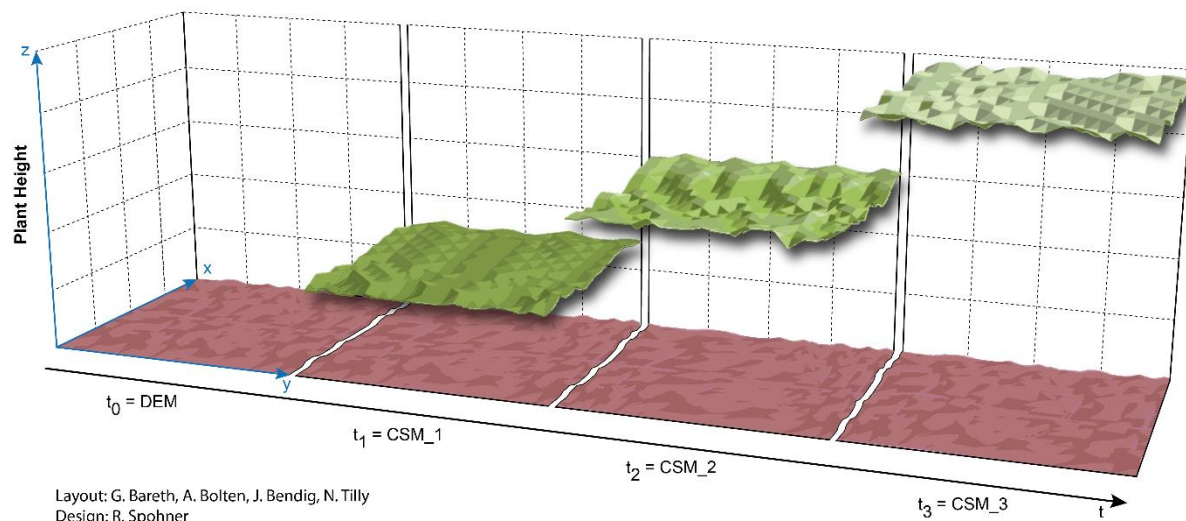


Figure 3-7. General concept of crop surface models (CSMs) (Bendig et al., 2013).

3.2.6 Statistical analysis

The statistical analyses were performed in Microsoft Excel 2010. For a better visualization, diagrams were plotted in OriginPro 8.5 by OriginLab. The plant height values, calculated pixel-wise for the CSMs, were averaged for each plot of the field experiment and each circular buffer area with a radius of 1 m around the bamboo sticks for the farmer's field, respectively. The plots of the field experiment were previously clipped with an inner buffer of 60 cm for preventing border effects. Additionally, the manually measured heights were averaged for each plot ($n = 54$) or area around the bamboo sticks ($n = 24$). These values were compared with the mean plant heights derived from the CSMs of the same respective spatial feature for evaluating and validating the laser scanning results.

3.2.7 Biomass regression model

As mentioned before, the problem of the non-destructive estimation of crop biomass on field level is not solved yet, while indirect approaches successfully used plant height as predictor. In order to investigate the correlation between plant height and biomass of rice plants, a regression model was derived from the results of the field experiment. The transferability of the model to the farmer's conventionally managed field was validated by comparing the simulated and measured biomass. As mentioned, different rice varieties were cultivated on both test sites. The two rice varieties from the field experiment were combined in the regression model to ensure an adequate number of measured values ($n = 90$) and attain a reasonable mean value for the transfer to the farmer's field. The combination of the different treatments covers the influence of the varying amount of used fertilizer. Previously, three test models were established for testing the general concept. For each test model the regression equation from two repetitions of the field experiment were used for simulating the biomass of the third repetition.

The workflow can be structured in five steps:

- VII. Generation of the test models, considering only the field experiment
- VIII. Evaluation of the correlation between all CSM-derived plant height and destructive biomass sampling for the field experiment and derivation of the regression model
- IX. Application of the regression model for simulating the biomass on the farmer's field based on the CSM-derived plant height
- X. Evaluation of the simulated and destructively measured biomass of the farmer's field
- XI. Validation of the regression model using the additional independent measurements of biomass of the overall farmer's field

3.3 Results

3.3.1 Spatial analysis

After the described data processing of the captured TLS point clouds, the CSMs for each date and both sites were generated and the plant heights were calculated pixel-wise. Thus, the following spatial and temporal patterns and variations within one CSM and between different CSMs can be obtained. As an example, **Figure 3-8** shows twelve maps of plant height

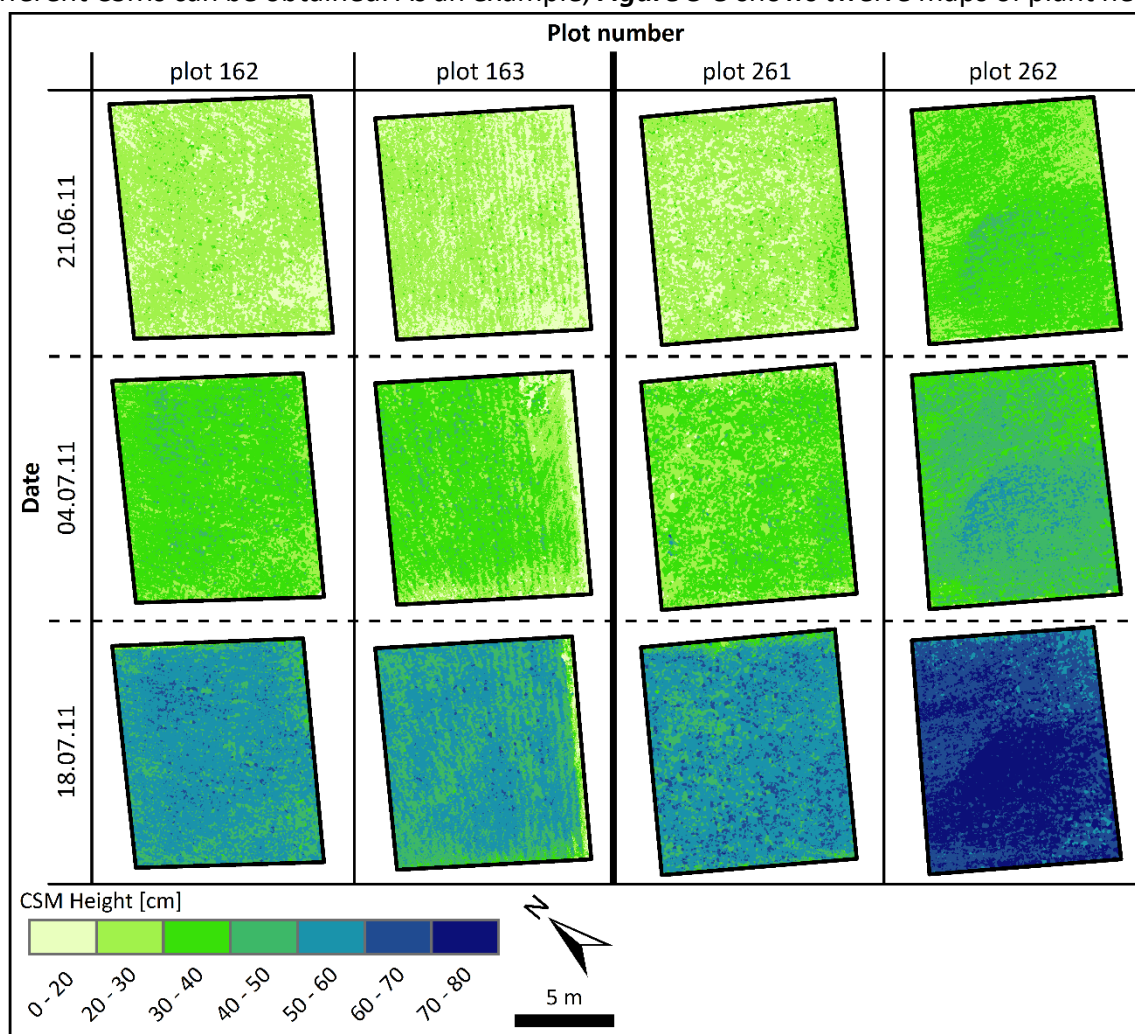


Figure 3-8. CSM-derived maps of plant height for four selected plots of the field experiment (left: Kongyu 131; right: Longjing 21, marked in Figure 3-3).

derived from the CSMs. For all three TLS campaign dates, the maps of two repetitions of the same fertilizer treatment for Kongyu 131 (plot 162 and 163) and Longjing 21 (plot 261 and 262) are shown. All field experiment plots and the whole farmer's field are represented in the way it is shown in **Figure 3-8**.

The linear structure of the rice plant rows within the plots is detectable at the first campaign but disappears later due to plant development. Regarding the field experiment, slight differences between the rice varieties can be identified. The latter difference is captured by examining the mean plant height per plot, which shows higher values for Longjing 21. The averaged difference between the varieties increases over time (4 cm, 5 cm, and 10 cm). In addition, the plant growth is observable, which is determined as height difference between consecutive CSMs and visualized as maps of plant growth. In **Figure 3-9** maps of Kongyu 131 (plot 133) and Longjing 21 (plot 232) for both time intervals are shown as an example. In both intervals, the growth patterns are almost homogeneous within the plots for both varieties. According to the increasing height difference between the varieties over time, the growth values are higher for Longjing 21.

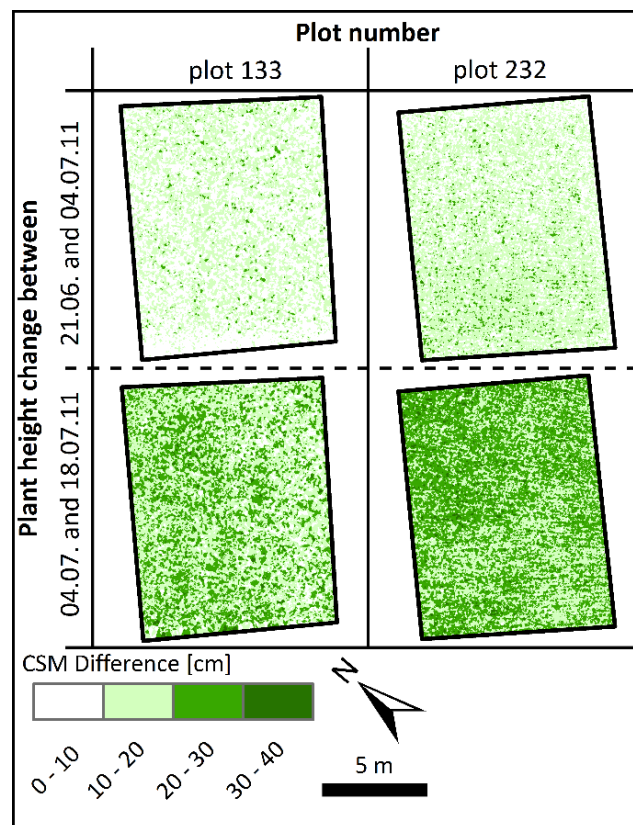


Figure 3-9. Maps of plant growth for two selected plots of the field experiment, derived from the difference between two consecutive CSMs (left: Kongyu 131; right: Longjing 21, marked in Figure 3-3).

The mean plant heights calculated from the CSMs were validated against the averaged manually measured plant heights for each plot or area around the bamboo sticks for verifying the results. **Figure 3-10** shows the difference between these values for the first campaign on the field experiment. The variance is quite small. About 40 % of the plots show a difference of less than 2 cm, further 45 % differ by 2 to 5 cm, and just 15 % show a higher error, reaching

the maximum at about 10 cm. The mean difference between all CSM-derived and manually measured plant heights is about 3 cm for the plots of the field experiment and about 9 cm for the buffer areas around the bamboo sticks of the intensively investigated units of the farmer's field, each with a standard deviation of about 5 cm.

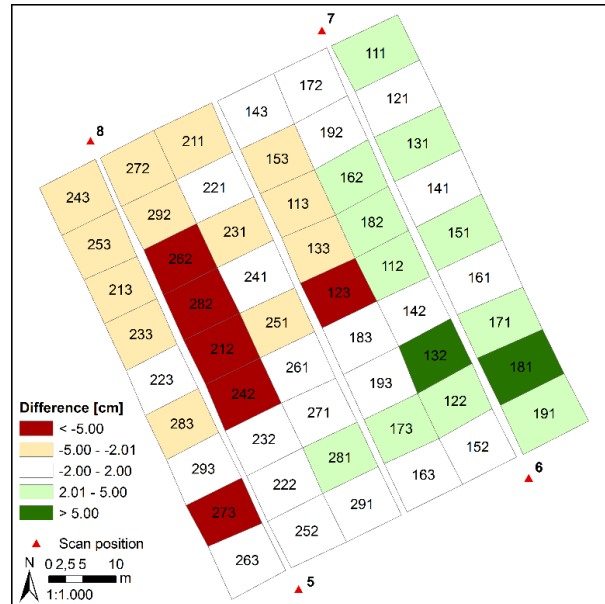


Figure 3-10. Difference between the averaged manually measured plant heights and the CSM-derived mean plant heights for each plot for the first campaign of the field experiment.

3.3.2 Statistical analysis

The CSM-derived and the manually measured plant heights, averaged for each plot or buffer area, were used for executing correlation and regression analyses. Common statistical values are shown in **Table 3-3**. For each campaign and both sites the mean heights are quite similar. The differences between the mean CSM-derived and manually measured plant heights are about 3 cm for the field experiment and 9 cm for the farmer's field. The standard deviation within each campaign is about 5 cm for both sites. All minimum values are lower for the CSM-derived mean plant heights, whereas the maximum values are more similar. All values and the resulting regression lines for both fields are shown in **Figure 3-11**. The correlation coefficients are very high for each field (both $R^2 = 0.91$).

Table 3-3. Mean CSM-derived and manually measured plant heights for both fields.

Date	n	Plant height from CSM (cm)				Measured plant height (cm)			
		\bar{x}	s	min	max	\bar{x}	s	min	max
Field experiment									
21.06.11	54	24.84	3.63	17.90	32.99	24.37	2.06	19.13	28.88
04.07.11	54	34.62	4.36	24.59	42.71	37.94	2.42	32.38	44.13
18.07.11	54	55.38	7.22	44.28	70.30	63.56	4.25	53.10	70.70
Farmer's field									
22.06.11	24	20.80	4.82	13.39	31.44	29.18	2.87	23.25	37.00
05.07.11	24	34.09	4.52	27.13	44.60	40.62	1.93	38.25	43.75
19.07.11	24	59.49	4.87	51.79	72.58	71.64	2.63	67.50	76.50

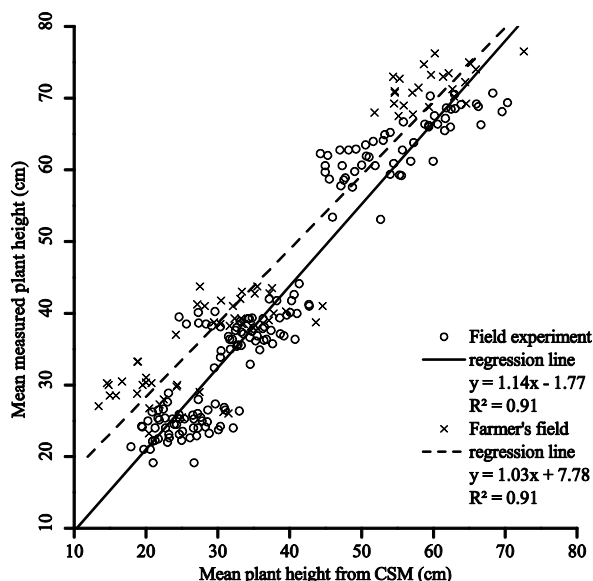


Figure 3-11. Regression of the mean CSM-derived and manually measured plant heights for the field experiment ($n = 162$) and the intensively investigated units on the farmer's field ($n = 72$).

3.3.3 Biomass regression model

As mentioned before, for destructive biomass sampling on the field experiment only treatments one to five were considered, with the main different levels of N fertilization. Hence, the number of samples and accordingly the averaged plant height values, differ from the comparison of the height measurement methods (**Table 3-3**). In the intensively investigated units of the farmer's field biomass was taken around all bamboo sticks. For each campaign the mean value, standard deviation, minimum, and maximum were calculated for the plant height and dry biomass (**Table 3-4**). The mean plant heights of each campaign are similar for the field experiment and the farmer's field, with a difference of less than 5 cm. In contrast, the averaged dry biomass values of the field experiment are 20 to 30 % lower than the values of the farmer's field at the second and third campaign.

Table 3-4. Mean CSM-derived plant heights and biomass values.

Date	n	Plant height from CSM (cm)				Dry biomass (g/m ²) ^a			
		\bar{X}	s	min	max	\bar{X}	s	min	max
Field experiment									
21.06.11	30	24.93	2.85	20.59	30.33	59.51	18.86	24.04	100.70
04.07.11	30	33.80	3.74	27.25	40.75	131.72	30.03	66.71	199.41
18.07.11	30	56.69	5.49	44.91	63.03	422.27	80.90	274.74	599.53
Farmer's field									
22.06.11	24	20.80	4.82	13.39	31.44	57.58	13.02	25.64	80.01
05.07.11	24	34.09	4.52	27.13	44.60	217.43	29.44	146.54	278.12
19.07.11	24	59.49	4.87	51.79	72.58	589.71	73.01	482.33	723.32

^a values for the field experiment are interpolated

The general concept of the biomass regression model was validated with three test models. Therefore, the regression equation achieved from two repetitions of the field experiment was used for calculating the biomass of the respective third repetition. The mean deviations of the simulated values from the actual measured values are 3 %, 16 %, and 19 %.

Considering now both fields, the relation between mean plant height and dry biomass is visualized in a scatterplot (**Figure 3-12**). The lower biomass values of the field experiment are also visible, but the linear correlation is similar for both sites. The regression equation from the field experiment ($y = 11.06x - 224.18$) was used for deriving the biomass regression model. Following, the biomass on the intensively investigated units of the farmer's field was estimated with the model, based on the CSM-derived plant heights. **Figure 3-13** shows the simulated biomass, with once the standard deviation calculated for each campaign, and the actual measured values. The reliability of the established model is supported by the strong correlation between simulated and measured values ($R^2 = 0.90$). The mean difference between the values is 90 g/m^2 (about $\frac{1}{4}$ of the mean measured dry biomass), with a standard deviation of 80 g/m^2 .

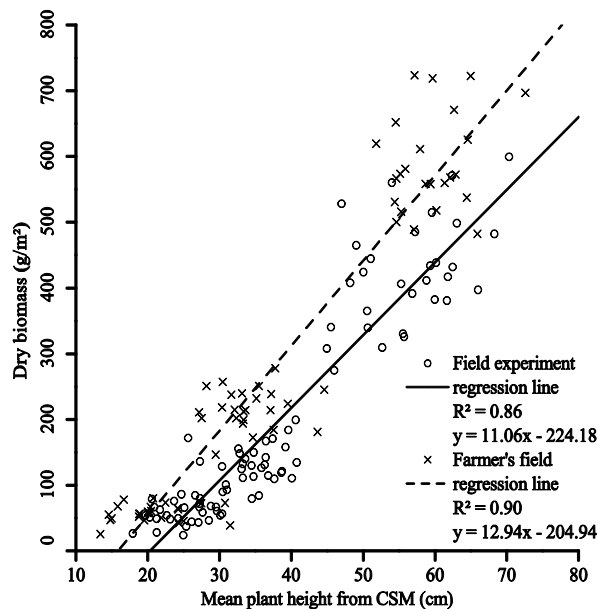


Figure 3-12. Regression of the mean CSM-derived plant height and dry biomass for the field experiment ($n = 90$) and the intensively investigated units on the farmer's field ($n = 72$).

The regression model was validated and the transferability to any point in time within the observation period was checked with the biomass measurements on the overall farmer's field. As the increase in plant height over time is almost linear in the observation period, a linear function achieved from all CSM-derived plant height values was used for interpolating the plant heights for the 26th of June. The theoretical biomass was estimated with the regression model and compared to the measured values. **Table 3-5** gives the basic statistics for the simulated and measured biomass values. The mean difference between both values is 15 g/m^2 (about 20 % of the mean measured dry biomass), with a standard deviation of 36 g/m^2 .

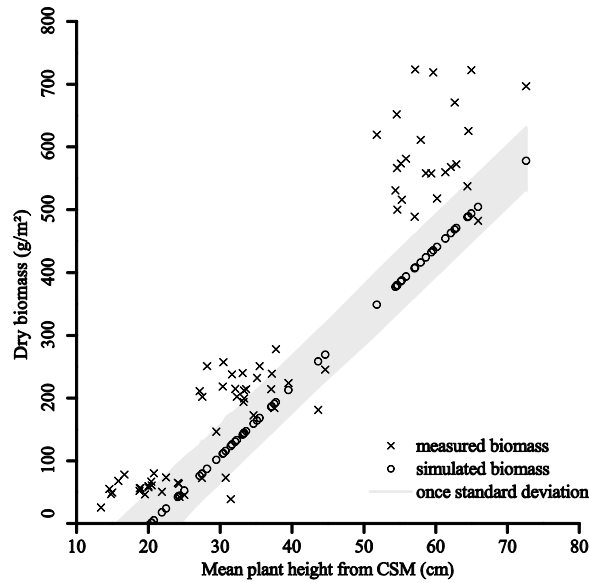


Figure 3-13. Theoretical biomass simulated with regression model and the measured values for the intensively investigated units on the farmer's field (each: $n = 72$).

Table 3-5 Biomass values for the overall farmer's field.

	n	Dry biomass (g/m ²)			
		\bar{X}	s	min	max
Simulated values	28	64.25	30.51	16.04	128.68
Measured values	28	79.32	15.91	50.02	113.23
Difference between related samples	28	15.07	36.36	0.50	84.88

3.4 Discussion

Generally, the data acquisition with the laser scanner in the field worked very well. The lightweight build-up of the Riegl VZ-1000 is quite helpful. Nevertheless, problems occur from noise in the point clouds, due to wind, rain, insects, or small particles in the air, reflections on water, and other effects. These issues for TLS applications in agriculture are also reported in Ehlert et al. (2009) and Lumme et al. (2008). The time-of-flight scanner, used in this study, reduces the noise already by the high measuring speed. Further improvements are possible with the software filter options in RiSCAN Pro. Earlier studies with a comparable setup (Hoffmeister et al., 2010) already showed the usability of this method, but further improvement is still desirable. Approaches for automatic corrections of internal errors focus on systematic error models and self-calibration methods (Lichti, 2010).

Further possibilities are the investigation of intensity values, which can be used for establishing a filtering scheme of separating laser returns on canopy from ground returns (Guarnieri et al., 2009) or for detecting single plants (Hoffmeister et al., 2012; Höfle, 2014), as already stated. In addition, the application of full-waveform analysis for identifying vegetation in point clouds is commonly known from ALS (Hyypä et al., 2008; Wagner et al., 2008). New TLS systems are also capable for retrieving the full-waveform of the reflected signal and their role for detection of vegetation gets increasingly important (Elseberg et al., 2011; Guarnieri et al., 2012).

A major advantage of the terrestrial laser scanner is the easily achievable and fast data acquisition of a whole field. Besides that, a higher spatial resolution and higher point density than achievable with airborne laser scanning (ALS) (McKinion et al., 2010) is reachable, which enables an accurate differentiation between the plots and allows the identification of small objects, like the bamboo sticks used on the farmer's field. Nevertheless, the approach leaves room for improvement, for example enhancing the evenness of the point cloud distribution. Recent developments in mobile laser scanning (MLS) brought up promising solutions (Kukko et al., 2012a). In general, MLS comprises all measurement systems with two-dimensional profiling scanners, attached to a moving ground vehicle for achieving an areal coverage. This method was already used in several studies for crop monitoring and detection purposes (Andújar et al., 2013; Ehlert et al., 2008; Gebbers et al., 2011; Kukko et al., 2012a). For the limited access on the small dikes of the paddy rice fields, the new Akhka MLS system (Kukko et al., 2012b), where the laser scanner is attached to a backpack, has promising potential.

In the literature (Ehlert and Heisig, 2013) the problem of overestimating the height of reflection points depending on the scanning angles is examined. In this study, the point clouds of all scan positions from one campaign date were merged for achieving an evenly distributed coverage of the field and a scheme for filtering the maximum points was used for detecting the crop surface. However, referring to Ehlert and Heisig (2013), the influence of the scanning angles has to be taken into account for further studies, in particular for MLS systems.

One source of error for validating the CSM measurements with the manual measurements, are the height variances within the observed spatial unit. Considering the manual measurements such within-field variations are already detectable. As mentioned, on the field experiment the heights of eight to ten hills per plot were measured. The mean standard deviations within those measurements are already 4 cm, 4.5 cm, and 5.5 cm for the respective three campaigns. Regarding the CSM-derived plant heights, many more measuring points exist, with one height value for each pixel. Hence, the whole area of the plot is captured, including lower parts. With respect to those within-field variations and differences between the measuring techniques the mean difference of 3 cm between averaged CSM-derived and manually measured plant heights is reasonable (**Table 3-3**). Considering **Figure 3-10** the few samples (15 %) with differences between 5 and 10 cm can probably be related to these uncertainties and variations. Moreover, for the first campaign a difference between the rice varieties on the field experiment might be detectable. While for Kongyu 131 mostly the manually measured plant heights are higher than the CSM-derived values (positive difference), contrasting patterns, resulting in negative differences, are observable for Longjing 21. However, those tendencies are not observable for the other campaigns.

Regarding the farmer's field similar patterns are clearly visible. In the intensively investigated units only the heights of four hills around each bamboo stick were manually measured, which assumably leads to the lower standard deviation (3 cm, 2.5 cm, and 4 cm for the three campaigns). However, the difference between the averaged manual measurements and CSM-derived plant heights is larger (9 cm), as the manual measurements covered only small parts of the area, mostly representing the highest parts of the crop surface. In contrast,

the scanner captures the whole area, including lower parts, resulting in a high number of measuring points. Thus, the mean values of the pixel-wise stored CSM-derived plant heights per circular buffer area are lower, which explains the overall lower minimum values for the CSM-derived plant heights (**Table 3-3**).

In summary, the manual measurements with strong correlations to the averaged CSM-derived values validate the accuracy of the TLS results. Due to the very different numbers of samplings per plot, only averaged values can be compared. As mentioned, the heights of less than ten hills per each spatial unit were manually measured. In contrast, the resolution of 1 cm of the CSMs results in a huge number of measuring points for each spatial unit (about 500,000 points for each plot and 30,000 point for each buffer area on the field experiment and farmer's field, respectively). Through this high resolution also smaller hills and lower parts of the plants are captured, which decreases the minimum values and increases the standard deviation (**Table 3-3**). Nevertheless, the comparable mean values of the measurement methods, with deviations of 2 to 15 % for the field experiment and 15 to 30 % for the farmer's field, lead to regressions with high correlation coefficients (**Figure 3-11**). The much higher spatial resolution and the acquisition of the whole area are the main benefits of the TLS approach and required for accurate crop monitoring in the context of precision agriculture. However, the precision of the CSMs can hardly be validated with the manual measurements. Other studies show that TLS measurements are supposed to be precise (Höfle, 2014; Keightley and Bawden, 2010; Lumme et al., 2008). The high accuracy and precision of the Riegl VZ-1000 is validated with performance test by the manufacturer (Riegl LMS GmbH, 2013). Moreover, the TLS approach immensely reduces the human error factor, which cannot be neglected for the manual measurements.

Although the TLS data acquisition worked well, some uncertainties remain. Due to the field management and construction, it was not possible to obtain a DEM from the AOI without any vegetation and water. Thus, the DEM had to be estimated from the point clouds of the respective first campaigns, containing already small plants. The low water height in the field of about 4 cm and the remaining ground at the edges and around the hills enabled this approach. Nevertheless, the high correlation coefficients and small differences between the CSM-derived and the manually measured plant heights justify this assumption.

For paddy rice fields, border effects have to be regarded, resulting in differences between internal and external rice plants in a plot (Wang et al., 2013). The executed application of a buffer, to cut off the outmost rows, is suitable for avoiding border effects. However, uncertainties still remain, for example about the appropriate size. The compiled CSMs show the applicability of the presented method of calculating crop heights in rice fields with a high spatial resolution (up to 1 cm, **Figure 3-8**) and accuracy. In contrast, spaceborne data, which is commonly used for rice field mapping reaches a spatial resolution not higher than 1 m (Koppe et al., 2012; Lopez-Sanchez et al., 2011; Ribbes and Le Toan, 1999). The results demonstrate the potential of TLS for accurate in-situ measurement on paddy rice fields, which could also be a validation for spaceborne remote sensing data. Furthermore, the transferability of virtual modeled rice plants to field level can be validated (Ding et al., 2011; Watanabe et al., 2005).

Reconsidering the model presented in Confalonieri et al. (2011), the CSM-derived plant heights can be used for predicting yield potential for rice. In this context, the mentioned influence of border effects is a general problem for estimating rice yield (Wang et al., 2013). The very high resolution of the TLS-derived CSMs might be useful for quantifying this effect and estimate differences between internal and external rows.

The strong correlation between plant height and biomass ($R^2 = 0.86$) enabled the derivation of the regression model for estimating the actual biomass of rice plants. Strong correlations between plant height and biomass were also reported in Ehlert et al. (2009) for different crops. The transferability of the established model to a larger-scale farmer's field was demonstrated. Differences between the theoretical biomass, simulated with the regression model and the actual measured values can be related to the mentioned differences between the investigated fields. The BBCH-values (**Table 3-2**) show that all varieties were almost in the same phenological stage, but differences in plant height and biomass are measurable. The biomass values of the field experiment are up to a third smaller than the values of the farmer's field (**Table 3-4**). Hence, the simulated values differ from the measured values with a mean difference of about 25 % of the mean measured dry biomass. Regarding the general concept of the biomass regression model, better simulations were possible with the established test models, where only the rice varieties on the field experiment were used. As mentioned, the mean differences between the simulated and measured values are 3 %, 16 %, and 19 %. Further investigations are required, regarding the differences and whether they are caused by the different rice varieties or fertilizer treatments. Other influencing factors might be different soil conditions or lower human impact and larger plot size on the farmer's field. In (Hosoi and Omasa, 2012), the authors achieved good results for estimating biomass of rice plants based on the vertical plant area density, measured with a portable scanner in combination with a mirror. However, the setup might be less practical for the application on larger-scale fields.

The estimated biomass values may be used for improving NNI calculations and N management strategies (Yao et al., 2012), as the actual biomass is a key factor for the evaluation of the field status and management decisions. Hence, the claimed improvement of the relation between input and output (Mulla, 2012) can be realized to reduce over-fertilization and shrink the gap between potential and current yield.

Accurate captured rice fields can also be used for modeling purposes. In My Phung et al. (2013), a model is presented for rating damages from rice field rats and corresponding yield losses. The extent of damages was assumed, based on the experiences of the involved farmers. Damages can also be caused by other sources like storms, rain, or plant diseases. Measurements with TLS could be more accurate for predicting the damaged biomass. Furthermore, crop simulation models can be used for estimating the potential and current yield (van Wart et al., 2013). Therefore, the CSM-derived height and estimated biomass values can be used as model input or validation data.

For the presented approach, the improvement of the temporal interpolation method for the plant height values to any point in time is desirable. In this study, the CSM-derived mean plant heights were interpolated. Better results might be reached with a pixel-wise raster

interpolation and subsequent averaging of the interpolated pixel values for estimating the mean plant height for a given day in the investigation period.

3.5 Conclusion

The presented method of producing multi-temporal CSMs based on TLS measurements is applicable for non-destructive capturing and monitoring of rice growth. The very high spatial resolution and accuracy of the point clouds are the most outstanding features of TLS. Regarding the varying performance of plant growth on the field experiment, further studies might focus on the different rice varieties and fertilizer treatments. Therefore, similar data sets of the same field experiment of consecutive years should be considered.

The Riegl VZ-1000 is comparatively expensive. However, for this study a TLS system, known for high precision and accuracy, was required to avoid system-based errors. Recent developments brought up cost-effective system, like the Velodyne HDL-64E LiDAR sensor (Velodyne, 2014). Such systems should be regarded for realizing the practical implementation and application for farmers. Further, more cost-effective approaches are conceivable with MLS systems like the ibeo ALASCA XT (Ehlert and Heisig, 2013).

In the context of precision agriculture, biomass is a key factor for management decisions. As mentioned, to this day, it is impossible to directly measure actual crop biomass non-destructively. Hence, remote and proximal sensing measurements for estimating actual values in-season are required. The results show the strong correlation between plant height and biomass ($R^2 = 0.86$; $R^2 = 0.90$) for the analyzed time of the growing period. The transferability of the established biomass regression model based on plant height measurements from a small-scale field experiment to a larger-scale farmer's conventionally managed field was supported. Differences between the two sites, e.g. rice varieties, plot size, and fertilizer treatment lead to differences between the simulated and measured values, but the strong correlation ($R^2 = 0.90$) demonstrates the coherence of the results. Furthermore, the independent biomass dataset from the overall field was used for validating the temporal transferability. In further studies, the transferability to other farmers' conventionally managed fields has to be checked. The accuracy of the simulated biomass shows the suitability of the established model and reveals the presented method as a promising approach for the non-destructive in-season estimation of biomass within-field resolution in paddy rice.

Acknowledgment

This work was financially supported by the International Bureau of the German Federal Ministry of Education and Research (BMBF, project number 01DO12013) and the German Research Foundation (DFG, project number BA 2062/8-1). We gratefully thank the Qixing Research and Development Centre, the Jiansanjiang Agricultural Research Station (both located in Heilongjiang Province, China) and Five Star Electronic Technologies (Beijing, China) for good cooperation. Furthermore, we like to thank Riegl LMS GmbH (Horn, Austria) for continuous support. We thank the anonymous reviewers for their valuable comments, which clearly enhanced the manuscript.

References

- Aasen, H., Gnyp, M.L., Miao, Y., Bareth, G., 2014. Automated hyperspectral vegetation index retrieval from multiple correlation matrices with HyperCor. *Photogramm. Eng. Remote Sens.* 80, 785–796. doi:10.14358/PERS.80.8.785
- Andújar, D., Escolà, A., Rosell-Polo, J.R., Fernández-Quintanilla, C., Doradoa, J., 2013. Potential of a terrestrial LiDAR-based system to characterise weed vegetation in maize crops. *Comput. Electron. Agric.* 92, 11–15. doi:10.1016/j.compag.2012.12.012
- Bendig, J., Bolten, A., Bareth, G., 2013. UAV-based Imaging for Multi-Temporal, very high Resolution Crop Surface Models to monitor Crop Growth Variability. *Photogramm. - Fernerkundung - Geoinf.* 6, 551–562. doi:10.1127/1432-8364/2013/0200
- Besl, P.J., McKay, N.D., 1992. A Method for Registration of 3D Shapes. *IEEE Trans. Pattern Anal. Mach. Intell.* 14, 239–256. doi:10.1117/12.57955
- Cao, Q., Miao, Y., Wang, H., Huang, S., Cheng, S., Khosla, R., Jiang, R., 2013. Non-destructive estimation of rice plant nitrogen status with Crop Circle multispectral active canopy sensor. *F. Crop. Res.* 154, 133–144. doi:10.1016/j.fcr.2013.08.005
- Casanova, D., Epema, G.F., Goudriaan, J., 1998. Monitoring rice reflectance at field level for estimating biomass and LAI. *F. Crop. Res.* 55, 83–92. doi:10.1016/S0378-4290(97)00064-6
- Confalonieri, R., Bregaglio, S., Rosenmund, A.S., Acutis, M., Savin, I., 2011. A model for simulating the height of rice plants. *Eur. J. Agron.* 34, 20–25. doi:10.1016/j.eja.2010.09.003
- Devienne-Barret, F., Justes, E., Mchet, J.M., Mary, B., 2000. Integrated Control of Nitrate Uptake by Crop Growth Rate and Soil Nitrate Availability under Field Conditions. *Ann. Bot.* 86, 995–1005. doi:10.1006/anbo.2000.1264
- Ding, W., Zhang, Y., Zhang, Q., Zhu, D., Chen, Q., 2011. Realistic Simulation of Rice Plant. *Rice Sci.* 18, 224–230. doi:10.1016/S1672-6308(11)60031-0
- Ding, Y., Chan, J.C.L., 2005. The East Asian summer monsoon: an overview. *Meteorol. Atmos. Phys.* 89, 117–142. doi:10.1007/s00703-005-0125-z
- Domrös, M., Gongbing, P., 1988. *The Climate of China*. Springer-Verlag, Berlin.
- Ehlert, D., Adamek, R., Horn, H.-J., 2009. Laser rangefinder-based measuring of crop biomass under field conditions. *Precis. Agric.* 10, 395–408. doi:10.1007/s11119-009-9114-4
- Ehlert, D., Heisig, M., 2013. Sources of angle-dependent errors in terrestrial laser scanner-based crop stand measurement. *Comput. Electron. Agric.* 93, 10–16. doi:10.1016/j.compag.2013.01.002
- Ehlert, D., Horn, H.-J., Adamek, R., 2008. Measuring crop biomass density by laser triangulation. *Comput. Electron. Agric.* 61, 117–125. doi:10.1016/j.compag.2007.09.013
- Eitel, J.U.H., Vierling, L.A., Long, D.S., Raymond Hunt, E., 2011. Early season remote sensing of wheat nitrogen status using a green scanning laser. *Agric. For. Meteorol.* 151, 1338–1345. doi:10.1016/j.agrformet.2011.05.015
- Elia, A., Conversa, G., 2012. Agronomic and physiological responses of a tomato crop to nitrogen input. *Eur. J. Agron.* 40, 64–74. doi:10.1016/j.eja.2012.02.001
- Elseberg, J., Borrmann, D., Nüchter, A., 2011. Full Wave Analysis in 3D laser scans for vegetation detection in urban environments, in: *2011 XXIII International Symposium on Information, Communication and Automation Technologies*. IEEE, pp. 1–7. doi:10.1109/ICAT.2011.6102101
- FAO, 2014. FAOSTAT. <http://faostat3.fao.org/faostat-gateway/go/to/home/E>

- Gao, J., Liu, Y., 2011. Climate warming and land use change in Heilongjiang Province, Northeast China. *Appl. Geogr.* 31, 476–482. doi:10.1016/j.apgeog.2010.11.005
- Gebbers, R., Ehler, D., Adamek, R., 2011. Rapid Mapping of the Leaf Area Index in Agricultural Crops. *Agron. J.* 103, 1532–1541. doi:10.2134/agronj2011.0201
- Gnyp, M.L., Yu, K., Aasen, H., Yao, Y., Huang, S., Miao, Y., Bareth, G., 2013. Analysis of crop reflectance for estimating biomass in rice canopies at different phenological stages. *Photogramm. - Fernerkundung - Geoinf.* 4, 351–365. doi:http://dx.doi.org/10.1127/1432-8364/2013/0182
- Greenwood, D.J., Gastal, F., Lemaire, G., Draycott, A., Millard, P., Neeteson, J.J., 1991. Growth rate and %N of field grown crops: Theory and experiments. *Ann. Bot.* 67, 181–190.
- Guarnieri, A., Pirotti, F., Vettore, A., 2012. Comparison of discrete return and waveform terrestrial laser scanning for dense vegetation filtering. *Int. Arch. Photogramm. Remote Sens. Spat. Inf. Sci.* 39 (Part B7) 511–516. doi:10.5194/isprsarchives-XXXIX-B7-511-2012
- Guarnieri, A., Vettore, A., Pirotti, F., Menenti, M., Marani, M., 2009. Retrieval of small-relief marsh morphology from Terrestrial Laser Scanner, optimal spatial filtering, and laser return intensity. *Geomorphology* 113, 12–20. doi:10.1016/j.geomorph.2009.06.005
- Henning, J.G., Radtke, P.J., 2006. Ground-based Laser Imaging for Assessing Three-dimensional Forest Canopy Structure. *Photogramm. Eng. Remote Sens.* 72, 1349–1358. doi:http://dx.doi.org/10.14358/PERS.72.12.1349
- Hoffmeister, D., Bolten, A., Curdt, C., Waldhoff, G., Bareth, G., 2010. High resolution Crop Surface Models (CSM) and Crop Volume Models (CVM) on field level by terrestrial laser scanning, in: Guo, H., Wang, C. (Eds.), *Proc. of SPIE, 6th International Symposium on Digital Earth*. Beijing, China. doi:10.1117/12.872315
- Hoffmeister, D., Tilly, N., Bendig, J., Curdt, C., Bareth, G., 2012. Detektion von Wachstumsvariabilität in vier Zuckerrübensorten, in: Clasen, M., Fröhlich, G., Bernhardt, H., Hildebrand, K., Theuvsen, B. (Eds.), *Informationstechnologie Für Eine Nachhaltige Landwirtschaft*, Proc. 32. GIL-Jahrestagung. Köllen Verlag, Bonn, Germany, Freising, pp. 135–138.
- Hoffmeister, D., Waldhoff, G., Curdt, C., Tilly, N., Bendig, J., Bareth, G., 2013. Spatial variability detection of crop height in a single field by terrestrial laser scanning, in: Stafford, J. (Ed.), *Precision Agriculture '13 SE - 31*. Wageningen Academic Publishers, pp. 267–274. doi:10.3920/978-90-8686-778-3_31
- Höfle, B., 2014. Radiometric Correction of Terrestrial LiDAR Point Cloud Data for Individual Maize Plant Detection. *Geosci. Remote Sens. Lett. IEEE* 11, 94–98. doi:10.1109/LGRS.2013.2247022
- Hosoi, F., Omasa, K., 2012. Estimation of vertical plant area density profiles in a rice canopy at different growth stages by high-resolution portable scanning lidar with a lightweight mirror. *ISPRS J. Photogramm. Remote Sens.* 74, 11–19. doi:10.1016/j.isprsjprs.2012.08.001
- Hosoi, F., Omasa, K., 2009. Estimating vertical plant area density profile and growth parameters of a wheat canopy at different growth stages using three-dimensional portable lidar imaging. *ISPRS J. Photogramm. Remote Sens.* 64, 151–158. doi:10.1016/j.isprsjprs.2008.09.003
- Hosoi, F., Omasa, K., 2006. Voxel-Based 3-D Modeling of Individual Trees for Estimating Leaf Area Density Using High-Resolution Portable Scanning Lidar. *IEEE Trans. Geosci. Remote Sens.* 44, 3610–3618. doi:10.1109/TGRS.2006.881743

- Huang, J., He, F., Cui, K., Buresh, R.J., Xu, B., Gong, W., Peng, S., 2008. Determination of optimal nitrogen rate for rice varieties using a chlorophyll meter. *F. Crop. Res.* 105, 70–80. doi:10.1016/j.fcr.2007.07.006
- Hyyppä, J., Hyyppä, H., Leckie, D., Gougeon, F., Yu, X., Maltamo, M., 2008. Review of methods of small-footprint airborne laser scanning for extracting forest inventory data in boreal forests. *Int. J. Remote Sens.* 29, 1339–1366. doi:10.1080/01431160701736489
- Johnston, K., Ver Hoef, J.M., Krivoruchko, K., Lucas, N., 2001. Using ArcGIS Geostatistical Analyst. ESRI, USA.
- Keightley, K.E., Bawden, G.W., 2010. 3D volumetric modeling of grapevine biomass using Tripod LiDAR. *Comput. Electron. Agric.* 74, 305–312. doi:10.1016/j.compag.2010.09.005
- Koppe, W., Gnyp, M.L., Hütt, C., Yao, Y., Miao, Y., Chen, X., Bareth, G., 2012. Rice monitoring with multi-temporal and dual-polarimetric TerraSAR-X data. *Int. J. Appl. Earth Obs. Geoinf.* 21, 568–576. doi:10.1016/j.jag.2012.07.016
- Kukko, A., Kaartinen, H., Hyyppä, J., Chen, Y., 2012a. Multiplatform Approach To Mobile Laser Scanning. *Int. Arch. Photogramm. Remote Sens. Spat. Inf. Sci.* 39 (Part B5) XXXIX-B5, 483–488. doi:10.5194/isprsarchives-XXXIX-B5-483-2012
- Kukko, A., Kaartinen, H., Hyyppä, J., Chen, Y., 2012b. Multiplatform Mobile Laser Scanning: Usability and Performance. *Sensors* 12, 11712–11733. doi:10.3390/s120911712
- Lefsky, M.A., Cohen, W.B., Parker, G.G., Harding, D.J., 2002. Lidar Remote Sensing for Ecosystem Studies. *Bioscience* 52, 19–30. doi:10.1641/0006-3568(2002)052[0019:LRSFES]2.0.CO;2
- Lemaire, G., Avice, J.-C., Kim, T.-H., Ourry, A., 2005. Developmental changes in shoot N dynamics of lucerne (*Medicago sativa* L.) in relation to leaf growth dynamics as a function of plant density and hierarchical position within the canopy. *J. Exp. Bot.* 56, 935–43. doi:10.1093/jxb/eri084
- Lemaire, G., Jeuffroy, M.-H., Gastal, F., 2008. Diagnosis tool for plant and crop N status in vegetative stage. *Eur. J. Agron.* 28, 614–624. doi:10.1016/j.eja.2008.01.005
- Li, W., Li, H., Zhao, L., 2011. Estimating Rice Yield by HJ-1A Satellite Images. *Rice Sci.* 18, 142–147. doi:10.1016/S1672-6308(11)60020-6
- Lichti, D.D., 2010. A review of geometric models and self-calibration methods for terrestrial laser scanners. *Bol. Ciências Geodésicas* 16, 3–19.
- Lopez-Sanchez, J.M., Ballester-Berman, J.D., Hajnsek, I., 2011. First Results of Rice Monitoring Practices in Spain by Means of Time Series of TerraSAR-X Dual-Pol Images. *IEEE J. Sel. Top. Appl. Earth Obs. Remote Sens.* 4, 412–422. doi:10.1109/JSTARS.2010.2047634
- Lovell, J.L., Jupp, D.L.B., Newnham, G.J., Culvenor, D.S., 2011. Measuring tree stem diameters using intensity profiles from ground-based scanning lidar from a fixed viewpoint. *ISPRS J. Photogramm. Remote Sens.* 66, 46–55. doi:10.1016/j.isprsjprs.2010.08.006
- Lumme, J., Karjalainen, M., Kaartinen, H., Kukko, A., Hyyppä, J., Hyyppä, H., Jaakkola, A., Kleemola, J., 2008. Terrestrial laser scanning of agricultural crops. *Int. Arch. Photogramm. Remote Sens. Spat. Inf. Sci.* 37 (Part B5) 563–566.
- McKinion, J.M., Willers, J.L., Jenkins, J.N., 2010. Spatial analyses to evaluate multi-crop yield stability for a field. *Comput. Electron. Agric.* 70, 187–198. doi:10.1016/j.compag.2009.10.005
- Meier, U., 2001. Growth stages of mono- and dicotyledonous plants, 2nd ed. Blackwell, Berlin.

- Miao, Y., Stewart, B.A., Zhang, F., 2011. Long-term experiments for sustainable nutrient management in China. A review. *Agron. Sustain. Dev.* 31, 397–414. doi:10.1051/agro/2010034
- Mistele, B., Schmidhalter, U., 2008. Estimating the nitrogen nutrition index using spectral canopy reflectance measurements. *Eur. J. Agron.* 29, 184–190. doi:10.1016/j.eja.2008.05.007
- Mulla, D.J., 2012. Twenty five years of remote sensing in precision agriculture: Key advances and remaining knowledge gaps. *Biosyst. Eng.* 114, 358–371. doi:10.1016/j.biosystemseng.2012.08.009
- My Phung, N.T., Brown, P.R., Leung, L.K.P., 2013. Use of computer simulation models to encourage farmers to adopt best rodent management practices in lowland irrigated rice systems in An Giang Province, the Mekong Delta, Vietnam. *Agric. Syst.* 116, 69–76. doi:10.1016/j.agsy.2012.11.003
- Ntanos, D.A., Koutroubas, S.D., 2002. Dry matter and N accumulation and translocation for Indica and Japonica rice under Mediterranean conditions. *F. Crop. Res.* 74, 93–101. doi:10.1016/S0378-4290(01)00203-9
- Omasa, K., Hosoi, F., Konishi, A., 2007. 3D lidar imaging for detecting and understanding plant responses and canopy structure. *J. Exp. Bot.* 58, 881–898. doi:10.1093/jxb/erl142
- Peng, S., Garcia, F.V., Laza, R.C., Sanico, A.L., Visperas, R.M., Cassman, K.G., 1996. Increased N-use efficiency using a chlorophyll meter on high-yielding irrigated rice. *F. Crop. Res.* 47, 243–252.
- Ribbes, F., Le Toan, T., 1999. Rice field mapping and monitoring with RADARSAT data. *Int. J. Remote Sens.* 20, 745–765. doi:10.1080/014311699213172
- Riegl LMS GmbH, 2013. Datasheet Riegl VZ-1000. http://www.riegl.com/uploads/tx_pxpriegldownloads/DataSheet_VZ-1000_18-09-2013.pdf
- Roelcke, M., Han, Y., Schleef, K.H., Zhu, J.-G., Liu, G., Cai, Z.-C., Richter, J., 2004. Recent trends and recommendations for nitrogen fertilization in intensive agriculture in eastern China. *Pedosphere* 14, 449–460.
- Ryu, C., Suguri, M., Umeda, M., 2011. Multivariate analysis of nitrogen content for rice at the heading stage using reflectance of airborne hyperspectral remote sensing. *F. Crop. Res.* 122, 214–224. doi:10.1016/j.fcr.2011.03.013
- Saeyns, W., Lenaerts, B., Craessaerts, G., De Baerdemaeker, J., 2009. Estimation of the crop density of small grains using LiDAR sensors. *Biosyst. Eng.* 102, 22–30. doi:10.1016/j.biosystemseng.2008.10.003
- Stroppiana, D., Boschetti, M., Brivio, P.A., Bocchi, S., 2009. Plant nitrogen concentration in paddy rice from field canopy hyperspectral radiometry. *F. Crop. Res.* 111, 119–129. doi:10.1016/j.fcr.2008.11.004
- Van der Zande, D., Hoet, W., Jonckheere, I., van Aardt, J., Coppin, P., 2006. Influence of measurement set-up of ground-based LiDAR for derivation of tree structure. *Agric. For. Meteorol.* 141, 147–160. doi:10.1016/j.agrformet.2006.09.007
- van Leeuwen, M., Hilker, T., Coops, N.C., Frazer, G., Wulder, M.A., Newnham, G.J., Culvenor, D.S., 2011. Assessment of standing wood and fiber quality using ground and airborne laser scanning: A review. *For. Ecol. Manage.* 261, 1467–1478. doi:10.1016/j.foreco.2011.01.032
- van Wart, J., Kersebaum, K.C., Peng, S., Milner, M., Cassman, K.G., 2013. Estimating crop yield potential at regional to national scales. *F. Crop. Res.* 143, 34–43. doi:10.1016/j.fcr.2012.11.018

- Velodyne, 2014. Velodyne HDL-64E User's Manual. [http://www.velodynelidar.com/lidar/products/manual/63-HDL64E S2 Manual_Rev D_2011_web.pdf](http://www.velodynelidar.com/lidar/products/manual/63-HDL64E%20Manual_Rev%20D_2011_web.pdf)
- Wagner, W., Hollaus, M., Briese, C., Ducic, V., 2008. 3D vegetation mapping using small-footprint full-waveform airborne laser scanners. *Int. J. Remote Sens.* 29, 1433–1452. doi:10.1080/01431160701736398
- Wang, K., Zhou, H., Wang, B., Jian, Z., Wang, F., Huang, J., Nie, L., Cui, K., Peng, S., 2013. Quantification of border effect on grain yield measurement of hybrid rice. *F. Crop. Res.* 141, 47–54. doi:10.1016/j.fcr.2012.11.012
- Watanabe, T., Hanan, J.S., Room, P.M., Hasegawa, T., Nakagawa, H., Takahashi, W., 2005. Rice morphogenesis and plant architecture: measurement, specification and the reconstruction of structural development by 3D architectural modelling. *Ann. Bot.* 95, 1131–1143. doi:10.1093/aob/mci136
- Yang, X., Huang, J., Wu, Y., Wang, J., Wang, P., Wang, X., Huete, A.R., 2011. Estimating biophysical parameters of rice with remote sensing data using support vector machines. *Sci. China. Life Sci.* 54, 272–281. doi:10.1007/s11427-011-4135-4
- Yao, Y., Miao, Y., Huang, S., Gao, L., Ma, X., Zhao, G., Jiang, R., Chen, X., Zhang, F., Yu, K., Gnyp, M.L., Bareth, G., Liu, C., Zhao, L., Yang, W., Zhu, H., 2012. Active canopy sensor-based precision N management strategy for rice. *Agron. Sustain. Dev.* 32, 925–933. doi:10.1007/s13593-012-0094-9
- Yi, Q.X., Huang, J.F., Wang, F.M., Wang, X.Z., Liu, Z.Y., 2007. Monitoring rice nitrogen status using hyperspectral reflectance and artificial neural network. *Environ. Sci. Technol.* 41, 6770–6775. doi:10.1021/es070144e
- Yu, K., Li, F., Gnyp, M.L., Miao, Y., Bareth, G., Chen, X., 2013. Remotely detecting canopy nitrogen concentration and uptake of paddy rice in the Northeast China Plain. *ISPRS J. Photogramm. Remote Sens.* 78, 102–115. doi:10.1016/j.isprsjprs.2013.01.008
- Zhang, L., Grift, T.E., 2012. A LIDAR-based crop height measurement system for *Miscanthus giganteus*. *Comput. Electron. Agric.* 85, 70–76. doi:10.1016/j.compag.2012.04.001

Nora Tilly studied geography at the University of Cologne and received her diploma in 2010. Currently, she is working in the GIS & Remote Sensing Group at the Institute of Geography, University of Cologne. Her research interests focus on terrestrial laser scanning for agricultural applications. In this context, her PhD thesis is related to the International Center for Agro-Informatics and Sustainable Development (ICASD).

Dirk Hoffmeister is a research assistant in the GIS & Remote Sensing Group at the Institute of Geography, University of Cologne, where he also received his PhD. His primary expertise is terrestrial laser scanning and corresponding applications for coastal geomorphology, agronomy, and geoarchaeology.

Biographies of the other authors are not available.

4 Transferability of Models for Estimating Paddy Rice Biomass from Spatial Plant Height Data

NORA TILLY^{1,*}, DIRK HOFFMEISTER¹, QIANG CAO², VICTORIA LENZ-WIEDEMANN¹, YUXIN MIAO²,
GEORG BARETH¹

Published in: *Agriculture* 2015, **5**, 538-560

DOI: 10.3390/agriculture5030538

Formatting and orthography of the manuscript is adapted to the dissertation style.

¹ International Center for Agro-Informatics and Sustainable Development, Institute of Geography (GIS & Remote Sensing Group), University of Cologne, 50923 Cologne, Germany

² International Center for Agro-Informatics and Sustainable Development, Department of Plant Nutrition, China Agricultural University, 100193 Beijing, China

* Corresponding author: Tel.: +49 221 470 6265, Fax: +49 221 470 8838,
Email: nora.tilly@uni-koeln.de

Abstract: It is known that plant height is a suitable parameter for estimating crop biomass. The aim of this study was to confirm the validity of spatial plant height data, which is derived from terrestrial laser scanning (TLS), as a non-destructive estimator for biomass of paddy rice on the field scale. Beyond that, the spatial and temporal transferability of established biomass regression models were investigated to prove the robustness of the method and evaluate the suitability of linear and exponential functions. In each growing season of two years, three campaigns were carried out on a field experiment and on a farmer's conventionally managed field. Crop surface models (CSMs) were generated from the TLS-derived point clouds for calculating plant height with a very high spatial resolution of 1 cm. High coefficients of determination between CSM-derived and manually measured plant heights (R^2 : 0.72 to 0.91) confirm the applicability of the approach. Yearly averaged differences between the measurements were ~7% and ~9%. Biomass regression models were established from the field experiment data sets, based on strong coefficients of determination between plant height and dry biomass (R^2 : 0.66 to 0.86 and 0.65 to 0.84 for linear and exponential models, respectively). The spatial and temporal transferability of the models to the farmer's conventionally managed fields is supported by strong coefficients of determination between estimated and measured values (R^2 : 0.60 to 0.90 and 0.56 to 0.85 for linear and exponential models, respectively). Hence, the suitability of TLS-derived spatial plant height as a non-destructive estimator for biomass of paddy rice on the field scale was verified and the transferability demonstrated.

Keywords: terrestrial laser scanning; plant height; biomass; rice; precision agriculture; field level

4.1 Introduction

Solutions to ensure the world's food security are required due to the growing world population. Focusing on the supply with staple food, the cultivation of rice is essential. This is

in particular for the Asian world important, where 2011 and 2012 about 90% of the estimated world rice production was cultivated, each year about 650 million tons (FAO, 2014). Miao et al. (2011) reviewed long-term experiments on sustainable field management and highlighted the required increase in cereal production to ensure food security in China. The authors emphasized the combination of traditional practices and modern sensor-based management approaches for addressing this challenge.

In this context, precision agriculture (PA) rises in importance, which focuses on spatial and temporal variabilities of natural conditions and an adequate dealing with resources (Oliver, 2013). PA-improved management methods support farmers in closing the gap between potential and current yield (van Wart et al., 2013). Based on analyses of long-term field experiments, Roelcke et al. (2004) concluded that there is a great need for on-farm experiments. Therefore accurate crop monitoring based on remote and proximal sensing has become increasingly important within PA in recent years (Marshall and Thenkabail, 2015; Mulla, 2012). A widely used indicator for quantifying the actual status of plants is the nitrogen nutrition index (NNI) (Elia and Conversa, 2012; Greenwood et al., 1991; Lemaire et al., 2008). The index shows the ratio between measured and critical N content. The latter is determined by the crop-specific N dilution curve, showing the relation between N concentration and biomass. Consequently, the accurate and non-destructive determination of biomass is a precondition for calculating the NNI.

For rice, it has been shown that grain yield is positively correlated to biomass and nitrogen (N) translocation efficiency (Ntanos and Koutroubas, 2002), but over-fertilization affects the nutrient balance in soil and groundwater. Consequently, the NNI should be used for optimizing rice production with PA-improved management methods. Therefore, non-invasive approaches for biomass estimation are of key importance as rice paddies should be entered with machinery as little as possible during the growing season. Satellite remote sensing images serve for estimating the actual biomass and yield of large paddy rice fields (Koppe et al., 2012b; Li et al., 2011; Lopez-Sanchez et al., 2011; Ribbes and Le Toan, 1999; Yang et al., 2011). However, for monitoring within-field variability and more accurately estimating biomass, a higher spatial resolution is required. The potential of ground-based plant parameter measurements as input for biomass estimation models was recently demonstrated for rice, maize, cotton, and alfalfa (Marshall and Thenkabail, 2015). However, therein, plant height was manually measured, which is prone to selection bias. A ground-based multi-sensor approach showed good results for predicting biomass of grassland (Reddersen et al., 2014). For biomass estimation of paddy rice, in-situ approaches with hand-held sensors for measuring canopy reflectance provided good results (Aasen et al., 2014; Casanova et al., 1998; Gnyp et al., 2013). Moreover, Confalonieri et al. (2011) emphasized rice plant height as a key factor for predicting yield potential and developed a model for estimating plant height increase, but accurate in-situ measurements of plant height on field level are rare. Although virtual geometric models of single rice plants in a high resolution exist (Ding et al., 2011; Watanabe et al., 2005), uncertainties remain about the transferability to the field, due to varying patterns of plant growth. Hence, accurate methods for determining plant height on field level are desirable.

Light detection and ranging (LiDAR) sensors have been increasingly used in vegetational studies since the 1980s (Lee et al., 2010). In-situ studies confirmed the potential of ground-based LiDAR methods, also known as terrestrial laser scanning (TLS), for the assessment of plant parameters in agricultural applications. Previous studies focused on the acquisition of plant height (Zhang and Grift, 2012), post-harvest growth (Koenig et al., 2015), leaf area index (Gebbers et al., 2011), crop density (Hosoi and Omasa, 2009; Saeys et al., 2009), nitrogen status (Eitel et al., 2011), or the detection of individual plants (Hoffmeister et al., 2012; Höfle, 2014). Moreover, the potential of TLS for estimating the biomass of small grain cereals was emphasized Ehlert et al. (2009, 2008), Hämmerle and Höfle (2014), and Lumme et al. (2008). Regarding the accuracy, Lumme et al. (2008) found that estimated heights of cereal plants correlated with tape measurements. The high precision for mapping of maize plants was shown by Höfle (2014). Little research has been done so far on TLS in-situ measurements of paddy rice. Hosoi and Omasa (2012) examined vertical plant area density as an estimator for biomass, achieved with a portable scanner in combination with a mirror. Besides, biomass estimations based on TLS-derived spatial plant height was evaluated for some of the fields considered in the presented study (Tilly et al., 2014, 2013) But as stated above, multi-annual on-farm experiments are necessary for achieving a comprehensive understanding of plant growth and developing objective sensor-based measuring methods and models for biomass estimations (Miao et al., 2011; Roelcke et al., 2004).

Based on the promising results of the single year analyses (Tilly et al., 2014, 2013), this study focused on (I) the robustness of the method, (II) the spatial and temporal transferability of the models, and (III) a model improvement. For the latter, in addition to partially existing linear models, exponential models were established, as a better suitability of these models is denoted in other studies of biomass estimations over different growth stages (Aasen et al., 2014; Hansen and Schjoerring, 2003; Thenkabail et al., 2000). In two consecutive growing seasons, rice fields were monitored during the pre-anthesis period. Based on the data sets of a field experiment, estimation models for biomass were established and then applied on a farmer's conventionally managed fields.

4.2 Data and methods

4.2.1 Study area

Heilongjiang Province in the northeast of China is an important region for agricultural production (Gao and Liu, 2011). Almost 25% of the total area is covered by the Sanjiang Plain (~120,000 km²). The regional climate with cold and dry winters and short but warm, humid summers is marked by the East Asian summer monsoon (Ding and Chan, 2005; Domrös and Gongbing, 1988). Three field sites around the city of Jiansanjiang (N 47°15'21" E 132°37'43") were considered in this study.

At the Keyansuo experimental station (Jiansanjiang, Heilongjiang Province, China) the same field experiment was monitored in 2011 and 2012 (**Figure 4-1**). For the experiment, nine N fertilizer treatments were repeated three times for the rice varieties Kongyu 131 and Longjing 21. Hence, the field with a spatial extent of 60 m by 63 m consisted of 54 plots, each

about 10 m by 7 m in size. A detailed description of the experimental set-up is given by Cao et al. (2013). Related to the amount of N input, variations in plant height and biomass were expected. These differences were useful for the TLS monitoring approach to capture varying patterns of plant growth at one growing stage.

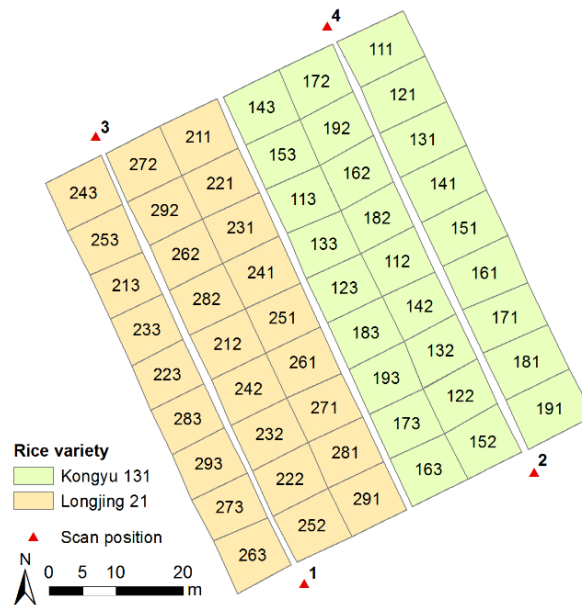


Figure 4-1. Design of the field experiment and scan positions. Three-digit number in the plot represents rice variety (1 = Kongyu 131; 2 = Longjing 21); treatment (1 to 9); and repetition (1 to 3). Modified from Tilly et al. (2014).

In addition, one farmer's conventionally managed field was investigated each year (hereafter referred to as farmer's field). The aim was to provide independent validation data sets for checking the spatial and temporal transferability of the findings from the field experiment data. For the following, they are termed village 69 (year 2011) and village 36 (year 2012). In both years, it was not possible to find a field with one of the field experiment rice varieties, where destructive sampling was possible several times during the growing season. In village 69 the variety Kenjiandao 6 was cultivated, in village 36 the variety Longjing 31. Moreover, in village 36 management units with very heterogeneous development were chosen, including parts without any plants (**Figure 4-2**). On each field two



Figure 4-2. One management unit with very heterogeneous plant growth in village 36.

management units were investigated. In village 69 and village 36 each unit was about 60 m by 40 m and 50 m by 70 m in size, respectively.

4.2.2 Field measurements

On each site, three TLS campaigns were carried out in June and July of the respective year to capture the key vegetative stages of the rice plants. During this pre-anthesis period, differences in plant development occur mainly due to the increase of tillers and plant height. This period is important for fertilizer management decisions. In both years, the campaigns on the field experiment and the farmer's field were carried out on two consecutive days to reach a best possible comparison regarding the plant development. For quantifying the phenological stages of plants and steps in plant development the BBCH scale was used (Lancashire et al., 1991; Meier, 2001). The abbreviation BBCH is derived from the funding organizations: Biologische Bundesanstalt (German Federal Biological Research Centre for Agriculture and Forestry), Bundessortenamt (German Federal Office of Plant Varieties), and Chemical industry. The campaign dates and BBCH-values for all sites are given in **Table 4-1**.

Table 4-1. Dates of the terrestrial laser scanning (TLS) campaigns and corresponding phenological stages.

Date/ BBCH scale ^a	2011		2012	
	Field experiment	Village 69	Field experiment	Village 36
1. Campaign	21 June 2011/ 13	22 June 2011/ 13	1 July 2012/ 37	30 June 2012/ 37
2. Campaign	4 July 2011/ 13 - 15; 22 - 23	5 July 2011/ 13; 21	9 July 2012/ 42	8 July 2012/ 37; 39
3. Campaign	18 July 2011/ 19; 29; 32	19 July 2011/ 19; 29; 34	17 July 2012/ 50	16 July 2012/ 19; 29; 34

^a Multiple values due to several samples.

Terrestrial laser scanners operating with the time-of-flight technique were used for all campaigns. The relative positions of survey points are calculated from the distances, as well as the horizontal and vertical angles between sensor and targets. For this, the time between transmitting and receiving a pulsed laser signal and its angles are measured. In 2011 and 2012, the Riegl VZ-1000 and Riegl LMS-Z420i, respectively, were provided by the company Five Star Electronic Technologies (Beijing, China) (Riegl LMS GmbH, 2013, 2010). Both devices operate with a near-infrared laser beam and have a beam divergence of 0.3 mrad (VZ-1000) and 0.25 mrad (LMS-Z420i). The angular resolution was set to 0.04 deg. All scans were conducted from the dikes between the paddies to avoid entering them, resulting in an oblique perspective. More detailed descriptions are given in Tilly et al. (2014).

The setup for the campaigns on the field experiment was similar in both years. Each time, nine scan positions were established for covering all fields of the Keyansuo experimental station and minimizing shadowing effects. For this analysis, the scans from all positions were used, but four positions were of major importance, as they were located close to the investigated field experiment. Following, the largest number of points was acquired from these positions. Point clouds from other positions were used to avoid gaps in the final point cover due to information signs close to the field. As shown in **Figure 4-1**, two positions respectively were set up at the north and south edges. At each position the scanner was mounted on a tripod which raised the sensor up to 1.5 m above ground. Additionally, a small

tractor-trailer system was used for the positions at the south edge of the field for achieving a greater height of about 3 m. The narrow dikes along the other edges made it impossible to reach those positions with the tractor-trailer system.

Due to a limited access on the dikes between the management units of both farmer's fields, it was also impossible to use a trailer. Hence, the sensor height of the scanner on the tripod was about 1.5 m above ground. In village 69 the scan positions were established close to the four corners of the management units (**Figure 4-3**). As the investigated units in village 36 were located at the edge of the whole field, this set-up was slightly changed. Two positions in the north were established on a small hill close to the field for reaching a higher position and an additional position was placed at the center of the edge (scan position 5 in **Figure 4-3**). Further two positions were set up close to the south corners. In both fields, twelve thin, long bamboo sticks per management unit were stuck in the ground. These bamboo sticks can be easily detected in the TLS point clouds and located in the field to ensure the spatial linkage to other plant parameter measurements.



Figure 4-3. Scan positions and bamboo stick positions on the farmer's fields.

Furthermore, ranging poles with high-reflective cylinders (Hoffmeister et al., 2010) were built upon the dikes between the fields, homogeneously distributed around the field. These can be detected by the laser scanner and act as tie points for merging the scan data in post-processing. In the first campaigns, the position of each pole was marked in the fields. By re-establishing the ranging poles at exactly the same position for the following campaigns, all scans of one site can be merged. In the data sets from 2011, alignment errors occurred due to imprecise re-establishing of the ranging poles or where an exact marking of the positions was difficult, particularly on the farmer's fields. These errors could be rectified with software options but caused time-consuming post-processing. In 2012, additional tie points were used to avoid this. As shown in **Figure 4-4** for village 36, five small, round reflectors were permanently attached to trees close to the fields and remained there during the observation period. A homogeneous distribution around the field was not possible, as no other stationary objects were available.



Figure 4-4. Small, round reflectors were permanently attached to trees in village 36.

At all sites, manual measurements of plant height and biomass were performed during the whole vegetation period. Corresponding to each TLS campaign on the field experiment, the heights of eight to ten and four hills per plot were measured in 2011 and 2012, respectively. Each hill consisted of four to six rice plants.

Regarding the measurement of biomass, differences between the sites and years must be pointed out. As part of the field experiment, destructive sampling was performed several times during the vegetation period. Samples were taken from both varieties, but only from the three repetitions of five treatments ($n = 30$). The dates of sampling differed from the TLS campaign dates in 2011, but due to the small plot size, it was not feasible to take additional samples. Thus, the biomass values were linearly interpolated. In 2012, the measurements could be carried out on the same day.

On the farmer's fields, four hills around each bamboo stick were destructively taken after the TLS measurements (each $n = 24$). For the following campaign, the bamboo sticks were moved in a defined direction to the center of four other hills. In each management unit of village 36, one bamboo stick was placed in the part without any plant and left at its position for all campaigns (no. 12 in **Figure 4-3**).

The cleaned above ground biomass was weighed after drying. All samples were oven dried at 105 °C for 30 min and dried to constant weight at 75 °C. The dry biomass per m^2 was calculated, considering the specific number of hills per m^2 .

4.2.3 Post-processing of the TLS data

The post-processing of the scan data was similar for all sites. A detailed description is given for the data sets from 2011 in Tilly et al. (2014). Riegl's software RiSCAN Pro, also applied for the data acquisition, was used for the first steps of the data handling. The scans from all campaigns were imported into one RiSCAN Pro project file for each site. Following, a co-registration of all scan positions was carried out, based on the reflectors acting as tie points. As mentioned above, the data sets of 2011 showed alignment errors, due to non-optimal positioning or imprecise re-establishing of the ranging poles. The iterative closest point (ICP) algorithm (Besl and McKay, 1992), implemented in RiSCAN Pro as Multi Station Adjustment, was used to modify the position and orientation of each scan position in multiple iterations for getting the best fitting result. For the campaigns in 2012, additional small reflectors were permanently established. By first registering one scan position of each

campaign based on these permanent tie points and aligning all other positions to these, an accurate alignment was possible. After optimizing the alignment with the ICP algorithm the error, measured as standard deviation between the used point-pairs, was 0.06 m and 0.01 m on average for both sites of 2011 and 2012, respectively.

Following, the point clouds were merged to one data set per campaign and the area of interest (AOI) was manually extracted. Clearly identifiable noise in the point clouds far below and above the field, caused by reflections on water in the field or on small particles in the air, was previously removed. The crop surface was then determined from the point clouds with a filtering scheme for selecting maximum points. A common reference surface is required for the calculation of plant heights. Therefore, the AOI is usually scanned without any vegetation. As it was not possible to obtain such data on the rice fields, the lowest parts in the point clouds from the first campaigns were selected. At this stage, the rice plants were small enough for clearly identifying points at the bottom of the hills, as shown in Tilly et al. (2014). The point clouds of the field experiment data sets were subdivided plot-wise to attain a common spatial base. Each management unit of the farmer's fields was regarded as one data set. All data sets were exported as ASCII files, which contained the XYZ coordinates of each point for spatial and statistical analyses.

4.2.4 Calculation of plant height and visualization as maps of plant height

For the spatial analyses, crop surface models (CSMs) were constructed from the TLS-derived point clouds. CSMs were introduced by (Hoffmeister et al., 2010) for an objective and non-invasive deriving of spatial crop height and crop growth patterns. A CSM represents the crop surface at a specific date with a high spatial resolution. Therefore, the exported point clouds were interpolated to raster data sets with a consistent spatial resolution of 1 cm with the inverse distance weighting (IDW) algorithm in ArcGIS Desktop 10 (Esri, Redlands, CA, USA). IDW is suitable for preserving the accuracy of measurements with a high density, as it is a deterministic, exact interpolation and retains a measured value at its location (Johnston et al., 2001). Likewise, a digital terrain model (DTM) was generated from the manually selected ground points as common reference surface. Next, the DTM was subtracted from the CSM for calculating the plant heights. In the same way, plant growth between two dates can be spatially measured by calculating the difference between two CSMs. Herein, growth is defined as spatio-temporal difference in height. Finally, maps of plant height were created for visualizing the pixel-wise calculated values.

For the following analyses, one plant height value per campaign for comparable spatial units was necessary. Therefore, the CSM-derived plant heights were averaged plot-wise for the field experiment ($n = 54$). Previously, each plot was clipped with an inner buffer of 60 cm for preventing border effects. As the manual measurements were used for validating the laser scanning results, these plant height values were also averaged plot-wise ($n = 54$). Around each bamboo stick on the farmer's fields, a circular buffer with a radius of 1 m was generated to attain a common spatial base, for which the CSM-derived plant heights were averaged (each $n = 24$).

4.2.5 Estimation of biomass

The field experiment analyses were taken to express the correlation between plant height and dry above ground biomass (hereafter referred to as biomass) in a biomass regression model (BRM). Since only the above ground plant height is determinable from the TLS data, statements about the subsurface cannot be done. As mentioned above, other studies showed that exponential models performed better for biomass estimations over different growth stages. For establishing exponential models in addition to the linear ones, the biomass values were natural log-transformed. The models were used for estimating the biomass on the farmer's fields based on the TLS-derived spatial plant height data. Previously, linear and exponential biomass regression models (BRMs) were established, only regarding the field experiment for checking the general concept and evaluating differences between the results for 2011 and 2012 (hereinafter referred to as trial BRMs). Afterwards, the transferability of the model to the farmer's fields was evaluated. The workflow can be structured as following:

- I. Examination of concept with trial BRMs: Each linear and exponential model was derived from the measurements of two field experiment repetitions from one year. The biomass of the remaining third repetition was estimated and validated against the destructive measurements.
- II. Generation of BRM: Overall six models were established based on the measurements of all field experiment repetitions, separately for each year and as a combination of both years, each as linear and exponential model.
- III. Application of the BRMs: Each model was used for estimating the biomass at all campaign dates on both farmer's fields based on the CSM-derived plant height of the buffer areas around the bamboo sticks.
- IV. Validation of the BRMs: By comparing estimated and destructively measured biomass values the general validity, robustness, and suitability of the linear and exponential BRMs were evaluated.

The accuracy of each BRM was evaluated based on the coefficient of determination, index of agreement and root mean square error, calculated for each estimated value in comparison with the destructively measured biomass. The coefficient of determination (R^2) is widely used as measure of the dependence between two variables, but often unrelated to the size of the difference between them. For validating models, Willmott's index of agreement (d) shows to which degree a measured value can be estimated (Willmott and Wicks, 1980; Willmott, 1981). The index ranges between 0 and 1, from total disagreement to entire agreement. In addition, the root mean square error (RMSE) indicates how well the estimated values fit to the measured values (Hair et al., 2010).

4.3 Results

4.3.1 Maps of CSM-derived plant height

The TLS-derived CSMs and the DTM were used to calculate plant height pixel-wise for all plots of the field experiment and each management unit of both farmer's fields. The resulting raster data sets have a high resolution of 1 cm. Maps of plant height were created for visualizing spatial and temporal patterns and variations. In **Figure 4-5**, maps of plant height

are shown for two field experiment plots for all campaigns of both years. The respective first repetition of two fertilizer treatments for the rice variety Kongyu 131 are selected as an example, whereby the plot numbers, 111 and 151, refer to the lower and higher amount of applied N fertilizer, respectively. In particular in the maps of plot 111, the linear structure of the rice plant rows is detectable in both years. In 2012, Plot 151 shows a discernible pattern with higher plant height values in the north corner, which is visible in all campaigns. Moreover, differences in plant height occur between the different fertilizer treatments. The mean plant heights are higher for plots with a higher amount of applied N fertilizer, with a difference ranging from ~7 cm to ~13 cm and ~4 cm to ~16 cm for 2011 and 2012, respectively.

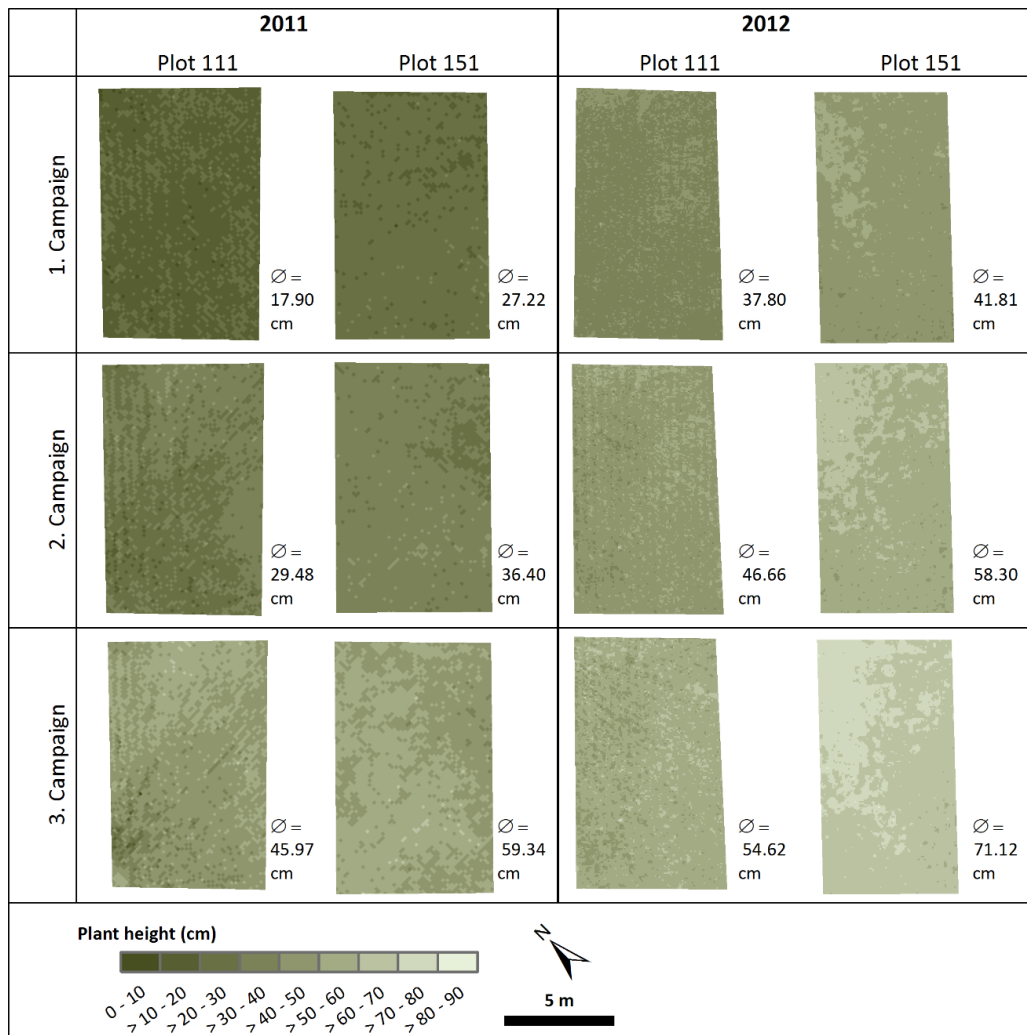


Figure 4-5. Crop surface model (CSM)-derived maps of plant height for two field experiment plots of both years, given with mean plant height per plot.

4.3.2 Analysis of plant height data

Regarding the field experiment, averaged CSM-derived and manually measured plant heights were used for validating the accuracy of the scan data (**Table 4-2**). The mean heights are quite similar for both years, with an average difference of ~7% and ~9% for 2011 and 2012, respectively. The standard deviation within each campaign increases over time. All values and the resulting regression lines are shown in **Figure 4-6**. The coefficients of determination are high for 2011 and 2012 with $R^2 = 0.91$ and $R^2 = 0.72$, respectively.

Table 4-2. Mean crop surface model (CSM)-derived and manually measured plant heights of the field experiment (n : number of samples; \bar{X} : mean value; SD: standard deviation; min: minimum; max: maximum).

Date	n	Plant height from CSM (cm)				Measured plant height (cm)				Difference
		\bar{X}	SD	min	max	\bar{X}	SD	min	max	%
21 June 11	54	24.84	3.63	17.90	32.99	24.37	2.06	19.13	28.88	1.89
04 July 11	54	34.62	4.36	24.59	42.71	37.94	2.42	32.38	44.13	9.59
18 July 11	54	55.38	7.22	44.28	70.30	63.56	4.25	53.10	70.70	14.77
01 July 12	54	44.72	3.08	37.80	53.25	40.85	4.87	31.00	49.50	8.64
09 July 12	54	57.09	3.61	48.87	64.64	46.84	4.30	37.50	56.50	17.95
17 July 12	54	67.04	5.25	54.62	76.46	65.84	5.38	53.00	75.50	1.78

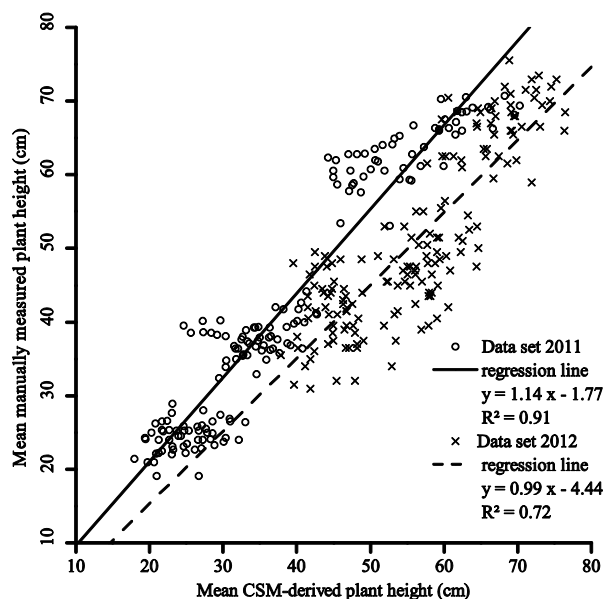


Figure 4-6. Regression of the mean CSM-derived and manually measured plant heights of the field experiment of both years (each $n = 162$).

4.3.3 Analysis of estimated biomass

Following the set-up of the field experiment, only five treatments were considered for the destructive biomass sampling ($n = 30$). Thus, the number of samples and averaged plant height values differ from the comparison shown in **Table 4-2**. On both farmer's fields, biomass was taken around all bamboo sticks (each $n = 24$). Mean value, standard deviation, minimum, and maximum were calculated for the plant height and dry biomass of all campaigns on each site (**Table 4-3**). The analysis of the mean plant heights can be summarized to: (I) the differences between the field experiment 2011 and village 69 are less than ~ 5 cm, (II) the data sets from the field experiment 2012 and village 36 show considerably larger differences with ~ 25 cm, (III) the difference between the data sets of the field experiment lies between ~ 10 cm and ~ 20 cm, (IV) comparing the farmer's fields, the difference increases over the growing season from ~ 2 cm to ~ 20 cm, and (V) the standard deviations within each campaign are almost similar and below ~ 5 cm, despite the results from village 36 with values between ~ 6 cm and ~ 8 cm.

Regarding the biomass measurements, comparative statements have to be limited, due to the interpolated values for the field experiment 2011. Nevertheless, the results can be

summed up as following: (I) all mean values are considerable higher for 2012, (II) the difference between the values of the field experiment 2011 and village 69 increases over time from less than 5% for the first campaign to ~40% and ~30% for the second and third campaign, respectively, (III) the difference between the values of the field experiment 2012 and village 36 is constantly less than 5% during the whole observation period, and (IV) the standard deviation is much higher for all measurements in 2012, ranging from ~75 g/m² to ~145 g/m², in contrast to ~15 g/m² to ~80 g/m² for the measurements in 2011.

Table 4-3. Mean CSM-derived plant heights and destructively measured biomass values of all sites (*n*: number of samples; \bar{x} : mean value; SD: standard deviation; min: minimum; max: maximum).

Site/ Date	n	Plant height from CSM (cm)				Biomass (g/m ²) ^a			
		\bar{x}	SD	min	max	\bar{x}	SD	min	max
Field experiment									
21.06.11	30	24.93	2.85	20.59	30.33	59.51	18.86	24.04	100.70
04.07.11	30	33.80	3.74	27.25	40.75	131.72	30.03	66.71	199.41
18.07.11	30	56.69	5.49	44.91	63.03	422.27	80.90	274.74	599.53
01.07.12	30	43.81	2.95	37.80	48.14	231.42	74.48	104.47	421.35
09.07.12	30	56.08	3.73	46.66	62.28	449.92	105.62	225.40	673.79
17.07.12	30	66.63	5.05	54.62	75.24	636.10	127.87	372.06	946.15
Village 69									
22.06.11	24	20.80	4.82	13.39	31.44	57.58	13.02	25.64	80.01
05.07.11	24	34.09	4.52	27.13	44.60	217.43	29.44	146.54	278.12
19.07.11	24	59.49	4.87	51.79	72.58	589.71	73.01	482.33	723.32
Village 36									
30.06.12	24	18.13	7.59	1.96	45.00	251.67	91.46	123.00	479.88
08.07.12	24	30.23	6.22	19.25	41.73	469.93	104.00	171.90	639.00
16.07.12	24	40.36	8.28	21.54	52.82	717.61	143.73	399.36	966.42

^a values for the field experiment 2011 are linearly interpolated from other dates.

The regression equations from the field experiment data were used to establish linear and exponential BRMs. Previously, the general concept was examined with trial BRMs, each achieved from two field experiment repetitions of one year, validated against the third repetition. **Table 4-4** shows the equations of the linear and exponential trial BRMs with the estimated and measured biomass values. In both years over- and underestimations occur, depending on the repetition combination and linear or exponential model. However, for the linear models the mean deviations of the estimated values from the actual measured values are small for 2011, less than 19% and very small for 2012, less than 1%. On the contrary, for 2011 the coefficients of determination (R^2) as well as the indices of agreement (*d*) between estimated and measured biomass values are higher and the root mean square error (RMSE) is lower. Similar R^2 and *d* values were achieved with the exponential models. Due to the log-transferred biomass values, the RMSE values cannot be directly compared. However, whereas the differences between estimated and measured values are much lower for 2011 (below 5%), they are slightly higher for 2012 (up to ~2.5%).

Table 4-4. Trial biomass regression models (BRMs) and validation of estimated against measured biomass (R^2 : coefficient of determination; d : index of agreement; RMSE: root mean square error).

Year/ Repetition	Trial BRMs ^a	Estimated repetition	Mean biomass (g/m ²)		Difference (%)	R^2	d	RMSE
			estimated	measured				
Linear								
2011								
1 & 2	$y = 11.06x - 211.23$	3	249.79	210.61	-18.60	0.92	0.96	61.54
1 & 3	$y = 11.12x - 237.97$	2	174.05	208.32	16.45	0.81	0.93	79.90
2 & 3	$y = 11.15x - 229.41$	1	189.38	194.56	2.66	0.88	0.97	52.90
2012								
1 & 2	$y = 14.33x - 379.96$	3	427.12	426.06	-0.25	0.72	0.91	93.27
1 & 3	$y = 14.87x - 413.65$	2	404.44	402.35	-0.52	0.55	0.85	125.13
2 & 3	$y = 14.36x - 379.12$	1	413.28	417.20	0.94	0.71	0.91	92.77
Exponential ^b								
2011								
1 & 2	$y = 0.06x + 2.76$	3	4.99	5.22	4.58	0.88	0.95	0.38
1 & 3	$y = 0.06x + 2.64$	2	5.01	4.83	-3.64	0.80	0.93	0.41
2 & 3	$y = 0.06x + 2.80$	1	4.91	5.05	2.91	0.91	0.97	0.30
2012								
1 & 2	$y = 0.04x + 3.79$	3	5.95	5.96	0.22	0.68	0.89	0.28
1 & 3	$y = 0.04x + 3.82$	2	5.88	6.02	2.44	0.58	0.82	0.36
2 & 3	$y = 0.04x + 3.67$	1	5.94	5.88	-1.03	0.72	0.91	0.25

^a x = plant height (cm); y = biomass (g/m²); ^b biomass values are natural log-transformed.

The final linear and exponential BRMs were established from the field experiment data sets for each year separately and for both years combined (**Table 4-5**). All values and the resulting regression lines are plotted in **Figure 4-7** for the linear and exponential models, the corresponding equations are given in **Table 4-5**. Strong coefficients of determination for all data sets prove the dependency of biomass on plant height during the regarded pre-anthesis period. Comparable results were achieved for linear (2011: $R^2 = 0.86$; 2012: $R^2 = 0.66$; combination: $R^2 = 0.81$) and exponential models (2011: $R^2 = 0.84$; 2012: $R^2 = 0.65$; combination: $R^2 = 0.84$). Each model was used for estimating the biomass of the buffer areas around the bamboo sticks on both farmer's fields based on the CSM-derived plant height. The reliability of the estimated values was validated against the measured biomass values. In **Table 4-5** the mean differences are given, averaged for each campaign and over all campaigns on each farmer's field. Further, the coefficient of determination (R^2), index of agreement (d), and root mean square error (RMSE) are given for each BRM. Generally, the estimations for village 69 are better overall, verifiable through smaller percentage deviations, higher R^2 and d as well as lower RMSE values for linear and exponential models. The differences between linear and exponential models for each site are small with slightly better R^2 values for the linear BRMs. Within each site, the three models yielded almost similar results. Regarding the BRMs of the single years, the linear function showed slightly lower percentage deviations with the data set from 2011, whereas the exponential with the one from 2012. For the combined data set, the linear model functioned slightly better than both single year BRMs, whereas with the exponential models it performed weaker.

Table 4-5. Biomass regression models (BRMs), derived from field experiment and validation of estimated against measured biomass for the farmer’s fields (R^2 : coefficient of determination; d : index of agreement; RMSE: root mean square error).

Site/ Data set	BRM ^a	Mean difference					R^2	d	RMSE
		per campaign (g/m ²)			all campaigns				
		1.	2.	3.	(g/m ²)	%			
Linear									
Village 69									
2011	$y = 11.06x - 224.18$	51.69	64.56	110.79	90.73	31.48	0.90	0.92	119.70
2012	$y = 14.51x - 390.58$	146.33	113.35	115.10	125.59	43.57	0.90	0.91	146.90
combination	$y = 12.37x - 273.19$	73.47	68.95	98.30	89.83	31.16	0.90	0.93	115.22
Village 36									
2011	$y = 11.06x - 224.18$	254.34	320.62	380.60	336.87	74.48	0.60	0.53	377.04
2012	$y = 14.51x - 390.58$	281.90	382.73	425.57	375.82	83.09	0.60	0.51	429.33
combination	$y = 12.37x - 273.19$	175.02	330.06	383.54	312.30	69.04	0.60	0.53	383.62
Exponential ^b									
Village 69									
2011	$y = 0.06x + 2.74$	0.04	0.59	0.32	0.23	4.35	0.85	0.95	0.46
2012	$y = 0.04x + 3.76$	-0.58	0.25	0.24	-0.03	-0.65	0.85	0.92	0.45
combination	$y = 0.05x + 2.95$	0.07	0.72	0.58	0.41	7.81	0.85	0.91	0.56
Village 36									
2011	$y = 0.06x + 2.74$	1.58	1.52	1.42	1.47	24.31	0.56	0.44	1.47
2012	$y = 0.04x + 3.76$	0.65	1.12	1.13	0.97	15.97	0.56	0.51	1.06
combination	$y = 0.05x + 2.95$	1.38	1.62	1.58	1.51	24.92	0.56	0.42	1.51

^a x = plant height (cm); y = biomass (g/m²); ^b biomass values are natural log-transformed.

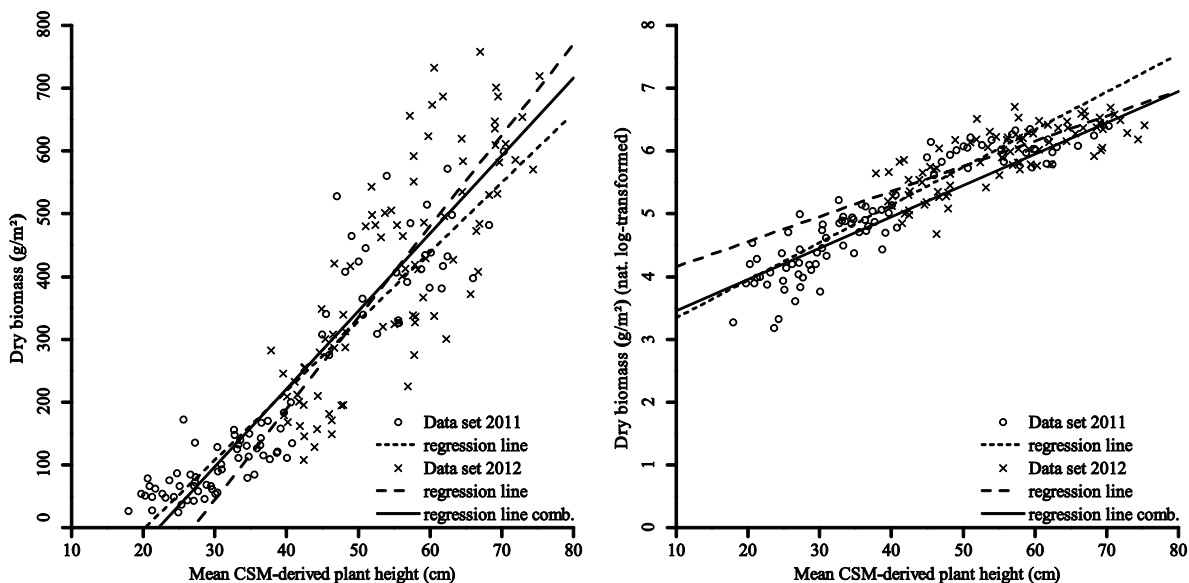


Figure 4-7. Linear (left) and exponential (right) regression between mean CSM-derived plant height and dry biomass for the field experiment of both years (each $n = 90$); regression equations are given in Table 4-5. Biomass values for the exponential regression are natural log-transformed.

4.4 Discussion

Overall, the acquisition with both laser scanners worked very well. The reliability of the devices was shown in earlier studies (Hoffmeister et al., 2010; Tilly et al., 2014, 2013). Due to the lightweight build-up and higher measurement rate the Riegl VZ-1000 is preferable to the Riegl LMS-Z420i, but was not available in 2012. As mentioned, alignment errors in the data sets from 2011 caused time-consuming post-processing. The positioning of additional reflectors was helpful for aligning the data sets from 2012 and led to better results, reflected

by the lower error after the whole alignment process. A further source of error in TLS measurements is noise in the point cloud, caused by reflections on rain, insects, or other small particles in the air. Due to the small size of the measured crops and uneven surfaces, this issue has to be regarded in particular for applications in agriculture, as also reported from other studies (Ehlert et al., 2009; Lumme et al., 2008). The measuring speed of the used time-of-flight scanners reduced the noise already and filter options in RiSCAN Pro simplified its removal, but further developments are desirable. In this context, intensity values should be investigated for establishing filtering schemes. So far, they are used for separating laser returns on canopy from ground returns (Guarnieri et al., 2012) or for detecting single plants (Hoffmeister et al., 2012; Höfle, 2014).

Regarding the practical implementation, this approach indicates advantages towards similar studies. Good results were achieved for estimating biomass of rice plants based on the vertical plant area density, measured with a portable scanner in combination with a mirror (Hosoi and Omasa, 2012). However, for the application on larger-scale fields their setup might be less practical. Through the non-invasive TLS acquisition from the edges of the field, undisturbed plant growth can be ensured and the scan positions with the tractor-trailer system profited from the greater height. As the linear structure of the rice plant rows is observable, a more precise acquisition of the crop surface can be assumed. Thus, lightweight scanners are desirable, which can easier be brought to a lifted position. Moreover, cost-effective systems like the Velodyne HDL-64E LiDAR sensor (Velodyne, 2014) and mobile laser scanning systems like the ibeo ALASCA XT (Jaakkola et al., 2010) should be considered for realizing practical applications of the presented approach for farmers.

Further, the oblique perspective of the scanner must be taken into account, which is unavoidable from a ground-based system without entering the field. Studies indicate that the height of reflection points might be overestimated through the influence of the scanning angle (Ehlert and Heisig, 2013). As the measured signal is influenced by the scanning geometry and beam divergence (Höfle, 2014; Kaasalainen et al., 2011), a radiometric calibration is supported for stationary TLS by other studies (Kaasalainen et al., 2011; Koenig et al., 2015). In this study, the merged and cleaned point clouds were filtered with a scheme for selecting maximum points. Hence, the crop surface was determined from an evenly distributed coverage of the field and overestimations should be precluded.

Manual measurements of plant height were conducted for validating the TLS data. However, therein differences between the measurement methods must be denoted. Whereas with less than ten hills per field experiment plot, only a small and mostly the highest part of the entire crop surface was considered for the manual measurements, the scanner captures the whole plot, including the lower parts. Hence, only plot-wise averaged values could be compared but the high R^2 values up to 0.91 between both measurements confirmed the accuracy of the TLS data. However, the approach of using the 90th percentile (Hämmerle and Höfle, 2014) instead of the maximum values for the CSM-based plant height calculation should be considered for achieving values which are more robust against low scanning resolutions. Generally, the precision of the TLS-derived CSMs is difficult to determine by the manual measurements due to these differences. The good performance of TLS measurements for

agricultural applications is presumed from other studies (Höfle, 2014; Lumme et al., 2008) and performance tests by the manufacturer validate the high accuracy and precision of the Riegl scanners (Riegl LMS GmbH, 2013, 2010). Nevertheless, a main advantage is the objective assessment of plant height by CSMs, which avoids the selection bias of manual measurements. The non-invasive acquisition of the whole area in a high spatial resolution is one of the main benefits of the presented approach. In the context of PA, this is required for accurate crop monitoring (Mulla, 2012).

Considering the upscaling of known plant information, the transferability of the virtually modeled geometry of single rice plants to field level might be evaluated with the high resolution CSMs (Ding et al., 2011; Watanabe et al., 2005). Referring to the model of predicting yield potential for rice (Confalonieri et al., 2011), the CSM-derived plant heights can be used as input data. Border effects cause problems in estimating rice yield, due to differences between internal and external rice plants in a plot (Wang et al., 2013). In this study, an inner buffer was used to avoid border effects. For further studies, the high resolution of the TLS-derived CSMs might be useful for determining the differences between internal and external rows.

The pixel-wise calculated plant heights were visualized in maps of plant height for discovering spatial or temporal patterns and variations. As shown in **Figure 4-5** the high resolution of 1 cm allowed an exact representation. In contrast, rice field mapping based on spaceborne data has not been carried out with resolutions finer than 1 m so far (Koppe et al., 2012; Lopez-Sanchez et al., 2011; Ribbes and Le Toan, 1999). However, new satellites like the WorldView-3 (DigitalGlobe, 2014), providing a panchromatic resolution of ~0.3 m, should enable a more detailed acquisition. The high resolution is one of the major advantages of TLS data and enables the usability as in-situ validation for spaceborne data. Although, the spatial extent of air- or spaceborne methods cannot be reached with ground-based methods and the data acquisition effort is high, they are more flexible for the application in the field. Consequently, the presented approach may offer a tool for comparative analyses between TLS and airborne laser scanning (ALS). As shown by Bendig et al. (2015) good results were achieved for the creation of CSMs from unmanned aerial vehicle (UAV)-based imaging for barley (R^2 up to 0.82 between CSM-derived and manually measured plant heights). Furthermore, promising results for the assessment of trees have already been achieved with UAV-based laser scanning systems (Jaakkola et al., 2010; Wallace et al., 2014). However, the influence of the oblique and nadir scanning perspectives of ground- and airborne measurements, respectively, have been less investigated so far. A comparative study on TLS and common plane-based ALS showed that the scanning angle and possible resolution influences the results (Luscombe et al., 2014). Therefore, multiple sensors and acquisition levels should be combined for comprehensive analyses.

For confirming the general validity of spatial plant height data as a non-destructive estimator for biomass of paddy rice and proving the robustness as well as the spatial and temporal transferability of all established models, destructive biomass sampling was performed on all sites, revealing differences between the fields (**Table 4-3**). Basic differences

were a lower human impact and larger size of the management units on the farmer's fields as well as the presence of different rice varieties and fertilizer treatments on all sites.

The three repetitions of each fertilizer treatment on the field experiment were useful to set up trial BRMs for proving the general concept (**Table 4-4**). High coefficients of determination and indices of agreement between the estimated and measured biomass values for each repetition of both years support linear and exponential models with comparable results. Nevertheless, further research is necessary for defining the differences between rice varieties and the influence of varying fertilizer treatments.

In addition to the final BRMs of each year, a model based on the combined data set of both years was established, each as a linear and an exponential model. The transferability of the BRMs from the small-scale field experiment for estimating biomass on larger scale farmer's fields was shown (**Table 4-5**). Besides the transferability of existing models, a model improvement through the combined data set and through additional exponential models was investigated. As shown in **Figure 4-7** for the data sets of the field experiment, the dependency of biomass on plant height can be described by linear and exponential regressions with similar high coefficients of determination. However, herein, only the pre-anthesis period was regarded. After anthesis, increasing biomass is mostly related to the development of grains while plant height remains almost constant. Thus, further studies are necessary for investigating the performance of linear and exponential BRMs for the estimation of rice biomass during the later stages.

The results of the linear and exponential models are almost similar for each site, with overall better values for village 69. As stated above the linear and exponential BRM yielded better results with the data sets from 2011 and 2012, respectively. A possible explanation might be the slightly different captured growth stages or the interpolated biomass values for 2011. Moreover, analyses are necessary, concerning the influence of different rice varieties, fertilizer treatments, or soil conditions. Additionally, the lower human impact on the farmer's fields might influence the plant development. For village 36 the heterogeneous plant development in the management units has to be stated as a source for the differences between estimated and measured values. The varying performance of the combined model might be caused by these differences. Of most importance might be the fact that the relation between plant height and biomass in the two regarded periods seems to be best represented by different models. Overall, the results support the applicability of BRMs for biomass estimations based on TLS-derived spatial plant height data and substantiate the potential of ground-based plant parameter measurements as input for biomass estimation models (Marshall and Thenkabail, 2015; Reddersen et al., 2014).

4.5 Conclusions

The applicability and high suitability of terrestrial laser scanning for monitoring plant height of paddy rice based on multi-temporal CSMs were confirmed. An outstanding feature is the objective assessment of the whole field in a very high spatial resolution. Moreover, as the scans are non-invasively acquired from the field edges, entering the rice paddies is avoided. By investigating a repeated field experiment and two farmer's conventionally managed fields in two years, varying patterns of plant development and growth were covered.

For PA, monitoring of plant parameters for adjusting site-specific fertilization is a major topic. Strong coefficients of determination between plant height and biomass show the applicability of spatial plant height data as a non-destructive estimator for biomass of rice plants. Based on the promising results of single year analyses (Tilly et al., 2014, 2013), in this contribution, the annual transferability of the BRMs and the applicability on different fields were regarded. Moreover, a model improvement through exponential models was examined. During the regarded pre-anthesis period, the linear and exponential models performed equally well. Further studies are necessary regarding a presumed differing performance during the later stages. However, the spatial and temporal transferability of the BRMs to a larger scale is supported by estimations of biomass on farmer's fields based on TLS-derived CSMs. High coefficients of determination and indices of agreement between estimated and measured values demonstrate the coherence of the results and prove the robustness of the method. Regarding the accuracy of the estimation, best results were achieved with different models, depending on the used data. Overall, higher R^2 values were achieved with the linear models, whereas the exponential models yielded smaller percentage deviations.

To summarize, the novelty in this contribution is the comparative analysis of linear and exponential models based on objectively assessed plant height as a reliable estimator for the biomass of paddy rice over different growing seasons and different fields. Further long-term experiments and comprehensive monitoring approaches are required for investigating the performance of linear and exponential models for the pre-anthesis and for later growing stages.

In the future, combined approaches involving plant height and spectral measurements should be developed for accurately determining the actual biomass and N content of plants. Following, spatially resolved NNI calculations could be executed for improving N management strategies (Yao et al., 2012). Thereby, over-fertilization could be reduced while keeping or enhancing the yield.

Acknowledgments

The accomplished field work was affiliated to the activities of the International Center for Agro-Informatics and Sustainable Development (ICASD). Founded in 2009 by the Department of Plant Nutrition of the China Agricultural University in Beijing and the Institute of Geography at the University of Cologne in Germany, ICASD is an open, international, and multidisciplinary cooperative research center (www.icasd.org).

We would like to thank all colleagues and student assistants for their great effort during the field work (Juliane Bendig, Simon Bennertz, Jonas Brands, Erik Boger, Martin Gnyp, Anne Henneken, and Maximilian Willkomm). Further we extend our thanks to Five Star Electronic Technologies (Beijing, China), the Qixing Research and Development Centre and the Jiansanjiang Agricultural Research Station (both located in Heilongjiang Province, China) for good cooperation as well as Riegl GmbH (Horn, Austria) for continuous support. This work was financially supported by the International Bureau of the German Federal Ministry of Education and Research (BMBF, project number 01DO12013) and the German Research Foundation (DFG, project number BA 2062/8-1).

Author Contributions

Nora Tilly with advice from Dirk Hoffmeister was responsible for the TLS measurements. The field experiment at the Keyansuo experimental station was carried out by Qiang Cao supervised by Yuxin Miao, who is scientific coordinator of the ICASD project, together with Victoria Lenz-Wiedemann. Nora Tilly carried out the post-processing and wrote this article, greatly supported by Dirk Hoffmeister and Victoria Lenz-Wiedemann. Georg Bareth directed the research and supervised the whole acquiring, analyzing, and writing process.

Conflicts of Interest

The authors declare no conflict of interest.

References

- Aasen, H., Gnyp, M.L., Miao, Y., Bareth, G., 2014. Automated hyperspectral vegetation index retrieval from multiple correlation matrices with HyperCor. *Photogramm. Eng. Remote Sens.* 80, 785–796. doi:10.14358/PERS.80.8.785
- Bendig, J., Yu, K., Aasen, H., Bolten, A., Bennertz, S., Broscheit, J., Gnyp, M.L., Bareth, G., 2015. Combining UAV-based plant height from crop surface models, visible, and near infrared vegetation indices for biomass monitoring in barley. *Int. J. Appl. Earth Obs. Geoinf.* 39, 79–87. doi:10.1016/j.jag.2015.02.012
- Besl, P.J., McKay, N.D., 1992. A Method for Registration of 3D Shapes. *IEEE Trans. Pattern Anal. Mach. Intell.* 14, 239–256. doi:10.1117/12.57955
- Cao, Q., Miao, Y., Wang, H., Huang, S., Cheng, S., Khosla, R., Jiang, R., 2013. Non-destructive estimation of rice plant nitrogen status with Crop Circle multispectral active canopy sensor. *F. Crop. Res.* 154, 133–144. doi:10.1016/j.fcr.2013.08.005
- Casanova, D., Epema, G.F., Goudriaan, J., 1998. Monitoring rice reflectance at field level for estimating biomass and LAI. *F. Crop. Res.* 55, 83–92. doi:10.1016/S0378-4290(97)00064-6
- Confalonieri, R., Bregaglio, S., Rosenmund, A.S., Acutis, M., Savin, I., 2011. A model for simulating the height of rice plants. *Eur. J. Agron.* 34, 20–25. doi:10.1016/j.eja.2010.09.003
- DigitalGlobe, 2014. Datasheet WorldView-3. https://www.digitalglobe.com/sites/default/files/DG_WorldView3_DS_forWeb_0.pdf
- Ding, W., Zhang, Y., Zhang, Q., Zhu, D., Chen, Q., 2011. Realistic Simulation of Rice Plant. *Rice Sci.* 18, 224–230. doi:10.1016/S1672-6308(11)60031-0
- Ding, Y., Chan, J.C.L., 2005. The East Asian summer monsoon: an overview. *Meteorol. Atmos. Phys.* 89, 117–142. doi:10.1007/s00703-005-0125-z
- Domrös, M., Gongbing, P., 1988. *The Climate of China*. Springer-Verlag, Berlin.
- Ehlert, D., Adamek, R., Horn, H.-J., 2009. Laser rangefinder-based measuring of crop biomass under field conditions. *Precis. Agric.* 10, 395–408. doi:10.1007/s11119-009-9114-4
- Ehlert, D., Heisig, M., 2013. Sources of angle-dependent errors in terrestrial laser scanner-based crop stand measurement. *Comput. Electron. Agric.* 93, 10–16. doi:10.1016/j.compag.2013.01.002
- Ehlert, D., Horn, H.-J., Adamek, R., 2008. Measuring crop biomass density by laser triangulation. *Comput. Electron. Agric.* 61, 117–125. doi:10.1016/j.compag.2007.09.013
- Eitel, J.U.H., Vierling, L.A., Long, D.S., Raymond Hunt, E., 2011. Early season remote sensing of wheat nitrogen status using a green scanning laser. *Agric. For. Meteorol.* 151, 1338–1345. doi:10.1016/j.agrformet.2011.05.015

- Elia, A., Conversa, G., 2012. Agronomic and physiological responses of a tomato crop to nitrogen input. *Eur. J. Agron.* 40, 64–74. doi:10.1016/j.eja.2012.02.001
- FAO, 2014. FAOSTAT. <http://faostat3.fao.org/faostat-gateway/go/to/home/E>
- Gao, J., Liu, Y., 2011. Climate warming and land use change in Heilongjiang Province, Northeast China. *Appl. Geogr.* 31, 476–482. doi:10.1016/j.apgeog.2010.11.005
- Gebbers, R., Ehler, D., Adamek, R., 2011. Rapid Mapping of the Leaf Area Index in Agricultural Crops. *Agron. J.* 103, 1532–1541. doi:10.2134/agronj2011.0201
- Gnyp, M.L., Yu, K., Aasen, H., Yao, Y., Huang, S., Miao, Y., Bareth, G., 2013. Analysis of crop reflectance for estimating biomass in rice canopies at different phenological stages. *Photogramm. - Fernerkundung - Geoinf.* 4, 351–365. doi:http://dx.doi.org/10.1127/1432-8364/2013/0182
- Greenwood, D.J., Gastal, F., Lemaire, G., Draycott, A., Millard, P., Neeteson, J.J., 1991. Growth rate and %N of field grown crops: Theory and experiments. *Ann. Bot.* 67, 181–190.
- Guarnieri, A., Pirotti, F., Vettore, A., 2012. Comparison of discrete return and waveform terrestrial laser scanning for dense vegetation filtering. *Int. Arch. Photogramm. Remote Sens. Spat. Inf. Sci.* 39 (Part B7) 511–516. doi:10.5194/isprsarchives-XXXIX-B7-511-2012
- Hair, J.F., Black, W.C., Babin, B.J., Anderson, R.E., 2010. *Multivariate Data Analysis*, 7th ed. Pearson, Upper Saddle River, N.J.
- Hämmerle, M., Höfle, B., 2014. Effects of Reduced Terrestrial LiDAR Point Density on High-Resolution Grain Crop Surface Models in Precision Agriculture. *Sensors* 14, 24212–24230. doi:10.3390/s141224212
- Hansen, P.M., Schjoerring, J.K., 2003. Reflectance measurement of canopy biomass and nitrogen status in wheat crops using normalized difference vegetation indices and partial least squares regression. *Remote Sens. Environ.* 86, 542–553. doi:10.1016/S0034-4257(03)00131-7
- Hoffmeister, D., Bolten, A., Curdt, C., Waldhoff, G., Bareth, G., 2010. High resolution Crop Surface Models (CSM) and Crop Volume Models (CVM) on field level by terrestrial laser scanning, in: Guo, H., Wang, C. (Eds.), *Proc. of SPIE, 6th International Symposium on Digital Earth*. Beijing, China. doi:10.1117/12.872315
- Hoffmeister, D., Tilly, N., Bendig, J., Curdt, C., Bareth, G., 2012. Detektion von Wachstumsvariabilität in vier Zuckerrübensorten, in: Clasen, M., Fröhlich, G., Bernhardt, H., Hildebrand, K., Theuvsen, B. (Eds.), *Informationstechnologie Für Eine Nachhaltige Landwirtschaft*, Proc. 32. GIL-Jahrestagung. Köllen Verlag, Bonn, Germany, Freising, pp. 135–138.
- Höfle, B., 2014. Radiometric Correction of Terrestrial LiDAR Point Cloud Data for Individual Maize Plant Detection. *Geosci. Remote Sens. Lett. IEEE* 11, 94–98. doi:10.1109/LGRS.2013.2247022
- Hosoi, F., Omasa, K., 2012. Estimation of vertical plant area density profiles in a rice canopy at different growth stages by high-resolution portable scanning lidar with a lightweight mirror. *ISPRS J. Photogramm. Remote Sens.* 74, 11–19. doi:10.1016/j.isprsjprs.2012.08.001
- Hosoi, F., Omasa, K., 2009. Estimating vertical plant area density profile and growth parameters of a wheat canopy at different growth stages using three-dimensional portable lidar imaging. *ISPRS J. Photogramm. Remote Sens.* 64, 151–158. doi:10.1016/j.isprsjprs.2008.09.003

- Jaakkola, A., Hyypä, J., Kukko, A., Yu, X., Kaartinen, H., Lehtomäki, M., Lin, Y., 2010. A low-cost multi-sensoral mobile mapping system and its feasibility for tree measurements. *ISPRS J. Photogramm. Remote Sens.* 65, 514–522. doi:10.1016/j.isprsjprs.2010.08.002
- Johnston, K., Ver Hoef, J.M., Krivoruchko, K., Lucas, N., 2001. Using ArcGIS Geostatistical Analyst. ESRI, USA.
- Kaasalainen, S., Jaakkola, A., Kaasalainen, M., Krooks, A., Kukko, A., 2011. Analysis of Incidence Angle and Distance Effects on Terrestrial Laser Scanner Intensity: Search for Correction Methods. *Remote Sens.* 3, 2207–2221. doi:10.3390/rs3102207
- Koenig, K., Höfle, B., Hämmerle, M., Jarmer, T., Siegmann, B., 2015. Comparative classification analysis of post-harvest growth detection from terrestrial LiDAR point clouds in precision agriculture. *ISPRS J. Photogramm. Remote Sens.* 104, 112–125. doi:10.1016/j.isprsjprs.2015.03.003
- Koppe, W., Gnyp, M.L., Hütt, C., Yao, Y., Miao, Y., Chen, X., Bareth, G., 2012. Rice monitoring with multi-temporal and dual-polarimetric TerraSAR-X data. *Int. J. Appl. Earth Obs. Geoinf.* 21, 568–576. doi:10.1016/j.jag.2012.07.016
- Lancashire, P.D., Bleiholder, H., van den Boom, T., Langelüddeke, P., Strauss, R., Weber, E., Witzemberger, A., 1991. A uniform decimal code for growth stages of crops and weeds. *Ann. Appl. Biol.* 119, 561–601. doi:10.1111/j.1744-7348.1991.tb04895.x
- Lee, W.S., Alchanatis, V., Yang, C., Hirafuji, M., Moshou, D., Li, C., 2010. Sensing technologies for precision specialty crop production. *Comput. Electron. Agric.* 74, 2–33. doi:10.1016/j.compag.2010.08.005
- Lemaire, G., Jeuffroy, M.-H., Gastal, F., 2008. Diagnosis tool for plant and crop N status in vegetative stage. *Eur. J. Agron.* 28, 614–624. doi:10.1016/j.eja.2008.01.005
- Li, W., Li, H., Zhao, L., 2011. Estimating Rice Yield by HJ-1A Satellite Images. *Rice Sci.* 18, 142–147. doi:10.1016/S1672-6308(11)60020-6
- Lopez-Sanchez, J.M., Ballester-Berman, J.D., Hajnsek, I., 2011. First Results of Rice Monitoring Practices in Spain by Means of Time Series of TerraSAR-X Dual-Pol Images. *IEEE J. Sel. Top. Appl. Earth Obs. Remote Sens.* 4, 412–422. doi:10.1109/JSTARS.2010.2047634
- Lumme, J., Karjalainen, M., Kaartinen, H., Kukko, A., Hyypä, J., Hyypä, H., Jaakkola, A., Kleemola, J., 2008. Terrestrial laser scanning of agricultural crops. *Int. Arch. Photogramm. Remote Sens. Spat. Inf. Sci.* 37 (Part B5) 563–566.
- Luscombe, D.J., Anderson, K., Gatis, N., Wetherelt, A., Grand-Clement, E., Brazier, R.E., 2014. What does airborne LiDAR really measure in upland ecosystems? *Ecohydrology* 8, 584–594. doi:10.1002/eco.1527
- Marshall, M., Thenkabail, P., 2015. Developing in situ Non-Destructive Estimates of Crop Biomass to Address Issues of Scale in Remote Sensing. *Remote Sens.* 7, 808–835. doi:10.3390/rs70100808
- Meier, U., 2001. Growth stages of mono- and dicotyledonous plants, 2nd ed. Blackwell, Berlin.
- Miao, Y., Stewart, B.A., Zhang, F., 2011. Long-term experiments for sustainable nutrient management in China. A review. *Agron. Sustain. Dev.* 31, 397–414. doi:10.1051/agro/2010034
- Mulla, D.J., 2012. Twenty five years of remote sensing in precision agriculture: Key advances and remaining knowledge gaps. *Biosyst. Eng.* 114, 358–371. doi:10.1016/j.biosystemseng.2012.08.009

- Ntanos, D.A., Koutroubas, S.D., 2002. Dry matter and N accumulation and translocation for Indica and Japonica rice under Mediterranean conditions. *F. Crop. Res.* 74, 93–101. doi:10.1016/S0378-4290(01)00203-9
- Oliver, M., 2013. An overview of precision agriculture, in: Oliver, M., Bishop, T., Marchant, B. (Eds.), *Precision Agriculture for Sustainability and Environmental Protection*. Springer, USA, pp. 3–19.
- Reddersen, B., Fricke, T., Wachendorf, M., 2014. A multi-sensor approach for predicting biomass of extensively managed grassland. *Comput. Electron. Agric.* 109, 247–260. doi:10.1016/j.compag.2014.10.011
- Ribbes, F., Le Toan, T., 1999. Rice field mapping and monitoring with RADARSAT data. *Int. J. Remote Sens.* 20, 745–765. doi:10.1080/014311699213172
- Riegl LMS GmbH, 2013. Datasheet Riegl VZ-1000. http://www.riegl.com/uploads/tx_pxpriegldownloads/DataSheet_VZ-1000_18-09-2013.pdf
- Riegl LMS GmbH, 2010. Datasheet Riegl LMS-Z420i. http://www.riegl.com/uploads/tx_pxpriegldownloads/10_DataSheet_Z420i_03-05-2010.pdf
- Roelcke, M., Han, Y., Schleef, K.H., Zhu, J.-G., Liu, G., Cai, Z.-C., Richter, J., 2004. Recent trends and recommendations for nitrogen fertilization in intensive agriculture in eastern China. *Pedosphere* 14, 449–460.
- Saeyes, W., Lenaerts, B., Craessaerts, G., De Baerdemaeker, J., 2009. Estimation of the crop density of small grains using LiDAR sensors. *Biosyst. Eng.* 102, 22–30. doi:10.1016/j.biosystemseng.2008.10.003
- Thenkabail, P.S., Smith, R.B., De Pauw, E., 2000. Hyperspectral Vegetation Indices and Their Relationships with Agricultural Crop Characteristics. *Remote Sens. Environ.* 71, 158–182. doi:10.1016/S0034-4257(99)00067-X
- Tilly, N., Hoffmeister, D., Cao, Q., Huang, S., Lenz-Wiedemann, V., Miao, Y., Bareth, G., 2014. Multitemporal crop surface models: accurate plant height measurement and biomass estimation with terrestrial laser scanning in paddy rice. *J. Appl. Remote Sens.* 8, 083671–1–22. doi:10.1117/1.JRS.8.083671
- Tilly, N., Hoffmeister, D., Cao, Q., Lenz-Wiedemann, V., Miao, Y., Bareth, G., 2013. Precise plant height monitoring and biomass estimation with Terrestrial Laser Scanning in paddy rice. *ISPRS Ann. Photogramm. Remote Sens. Spat. Inf. Sci.* II-5/W2, 295–300. doi:10.5194/isprsannals-II-5-W2-295-2013
- van Wart, J., Kersebaum, K.C., Peng, S., Milner, M., Cassman, K.G., 2013. Estimating crop yield potential at regional to national scales. *F. Crop. Res.* 143, 34–43. doi:10.1016/j.fcr.2012.11.018
- Velodyne, 2014. Velodyne HDL-64E User's Manual. http://www.velodynelidar.com/lidar/products/manual/63-HDL64E_S2_Manual_Rev_D_2011_web.pdf
- Wallace, L., Watson, C., Lucieer, A., 2014. Detecting pruning of individual stems using airborne laser scanning data captured from an Unmanned Aerial Vehicle. *Int. J. Appl. Earth Obs. Geoinf.* 30, 76–85. doi:10.1016/j.jag.2014.01.010
- Wang, K., Zhou, H., Wang, B., Jian, Z., Wang, F., Huang, J., Nie, L., Cui, K., Peng, S., 2013. Quantification of border effect on grain yield measurement of hybrid rice. *F. Crop. Res.* 141, 47–54. doi:10.1016/j.fcr.2012.11.012

- Watanabe, T., Hanan, J.S., Room, P.M., Hasegawa, T., Nakagawa, H., Takahashi, W., 2005. Rice morphogenesis and plant architecture: measurement, specification and the reconstruction of structural development by 3D architectural modelling. *Ann. Bot.* 95, 1131–1143. doi:10.1093/aob/mci136
- Willmott, C.J., 1981. On the validation of models. *Phys. Geogr.* 2, 184–194. doi:10.1080/02723646.1981.10642213
- Willmott, C.J., Wicks, D.E., 1980. An Empirical Method for the Spatial Interpolation of Monthly Precipitation within California. *Phys. Geogr.* 1, 59–73. doi:10.1080/02723646.1980.10642189
- Yang, X., Huang, J., Wu, Y., Wang, J., Wang, P., Wang, X., Huete, A.R., 2011. Estimating biophysical parameters of rice with remote sensing data using support vector machines. *Sci. China. Life Sci.* 54, 272–281. doi:10.1007/s11427-011-4135-4
- Yao, Y., Miao, Y., Huang, S., Gao, L., Ma, X., Zhao, G., Jiang, R., Chen, X., Zhang, F., Yu, K., Gnyp, M.L., Bareth, G., Liu, C., Zhao, L., Yang, W., Zhu, H., 2012. Active canopy sensor-based precision N management strategy for rice. *Agron. Sustain. Dev.* 32, 925–933. doi:10.1007/s13593-012-0094-9
- Zhang, L., Grift, T.E., 2012. A LIDAR-based crop height measurement system for *Miscanthus giganteus*. *Comput. Electron. Agric.* 85, 70–76. doi:10.1016/j.compag.2012.04.001
- © 2015 by the authors; licensee MDPI, Basel, Switzerland. This article is an open access article distributed under the terms and conditions of the Creative Commons Attribution license (<http://creativecommons.org/licenses/by/4.0/>).

5 Terrestrial laser scanning for plant height measurement and biomass estimation of maize

NORA TILLY^{1,*}, DIRK HOFFMEISTER¹, HENNING SCHIEDUNG², CHRISTOPH HÜTT¹, JONAS BRANDS¹,
GEORGE BARETH¹

Published in: The International Archives of the Photogrammetry, Remote Sensing
and Spatial Information Sciences, 2014, **XL-7**, 7p

Formatting and orthography of the manuscript is adapted to the dissertation style.

¹ Institute of Geography (GIS & Remote Sensing Group), University of Cologne, 50923
Cologne, Germany

² Institute of Crop Science and Resource Conservation, University of Bonn, 53121 Bonn,
Germany

* Corresponding author: Tel.: +49 221 470 6265, Fax: +49 221 470 8838,
Email: nora.tilly@uni-koeln.de

Abstract: Over the last decades, the role of remote sensing gained in importance for monitoring applications in precision agriculture. A key factor for assessing the development of crops during the growing period is the actual biomass. As non-destructive methods of directly measuring biomass do not exist, parameters like plant height are considered as estimators. In this contribution, first results of multi-temporal surveys on a maize field with a terrestrial laser scanner are shown. The achieved point clouds are interpolated to generate crop surface models (CSM) that represent the top canopy. These CSMs are used for visualizing the spatial distribution of plant height differences within the field and calculating plant height above ground with a high resolution of 1 cm. In addition, manual measurements of plant height were carried out corresponding to each TLS campaign to verify the results. The high coefficient of determination ($R^2 = 0.93$) between both measurement methods shows the applicability of the presented approach. The established regression model between CSM-derived plant height and destructively measured biomass shows a varying performance depending on the considered time frame during the growing period. This study shows that TLS is a suitable and promising method for measuring plant height of maize. Moreover, it shows the potential of plant height as a non-destructive estimator for biomass in the early growing period. However, challenges are the non-linear development of plant height and biomass over the whole growing period.

Keywords: TLS; multi-temporal; agriculture; crop; change detection; monitoring

5.1 Introduction

A major topic in the field of precision agriculture (PA) is the enhancement of crop management due to the constant or even decreasing cultivation area but concurrently growing world population (Oliver, 2013). Therefore an accurate determination of the crop status during the growing period is required. In the last decades, remote and proximal sensing methods are widely used for crop monitoring. Depending on the investigated parameters and

desired resolution various sensors and methods are applied. An overview is given in Mulla (2012).

Studies focusing on maize plants have a particular challenge in common. In contrast to other crops, tall maize plants with heights of about 3 m complicate ground-based nadir measurements. As demonstrated by Claverie et al. (2012), spectral satellite data has promising potential for large-scale crop monitoring and biomass estimation. However, ground-based observations are conducted to achieve a high resolution and thus enable the detection of in-field variability. Studies show the potential of passive hyperspectral hand-held sensors for biomass estimations (Osborne et al., 2002; Teal et al., 2006). Perbandt et al. (2010) compared nadir and off-nadir hyperspectral measurements and detected a significant influence of sensor height and measuring angle.

A major disadvantage of passive sensors is the dependency on solar radiation. By contrast, studies show that terrestrial laser scanning (TLS), as an active system, can be applied for agricultural purposes. Investigated plant parameters are plant height (Zhang and Grift, 2012), biomass (Ehlert et al., 2009, 2008; Keightley and Bawden, 2010), crop density (Hosoi and Omasa, 2012, 2009; Saeys et al., 2009), and leaf area index (Gebbers et al., 2011). As mentioned the large height of maize plants causes difficulties for ground-based system. Solely, Höfle (2014) used the measured intensity values from TLS for detecting single plants of maize.

In this contribution, the first results of multi-temporal surveys on a maize field with a TLS system are shown. The scanner was mounted on a cherry picker to reach a high position above the canopy. The TLS-derived point clouds are interpolated to generate crop surface models (CSM) that represent the top canopy. The concept of CSMs for determining plant height and estimating biomass was tested for sugar beet (Hoffmeister et al., 2013, 2010), barley (Tilly et al., 2014a) and paddy rice (Tilly et al., 2014b).

5.2 Methods

5.2.1 Data acquisition

In the growing period 2013, surveys were carried out on a maize field in Selhausen, about 40 km away from Cologne, Germany (N 50°52'5", E 6°27'11"). The field with a spatial extent of about 60 m by 160 m was chosen, due to heterogeneous soil conditions and thereby expected differences in plant development within the field. Six field campaigns were carried out between the 22nd of May and 24th of September 2013 for monitoring plant height. Thus, almost the whole growing period of maize is covered. For an accurate acquisition of the ground surface the first campaign was scheduled after sowing, before the plants are visible above ground. For all campaigns, the terrestrial laser scanner Riegl LMS-Z420i was used, which applies the time-of-flight method (Riegl LMS GmbH, 2010) (**Figure 5-1 a**). From the known position of the scanner, the position of targets is calculated by measuring the distance through the time shift between transmitting and receiving a pulsed signal and the respective direction. The laser beam is generated in the bottom of the device with a measurement rate of up to 11,000 points/sec. Parallel scan lines are achieved with a rotating multi-facet polygon mirror and the rotation of the scanners head. Thereby a wide field of view can be achieved, up to 80° in vertical and 360° in horizontal direction. Furthermore, a digital camera, Nikon D200, was

mounted on the laser scanner. From the recorded RGB-images, the point clouds recorded by the scanner can be colored and the corresponding surfaces can be textured.

The scanner was mounted on a cherry picker to achieve a high position above the canopy (**Figure 5-1 a**). The height of the sensor was about 8 m above ground. All positions of the scanner were measured with the highly accurate RTK-DGPS system Topcon HiPer Pro (Topcon Positioning Systems, 2006). The relative accuracy of this system is ~ 1 cm. Additional reference targets are required to enable a direct georeferencing in the post-processing. Therefore, highly reflective cylinders arranged on ranging poles were used, which can be easily detected by the laser scanner and their coordinates were measured with the RTK-DGPS system (**Figure 5-1 b**). In each campaign, the field was scanned from its four corners for achieving a uniform spatial resolution and lower shadowing effects. For all scans a resolution of 0.7 cm at a distance of 10 m was used.



Figure 5-1. a) TLS system (marked with arrow) mounted on a cherry picker; b) highly reflective cylinders arranged on ranging pole.

With exception of the first campaign, manual measurements of plant height and biomass were carried out, corresponding to the TLS measurements. Therefore twelve sample points, well distributed in the field, were marked in the first campaign and their positions were measured with the RTK-DGPS system. Hence, the manual and TLS measurements can be accurately linked. In each campaign, the heights of five plants per sample point were measured. In the last four campaigns, destructive sampling of biomass was performed.

Around each sample point, five plants were taken after the TLS and manual height measurements.

5.2.2 Data processing

The workflow for the post-processing can be divided in three main steps: (I) the registration and merging of all point clouds; (II) the extraction of the area of interest (AOI), both executed in Riegl's software RiSCAN Pro; (III) spatial analyses, conducted in ArcGIS Desktop 10 by Esri; and (IV) statistical analyses, calculated with Microsoft Excel 2013 and diagrams plotted in OriginPro 8.5 by OriginLab.

At first, the scan data from all campaigns and the GPS-derived coordinates were imported into one RiSCAN Pro project file. Based on the positions of the scanner and the reflectors, a direct georeferencing method was used for the registration of the scan positions. However, small alignment errors occur between the point clouds of one campaign and between different campaigns. Thus, a further adjustment was applied. RiSCAN Pro offers the Multi Station Adjustment, where the position and orientation of each scan position are modified in multiple iterations to get the best fitting result for all of them. The calculations are based on the iterative closest point (ICP) algorithm (Besl and McKay, 1992).

Following, all point clouds of one date were merged to one data set and the AOI was manually extracted. Moreover, points regarded as noise were removed, caused by reflections on insects or other small particles in the air. The crop surface was then determined from the data sets with a filtering scheme for selecting maximum points. Similar, for the data set of the first campaign a filtering scheme for selecting minimum points was used to extract ground points. Finally, the data sets were exported for the following analyses.

In ArcGIS Desktop 10, the exported point cloud data sets were interpolated with the inverse distance weighting (IDW) algorithm. For retaining the accuracy of measurements with a high density, this exact, deterministic algorithm is well suitable as measured values are retained at their sample location (Johnston et al., 2001). The result are raster data sets with a consistent spatial resolution of 1 cm, introduced by (Hoffmeister et al., 2010) as crop surface models (CSMs). For each date, the CSM represents the crop surface of the whole field in a high resolution. Hence, in-field variability can be spatially measured. A digital elevation model (DEM) is interpolated from the ground points of the first campaign as a common reference surface for the calculation of plant heights. By subtracting the DEM from a CSM, the actual plant height is calculated with the same spatial resolution. Likewise, by calculating the difference between two CSMs the plant growth can be spatially measured for the respective period of time. Herein, growth is defined as a temporal difference in height.

Furthermore, statistical analyses were performed, taking account of the manual measurements. For validating the TLS results, a common spatial base was required. Therefore, a circular buffer with a radius of 1 m was generated around each sample point, where the CSM-derived plant heights were averaged ($n = 12$). The manually measured plant heights and destructively taken biomass were also averaged for each sample point. Consequently, correlation and regression analyses were carried out to investigate the accuracy of the TLS results and examining the usability of plant height as predictor for biomass of maize.

5.3 Results

5.3.1 Spatial analysis

The TLS-derived point clouds were interpolated to generate a CSM of the whole maize field for each campaign. By subtracting the DEM from each CSM, the plant heights are calculated pixel-wise for the whole field and visualized as map of plant height for each campaign. Thus, spatial differences in plant height and their temporal development can be detected. As an example, **Figure 5-2** shows the maps of plant height for the whole field on the last campaign date and for the buffer area around sample point 5 on each date. Regarding the whole field, spatial patterns are observable. It has to be mentioned that the whole field was clipped with an inner buffer of 1 m for avoiding border effects. However, in particular in the corners such influences cannot be completely excluded and the south edge of the field seems to be more affected. Nevertheless, spatial patterns are noticeable. Lower plant height values are detectable (I) in a stripe of ~20 m at the west edge, (II) in an almost circular area with a diameter of ~15 m eastward of sample point 7, and (III) in a small area at the south edge between the sample points 10 and 11. Regarding the detailed view of the buffer area around sample point 5, the plant height increase between the campaigns is clearly detectable for the first half of the observation period. However, as also supported by the mean values, the plant height is almost constant from late July to the end of the observation period in late September.

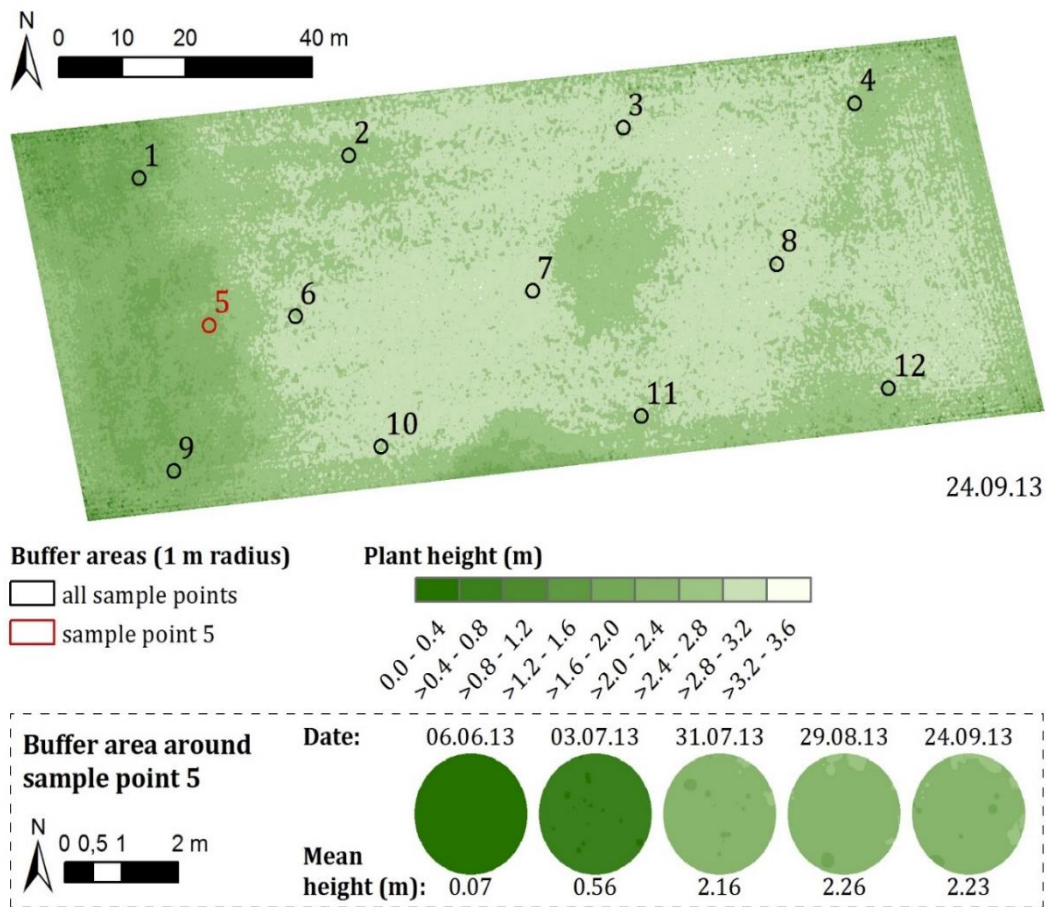


Figure 5-2. CSM-derived maps of plant height for the whole maize field on the last campaign date (top) and for the buffer area around sample point 5 on each date (bottom).

The spatial distribution of plant height differences between the campaigns is measured by subtracting the CSM of an earlier date from the CSM of a later date and visualized in maps of plant growth. In **Figure 5-3**, maps of plant growth are shown for two time periods. At the top, the plant growth between the 3rd and 31st of July and at the bottom between the 31st of July and the 24th of September are shown. Thereby the above stated results are supported. On the one hand, for the earlier period, the same spatial patterns with areas of lower plant growth are detectable at the west edge, in the almost circular area in the middle, and in the small area at the south edge. On the other hand, the temporal development, stated for the buffer area around sample point 5 is also observable. The main increase occurred in July with a mean plant growth of about 2 m for the whole field, whereas afterwards the plant heights are almost constant with a mean growth of 0.08 m for the whole field until the end of September.

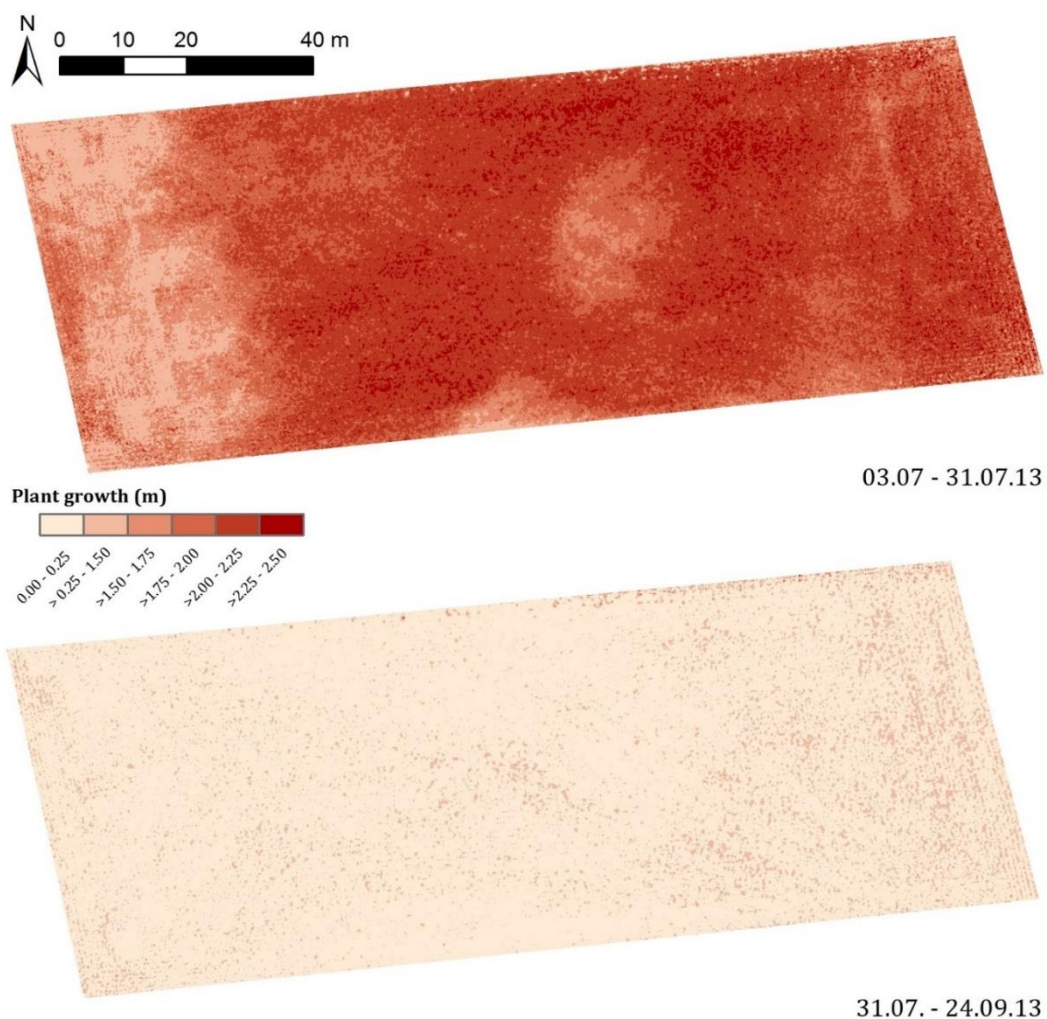


Figure 5-3. CSM-derived maps of plant growth for the whole maize field (at the top between 3rd and 31st of July; at the bottom between the 31st of July and the 24^h of September).

5.3.2 Statistical analysis

Besides the visualization of spatial patterns, the quantification of plant height differences and the correlation between plant height and biomass was an object of this study. The analyses are based on the averaged values, measured in the buffer areas around the sample points. **Table 5-1** gives the mean value (\bar{x}), standard deviation (s), minimum (\min), and

maximum (max) for the CSM-derived and manually measured plant heights, as well as for the destructively taken biomass. Regarding the plant height, the results of both measuring methods are similar. The differences can be summarized as: (I) except of the first campaign, the CSM-derived values are always a little higher, (II) the standard deviations are very similar, (III) in conformity with the mean values, the minimum and maximum values are mainly a bit lower for the CSM-derived values. As already stated for the maps of plant growth, the main increase occurred in July. Afterwards the plant heights are almost constant.

Table 5-1. CSM-derived and manually measured plant heights as well as destructively taken biomass, based on the averaged values for the buffer areas (each date $n = 12$).

Date	Plant height from CSM (m)				Manually measured plant height (m)				Dry biomass (g/sample point)			
	\bar{x}	s	min	max	\bar{x}	s	min	max	\bar{x}	s	min	max
06.06.13	0.07	0.02	0.05	0.14	0.04	0.01	0.03	0.05	N/A ^a	N/A ^a	N/A ^a	N/A ^a
03.07.13	0.60	0.10	0.38	0.72	0.82	0.11	0.60	0.96	13.08	4.05	5.90	18.40
31.07.13	2.56	0.32	1.99	2.84	2.68	0.32	2.10	2.98	783.00	243.79	475.95	1153.00
29.08.13	2.63	0.35	2.01	2.99	2.78	0.37	2.08	3.19	843.85	200.09	513.50	1188.80
24.09.13	2.59	0.35	1.96	2.97	2.71	0.38	1.94	3.15	1059.68	300.97	524.60	1435.90

^a No biomass sampling performed

Regarding the biomass, no comparative statements can be done. Nonetheless, it is noteworthy that in contrast to the almost constant plant height in the second half of the observation period, the biomass still increases. However, the main increase occurred in the first half, between the 3rd and 31st of July where the amount increased about 60 times. It has to be mentioned, that the values for the samples of the 31st of July are a little too high. Due to technical problems, some plants were not completely dry while weighing. Consequently the plants were heavier owing to the remaining water. As the problem could not be fixed and the amount of water could not be determined afterwards, the values were used for the analyses. Otherwise the time frame between the previous and following campaign would have been too long.

For validating the CSM-derived heights, regression analyses were carried out with the results of both measuring methods. **Figure 5-4** shows the related values of all campaigns ($n = 60$) and the resulting regression line with a very high coefficient of determination ($R^2 = 0.93$).

Moreover, regression analyses were carried out for investigating the dependence of the actual biomass from plant height. **Figure 5-5** shows the related values only for the last four campaigns, as no destructive sampling was performed on the 6th of June ($n = 48$). The regression lines and coefficients of determination were calculated for different periods. First, for the data set of the whole observation time, second and third, without the values of first or last campaign, respectively. As mentioned, the main increase took place between the first and second destructive biomass measurements. These clusters are visible in the scatterplot. A small cluster of values with plant heights between 0.5 and 1 m and a low degree of scattering in the biomass values and a larger cluster of values with plant heights between 2 and 3 m and a high degree of scattering in the biomass values. Following, the high coefficients of determination for the periods including the first destructive sampling ($R^2 = 0.70$ and $R^2 = 0.80$), have to be regarded as spurious correlations. Regarding the period excluding the first

measurements, any correlation is detectable ($R^2 = 0.03$). The uncertain values from the 31st of July have to be taken in to account.

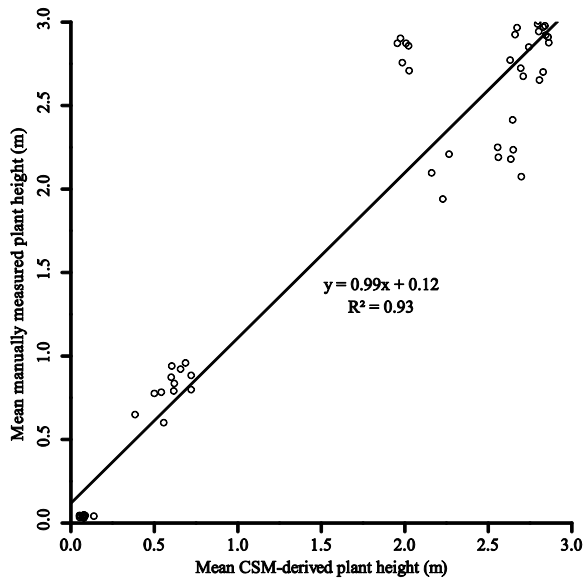


Figure 5-4. Regression of the mean CSM-derived and manually measured plant heights ($n = 60$).

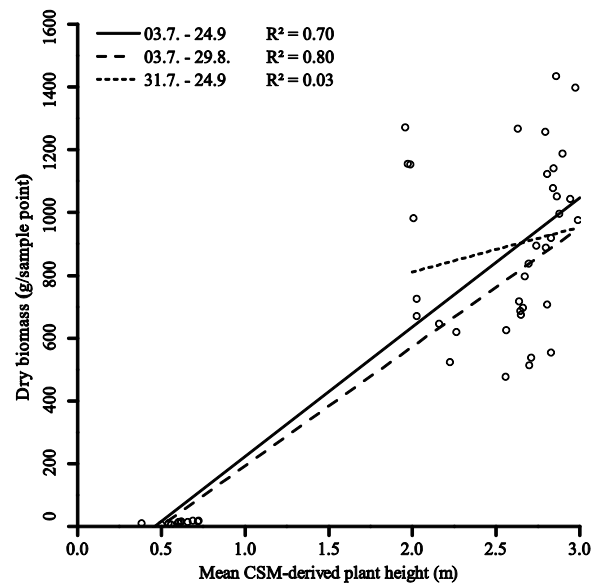


Figure 5-5. Regression of the mean CSM-derived plant height and the dry biomass ($n = 48$).

5.4 Discussion

The data acquisition with the laser scanner worked very well. As mentioned, the presented approach of generating CSMs was successfully applied with low growing crops like sugar beet (Hoffmeister et al., 2013, 2010), barley (Tilly et al., 2014a) and paddy rice (Tilly et al., 2014b). The height of tall maize plants is a challenge for ground-based measurements. In the study presented in this paper, the laser scanner was mounted on a cherry picker. Following, the sensor height of about 8 m above ground was helpful for reaching a position above the canopy. Obviously, this setup can hardly be implemented for realizing practical applications for farmers. However, as this was the first approach of determining maize plant height with TLS-derived CSMs, the preconditions ought to be comparable to earlier studies, like the relative height of the sensor above the canopy. Further studies are required regarding other platforms and acquisition methods.

An issue of TLS measurements with fixed scan positions at the edges of a field, is the radial measuring view of the scanner. Closer to the edges, the viewing perspective is steeper and allows a deeper penetration of the vegetation. Thus, also lower parts of the plants are captured. This influence of the scanning angles is also stated by Ehlert and Heisig (2013). However they detected overestimations in the height of reflection points. For the generation of the CSMs in this study, point clouds were merged from all positions of one campaign and a filtering scheme for selecting maximum points was used for determining the crop surface. Hence, it was determined from an evenly distributed coverage of the field with a mean point density of 11,000 points per m^2 . Nonetheless, further studies are required for analyzing the influence of the scanning angle.

Reconsidering alternative platforms for practical applications, ways of avoiding effects due to the radial measuring view should also be regarded. Promising systems are brought up

through recent developments in mobile laser scanning (MLS). Those systems apply a two-dimensional profiling scanners based on a moving ground vehicle for achieving an areal coverage. Conceivable MLS approaches are presented by Ehlert and Heisig (2013) and Kukko et al. (2012).

The high resolution and acquisition of the whole field, achievable with the TLS system, allow to calculate the plant heights pixel-wise and visualize them as maps of plant height for several steps in the growing period. Thus, spatial and temporal patterns and variations can be detected, as shown in **Figure 5-2**. Moreover, the plant growth between two campaigns can be calculated and visualized as maps of plant growth, as shown in **Figure 5-3**.

The very high coefficients of determination ($R^2 = 0.93$) and low differences between the mean CSM-derived and manually measured plant heights show the usability of the presented approach for determining maize plant height. Regarding the differences between the mean values (**Table 5-1**), the differences between the measuring methods are on source of error. Whereas the scanner captured the whole field, including lower parts of the canopy, only five plants per sample point were considered for the manual measurements, which represent the highest parts of the canopy. Thus, the manual measurements can solely be regarded as an indicator for the accuracy of the CSM-derived heights. Due to the high resolution of the scan data a more precise acquisition of the field can be assumed. However, as visible in **Figure 5-4** there is a data gap between heights of 1 m to 2 m. Due to technical problems, the measurements of one campaign in the middle of July could not be used for the analyses. Consequently, this period, with the main increase in plant height is not well covered with data. Further monitoring studies in the following years are necessary to fill this gap.

Furthermore, additional studies are required to enhance the knowledge about the correlation between plant height and biomass. Due to the unusable data set from the middle of July and the technical problems with drying some plants at the 31st of July, several uncertainties remain. As the main increase in plant height and biomass occurred in this period, more measurements are necessary for establishing a reliable regression model. Nevertheless, the results suggest a linear regression between plant height and biomass for the first half of the growing period. Furthermore, it has to be evaluated whether an exponential function can better model the increase of biomass while almost constant plant heights in the later growing period occur.

5.5 Conclusion and outlook

In summary, the main benefits of the TLS approach are the easily acquisition of a large area and the high resolution of the resulting data. In addition, applying the cherry picker to reach a high position above the canopy turns out to be useful in particular for large plants, like maize. Nevertheless, further research is required regarding the differences between CSM-derived and manually measured plant heights. Moreover, as also mentioned, further field studies are necessary to achieve more data for the period of main increase in plant height and biomass for investigating the applicability of plant height as an estimator for the actual biomass of maize. Challenges therein are the height differences within one CSM, in particular in the early stages, before the canopy closure and the non-linear development of plant height and biomass over the whole growing period.

References

- Besl, P.J., McKay, N.D., 1992. A Method for Registration of 3D Shapes. *IEEE Trans. Pattern Anal. Mach. Intell.* 14, 239–256. doi:10.1117/12.57955
- Claverie, M., Demarez, V., Duchemin, B., Hagolle, O., Ducrot, D., Marais-Sicre, C., Dejoux, J.-F., Huc, M., Keravec, P., Béziat, P., Fieuzal, R., Ceschia, E., Dedieu, G., 2012. Maize and sunflower biomass estimation in southwest France using high spatial and temporal resolution remote sensing data. *Remote Sens. Environ.* 124, 844–857. doi:10.1016/j.rse.2012.04.005
- Ehlert, D., Adamek, R., Horn, H.-J., 2009. Laser rangefinder-based measuring of crop biomass under field conditions. *Precis. Agric.* 10, 395–408. doi:10.1007/s11119-009-9114-4
- Ehlert, D., Heisig, M., 2013. Sources of angle-dependent errors in terrestrial laser scanner-based crop stand measurement. *Comput. Electron. Agric.* 93, 10–16. doi:10.1016/j.compag.2013.01.002
- Ehlert, D., Horn, H.-J., Adamek, R., 2008. Measuring crop biomass density by laser triangulation. *Comput. Electron. Agric.* 61, 117–125. doi:10.1016/j.compag.2007.09.013
- Gebbers, R., Ehlert, D., Adamek, R., 2011. Rapid Mapping of the Leaf Area Index in Agricultural Crops. *Agron. J.* 103, 1532–1541. doi:10.2134/agronj2011.0201
- Hoffmeister, D., Bolten, A., Curdt, C., Waldhoff, G., Bareth, G., 2010. High resolution Crop Surface Models (CSM) and Crop Volume Models (CVM) on field level by terrestrial laser scanning, in: Guo, H., Wang, C. (Eds.), *Proc. of SPIE, 6th International Symposium on Digital Earth*. Beijing, China. doi:10.1117/12.872315
- Hoffmeister, D., Waldhoff, G., Curdt, C., Tilly, N., Bendig, J., Bareth, G., 2013. Spatial variability detection of crop height in a single field by terrestrial laser scanning, in: Stafford, J. (Ed.), *Precision Agriculture '13 SE - 31*. Wageningen Academic Publishers, pp. 267–274. doi:10.3920/978-90-8686-778-3_31
- Höfle, B., 2014. Radiometric Correction of Terrestrial LiDAR Point Cloud Data for Individual Maize Plant Detection. *Geosci. Remote Sens. Lett. IEEE* 11, 94–98. doi:10.1109/LGRS.2013.2247022
- Hosoi, F., Omasa, K., 2012. Estimation of vertical plant area density profiles in a rice canopy at different growth stages by high-resolution portable scanning lidar with a lightweight mirror. *ISPRS J. Photogramm. Remote Sens.* 74, 11–19. doi:10.1016/j.isprsjprs.2012.08.001
- Hosoi, F., Omasa, K., 2009. Estimating vertical plant area density profile and growth parameters of a wheat canopy at different growth stages using three-dimensional portable lidar imaging. *ISPRS J. Photogramm. Remote Sens.* 64, 151–158. doi:10.1016/j.isprsjprs.2008.09.003
- Johnston, K., Ver Hoef, J.M., Krivoruchko, K., Lucas, N., 2001. *Using ArcGIS Geostatistical Analyst*. ESRI, USA.
- Keightley, K.E., Bawden, G.W., 2010. 3D volumetric modeling of grapevine biomass using Tripod LiDAR. *Comput. Electron. Agric.* 74, 305–312. doi:10.1016/j.compag.2010.09.005
- Kukko, A., Kaartinen, H., Hyypä, J., Chen, Y., 2012. Multiplatform Approach To Mobile Laser Scanning. *Int. Arch. Photogramm. Remote Sens. Spat. Inf. Sci.* 39 (Part B5) XXXIX-B5, 483–488. doi:10.5194/isprsarchives-XXXIX-B5-483-2012
- Mulla, D.J., 2012. Twenty five years of remote sensing in precision agriculture: Key advances and remaining knowledge gaps. *Biosyst. Eng.* 114, 358–371. doi:10.1016/j.biosystemseng.2012.08.009

- Oliver, M., 2013. An overview of precision agriculture, in: Oliver, M., Bishop, T., Marchant, B. (Eds.), *Precision Agriculture for Sustainability and Environmental Protection*. Springer, USA, pp. 3–19.
- Osborne, S.L., Schepers, J.S., Francis, D.D., Schlemmer, M.R., 2002. Use of Spectral Radiance to Estimate In-Season Biomass and Grain Yield in Nitrogen- and Water-Stressed Corn. *Crop Sci.* 42, 165–171. doi:10.2135/cropsci2002.0165
- Perbandt, D., Fricke, T., Wachendorf, M., 2010. Off-nadir hyperspectral measurements in maize to predict dry matter yield, protein content and metabolisable energy in total biomass. *Precis. Agric.* 12, 249–265. doi:10.1007/s11119-010-9175-4
- Riegl LMS GmbH, 2010. Datasheet Riegl LMS-Z420i. http://www.riegl.com/uploads/tx_pxpriegldownloads/10_DataSheet_Z420i_03-05-2010.pdf
- Saeyes, W., Lenaerts, B., Craessaerts, G., De Baerdemaeker, J., 2009. Estimation of the crop density of small grains using LiDAR sensors. *Biosyst. Eng.* 102, 22–30. doi:10.1016/j.biosystemseng.2008.10.003
- Teal, R.K., Tubana, B., Girma, K., Freeman, K.W., Arnall, D.B., Walsh, O., Raun, W.R., 2006. In-Season Prediction of Corn Grain Yield Potential Using Normalized Difference Vegetation Index. *Agron. J.* 98, 1488–1494. doi:10.2134/agronj2006.0103
- Tilly, N., Hoffmeister, D., Aasen, H., Brands, J., Bareth, G., 2014a. Multi-temporal Crop Surface Models derived from terrestrial laser scanning for accurate plant height measurement and biomass estimation of barley. *Kölner Geogr. Arb.* 94, 83–91. doi:10.5880/TR32DB.KGA94.12
- Tilly, N., Hoffmeister, D., Cao, Q., Huang, S., Lenz-Wiedemann, V., Miao, Y., Bareth, G., 2014b. Multitemporal crop surface models: accurate plant height measurement and biomass estimation with terrestrial laser scanning in paddy rice. *J. Appl. Remote Sens.* 8, 083671–1–22. doi:10.1117/1.JRS.8.083671
- Topcon Positioning Systems, I., 2006. HiPer Pro Operator's Manual. http://www.top-survey.com/top-survey/downloads/HiPerPro_om.pdf
- Zhang, L., Grift, T.E., 2012. A LIDAR-based crop height measurement system for *Miscanthus giganteus*. *Comput. Electron. Agric.* 85, 70–76. doi:10.1016/j.compag.2012.04.001

6 Fusion of Plant Height and Vegetation Indices for the Estimation of Barley Biomass

NORA TILLY^{1,*}, HELGE AASEN¹, GEORGE BARETH¹

Published in: Remote sensing 2015, **7**, 11449-11480

DOI: 10.3390/rs70911449

Formatting and orthography of the manuscript is adapted to the dissertation style.

¹ Institute of Geography (GIS & Remote Sensing Group), University of Cologne, 50923 Cologne, Germany

* Corresponding author: Tel.: +49 221 470 6265, Fax: +49 221 470 8838,
Email: nora.tilly@uni-koeln.de

Abstract: Plant biomass is an important parameter for crop management and yield estimation. However, since biomass cannot be determined non-destructively, other plant parameters are used for estimations. In this study, plant height and hyperspectral data were used for barley biomass estimations with bivariate and multivariate models. During three consecutive growing seasons a terrestrial laser scanner was used to establish crop surface models for a pixel-wise calculation of plant height and manual measurements of plant height confirmed the results (R^2 up to 0.98). Hyperspectral reflectance measurements were conducted with a field spectrometer and used for calculating six vegetation indices (VIs), which have been found to be related to biomass and LAI: GnyLi, NDVI, NRI, RDVI, REIP, and RGBVI. Furthermore, biomass samples were destructively taken on almost the same dates. Linear and exponential biomass regression models (BRMs) were established for evaluating plant height and VIs as estimators of fresh and dry biomass. Each BRM was established for the whole observed period and pre-anthesis, which is important for management decisions. Bivariate BRMs supported plant height as a strong estimator (R^2 up to 0.85), whereas BRMs based on individual VIs showed varying performances (R^2 : 0.07 - 0.87). Fused approaches, where plant height and one VI were used for establishing multivariate BRMs, yielded improvements in some cases (R^2 up to 0.89). Overall, this study reveals the potential of remotely sensed plant parameters for estimations of barley biomass. Moreover, it is a first step towards the fusion of 3D spatial and spectral measurements for improving non-destructive biomass estimations.

Keywords: terrestrial laser scanning; spectrometer; plant height; hyperspectral vegetation indices; biomass; precision agriculture; plot level; multi-temporal

6.1 Introduction

Over the past several decades remote sensing has increased in importance for precision agriculture (Atzberger, 2013; Liaghat and Balasundram, 2010; Mulla, 2012). Since the world population is expected to increase by more than one third until 2050 a main goal is shrinking the gap between potential and current yield (UNFPA, 2010; van Wart et al., 2013). Field management strategies in precision agriculture that aim to maximize yield must involve a reasonable use of natural resources and have to take spatial and temporal variabilities into account (Oliver, 2013), as agricultural production is influenced by the physical landscape,

climatic variables, and agricultural management practices (Atzberger, 2013). Studies reveal that grain yield is correlated with total biomass (Boukerrou and Rasmusson, 1990; Fischer, 1993). A quantitative measure is the harvest index, which expresses yield vs. total biomass (Price and Munns, 2010). Moreover, adequate crop condition in early growing stages could buffer the yield against environmental stresses, such as droughts, during later stages (Bidinger et al., 1977). In-season, the nitrogen nutrition index, the ratio between actual and critical nitrogen (N) content, is widely used as a measure of the plant status (Greenwood et al., 1991). The critical value is defined by a crop-specific N dilution curve, showing the relation between N concentration and biomass. Hence, an exact in-season acquisition of biomass is important in precision agriculture.

Since plant biomass cannot be determined non-destructively, other plant parameters are used as estimators. Therefore, remote sensing measurements enable an objective and accurate acquisition in a high temporal frequency (Atzberger, 2013). A review of remote sensing methods for assessing biomass is given by Ahamed et al. (2011). At the field level, ground-based methods are commonly used to achieve sufficiently high resolutions and over the last several decades, several studies investigated the relationship between spectral reflectance measurements and crop characteristics. For extracting information, various vegetation indices (VIs) were developed from the reflectance in determined wavelengths. Two band VIs like the normalized difference vegetation index (NDVI) were traditionally used with multispectral broad band systems to estimate biomass or biomass-related parameters, like LAI. Such VIs have been adapted to narrow band hyperspectral data and other band combinations (Aasen et al., 2014; Marshall and Thenkabail, 2015; Thenkabail et al., 2013, 2000). Additionally, other VIs with more than two bands, such as the GnyLi, have been developed for the same purpose (Gnyp et al., 2014b).

Moreover, active sensors based on light detection and ranging (LiDAR) have been increasingly used in vegetation studies since the 1980s (Lee et al., 2010). Indeed, a main benefit of LiDAR is the very high resolution, which enables the acquisition of complex canopies (Danson et al., 2009). In agricultural applications, for example, ground-based LiDAR methods, also known as terrestrial laser scanning (TLS), reveal potential for assessing plant height (Zhang and Grift, 2012), leaf area index (Gebbers et al., 2011), crop density (Hosoi and Omasa, 2012, 2009; Saeys et al., 2009), or post-harvest growth (Koenig et al., 2015). Furthermore, the potential for estimating biomass with TLS is supported through studies on small grain cereals (Ehlert et al., 2009, 2008; Lumme et al., 2008), sagebrush (Olsoy et al., 2014), and paddy rice (Tilly et al., 2015, 2014b). The 3D architecture of single plants was modeled under laboratory conditions (Paulus et al., 2014a, 2014b), however the transferability of those laboratory results to field conditions has not yet been shown.

Generally, the accuracy of estimations is a major issue, with the accuracy being limited when calculations are based on one estimator. Whilst biomass estimations based on VIs are affected by saturation effects (Blackburn, 1998; Reddersen et al., 2014; Thenkabail et al., 2000), plant height may reach limitations when differences in plant height are low. Consequently, the fusion of multiple parameters should be examined to enhance estimations. So far, studies on the fusion of spectral and non-spectral information have been

applied for characterization of forest ecosystems (Torabzadeh et al., 2014) and modeling of corn yield (Geipel et al., 2014). As both studies applied airborne methods, the spatial resolution was low. A ground-based multi-sensor approach for predicting biomass of grassland based on measurements of plant height, leaf area index (LAI), and spectral reflectance showed that combining multiple sensors can improve the estimation (Reddersen et al., 2014). However, in that study, spectral data were not well suited. Recently, the potential of the combined use of spectral and non-spectral ground-based measurements for estimating biomass was demonstrated for rice, maize, cotton, and alfalfa (Marshall and Thenkabail, 2015).

The overall aim of this study was to compare the potential of plant height (PH), VIs, and a fusion of PH and VIs for estimations of above ground fresh and dry barley biomass. More specifically, this study compares the potential of 3D spatial and spectral information for different time frames during the growing season and investigates if a fusion of both can improve the estimation. Therefore, a spring barley experiment was monitored during three growing seasons in various campaigns with a TLS system and a field spectrometer. PH was derived from the TLS data and VIs from the hyperspectral data. Four major working tasks were carried out: (I) conduct extensive multi-annual field measurements during the growing seasons, (II) derive bivariate biomass regression models (BRMs) from 3D spatial and spectral measurements for biomass estimations, (III) fuse the 3D spatial and spectral data in multivariate BRMs to estimate biomass based on this extensive data set, and (IV) evaluate the robustness of the BRMs with a cross-validation.

6.2 Methods

6.2.1 Field measurements

In three growing seasons (2012, 2013, and 2014), field experiments were carried out at the Campus Klein-Altendorf (50°37'51"N, E 6°59'32") belonging to the Faculty of Agriculture at the University of Bonn, Germany. Due to crop rotation, the locations of the fields were slightly different between the years. However, soil and climatic conditions were similar with the surface of the soil being flat with a clayey silt luvisol and well suited for crop cultivation (Uni Bonn, 2010a). According to the campus' own weather records, the long-term average yearly precipitation was about 600 mm with a daily average temperature of 9.3 °C (Uni Bonn, 2010b).

Each year, the field consisted of 36 small-scale plots (3 × 7 m) where different cultivars of barley were cultivated with two levels of N fertilization. For half of the plots, a farmer's common rate of 80 kg/ha N fertilizer was applied, for the other half a reduced rate of 40 kg/ha. In 2012 and 2013 each fertilization scheme was carried out once for 18 cultivars of spring barley (Barke, Wiebke, Beatrix, Eunova, Djamila, Streif, Ursa, Victoriana, Sissy, Perun, Apex, Isaria, Trumpf, Pflugs Intensiv, Heils Franken, Ackermanns Bavaria, Mauritia and Sebastian). In 2014, the set-up for the experiment was changed in that each fertilization scheme was repeated three times for six selected cultivars (Barke, Beatrix, Eunova, Trumpf, Mauritia and Sebastian). The experiments were carried out within the interdisciplinary research network CROP.SENSE.net (www.cropsense.uni-bonn.de). The research focus of this project was

non-destructive sensor-based methods for detecting crop status such as nutrients, stress, and quality.

In this study, 3D spatial measurements from a TLS system, spectral measurements from a field spectrometer, and manual reference measurements were used. Due to the weather conditions the time of seeding changed and therefore so did the start of the growing season. The seeding dates were 21 March 2012, 9 April 2013, and 13 March 2014. In **Table 6-1**, all dates of TLS and spectrometer campaigns are listed as day after seeding (DAS) and a universal scale, known as the BBCH scale, was used to describe phenological stages and steps in the plant development, encoded in a decimal code (Lancashire et al., 1991; Meier, 2001).

Table 6-1. Dates of the terrestrial laser scanning (TLS) and spectrometer (S) campaigns listed as day after seeding (DAS). Averaged codes for the developmental steps are given for the dates of manual plant parameter measurements (BBCH). For some dates BBCH codes were not determined (N/A).

DAS	2012		2013		2014		DAS	2012		2013		2014		DAS	2012		2013		2014	
	Sensor	BBCH	Sensor	BBCH	Sensor	BBCH		Sensor	BBCH	Sensor	BBCH	Sensor	BBCH		Sensor	BBCH	Sensor	BBCH	Sensor	BBCH
15					TLS		45						75	TLS						
16							46						76							
17							47						77							
18							48						78			TLS/S	57			
19							49			TLS/S	30		79							
20			TLS/S	N/A			50	TLS/S					80							
21							51						81							
22							52						82							S
23							53						83		N/A					
24							54		30			S	84	S					TLS	56
25							55						85							
26							56					TLS	31	86	TLS					
27							57						87							
28							58	TLS					88							
29							59						89							
30							60						90							
31							61						91				S	68		
32							62						92				TLS			
33							63						93							
34			TLS				64			TLS/S	41		94							
35			S	18			65						95							
36							66						96							74
37							67						97							TLS/S
38							68						98							
39							69						99							
40							70	S	49			TLS/S	49	100						
41					TLS/S	29	71						101							
42							72						102							
43		N/A					73						103							
44							74						104			TLS/S	81			

The acronym BBCH is derived from the funding organizations: Biologische Bundesanstalt (German Federal Biological Research Centre for Agriculture and Forestry), Bundessortenamt (German Federal Office of Plant Varieties), and Chemical industry. The first number of the two-digit code represents the principal growth stage (**Table 6-2**) and the second subdivides further in short developmental steps. Through determining the BBCH codes during the growing seasons, the annual comparability was ensured. For each plot, the BBCH

developmental step was determined as a mean of three plants. In **Table 6-1**, BBCH codes are given for the dates where plant parameters were manually measured. The codes are averaged per campaign, as the values were almost similar for all cultivars. Although the plant development varied among the years it can be seen that the BBCH codes indicate a comparable development.

Table 6-2. Principal growth stages of the BBCH scale.

Principal Growth Stage ^a	Stage Description	Time Frames Regarded for Biomass Estimation	
0	Germination		
1	Leaf development		
2	Tillering		
3	Stem elongation	Pre-	
4	Booting	anthesis	Whole
5	Inflorescence emergence, heading		observed
6	Flowering, anthesis		period
7	Development of fruit		
8	Ripening		
9	Senescence		

^a first number of the two-digit code.

As reference measurements, the heights of ten plants were measured for each plot and averaged in the post-processing. Moreover, in a defined sampling area of each plot, the above ground biomass of a 0.2 × 0.2 m area was destructively taken each time. The sampling area was neglected for the remote sensing measurements. In the laboratory, plants were cleaned and fresh weights were measured. After drying the samples for 120 h at 70 °C, dry biomass was weighted and extrapolated across the plot (g/m²).

Furthermore, a digital terrain model (DTM) is required as a common reference surface for calculating plant height from the TLS data. In 2014, the bare ground of the field was scanned after seeding but before any vegetation was visible (**Table 6-1**: DAS 15). For technical reasons, it was not possible to acquire such data in 2012 and 2013, however, the ground was identifiable in the point cloud of the first campaigns due to the low and less dense vegetation.

6.2.1.1 Terrestrial laser scanning

The TLS configuration and setup was almost equal in all years. Thus for each campaign, the time-of-flight scanner Riegl LMS-Z420i was used (**Figure 6-1 A**) (Riegl LMS GmbH, 2010). The sensor operates with a near-infrared laser beam, has a beam divergence of 0.25 mrad, and a measurement rate of up to 11,000 points/sec. In addition its field of view is up to 80° in the vertical and 360° in the horizontal direction and this study used resolutions between 0.034° and 0.046°. The digital camera Nikon D200 was mounted on the laser scanner and the TLS point clouds were colorized from the images captured. Furthermore the sensor should be as high as possible above ground, resulting in a steep angle between scanner and investigated area enabling the best possible coverage of the crop surface and a homogenous penetration of the vegetation. Accordingly the scanner was mounted on the hydraulic platform of a tractor, raising the sensor to approximately 4 m above ground (**Figure 6-1 B**). In order to lower shadowing effects and to attain an almost uniform spatial coverage, the field was scanned from its four corners. The coordinates of all scan positions and an additional target were required for the georeferencing and co-registration of the positions in the post-

processing. Highly reflective cylinders arranged on ranging poles were used as targets (**Figure 6-1 C**). These reflective cylinders can be easily detected by the scanner meaning their exact position in relation to the scan position can be measured (Hoffmeister et al., 2010). The coordinates of the scan positions and ranging poles were measured with the highly accurate RTK-DGPS system Topcon HiPer Pro (Topcon Positioning Systems, 2006). By establishing an own reference station each year, the precise merging of all data sets per year was ensured with the relative accuracy of this system being approximately 1 cm.

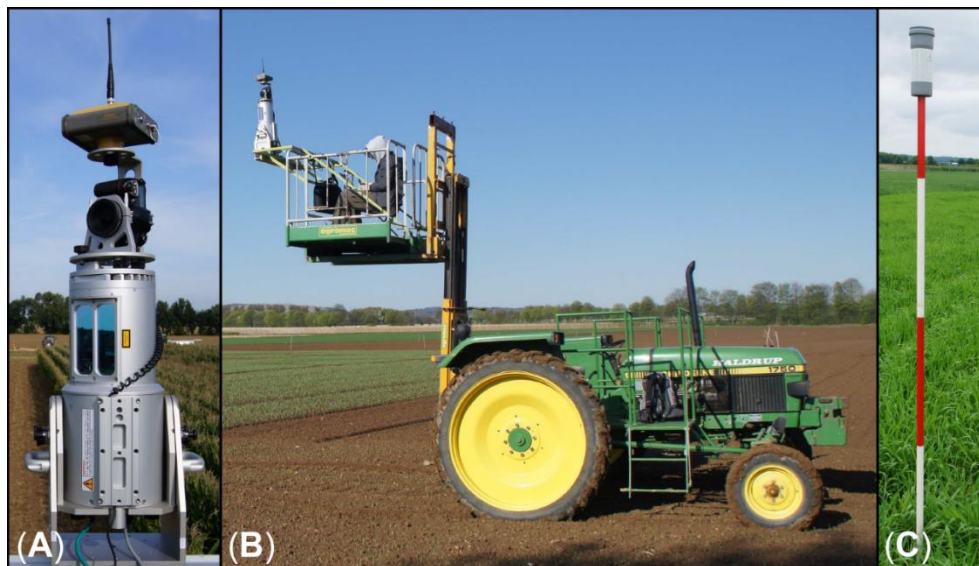


Figure 6-1. Instrumental set-up: (A) terrestrial laser scanner Riegl LMS-Z420i; (B) tractor with hydraulic platform; (C) ranging pole with reflective cylinder.

6.2.1.2 Field spectrometer measurements

The ASD[®] FieldSpec3 was used for measuring the reflectance several times during the growing seasons (all dates are listed in **Table 6-1** above). This spectrometer measures the incoming light from 350 to 2500 nm with a sampling interval of 1.4 nm in the VNIR (350 - 1000 nm) and 2 nm in the SWIR (1001 - 2500 nm). These measurements are resampled to spectra with 1 nm resolution by the manufacturer's software. At each position, ten measurements were taken and instantly averaged by the software, from 1 m above the canopy with a pistol grip, which was mounted on a cantilever to avoid shadows obscuring the sampling area. Additionally, a water level was used to ensure nadir view and no fore optic was used, resulting in a field of view of 25° and thus, a footprint area on the canopy with a radius of approximately 22 cm was achieved. Before the measurements, the spectrometer warmed up for at least 30 min and every 10 min or after illumination change, the spectrometer was optimized and calibrated with a spectralon calibration panel (polytetrafluoroethylene reference panel). Six positions were measured within each plot and for each position, the detector offset was corrected (Aasen et al., 2014). Then the six spectra were averaged, resulting in one spectrum per field plot, which was used in the further analysis.

6.2.2 Post-processing

6.2.2.1 TLS data

In the scanner software RiSCAN Pro, the DGPS data and the scans of all campaigns were imported into one project file per year. Based on the coordinates of the scan positions and reflectors, a direct georeferencing method was applied for the registration of all scan positions. However, a further adjustment was required due to small alignment errors between the point clouds. Based on the iterative closest point (ICP) algorithm (Besl and McKay, 1992), the Multi Station Adjustment in RiSCAN Pro allows the position and orientation of each scan position to be modified in multiple iterations and thus the best fitting result for all of them to be acquired. After optimizing the alignment with the ICP algorithm, the error, measured as standard deviation between used point-pairs, was 0.04 m on average for each campaign.

The point clouds were then merged to one dataset per campaign, and the area of interest was extracted. As reflections on insects or small particles in the air produced noise those points were manually removed. In addition a filtering scheme for selecting maximum points was used for determining the crop surface and in the same way, a filtering scheme for selecting minimum points was applied to extract ground points from the data sets of each first campaign. Finally, the data sets with XYZ coordinates of each point were exported.

The spatial analyses and visualization of the data were carried out in Esri ArcGIS Desktop 10.2.1. All point clouds were interpolated using the inverse distance weighting (IDW) algorithm, resulting in a raster with a consistent spatial resolution of 1 cm. IDW is an exact, deterministic algorithm that retains measured values at their sample location. The accuracy of measurements with a high density is maintained as all values are kept at their discrete location and not moved to fit the interpolation better (Johnston et al., 2001). As introduced by Hoffmeister et al. (2010), the created raster data sets are referred to as crop surface models (CSMs). Similarly, a digital terrain model (DTM) was generated from the ground points and by subtracting the DTM from a CSM, plant heights were calculated pixel-wise. Moreover, by calculating the difference between two CSMs, plant growth was spatially measured. Hereinafter, growth is defined as temporal difference in height (for a detailed description of the CSMs creation and the calculation of plant heights see Tilly et al. (2014b)). The raster data sets with pixel-wise stored plant heights and growth were visualized as maps of plant height and growth, respectively. Then the plant heights were averaged plot-wise, allowing a common spatial base with the other measurements to be attained. It should be noted that previously, each plot was clipped with an inner buffer of 0.5 m to prevent border effects.

6.2.2.2 Spectral data

For this study, established VIs were used to extract information from the hyperspectral data, measured with the field spectrometer. From the widespread of known hyper- and multispectral VIs for deriving different vegetation properties, six VIs were selected from the literature which have been found to be related to biomass and LAI. The selection was based on two criteria: Firstly, to make this study comparable to other studies VIs were selected which have been widely used in literature. Secondly, VIs with different spectral domains were used to examine if this would influence the prediction power of the fused models.

The NDVI was originally created for broad band satellite remote sensing (Rouse et al., 1974) and has been widely used in the literature. It has been adapted to hyperspectral narrow bands and was specified for sensors such as GreenSeeker™ and Crop Circle™ (Gnyp et al., 2014b). Several articles reported relationships between the NDVI and biomass or LAI. However, NDVI has been shown to saturate in cases of dense and multi-layered canopy (Thenkabail et al., 2000) and to have a non-linear relationship with biophysical parameters such as green LAI (Haboudane et al., 2004).

On this basis, Roujean and Breon (1995) developed the renormalized difference vegetation index (RDVI) for estimating the fraction of photosynthetically active radiation absorbed by vegetation, independent of a priori knowledge of the vegetation cover (Roujean and Breon, 1995). The RDVI showed strong relationships to LAI for different crops below an LAI of 5 (Broge and Leblanc, 2001; Haboudane et al., 2004). In dense crop canopies with an LAI above five, RDVI tended to overestimate the LAI (Haboudane et al., 2004). Simulations with the radiative transfer models PROSPECT and SAIL indicated that the RDVI is less affected by canopy structure, biochemistry, and soil background when estimating the LAI (Broge and Leblanc, 2001).

The red edge inflection point (REIP) was introduced by Guyot and Baret (1988). The REIP characterizes the inflection in the spectral red edge by calculating the wavelength with maximum slope. A variation of the inflection is mainly related to leaf chlorophyll content, leaf area index, and leaf inclination angle. Furthermore, soil reflectance and sun position have a limited effect (Guyot et al., 1992).

GnyLi is a four-band VI for estimating biomass in the NIR and SWIR domain (Gnyp et al., 2014b). This VI was developed for winter wheat and showed good performance on different scales from plot to regional level and across several growth stages (Gnyp et al., 2014b). The GnyLi considers the two reflectance maxima and minima between 800 and 1300 nm. While the high reflectance is caused by the plants intercellular structure, the absorption at the minima is caused by cellulose, starch lignin, and water. These components contribute substantially to dry and fresh biomass and combining the two products helps to avoid saturation problems—this is a major advantage of this VI.

Similar to the GnyLi, the normalized reflectance index (NRI) was also developed for estimating biomass in winter wheat. The NRI was empirically developed by combining the shape of the NDVI and the best two band combination for biomass estimation with EO-1 Hyperion satellite data (Koppe et al., 2010).

The red green blue vegetation index (RGBVI) was developed for estimating biomass based on bands available in a standard digital camera (Bendig et al., 2015). In this study, the RGB data was simulated from hyperspectral data where green, red, and blue values were calculated as the mean of the reflectance from 530 to 560 nm, 645 to 765 nm, and 465 to 495 nm, respectively. Thus, in contrast to other studies (Bareth et al., 2015; Bendig et al., 2015; Geipel et al., 2014), the RGBVI was derived from radiometrically and spectrally calibrated data.

The six VIs used in this study can be categorized by the wavelength domains that are used in their formula. The NDVI, RDVI, and REIP use wavelengths in the visible and near-infrared domain (VISNIR VIs), the GnyLi and NRI use wavelengths in the near-infrared domain (NIR VIs),

while the RGBVI uses wavelengths in the visible domain (VIS VI). The formulas of the VIs used in this study are given in **Table 6-3** (Bendig et al., 2015; Gnyp et al., 2014a; Guyot and Baret, 1988; Koppe et al., 2010; Roujean and Breon, 1995; Rouse et al., 1974).

Table 6-3. Vegetation indices used in this study.

Wave-length Domains	Vegetation Index	Formula	References
NIR	GnyLi	$(R900 \times R1050 - R955 \times R1220)/(R900 \times R1050 + R955 \times R1220)$	(Gnyp et al., 2014a)
	NRI	$(R874 - R1225)/(R874 + R1225)$	(Koppe et al., 2010)
VISNIR	NDVI	$(R798 - R670)/(R798 + R670)$	(Rouse et al., 1974)
	RDVI	$(R798 - R670)/(\sqrt{R798 + R670})$	(Roujean and Breon, 1995)
	REIP	$700 + 40 * \frac{(R670 + R780)/2 - R700}{R740 - R700}$	(Guyot and Baret, 1988)
VIS	RGBVI	$(R_{green}^2 - R_{blue} \times R_{red})/(R_{green}^2 + R_{blue} \times R_{red})$	(Bendig et al., 2015)

6.2.3 Biomass regression models

The main aim of this study was to establish biomass regression models (BRMs) and compare the potential of PH, VIs, and a fusion of PH and VIs for estimating barley biomass. The workflow for the BRM calibration and validation and the distinction of considered cases are shown in **Figure 6-2**. All calculations were performed in the R software environment (R Development Core Team, 2015). The measurements from 2012 were excluded because the spectral data set was inconsistent, since due to unsuitable weather, no spectral data or only data for less than half of the plots could be acquired corresponding to the second and fourth TLS campaign, respectively (**Table 6-1**). Furthermore, as mentioned above, the number of cultivars was reduced in 2014 so as a result only these six cultivars were used from the 2013 data set to ensure comparability.

The reduced data set was split into four subsets to obtain independent values for calibration and validation. The first subset contained the plot-wise averaged measurements of plant height, calculated VIs and destructively taken biomass from 2013 (n = 48). Each other subset contained the same measurements of one repetition from 2014 (each n = 60). Thus, each subset contained the measurements of each cultivar from one plot with low and one with high N fertilizer level for the given campaign dates. A cross-validation was performed using these data sets: For each run, one subset was excluded from the BRM calibration and used for validating the resulting BRM.

First, bivariate BRMs for fresh and dry biomass were developed based on the CSM-derived PH or one of the six VIs. Linear and exponential BRMs were established since no trend regarding their usability for biomass estimations based on PH was clearly identifiable in earlier studies (Tilly et al., 2015). However, the biomass accumulation during the vegetative phase is exponential and other studies have shown that it is best estimated with exponential models

(Aasen et al., 2014; Thenkabail et al., 2000). For the exponential BRMs, the fresh and dry biomass values were natural log-transformed. Each BRM was calculated for two time frames, the whole observed period from tillering (BBCH stage 2) till the end of fruit development (BBCH stage 7) and the pre-anthesis period (till BBCH stage 6) (**Table 6-2**).

The latter period is important as, for example, adequate crop conditions could buffer the grain yield against later environmental stress (Bidinger et al., 1977). Thus, campaign numbers 3 to 6 and 2 to 6 were considered for 2013 and 2014, respectively, whereas each final campaign was excluded for the pre-anthesis BRMs. Considering the four possible subset combinations, overall 224 bivariate BRMs were established. Second, multivariate BRMs were established based on PH fused with each VI. Since they were also established as linear and exponential BRMs for fresh and dry biomass for both time frames, the four possible subset combinations led to 192 multivariate BRMs in total.

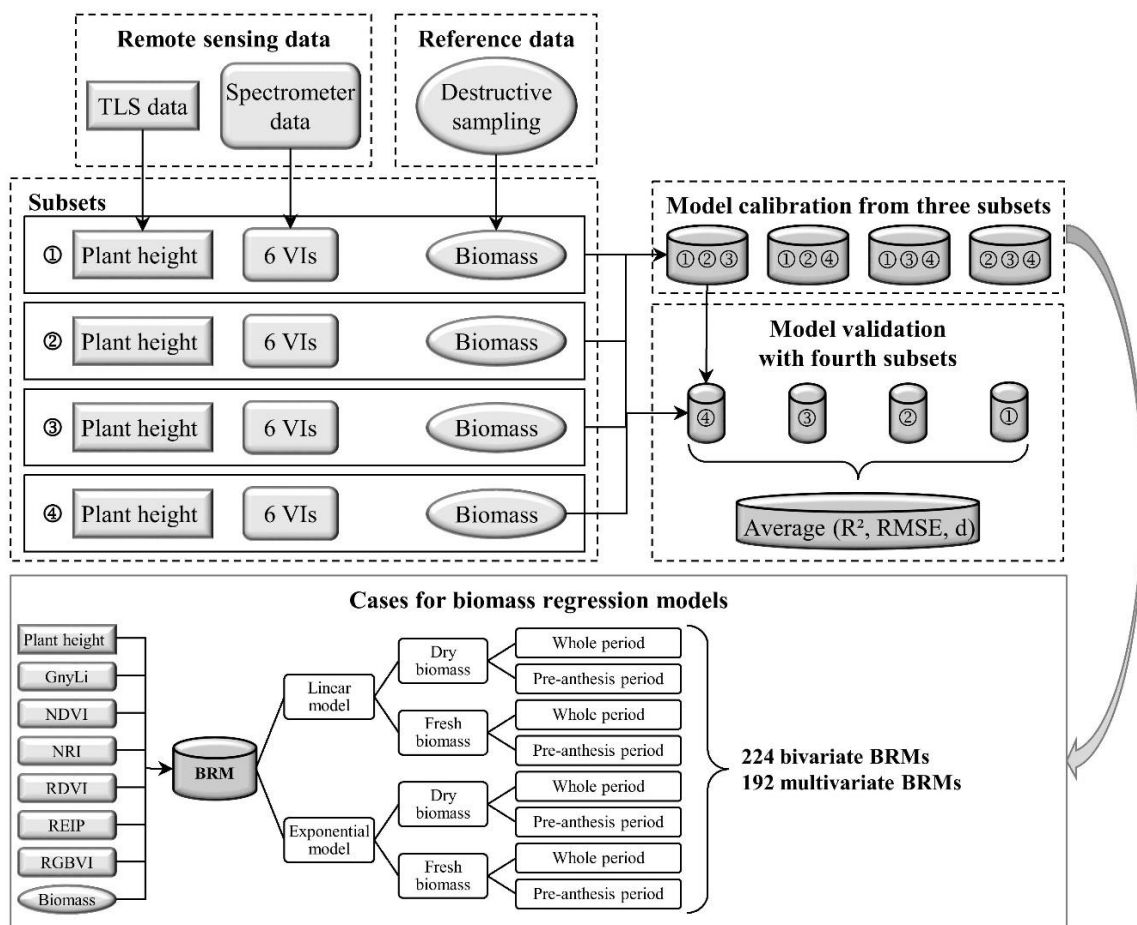


Figure 6-2. Workflow for the calibration and validation of the biomass regression models and distinction of cases for each model.

The calibration was evaluated by calculating the coefficient of determination (R^2) for PH or VI vs. measured biomass and the standard error of the estimate (SE_E) (Hair et al., 2010). For the validation, besides the R^2 (estimated vs. measured biomass), the root mean square error (RMSE), and Willmott’s index of agreement (d) (Willmott and Wicks, 1980; Willmott, 1981) were determined. For each case, the results from the four runs were averaged. Finally, the robustness of the BRMs was evaluated by calculating the ratio between the R^2 values of BRM calibration and validation.

6.3 Results

6.3.1 Acquired plant parameters

The TLS-derived point clouds were used to establish CSMs and spatially calculate plant height. Results of the pixel-wise calculation were visualized in maps of plant height for each plot. As an example for this, maps of four plots and corresponding mean heights are shown in **Figure 6-3** for the barley cultivar Trumpf. In the first campaign of 2013, plants were too small to obtain reasonable results. Thus, maps are presented for the last six and five campaigns of

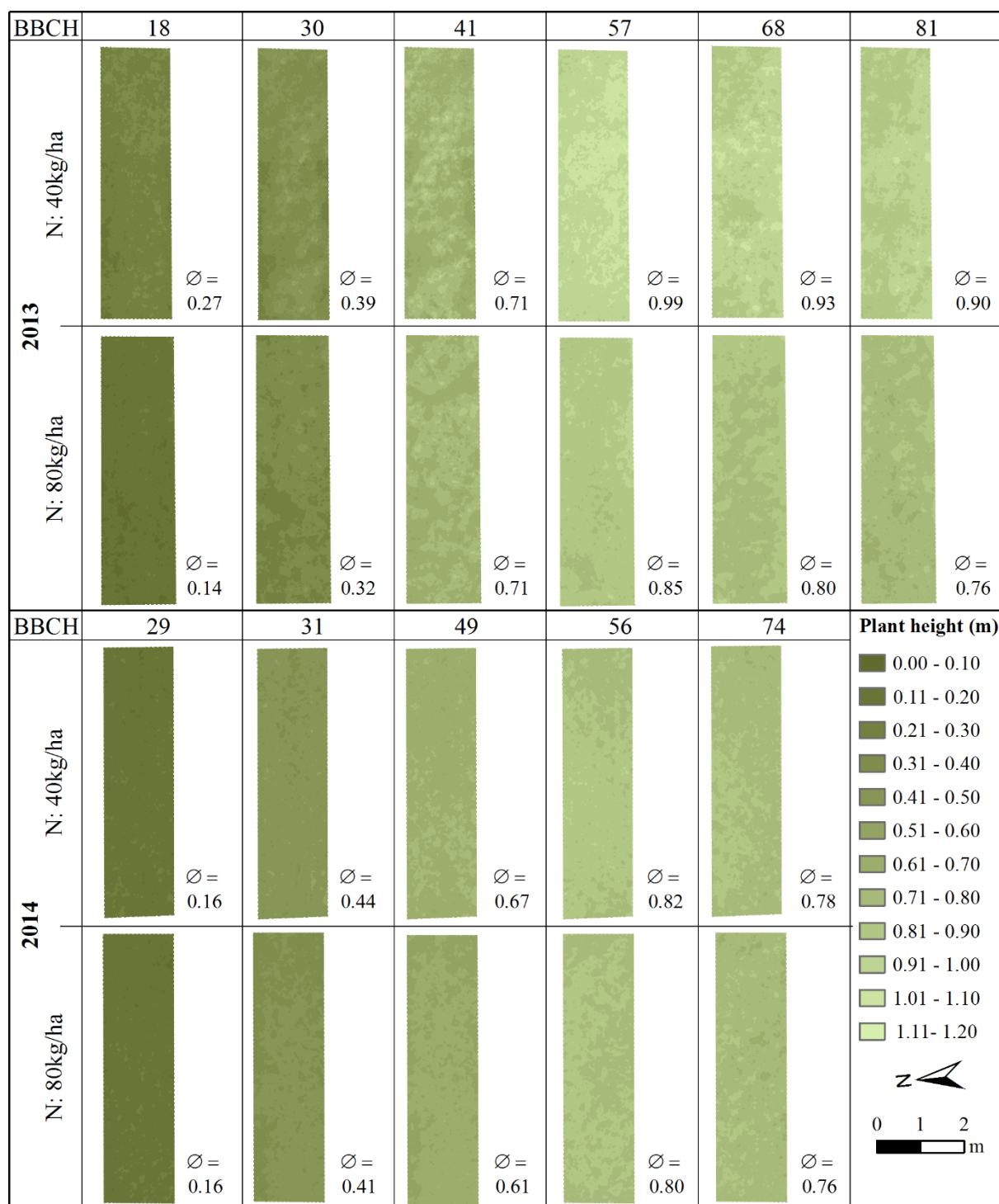


Figure 6-3. Maps of four plots from the last six and five campaigns of 2013 and 2014, respectively. One plot of each N fertilizer level of the barley cultivar Trumpf is shown for each year (\varnothing : Plot mean height).

2013 and 2014, respectively. One plot of each N fertilizer level is shown for both years. For the temporal development, an increase in plant height is observable until anthesis (BBCH stage 6) and afterwards, the development of ears begins and plant heights decrease due to the associated sinking of heads. Within all plots, the detailed representation of plant height is visible, which enables spatial differences in plant height to be detected. As a result, the exact calculation of mean heights can be assumed. A comparison of the plot-wise averaged values does not show that the fertilization rate directly influenced plant height.

The plot-wise averaged plant heights were used for statistical analysis and a comparison with the manual measurements. The linear regressions between all mean CSM-derived and manual measured plant heights for each of the three years is illustrated below in **Figure 6-4**. High coefficients of determination (R^2) confirm the TLS-derived results. The R^2 across all years is 0.92, yearly separated values are also given in **Figure 6-4**. Moreover, a varying scattering between the years is indicated. The scattering is the lowest in the 2014 data set, which is presumably caused by the reduced number of cultivars in 2014 and associated with more similar plant heights. **Table A 6-1** in the Appendix gives the mean, minimum, and maximum values of all plot-wise averaged values as well as the standard deviation per campaign of the CSM-derived and manual measured plant heights. Clearly observable lodging occurred in some plots between the second and third or fourth and fifth campaign in 2012 and 2013, respectively (for more details see Tilly et al. (2014a)). Those plots were neglected for the analysis and thus reduced the number of samples for the affected campaigns. As already stated for the visualized plots (**Figure 6-3**), an increase in plant height is detectable during pre-anthesis and a slight decrease is detectable afterwards. In addition, the difference

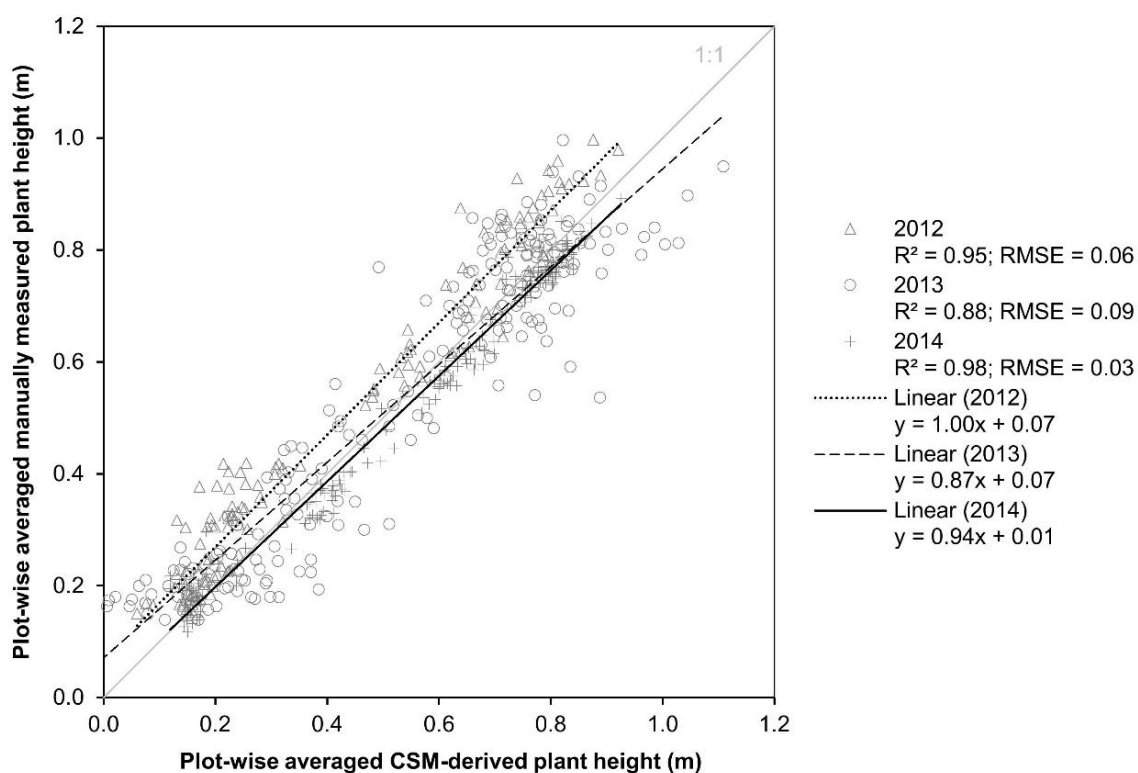


Figure 6-4. Regression of the mean CSM-derived and manual measured plant heights (2012: $n = 131$; 2013: $n = 196$; 2014: $n = 180$).

between the mean values of both measurement methods is lower than 10% for almost all campaigns.

The field spectrometer measurements were used for calculating the six VIs (GnyLi, NDVI, NRI, RDVI, REIP, and RGBVI). As the spectral measurements from 2012 were not usable for a linkage with the TLS data, only the data sets from 2013 to 2014 were used. Moreover, from the data set of 2013 only measurements of the cultivars selected in 2014 were considered and the data sets of plant height and biomass were accordingly adapted to ensure comparability. For each campaign, the values for both N fertilizer levels were averaged. **Table 6-4** shows the statistics for the reduced data sets of the nine regarded campaigns. Additionally, the yearly mean biomass values were calculated for the pre-anthesis and whole observed period, as reference for the later evaluation of the biomass estimation.

Table 6-4. Statistics for the plot-wise averaged CSM-derived plant heights and destructively taken biomass for the reduced data sets of 2013 and 2014 (*n*: number of samples; \bar{x} : mean value; min: minimum; max: maximum; SD: standard deviation).

	n	CSM-derived plant height (m)				Fresh biomass (g/m ²)				Dry biomass (g/m ²)			
		\bar{x}	min	max	SD	\bar{x}	min	max	SD	\bar{x}	min	max	SD
2013													
3	12	0.22	0.01	0.39	0.13	1282.92	491.00	2172.50	473.20	168.31	52.00	272.00	56.59
4	12	0.47	0.24	0.71	0.17	2891.54	1560.25	4465.50	806.12	415.31	205.00	725.00	146.02
5	12	0.78	0.58	0.99	0.13	5070.42	2668.75	7730.00	1561.62	883.38	434.50	1429.25	328.93
6	12	0.78	0.65	0.93	0.07	4631.73	2986.25	7655.75	1193.95	1258.88	886.75	1687.50	219.92
Mean pre-anthesis period					3081.63	1573.33	4789.33	946.98	489.00	230.50	808.75	177.18	
Mean whole observed period					3469.15	1926.56	5505.94	1008.72	681.47	394.56	1028.44	187.86	
2014													
2	36	0.17	0.12	0.25	0.03	656.28	266.25	1116.50	202.07	89.01	33.00	155.25	27.66
3	36	0.41	0.34	0.52	0.04	2227.08	1226.75	3236.50	531.72	289.83	165.75	417.75	66.03
4	36	0.63	0.53	0.70	0.04	2825.48	1643.75	4162.00	603.19	465.49	276.62	706.65	97.89
5	36	0.81	0.69	0.99	0.05	3185.13	2106.50	5433.25	687.74	777.23	486.35	1271.35	156.02
6	36	0.78	0.66	0.99	0.05	3569.34	1994.75	6044.00	898.59	1166.38	652.60	1876.35	276.46
Mean pre-anthesis period					2223.49	1310.81	3487.06	506.18	405.39	240.43	637.75	86.90	
Mean whole observed period					2492.66	1447.60	3998.45	584.66	557.59	322.86	885.47	124.81	

6.3.2 Biomass estimation

The barley biomass was estimated by establishing 224 bivariate and 192 multivariate biomass regression models (BRMs) based on plant height (PH) and vegetation indices (VIs). **Table 6-5** shows the statistical parameters for the BRM calibration. The table is vertically divided into bivariate or multivariate BRMs and the regarded time frames. Horizontally it distinguishes between dry or fresh biomass and linear or exponential BRMs. However, the results of the linear and exponential BRMs cannot be directly compared due to the log-transformation of biomass for the latter ones. Since the biomass accumulation during the vegetative phase is exponential and other studies have shown that it is best estimated with exponential BRMs (Aasen et al., 2014; Thenkabail et al., 2000) only the exponential BRMs are regarded in the following. For each model the coefficient of determination (R^2) and the standard error of the estimate (SE_E) are given as mean values of the four possible subset combinations.

Each established BRM was validated with the remaining fourth subsets. **Table 6-6** shows the R^2 , root mean square error (RMSE), and Willmott's index of agreement (d) for the model validation as mean values of the four subset combinations. The subdivision of the table is equivalent to that of **Table 6-5**. The results of the bivariate BRMs are regarded in the following subsection; the fusion of both plant parameters to multivariate BRMs is examined in the last subsection of this chapter. As the results of the calibration and validation show a similar tendency, only the values of the validation are stated. However, to evaluate the robustness of the BRMs, an overall comparison of differences between calibration and validation is given at the end of this chapter.

Table 6-5. Statistics for the model calibration as mean values of the four subset combinations (R^2 : coefficient of determination; SE_E : standard error of the estimate).

	Estimator	Bivariate BRMs				Multivariate BRMs					
		Whole period		Pre-anthesis		Whole period		Pre-anthesis		Estimator ^b	
		R^2	SE_E^a	R^2	SE_E^a	R^2	SE_E^a	R^2	SE_E^a		
Dry biomass	Linear	PH	0.65	10.03	0.76	5.73					
		GnyLi	0.52	11.75	0.68	6.67	GnyLi	0.65	34.63	0.77	25.41
		NDVI	0.07	16.38	0.34	9.56	NDVI	0.69	21.49	0.76	20.73
		NRI	0.54	11.58	0.70	6.40	NRI	0.65	35.04	0.77	24.86
		RDVI	0.13	15.87	0.39	9.21	RDVI	0.69	19.18	0.76	21.40
		REIP	0.12	15.92	0.58	7.60	REIP	0.73	1933.86	0.76	258.29
		RGBVI	0.05	16.55	0.26	10.10	RGBVI	0.68	22.28	0.76	23.23
	Exponential	PH	0.84	0.37	0.84	0.34					
		GnyLi	0.80	0.42	0.85	0.32	GnyLi	0.86	2.43	0.88	2.14
		NDVI	0.30	0.77	0.61	0.53	NDVI	0.85	2.84	0.88	3.99
		NRI	0.81	0.40	0.87	0.30	NRI	0.87	2.29	0.89	1.96
		RDVI	0.41	0.71	0.68	0.48	RDVI	0.85	2.52	0.88	2.84
		REIP	0.37	0.73	0.77	0.40	REIP	0.84	30.37	0.86	48.49
		RGBVI	0.23	0.81	0.48	0.60	RGBVI	0.85	2.51	0.87	2.73
Fresh biomass	Linear	PH	0.59	901.99	0.60	843.32					
		GnyLi	0.58	913.81	0.62	829.48	GnyLi	0.62	3295.30	0.64	2968.91
		NDVI	0.25	1222.39	0.42	1022.79	NDVI	0.60	4561.69	0.63	5008.60
		NRI	0.59	909.94	0.62	821.35	NRI	0.62	3056.34	0.64	2718.09
		RDVI	0.35	1143.49	0.50	945.26	RDVI	0.61	3813.94	0.64	3955.80
		REIP	0.30	1180.82	0.55	894.62	REIP	0.60	14599.87	0.63	59169.39
		RGBVI	0.22	1243.84	0.37	1066.53	RGBVI	0.61	4007.93	0.64	3881.46
	Exponential	PH	0.70	0.37	0.68	0.39	PH				
		GnyLi	0.76	0.33	0.76	0.34	GnyLi	0.77	1.87	0.77	1.77
		NDVI	0.46	0.50	0.65	0.41	NDVI	0.77	3.74	0.79	4.30
		NRI	0.77	0.33	0.77	0.33	NRI	0.77	1.67	0.77	1.56
		RDVI	0.59	0.43	0.74	0.35	RDVI	0.79	2.69	0.82	2.89
		REIP	0.47	0.49	0.71	0.37	REIP	0.72	22.27	0.74	73.05
		RGBVI	0.38	0.53	0.55	0.47	RGBVI	0.77	2.58	0.78	2.68

^a The SE_E for exponential models is calculated from natural log-transformed biomass values; ^b each fused with PH.

Table 6-6. Statistics for the model validation as mean values of the four subset combinations (R^2 : coefficient of determination; RMSE: root mean square error (g/m^2); d: Willmott's index of agreement).

	Estimator	Bivariate BRMs						Multivariate BRMs							
		Whole period			Pre-anthesis			Whole period			Pre-anthesis				
		R^2	RMSE ^a	d	R^2	RMSE ^a	d	R^2	RMSE ^a	d	R^2	RMSE ^a	d		
Dry biomass	Linear	PH	0.66	257.57	0.88	0.80	147.75	0.92							
		GnyLi	0.54	299.67	0.81	0.72	173.31	0.88	GnyLi	0.65	262.19	0.88	0.79	148.20	0.92
		NDVI	0.07	412.70	0.33	0.38	244.47	0.64	NDVI	0.71	250.35	0.89	0.80	148.32	0.92
		NRI	0.55	295.41	0.82	0.74	166.41	0.89	NRI	0.66	261.77	0.88	0.80	147.67	0.92
		RDVI	0.13	400.36	0.44	0.41	233.53	0.71	RDVI	0.72	247.16	0.89	0.80	148.27	0.92
		REIP	0.15	404.95	0.46	0.68	197.50	0.83	REIP	0.73	228.46	0.91	0.80	147.88	0.92
		RGBVI	0.04	416.42	0.26	0.28	254.41	0.58	RGBVI	0.70	261.30	0.88	0.80	149.33	0.92
	Exponential	PH	0.85	0.39	0.95	0.85	0.36	0.95							
		GnyLi	0.80	0.42	0.94	0.86	0.33	0.95	GnyLi	0.87	0.36	0.96	0.89	0.31	0.96
		NDVI	0.29	0.77	0.63	0.59	0.54	0.81	NDVI	0.85	0.38	0.95	0.87	0.30	0.96
		NRI	0.81	0.40	0.94	0.87	0.31	0.96	NRI	0.87	0.36	0.96	0.89	0.29	0.96
		RDVI	0.40	0.71	0.73	0.66	0.48	0.87	RDVI	0.85	0.38	0.95	0.88	0.30	0.96
		REIP	0.40	0.75	0.72	0.82	0.43	0.90	REIP	0.85	0.39	0.95	0.89	0.34	0.95
		RGBVI	0.22	0.82	0.55	0.48	0.62	0.75	RGBVI	0.85	0.38	0.95	0.86	0.31	0.96
Fresh biomass	Linear	PH	0.67	963.45	0.84	0.70	892.55	0.85							
		GnyLi	0.65	970.70	0.83	0.72	886.24	0.84	GnyLi	0.69	939.84	0.85	0.74	861.73	0.86
		NDVI	0.27	1254.02	0.58	0.51	1053.83	0.70	NDVI	0.67	952.58	0.84	0.73	862.84	0.85
		NRI	0.65	962.49	0.83	0.72	873.75	0.85	NRI	0.69	938.46	0.85	0.74	857.99	0.86
		RDVI	0.38	1175.32	0.67	0.59	964.42	0.77	RDVI	0.68	943.96	0.85	0.74	841.36	0.86
		REIP	0.41	1244.11	0.66	0.77	951.74	0.81	REIP	0.67	966.67	0.84	0.77	908.74	0.84
		RGBVI	0.21	1260.32	0.53	0.41	1066.26	0.67	RGBVI	0.66	948.90	0.85	0.71	852.97	0.86
	Exponential	PH	0.73	0.40	0.89	0.71	0.42	0.88							
		GnyLi	0.78	0.35	0.92	0.79	0.36	0.91	GnyLi	0.79	0.34	0.92	0.80	0.36	0.92
		NDVI	0.44	0.51	0.73	0.64	0.42	0.83	NDVI	0.78	0.34	0.92	0.79	0.34	0.92
		NRI	0.77	0.34	0.92	0.79	0.35	0.92	NRI	0.79	0.34	0.92	0.79	0.35	0.92
		RDVI	0.57	0.44	0.82	0.73	0.36	0.89	RDVI	0.80	0.33	0.93	0.83	0.31	0.93
		REIP	0.54	0.53	0.77	0.82	0.42	0.87	REIP	0.77	0.39	0.90	0.82	0.40	0.88
		RGBVI	0.36	0.54	0.68	0.53	0.47	0.78	RGBVI	0.76	0.34	0.92	0.76	0.34	0.92

^a The RMSE for exponential models is calculated from natural log-transformed biomass values; ^b each fused with PH.

6.3.2.1 Bivariate models

All cases show moderate to good results for bivariate BRMs based on PH. For each time frame, PH shows the same and similar relationship with dry and fresh biomass, respectively (**Table 6-6**). Scatterplots of measured vs. estimated biomass for selected examples are shown in the last subsection in comparison with multivariate BRMs.

Most VIs lead to better results for pre-anthesis than for the whole observed period. For dry biomass, the RGBVI performs worst for both time frames (**Table 6-6**, top left quarter). The largest difference between the whole observed period and the pre-anthesis can be found for the NDVI ($R^2 = 0.29$ vs. 0.59), while the NIR VIs as the GnyLi perform more consistently ($R^2 = 0.80$ vs. 0.86). Both, the NRI and the GnyLi also reveal best results for pre-anthesis ($R^2 = 0.87$, 0.86) and for the whole observed period ($R^2 = 0.81$, 0.80). In pre-anthesis, the relative difference between the NIR VIs and VISNIR VIs is smaller. **Figure 6-5** shows scatterplots of measured vs. estimated dry biomass of one validation dataset for selected VIs and as expected from the high R^2 values, the estimated biomass from the GnyLi BRM corresponds well with the measured biomass (close to the 1:1 line). In pre-anthesis, the same applies the REIP whereas the NDVI and RGBVI saturate at about $185 g/m^2$. For the whole

observed period, biomass estimated by the BRM of REIP, NDVI and RGBVI does not align well with what was measured. The scatterplots reveal that the dynamic range of the models does not cover the range of the measured biomass values.

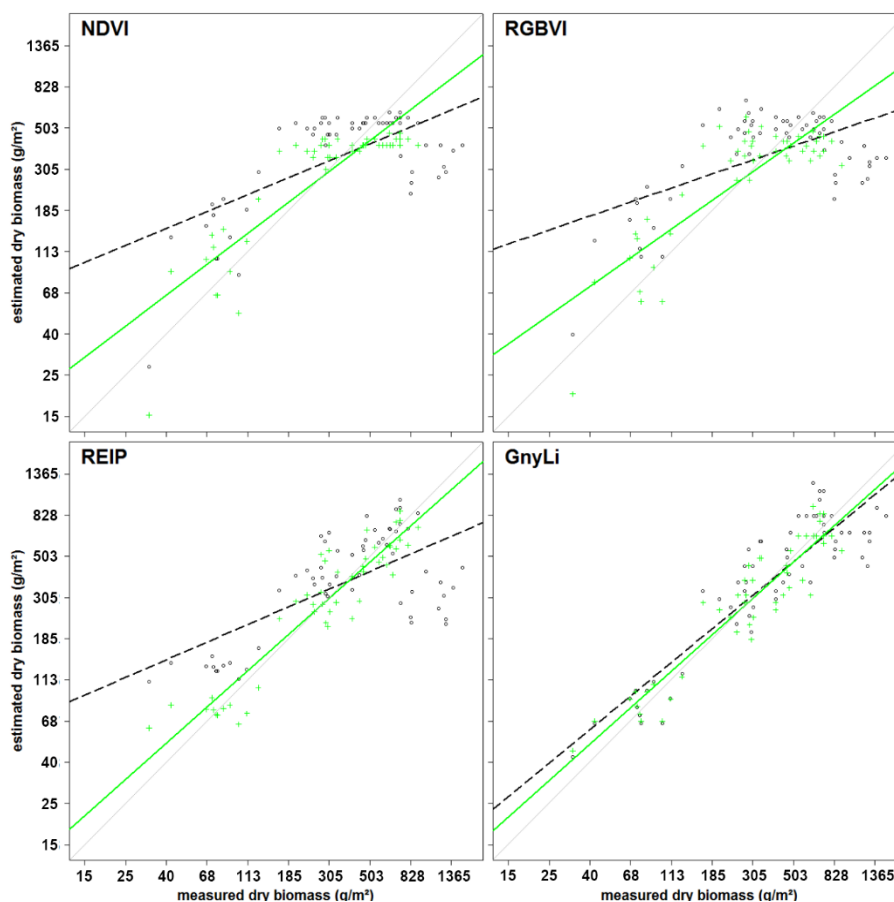


Figure 6-5. Scatterplots of measured vs. estimated dry biomass for one validation data set for NDVI, RGBVI, REIP, and GnyLi (exponential model). Pre-anthesis: crosses and solid green line; whole observed period: circles and dashed black line; 1:1 line: light grey.

Better results are also obtained for pre-anthesis of fresh biomass than for the whole observed period, although the differences are smaller than for dry biomass. The NIR VIs perform most consistently for both periods and have the highest R^2 values for the whole observed period. However, particularly for the whole observed period, the relative difference between the NIR VIs and the VIS and VISNIR VIs is smaller than for dry biomass and in pre-anthesis, the relative difference between the NIR VIs and other VIs is further reduced. Additionally, the REIP ($R^2 = 0.82$) yields better results than the NIR VIs (each $R^2 = 0.79$). Again, the RGBVI performs worst. **Figure 6-6** shows scatterplots of measured vs. estimated fresh biomass of one validation dataset for selected VIs. As expected from the high R^2 values, biomass estimated from the GnyLi BRM corresponds well with the measured values (close to the 1:1 line). In pre-anthesis, the same applies for the REIP, whereas the NDVI and RGBVI saturate at about 1,375 g/m². As for dry biomass, the BRMs based on the REIP and particularly the NDVI and RGBVI show a poor relationship between estimated and measured fresh biomass. Overall, most VISNIR VIs and the RGBVI yield better results for fresh biomass than

for dry biomass. The NIR VIs perform best and most consistently (**Table 6-6**, bottom left quarter).

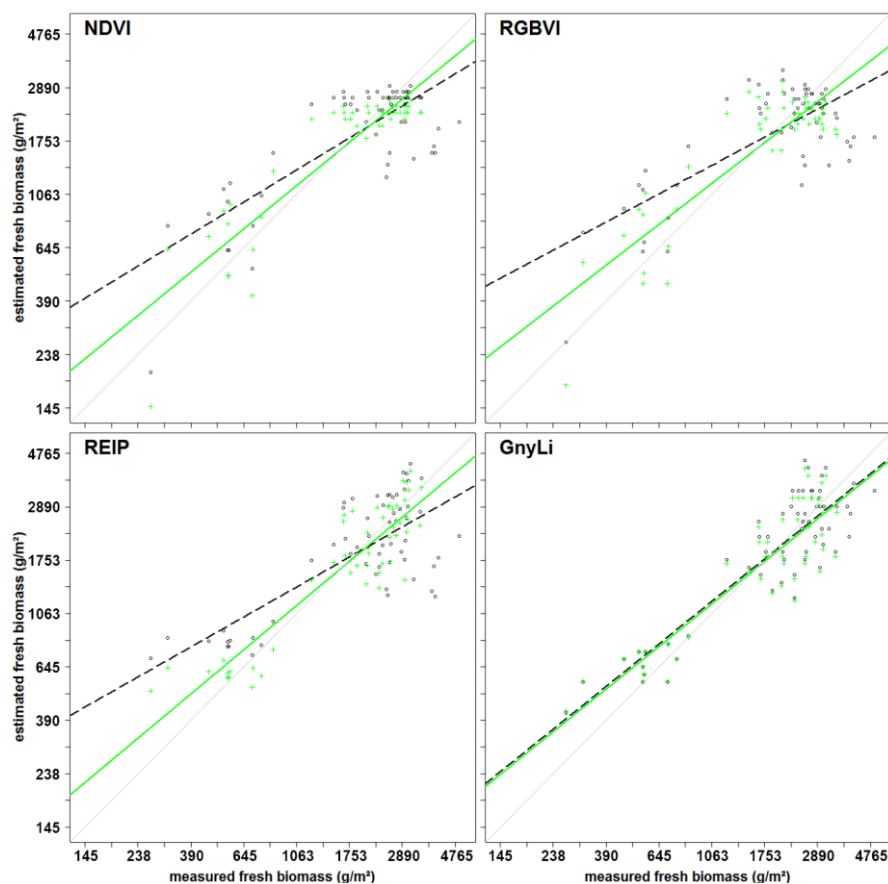


Figure 6-6. Scatterplots of measured vs. estimated fresh biomass for one validation data set for NDVI, RGBVI, REIP, and GnyLi (exponential model). Pre-anthesis: crosses and solid green line; whole observed period: circles and dashed black line; 1:1 line: light grey.

6.3.2.2 Multivariate models

For dry biomass, PH is the best individual estimator across the whole observed period ($R^2 = 0.85$) and a slight improvement is only achieved when fused with one of the NIR VIs in a multivariate BRM (both $R^2 = 0.87$). In pre-anthesis, PH and the NIR VIs perform similarly to the bivariate BRMs ($R^2 = 0.85, 0.86, 0.87$) and when PH is fused with the NIR VIs or the REIP, the predictability slightly increases ($R^2 = 0.89$).

For fresh biomass across the whole observed period, PH ($R^2 = 0.73$) yields comparable results to the NIR VIs (both $R^2 = 0.77$) although the fusion of PH with NIR VIs slightly improves the estimation (both $R^2 = 0.79$). Only the multivariate BRM from PH and RDVI is very slightly better ($R^2 = 0.80$). In pre-anthesis, REIP, GnyLi, NRI, and RDVI explain up to 11% more variation ($R^2 = 0.82, 0.79, 0.79, 0.73$) than PH ($R^2 = 0.71$). When PH is fused with any VI, the predictability is improved compared to most individual estimators and even the RGBVI in combination with PH improves the estimation of dry and fresh biomass for pre-anthesis yielding an R^2 of 0.71 and 0.76, respectively. In the fused analysis, the RGBVI performs only slightly weaker than the other VIs. Nevertheless, only the RDVI fused with PH slightly increases the predictability ($R^2 = 0.83$) compared to the bivariate BRM based on the RDVI.

Figure 6-7 shows the scatterplots of measured vs. estimated values of one validation dataset from the bivariate BRM of PH and the multivariate BRM of PH and GnyLi for dry biomass in pre-anthesis and fresh biomass across the whole observed period. The model fit is only slightly improved by fusing PH with the VI.

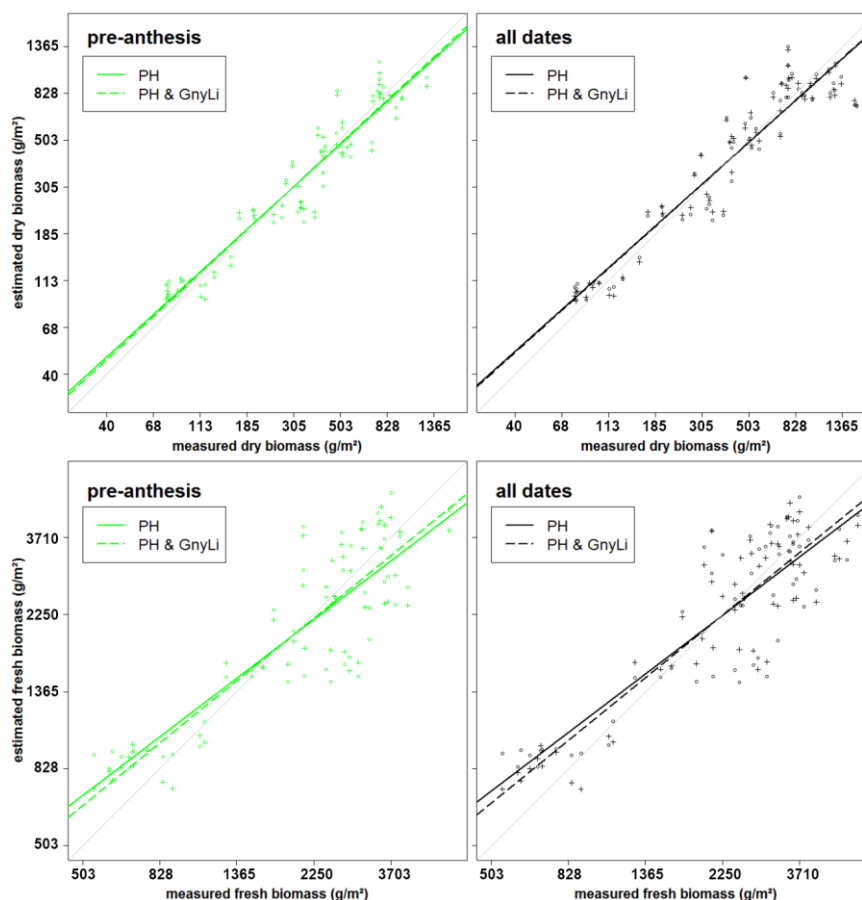


Figure 6-7. Scatterplot for one validation data set for the pre-anthesis (green) and for the whole observed period (black) of the bivariate BRM of PH (circles and solid regression line) and multivariate BRM of PH and GnyLi (crosses and dashed regression line) for dry biomass (top) and fresh biomass (bottom) (all exponential models); 1:1 line: light grey.

The robustness of the models was evaluated by calculating the ratio between the R^2 values of model calibration and validation for each BRM (Appendix **Table A 6-2**). Since the R^2 of calibration was divided through the R^2 of validation, values above 1 indicate better results from the calibration and below 1 indicate better results from the validation. Consequently, values close to 1 show a robust performance. For the bivariate BRMs, PH and almost all VIs are supported as robust estimators by ratios close to 1 for all cases. The weakest ratios are attained for the REIP, in particular for fresh biomass with linear BRMs (0.73, 0.71). For the multivariate BRMs, good ratios are found for all cases. Only the linear BRMs for fresh biomass show slightly weaker values for the pre-anthesis period.

6.4 Discussion

The overall aim of this study was to evaluate whether the fusion of PH and VIs can improve the predictability of dry and fresh barley biomass compared to each parameter as individual

estimator. For this work, the use of TLS to derive PH was verified and bivariate BRMs based on PH or one of six VIs as well as multivariate BRMs based on the fusion of PH with each VI were established. Extensive fieldwork over three years supported the practical application of the presented methods for monitoring crop development on plot level. The same instruments were used for all measurements whereby variations through different sensors could be excluded. However, the design of the field experiment and the measurement program was slightly modified and optimized over the years. Hence, only a part of the acquired data was used for the final model generation in order to ensure the comparability between the data sets. In the following, first the retrieval of PH from TLS data is discussed before the different BRMs are examined.

6.4.1 TLS-derived plant height

The presented study verified the reliability of the laser scanner Riegl LMS-Z420i for capturing crop surfaces. In comparison with past studies (Hoffmeister et al., 2010; Tilly et al., 2015), the scanning angle to the field was optimized through the elevated position on the hydraulic platform. However, uncertainties still remain about the influence of the scanning angle and the fixed position of the scanner during the measurements. As maintained by Ehlert and Heisig (2013)—the scanning angle can cause overestimations in the height of reflection points and should be considered in the calculation of heights. In this study, the crop surface was determined from the merged and cleaned point clouds of four scan positions, filtered with a scheme for selecting maximum points. Overestimations should therefore be precluded.

For the practical implementation of CSM-derived plant height measurements, further aspects have to be considered. Usually, the factors time and cost have a major influence on choosing a system. As shown by Hämmerle and Höfle (2014) the appropriate point density for generating a CSM varies depending on the application. In further studies, cost-efficient systems, such as the Velodyne HDL-64E (Velodyne, 2014), should be considered to investigate their potential for capturing crop surfaces in an adequate resolution. In the distant future, low-cost stationary systems might get permanently established for monitoring plant growth on field level. Moreover, recent developments have brought up new laser scanning platforms that might accelerate the field measurement process and optimize the scanning angle. First, ground-based mobile laser scanning (MLS) systems (Kukko et al., 2012) should be taken into account for increasing the homogeneous distribution in the point cloud and thus enhancing a uniform field coverage. Second, unmanned aerial vehicles (UAVs), such as the recently introduced Riegl RiCOPTER (Riegl LMS GmbH, 2015), should be examined as a potential platform of a lightweight airborne laser scanning (ALS) systems. Promising results have already been achieved for measuring tree heights (Jaakkola et al., 2010) or detecting pruning of individual stems (Wallace et al., 2014) with UAV-based laser scanning. However, as examined in a comparative study for TLS and common plane-based ALS, the scanning angle and possible resolution influence the results (Luscombe et al., 2014) and thus have also to be taken into account for studies on UAV-based scanning systems.

In this study, TLS measurements were used to derive 3D information of points. As shown in other studies, captured intensity values could be used for qualitative analyses of the points,

such as detecting single plants (Hoffmeister et al., 2012; Höfle, 2014). Whilst such analyses were not an object of this study they should be considered for further investigations. Moreover, full-waveform analysis, commonly known from ALS, can simplify the distinction between laser returns on canopy and ground returns in TLS data (Elseberg et al., 2011; Pirotti et al., 2013). The scanner used in this study however is not capable of capturing the full waveform.

The maps of plant height demonstrate the potential of the present approach for deriving plant height information on plot level in a very high resolution. The methodology of spatial plant height mapping can be scaled to field level, as long as the maximum range of the scanner is regarded and the point density is above the required minimum. As shown by Hämmerle and Höfle (2014), the coverage of the field and attained mean heights are influenced by the point density. The approach of pixel-wise calculating plant height from TLS-derived CSMs has already shown good results at the field level for monitoring a maize field, about 80 m by 160 m in size (Tilly et al., 2014c) and a sugar beet field, about 300 m by 500 m in size (Hoffmeister et al., 2010) captured from four and eight scan positions, respectively. Further studies are necessary for determining crop- or case-specific minimum values for the point density. In this context, the used sensor and its maximum range influence the required number of scan positions.

Nevertheless, for this study, high coefficients of determination between averaged CSM-derived and manual measured plant heights validate the TLS measurements. For the absolute values, differences between the measurement methods have to be considered. Whereas for the manual measurement the heights of ten plants were averaged per plot, the CSM captured the entire crop surface. Consequently, differences in the mean heights occurred, which make precision analysis between TLS data and manual measurements infeasible. The precision of TLS measurements for agricultural applications is presumed from other studies (Höfle, 2014; Lumme et al., 2008). It is important to note that a key advantage of the TLS data is that while plants for the manual measurements are subjectively selected, CSMs enable an objective assessment of spatially continuous plant height.

6.4.2 Biomass estimation from plant height

Generally, PH performed well for the estimation of biomass in the pre-anthesis and the whole observed period. For dry biomass, PH was the best predictor for the whole observed period and similar good predictor as the best performing VIs for the pre-anthesis. However, PH performed far better for dry biomass than for fresh biomass, although these values are only distinguished by the water content of the sample. Thus, a possible explanation is the fact that the water content is not only influenced by the changing plant phenology across the growing season, but also by varying weather conditions. Moreover, during each day the available soil water and transpiration conditions vary. Hence, the amount of fresh biomass might vary more between the campaigns while the dry biomass is less influenced. Since PH is hardly affected by the water content of the plants, the varying water content in the fresh biomass adds noise to the BRM based on PH which results in lower R^2 values.

6.4.3 Biomass estimation from vegetation indices

All VIs in this study have previously shown a relationship with biomass and LAI. Since the VIs use different bands within the spectral range, they were subdivided into three categories VIS VIs (RGBVI), VISNIR VIs (NDVI, RDVI, REIP), and NIR VIs (NRI, GnyLi). The VIs showed varying performances for the estimation of dry and fresh biomass, also depending on the regarded time frame of the growing season. Generally, the VIs within a category showed a similar behavior.

The saturation problem of the NDVI type VISNIR VIs was confirmed: Typically, crops reach 100% canopy cover around mid-vegetative phase. However, most crops continue to accumulate biomass and LAI afterwards. At a LAI of about 2.5 - 3, the absorbed amount of red light reaches a peak while the NIR scattering by leaves continues to increase. Thus, the ratio of NDVI type VISNIR VIs will only show slight changes (Thenkabail et al., 2000). In this study, the sensitivity thresholds were about 185 g/m² and 1,375 g/m² for dry and fresh biomass, respectively. Additionally, after heading the canopy de-greens due to flowering and fruit development (after BBCH 5, **Table 6-2**) This leads to an increased reflectance in the red part of the spectrum and thus, decreases values of the VISNIR VIs, while the biomass does not decrease. Herein, this discrepancy resulted in an inadequate model parameterization for the BRMs of the VISNIR VIs and poorer results for the whole observed period than for pre-anthesis.

A similar behavior was observable for the RGBVI. The inferior results might be explained by the fact that this VI does not take the reflectance in the NIR region into account, where most of the absorption features for biomass-related plant compounds are situated (Kumar et al., 2001). These results align well with the ones presented by Bendig et al. (2015), where low correlations were found for the RGBVI with biomass after booting stage (BBCH 4, **Table 6-2**).

In pre-anthesis, relationships of the RGBVI with dry and fresh biomass were similar. These results suggest that the RGBVI is mostly related with vegetation cover and not directly with biomass.

In contrast, NIRVIs, such as GnyLi and NRI, use bands only in the NIR and are thus not affected by the absorption in the red part of the spectrum, which could explain the overall more consistent and better performance of the NIR VIs, particularly after anthesis. A later saturation of these VIs aligns well with other studies (Gnyp et al., 2014a; Koppe et al., 2010). Similarly, the REIP did not show any saturation effects in the pre-anthesis and yielded very good results for dry and fresh biomass. These findings can be explained by the major influence of the NIR bands that are not normalized as they are in the NDVI type VIs. Thus, the REIP saturated later than the VISNIR and VIS VIs. Nevertheless, across the whole observed period, the performance of the REIP also decreased due to saturation. The importance of the NIR domain for biomass estimation aligns with other studies (Aasen et al., 2014; Gnyp et al., 2014a; Koppe et al., 2010; Marshall and Thenkabail, 2015) and should be further investigated. Similar to PH, the NIR VIs performed better for dry than for fresh biomass while the VISNIR VIs generally performed better with fresh biomass. This suggests that the VISNIR

VIs respond more to the canopy water content and the related reflectance change in the NIR shoulder rather than directly to the biomass.

Overall, the results show that the NIR VIs perform best in the prediction of fresh and dry biomass. Moreover, the results indicate that the VIS and VISNIR VIs might not be directly related to biomass. However, no rigorous sensitivity analysis was carried out in this study but, as indicated by the results, such analyses should be carried out in the future.

In general, hyperspectral field measurements have been shown to be useful in earlier studies to estimate biomass (Aasen et al., 2014; Gnyp et al., 2014b; Marshall and Thenkabail, 2015; Thenkabail et al., 2013). However, VIs are prone to errors by illumination changes (Damm et al., 2015) and multiangular reflection effects (Burkart et al., 2015). So far, the influence of these effects on the estimation of plant parameters have not been comprehensively investigated and should be examined for evaluating the potential of VIs for plant parameter estimations. Moreover, ground-based spectrometer measurements are laborious and time-consuming. Automated platforms are under development in different fields of remote sensing to overcome this difficulty but they have not yet become standard. Kicherer et al. (2015) developed a robotic platform for phenotyping grapevine based on automatic image acquisition. Results of a mobile multi-sensor phenotyping platform for phenotyping of winter wheat are presented by Kipp et al. (2014). Moreover, hyperspectral UAV-based systems showed promise (Aasen et al., 2015; Bareth et al., 2015; Honkavaara et al., 2013; Quemada et al., 2014; Suomalainen et al., 2014). Unfortunately, the promising NIR domain is currently not well covered by UAV sensing systems.

6.4.4 Biomass estimation with fused models

Leaves make up a major part of the biomass, and VIs related to biomass are often also responsive to LAI (Thenkabail et al., 2002, 2000). Thus, it was assumed that the spectral information would complement the PH information by adding information about the canopy density and cover.

As described above, PH and VIs showed varying performances in the estimation of fresh and dry biomass and for pre-anthesis or the whole observed period. For dry biomass in pre-anthesis, the NIR VIs performed slightly better than PH. Here, the fusion with all VIs improved the predictability, whereby the NIR and VISNIR VIs yielded the best results. This can be explained by the sensitivity of the VIs to the vegetation cover in early growth stages. For the whole observed period, PH clearly outperformed the VIs in the multivariate BRMs and only the fusion with the NIR VIs increased the predictability slightly compared to PH alone. For the VIS and VISNIR VIs, the above described saturation effects might have counteracted the positive effect of the vegetation cover estimation in the early growth stages. Additionally, for pre-anthesis and across the whole observed period, the multivariate BRMs performed similarly regardless which VI was used. This indicates that most of the prediction power can be accounted to PH.

For fresh biomass across the whole observed period, the NIR VIs performed best, followed by PH. Although the VISNIR VIs did not perform well in the bivariate BRMs, they could improve the results when fused with PH. As described above, VISNIR VIs respond to the water content. Thus, they might have complement the PH information for the estimation of fresh biomass.

Still, only a slight improvement was achieved with the fused models compared to the NIR VIs alone and overall, the results of multivariate BRMs with different VIs differed only slightly.

In pre-anthesis, only the NDVI and RGBVI performed poorer than PH while the REIP performed best for the fresh biomass. In combination with PH, the results of the NDVI and RDVI were improved the most, while the latter one also achieved the best results of all fused models. For the NIR VIs and REIP none or only very minor improvements were achieved and as for the whole observed period, the water was important because it influences the reflectance in the NIR. Additionally, the VIs correspond to vegetation cover in the early growth stages. Thus, in pre-anthesis already the VIs performed well and PH only rarely contributed to the prediction power. Only the RGBVI, NDVI, and RDVI might have carried complementary information to the PH.

In this study, the NIR VIs showed the overall best performance of the VIs and seemed to carry similar information as PH. Overall, PH and NIR VIs showed the best potential for biomass estimation as individual and fused estimators. This aligns with a recent study by Marshall and Thenkabail (2015), in which they have shown the importance of PH and the NIR domain for fresh biomass estimations. The VISNIR VIs seemed to be influenced by the water content and their performance strongly depended on the regarded time frame of the growing season. Although, no comprehensive sensitivity analysis was carried out, these findings align well with other studies (Gnyp et al., 2014a, 2013). Further studies are needed to investigate the influence of the growing stage on the estimation, and whether estimators, which have been found as suitable in across growth stage estimations, are suitable for estimation at individual growth stages. Such in-season estimations are particularly important for applications in precision agriculture. Additionally, in this study VIs known for estimating biomass from hyperspectral data were used. Thus, the full potential of the fusion of 3D spatial and spectral data may not have been explored. Future studies should investigate whether other parts of the spectral range complement PH information better.

Overall, this study demonstrated the strength of bivariate BRMs based on PH and NIR VIs for estimating biomass, with only slight improvements achievable through multivariate models. In contrast, the weak performances of the VIS and VISNIR VIs as individual estimators were compensated through the fusion with PH. However, statements have to be limited, since the models indicated that PH contributed the most to the prediction power. In this context, it has to be noted that neither linear nor exponential models reflected the relation between estimators and biomass perfectly and thus more complex functions have to be considered, which might take the benefits of VIs, like sensitivity to water content, better in to account.

For practical applications the benefit of the fused models might be outweighed by the expenses to deploy two different systems. Referring to this, limitations through the attainable spatial and temporal resolution of each system have to be regarded. As already mentioned, TLS measurements can be scaled up to larger fields, as long as a sufficiently point density can be achieved, which has to be determined crop- and case-specific in further studies. Apart from that, laser scanning appeared as powerful tool for the non-destructive and objective assessment of spatially resolved plant height data. Statements about the accuracy of the measured plant heights are hardly possible due to the already mentioned different spatial

resolution of the plant height measurements, however the averaged difference of 0.05 m between TLS-derived and manual measured plant heights corroborate the results (**Table A 6-1**). A main benefit of the field spectrometer measurements is the high credibility of the acquired spectral data, based on a large number of former studies, however the dependence on solar radiation and the small numbers of measurements per regarded spatial area, herein per plot, are the main disadvantages. Consequently, systems are required which are capable to assess larger areas in less time with the same accuracy of the results. Ideally, spatial and spectral information should be acquired directly through one sensor. For example, recently developed sensing systems and techniques allow to create hyperspectral point clouds (Vauhkonen et al., 2013) and hyperspectral digital surface models (Aasen et al., 2015) with only one sensor and thus, derive 3D spatial and hyperspectral information at the same time. Thus, it can be expected that 3D hyperspectral information will become increasingly available and combined analysis approaches should be further developed.

6.5 Conclusion and outlook

Continuously conducting a field experiment with different barley cultivars and the related TLS, field spectrometer, and manual measurements enabled the acquisition of an extensive data set. High R^2 values up to 0.89, between TLS-derived and manual measured plant heights verified the applicability of the presented approach for a pixel-wise calculation of plant height (PH) from high resolution crop surface models (CSMs). Six established vegetation indices (VIs) were used to extract information from the hyperspectral data. Based on PH and VIs, bivariate and multivariate biomass regression models (BRMs) were established, with varying performances. Whereas PH was supported as strong estimator in the bivariate models (R^2 up to 0.85), VIs showed highly different results (R^2 : 0.07 - 0.87). The multivariate models yielded improvements in some cases (R^2 up to 0.89), however in most cases PH had the greatest contribution to the prediction power.

Different models appeared best suitable for dry or fresh biomass estimations, also depending on the regarded time frame of the growing season, but in all cases exponential models performed better than the linear ones: For dry biomass, the bivariate BRM with PH showed the best results for the whole observed period ($R^2 = 0.85$), whereas for the pre-anthesis the REIP and the near-infrared (NIR) VIs GnyLi and NRI showed slightly better results than PH ($R^2 = 0.86, 0.87$). Multivariate BRMs from PH and one VI slightly improved the R^2 values compared to the bivariate BRMs in some cases. For fresh biomass, the bivariate BRMs of the NIR VIs showed the best results for the whole observed period (both $R^2 = 0.77$). For pre-anthesis, the REIP ($R^2 = 0.82$) showed slightly better results than the NIR VIs (both $R^2 = 0.79$). The multivariate BRM could slightly improve the results in some cases. Additionally, it can be noted that also weakly performing VIs, such as the NDVI or RGBVI, improved the estimations slightly when fused with PH in the multivariate BRMs, both for fresh and dry biomass. These results suggest that specific models should be chosen for specific applications, and a fusion of PH and VIs does not always substantially improve the results. Additionally, when PH and VIs are fused, the choice of the VI does not seem critical in all cases.

Altogether, it should be noted that the presented results are a first step towards the fusion of remotely sensed 3D spatial and spectral data for a precise and non-destructive estimation of crop biomass. Other ways of data fusion may further increase the prediction power. Further studies are also necessary to investigate differences between the years, cultivars, and fertilizer treatments. Moreover, as already mentioned, in-season biomass estimations are important for precision agriculture. Therefore models should be established based on data sets from only one campaign to investigate the potential for timely monitoring and in-season estimations. Accurate and rapidly ascertainable estimations in a high spatial resolution during the growing season could support spatially resolved nitrogen nutrition index calculations. Thereby in-field variations can be considered for optimizing fertilizer application and shrinking the gap between potential and current yield. The fusion of 3D spatial and spectral data might improve such calculations as weaknesses and limitations of one estimator might be compensated through the other one.

With regard to the application in the field, the usability of new platforms should be further investigated. UAV-based lightweight ALS systems reveal potential for vegetation mapping. Furthermore, new technologies like hyperspectral snapshot camera systems which enable the derivation of 3D spatial and hyperspectral information at the same time carry great potential for agricultural applications. Combined with estimation models based on structural and spectral and information, such approaches can become a powerful tool for applications in precision agriculture and biomass monitoring.

Acknowledgments

We would like to thank Dirk Hoffmeister for his knowledgeable support of the TLS measurements and Martin Gnyp for his expertise and effort in collecting the spectral data. Further we extend our thanks to the student assistants for their great work in the field and during the post-processing (Simon Bennertz, Jonas Brands, Janis Broscheit, Markus Drahs, Silas Eichfuss, Sven Ortloff, Maximilian Willkomm), the staff of the Campus Klein-Altendorf for carrying out the experiment (Bernd Bünthen, Winfried Bungert, Georg Völkering, Helmut Rehkopf), and the collaborators at the Forschungszentrum Jülich for supporting the laboratory work (Uwe Rascher, Edelgard Schölgens, Mark Müller-Linow, Francisco Pinto). Agim Ballvola is acknowledged for the coordination of the CROP.SENSE.net research group barley. We thank the anonymous reviewers for their valuable comments and Anne Wegner and Lesley-Anne Weiling for the English editing of the manuscript. Helge Aasen was supported by the Grant No. GSGS-2015B-F01 of the Graduate School of Geosciences, University of Cologne during the preparation of this manuscript. This work was carried out within the CROP.SENSE.net project in context of the Ziel 2-Programms NRW 2007–2013 “Regionale Wettbewerbsfähigkeit und Beschäftigung”, financially supported by the Ministry for Innovation, Science and Research (MIWF) of the state North Rhine Westphalia (NRW) and European Union Funds for regional development (EFRE) (005-1103-0018).

Author Contributions

Nora Tilly and Helge Aasen were responsible for the TLS and spectrometer measurements, respectively. The post-processing of the TLS data was carried out by Nora Tilly. Helge Aasen

and Georg Bareth selected the used vegetation indices. Nora Tilly substantially designed and established the analysis and mainly wrote this article. Helge Aasen carried out large parts of the analysis and added extensive sections to the manuscript. The research was directed by Georg Bareth, who supervised the whole acquiring, analyzing, and writing process.

Appendix

Table A 6-1. Statistics for the plot-wise averaged CSM-derived and manual measured plant heights (*n*: number of samples; \bar{x} : mean value; min: minimum; max: maximum; SD: standard deviation).

	BBCH	N level	n	CSM-derived plant height (m)				Manual measured plant height (m)			
				\bar{x}	min	max	SD	\bar{x}	min	max	SD
2012											
1	N/A	40	18	0.15	0.06	0.22	0.04	0.20	0.15	0.25	0.03
		80	18	0.18	0.14	0.24	0.03	0.20	0.15	0.26	0.03
2	30	40	18	0.21	0.13	0.28	0.04	0.35	0.28	0.42	0.05
		80	18	0.27	0.20	0.35	0.04	0.35	0.30	0.42	0.04
3	49	40	16	0.58	0.47	0.72	0.08	0.63	0.52	0.80	0.09
		80	15	0.64	0.48	0.80	0.11	0.66	0.54	0.79	0.08
4	N/A	40	14	0.73	0.61	0.81	0.06	0.86	0.74	0.96	0.06
		80	14	0.81	0.71	0.92	0.06	0.89	0.80	1.00	0.06
2013											
2	18	40	18	0.21	0.05	0.37	0.09	0.19	0.14	0.25	0.03
		80	18	0.11	-0.07	0.25	0.08	0.20	0.16	0.27	0.03
3	30	40	18	0.33	0.15	0.51	0.11	0.29	0.19	0.56	0.09
		80	18	0.25	0.01	0.40	0.11	0.28	0.17	0.45	0.08
4	41	40	18	0.57	0.33	0.83	0.17	0.52	0.39	0.70	0.09
		80	18	0.56	0.24	0.79	0.18	0.57	0.31	0.81	0.13
5	57	40	16	0.84	0.64	1.11	0.13	0.77	0.66	0.95	0.07
		80	16	0.79	0.58	1.04	0.12	0.81	0.54	0.94	0.11
6	68	40	14	0.78	0.65	0.97	0.09	0.77	0.66	0.84	0.05
		80	14	0.77	0.66	0.90	0.08	0.83	0.76	1.00	0.06
7	81	40	14	0.75	0.62	0.96	0.10	0.72	0.65	0.82	0.06
		80	14	0.72	0.62	0.83	0.07	0.79	0.67	0.89	0.07
2014											
2	29	40	18	0.16	0.12	0.24	0.03	0.19	0.12	0.30	0.04
		80	18	0.18	0.15	0.25	0.03	0.18	0.13	0.27	0.04
3	31	40	18	0.41	0.36	0.51	0.04	0.38	0.31	0.52	0.05
		80	18	0.42	0.34	0.52	0.05	0.36	0.27	0.45	0.05
4	49	40	18	0.63	0.53	0.70	0.04	0.59	0.53	0.65	0.03
		80	18	0.63	0.57	0.70	0.04	0.57	0.51	0.64	0.04
5	56	40	18	0.80	0.69	0.87	0.04	0.78	0.68	0.85	0.04
		80	18	0.81	0.75	0.93	0.04	0.78	0.72	0.89	0.04
6	74	40	18	0.76	0.66	0.84	0.04	0.77	0.68	0.83	0.03
		80	18	0.79	0.73	0.85	0.03	0.75	0.71	0.82	0.03

Table A 6-2. Ratio between model calibration and validation (R^2_{cal} : coefficient of determination from calibration; R^2_{val} : coefficient of determination from validation).

	Estimator	Bivariate BRMs		Multivariate BRMs			
		Whole period		Pre-anthesis	Whole period		Pre-anthesis
		R^2_{cal} / R^2_{val}					
Dry biomass	Linear	PH	0.98	0.95			
		GnyLi	0.96	0.94	GnyLi	1.00	0.97
		NDVI	1.00	0.89	NDVI	0.97	0.95
		NRI	0.98	0.95	NRI	0.98	0.96
		RDVI	1.00	0.95	RDVI	0.96	0.95
		REIP	0.80	0.85	REIP	1.00	0.95
		RGBVI	1.25	0.93	RGBVI	0.97	0.95
	Exponential	PH	0.99	0.99			
		GnyLi	1.00	0.99	GnyLi	0.99	0.99
		NDVI	1.03	1.03	NDVI	1.00	1.01
		NRI	1.00	1.00	NRI	1.00	1.00
		RDVI	1.03	1.03	RDVI	1.00	1.00
		REIP	0.93	0.94	REIP	0.99	0.97
		RGBVI	1.05	1.00	RGBVI	1.00	1.01
	Estimator	R^2_{cal} / R^2_{val}	R^2_{cal} / R^2_{val}	Estimator ^a	R^2_{cal} / R^2_{val}	R^2_{cal} / R^2_{val}	
Fresh biomass	Linear	PH	0.88	0.86			
		GnyLi	0.89	0.86	GnyLi	0.90	0.86
		NDVI	0.93	0.82	NDVI	0.90	0.86
		NRI	0.91	0.86	NRI	0.90	0.86
		RDVI	0.92	0.85	RDVI	0.90	0.86
		REIP	0.73	0.71	REIP	0.90	0.82
		RGBVI	1.05	0.90	RGBVI	0.92	0.90
	Exponential	PH	0.96	0.96			
		GnyLi	0.99	0.96	GnyLi	0.97	0.96
		NDVI	1.05	1.02	NDVI	0.99	1.00
		NRI	1.00	0.97	NRI	0.97	0.97
		RDVI	1.04	1.01	RDVI	0.99	0.99
		REIP	0.87	0.87	REIP	0.94	0.90
		RGBVI	1.06	1.04	RGBVI	1.01	1.03

Conflicts of Interest

The authors declare no conflict of interest.

References

- Aasen, H., Burkart, A., Bolten, A., Bareth, G., 2015. Generating 3D Hyperspectral Information with Lightweight UAV Snapshot Cameras for Vegetation Monitoring: From Camera Calibration to Quality Assurance. *ISPRS J. Photogramm. Remote Sens.* 108, 245–259. doi:10.1016/j.isprsjprs.2015.08.002
- Aasen, H., Gnyp, M.L., Miao, Y., Bareth, G., 2014. Automated hyperspectral vegetation index retrieval from multiple correlation matrices with HyperCor. *Photogramm. Eng. Remote Sens.* 80, 785–796. doi:10.14358/PERS.80.8.785
- Ahamed, T., Tian, L., Zhang, Y., Ting, K.C., 2011. A review of remote sensing methods for biomass feedstock production. *Biomass and Bioenergy* 35, 2455–2469. doi:10.1016/j.biombioe.2011.02.028
- Atzberger, C., 2013. Advances in Remote Sensing of Agriculture: Context Description, Existing Operational Monitoring Systems and Major Information Needs. *Remote Sens.* 5, 949–981. doi:10.3390/rs5020949

- Bareth, G., Aasen, H., Bendig, J., Gnyp, M.L., Bolten, A., Jung, A., Michels, R., Soukkamäki, J., 2015. Low-weight and UAV-based Hyperspectral Full-frame Cameras for Monitoring Crops: Spectral Comparison with Portable Spectroradiometer Measurements. *Photogramm. - Fernerkundung - Geoinf.* 1, 69–79. doi:10.1127/pfg/2015/0256
- Bendig, J., Yu, K., Aasen, H., Bolten, A., Bennertz, S., Broscheit, J., Gnyp, M.L., Bareth, G., 2015. Combining UAV-based plant height from crop surface models, visible, and near infrared vegetation indices for biomass monitoring in barley. *Int. J. Appl. Earth Obs. Geoinf.* 39, 79–87. doi:10.1016/j.jag.2015.02.012
- Besl, P.J., McKay, N.D., 1992. A Method for Registration of 3D Shapes. *IEEE Trans. Pattern Anal. Mach. Intell.* 14, 239–256. doi:10.1117/12.57955
- Bidinger, F., Musgrave, R.B., Fischer, R.A., 1977. Contribution of stored pre-anthesis assimilate to grain yield in wheat and barley. *Nature* 270, 431–433. doi:10.1038/270431a0
- Blackburn, G.A., 1998. Quantifying Chlorophylls and Carotenoids at Leaf and Canopy Scales. *Remote Sens. Environ.* 66, 273–285. doi:10.1016/S0034-4257(98)00059-5
- Boukerrou, L., Rasmusson, D.D., 1990. Breeding for High Biomass Yield in Spring Barley. *Crop Sci.* 30, 31–35. doi:10.2135/cropsci1990.0011183X003000010007x
- Broge, N.H., Leblanc, E., 2001. Comparing prediction power and stability of broadband and hyperspectral vegetation indices for estimation of green leaf area index and canopy chlorophyll density. *Remote Sens. Environ.* 76, 156–172. doi:10.1016/S0034-4257(00)00197-8
- Burkart, A., Aasen, H., Alonso, L., Menz, G., Bareth, G., Rascher, U., 2015. Angular Dependency of Hyperspectral Measurements over Wheat Characterized by a Novel UAV Based Goniometer. *Remote Sens.* 7, 725–746. doi:10.3390/rs70100725
- Damm, A., Guanter, L., Verhoef, W., Schläpfer, D., Garbari, S., Schaepman, M.E., 2015. Impact of varying irradiance on vegetation indices and chlorophyll fluorescence derived from spectroscopy data. *Remote Sens. Environ.* 156, 202–215. doi:10.1016/j.rse.2014.09.031
- Danson, F.M., Morsdorf, F., Koetz, B., 2009. Airborne and Terrestrial Laser Scanning for Measuring Vegetation Canopy Structure, in: Heritage, G.L., Large, A.R.G. (Eds.), *Laser Scanning for the Environmental Sciences*. Wiley-Blackwell, West Sussex, UK, pp. 201–219. doi:10.1002/9781444311952.ch13
- Ehlert, D., Adamek, R., Horn, H.-J., 2009. Laser rangefinder-based measuring of crop biomass under field conditions. *Precis. Agric.* 10, 395–408. doi:10.1007/s11119-009-9114-4
- Ehlert, D., Heisig, M., 2013. Sources of angle-dependent errors in terrestrial laser scanner-based crop stand measurement. *Comput. Electron. Agric.* 93, 10–16. doi:10.1016/j.compag.2013.01.002
- Ehlert, D., Horn, H.-J., Adamek, R., 2008. Measuring crop biomass density by laser triangulation. *Comput. Electron. Agric.* 61, 117–125. doi:10.1016/j.compag.2007.09.013
- Elseberg, J., Borrmann, D., Nüchter, A., 2011. Full Wave Analysis in 3D laser scans for vegetation detection in urban environments, in: *2011 XXIII International Symposium on Information, Communication and Automation Technologies*. IEEE, pp. 1–7. doi:10.1109/ICAT.2011.6102101
- Fischer, R.A., 1993. Irrigated spring wheat and timing and amount of nitrogen fertilizer. II. Physiology of grain yield response. *F. Crop. Res.* 33, 57–80. doi:10.1016/0378-4290(93)90094-4
- Gebbers, R., Ehlert, D., Adamek, R., 2011. Rapid Mapping of the Leaf Area Index in Agricultural Crops. *Agron. J.* 103, 1532–1541. doi:10.2134/agronj2011.0201

- Geipel, J., Link, J., Claupein, W., 2014. Combined Spectral and Spatial Modeling of Corn Yield Based on Aerial Images and Crop Surface Models Acquired with an Unmanned Aircraft System. *Remote Sens.* 6, 10335–10355. doi:10.3390/rs61110335
- Gnyp, M.L., Bareth, G., Li, F., Lenz-Wiedemann, V.I.S., Koppe, W., Miao, Y., Hennig, S.D., Jia, L., Laudien, R., Chen, X., Zhang, F., 2014a. Development and implementation of a multiscale biomass model using hyperspectral vegetation indices for winter wheat in the North China Plain. *Int. J. Appl. Earth Obs. Geoinf.* 33, 232–242. doi:10.1016/j.jag.2014.05.006
- Gnyp, M.L., Miao, Y., Yuan, F., Ustin, S.L., Yu, K., Yao, Y., Huang, S., Bareth, G., 2014b. Hyperspectral canopy sensing of paddy rice aboveground biomass at different growth stages. *F. Crop. Res.* 155, 42–55. doi:10.1016/j.fcr.2013.09.023
- Gnyp, M.L., Yu, K., Aasen, H., Yao, Y., Huang, S., Miao, Y., Bareth, G., 2013. Analysis of crop reflectance for estimating biomass in rice canopies at different phenological stages. *Photogramm. - Fernerkundung - Geoinf.* 4, 351–365. doi:http://dx.doi.org/10.1127/1432-8364/2013/0182
- Greenwood, D.J., Gastal, F., Lemaire, G., Draycott, A., Millard, P., Neeteson, J.J., 1991. Growth rate and %N of field grown crops: Theory and experiments. *Ann. Bot.* 67, 181–190.
- Guyot, G., Baret, F., 1988. Utilisation de la haute resolution spectrale pour suivre l'état des couverts vegetaux, in: NASA Astrophysics Data System (Ed.), Proceedings of the 4th International Colloquium on Spectral Signatures of Objects in Remote Sensing. Aussois, France, pp. 279–286.
- Guyot, G., Baret, F., Jacquemoud, S., 1992. Imaging spectroscopy for vegetation studies, in: Toselli, F., Bodechtel, J. (Eds.), *Imaging Spectroscopy for Vegetation Studies*. Kluwer, Dordrecht, Netherlands, pp. 145–165.
- Haboudane, D., Miller, J.R., Pattey, E., Zarco-Tejada, P.J., Strachan, I.B., 2004. Hyperspectral vegetation indices and novel algorithms for predicting green LAI of crop canopies: Modeling and validation in the context of precision agriculture. *Remote Sens. Environ.* 90, 337–352. doi:10.1016/j.rse.2003.12.013
- Hair, J.F., Black, W.C., Babin, B.J., Anderson, R.E., 2010. *Multivariate Data Analysis*, 7th ed. Pearson, Upper Saddle River, N.J.
- Hämmerle, M., Höfle, B., 2014. Effects of Reduced Terrestrial LiDAR Point Density on High-Resolution Grain Crop Surface Models in Precision Agriculture. *Sensors* 14, 24212–24230. doi:10.3390/s141224212
- Hoffmeister, D., Bolten, A., Curdt, C., Waldhoff, G., Bareth, G., 2010. High resolution Crop Surface Models (CSM) and Crop Volume Models (CVM) on field level by terrestrial laser scanning, in: Guo, H., Wang, C. (Eds.), *Proc. of SPIE, 6th International Symposium on Digital Earth*. Beijing, China. doi:10.1117/12.872315
- Hoffmeister, D., Tilly, N., Bendig, J., Curdt, C., Bareth, G., 2012. Detektion von Wachstumsvariabilität in vier Zuckerrübensorten, in: Clasen, M., Fröhlich, G., Bernhardt, H., Hildebrand, K., Theuvsen, B. (Eds.), *Informationstechnologie Für Eine Nachhaltige Landwirtschaft*, Proc. 32. GIL-Jahrestagung. Köllen Verlag, Bonn, Germany, Freising, pp. 135–138.
- Höfle, B., 2014. Radiometric Correction of Terrestrial LiDAR Point Cloud Data for Individual Maize Plant Detection. *Geosci. Remote Sens. Lett. IEEE* 11, 94–98. doi:10.1109/LGRS.2013.2247022

- Honkavaara, E., Saari, H., Kaivosoja, J., Pölönen, I., Hakala, T., Litkey, P., Mäkynen, J., Pesonen, L., 2013. Processing and assessment of spectrometric, stereoscopic imagery collected using a lightweight UAV spectral camera for precision agriculture. *Remote Sens.* 5, 5006–5039. doi:10.3390/rs5105006
- Hosoi, F., Omasa, K., 2012. Estimation of vertical plant area density profiles in a rice canopy at different growth stages by high-resolution portable scanning lidar with a lightweight mirror. *ISPRS J. Photogramm. Remote Sens.* 74, 11–19. doi:10.1016/j.isprsjprs.2012.08.001
- Hosoi, F., Omasa, K., 2009. Estimating vertical plant area density profile and growth parameters of a wheat canopy at different growth stages using three-dimensional portable lidar imaging. *ISPRS J. Photogramm. Remote Sens.* 64, 151–158. doi:10.1016/j.isprsjprs.2008.09.003
- Jaakkola, A., Hyypä, J., Kukko, A., Yu, X., Kaartinen, H., Lehtomäki, M., Lin, Y., 2010. A low-cost multi-sensoral mobile mapping system and its feasibility for tree measurements. *ISPRS J. Photogramm. Remote Sens.* 65, 514–522. doi:10.1016/j.isprsjprs.2010.08.002
- Johnston, K., Ver Hoef, J.M., Krivoruchko, K., Lucas, N., 2001. Using ArcGIS Geostatistical Analyst. ESRI, USA.
- Kicherer, A., Herzog, K., Pflanz, M., Wieland, M., Rüger, P., Kecke, S., Kuhlmann, H., Töpfer, R., 2015. An Automated Field Phenotyping Pipeline for Application in Grapevine Research. *Sensors* 15, 4823–4836. doi:10.3390/s150304823
- Kipp, S., Mistele, B., Baresel, P., Schmidhalter, U., 2014. High-throughput phenotyping early plant vigour of winter wheat. *Eur. J. Agron.* 52, 271–278. doi:10.1016/j.eja.2013.08.009
- Koenig, K., Höfle, B., Hämmerle, M., Jarmer, T., Siegmann, B., 2015. Comparative classification analysis of post-harvest growth detection from terrestrial LiDAR point clouds in precision agriculture. *ISPRS J. Photogramm. Remote Sens.* 104, 112–125. doi:10.1016/j.isprsjprs.2015.03.003
- Koppe, W., Li, F., Gnyp, M.L., Miao, Y., Jia, L., Chen, X., Zhang, F., Bareth, G., 2010. Evaluating Multispectral and Hyperspectral Satellite Remote Sensing Data for Estimating Winter Wheat Growth Parameters at Regional Scale in the North China Plain. *Photogramm. - Fernerkundung - Geoinf.* 3, 167–178. doi:10.1127/1432-8364/2010/0047
- Kukko, A., Kaartinen, H., Hyypä, J., Chen, Y., 2012. Multiplatform Mobile Laser Scanning: Usability and Performance. *Sensors* 12, 11712–11733. doi:10.3390/s120911712
- Kumar, L., Schmidt, K., Dury, S., Skidmore, A., 2001. Imaging Spectrometry and Vegetation Science, in: Meer, F. va. der, Jong, S.D. (Eds.), *Imaging Spectrometry: Basic Principles and Prospective Applications, Remote Sensing and Digital Image Processing*. Springer Netherlands, Dordrecht, pp. 111–155. doi:10.1007/978-0-306-47578-8_5
- Lancashire, P.D., Bleiholder, H., van den Boom, T., Langelüddeke, P., Strauss, R., Weber, E., Witzemberger, A., 1991. A uniform decimal code for growth stages of crops and weeds. *Ann. Appl. Biol.* 119, 561–601. doi:10.1111/j.1744-7348.1991.tb04895.x
- Lee, W.S., Alchanatis, V., Yang, C., Hirafuji, M., Moshou, D., Li, C., 2010. Sensing technologies for precision specialty crop production. *Comput. Electron. Agric.* 74, 2–33. doi:10.1016/j.compag.2010.08.005
- Liaghat, S., Balasundram, S.K., 2010. A Review : The role of remote sensing in precision agriculture. *Am. Soc. Agric. Biol. Eng.* 5, 50–55. doi:10.3844/ajabssp.2010.50.55
- Lumme, J., Karjalainen, M., Kaartinen, H., Kukko, A., Hyypä, J., Hyypä, H., Jaakkola, A., Kleemola, J., 2008. Terrestrial laser scanning of agricultural crops. *Int. Arch. Photogramm. Remote Sens. Spat. Inf. Sci.* 37 (Part B5) 563–566.

- Luscombe, D.J., Anderson, K., Gatis, N., Wetherelt, A., Grand-Clement, E., Brazier, R.E., 2014. What does airborne LiDAR really measure in upland ecosystems? *Ecohydrology* 8, 584–594. doi:10.1002/eco.1527
- Marshall, M., Thenkabail, P., 2015. Developing in situ Non-Destructive Estimates of Crop Biomass to Address Issues of Scale in Remote Sensing. *Remote Sens.* 7, 808–835. doi:10.3390/rs70100808
- Meier, U., 2001. Growth stages of mono- and dicotyledonous plants, 2nd ed. Blackwell, Berlin.
- Mulla, D.J., 2012. Twenty five years of remote sensing in precision agriculture: Key advances and remaining knowledge gaps. *Biosyst. Eng.* 114, 358–371. doi:10.1016/j.biosystemseng.2012.08.009
- Oliver, M., 2013. An overview of precision agriculture, in: Oliver, M., Bishop, T., Marchant, B. (Eds.), *Precision Agriculture for Sustainability and Environmental Protection*. Springer, USA, pp. 3–19.
- Olsoy, P.J., Glenn, N.F., Clark, P.E., 2014. Estimating sagebrush biomass using terrestrial laser scanning. *Rangel. Ecol. Manag.* 67, 224–228. doi:10.2111/REM-D-12-00186.1
- Paulus, S., Dupuis, J., Riedel, S., Kuhlmann, H., 2014a. Automated analysis of barley organs using 3D laser scanning: an approach for high throughput phenotyping. *Sensors* 14, 12670–12686. doi:10.3390/s140712670
- Paulus, S., Schumann, H., Kuhlmann, H., Léon, J., 2014b. High-precision laser scanning system for capturing 3D plant architecture and analysing growth of cereal plants. *Biosyst. Eng.* 121, 1–11. doi:10.1016/j.biosystemseng.2014.01.010
- Pirotti, F., Guarnieri, A., Vettore, A., 2013. Vegetation filtering of waveform terrestrial laser scanner data for DTM production. *Appl. Geomatics* 5, 311–322. doi:10.1007/s12518-013-0119-3
- Price, C., Munns, R., 2010. Growth analysis: a quantitative approach, in: Munns, R., Schmidt, S., Beveridge, C. (Eds.), *Plants in Action*. Australia.
- Quemada, M., Gabriel, J., Zarco-Tejada, P., 2014. Airborne Hyperspectral Images and Ground-Level Optical Sensors As Assessment Tools for Maize Nitrogen Fertilization. *Remote Sens.* 6, 2940–2962. doi:10.3390/rs6042940
- R Development Core Team, 2015. The R Project for Statistical Computing. <http://www.r-project.org/>
- Reddersen, B., Fricke, T., Wachendorf, M., 2014. A multi-sensor approach for predicting biomass of extensively managed grassland. *Comput. Electron. Agric.* 109, 247–260. doi:10.1016/j.compag.2014.10.011
- Riegl LMS GmbH, 2015. Infosheet RiCOPTER. http://www.riegl.com/uploads/tx_pxpriegldownloads/RiCOPTER_at_a_glance_2015-03-31.pdf
- Riegl LMS GmbH, 2010. Datasheet Riegl LMS-Z420i. http://www.riegl.com/uploads/tx_pxpriegldownloads/10_DataSheet_Z420i_03-05-2010.pdf
- Roujean, J.L., Breon, F.M., 1995. Estimating PAR absorbed by vegetation from bidirectional reflectance measurements. *Remote Sens. Environ.* 51, 375–384. doi:10.1016/0034-4257(94)00114-3
- Rouse, J.W., Haas, R.H., Schell, J.A., Deering, D.W., 1974. Monitoring Vegetation Systems in the Great Plains with ERTS, in: NASA (Ed.), *Third Earth Resources Technology Satellite-1 Symposium*. Washington, D.C., pp. 309–317.

- Saeyes, W., Lenaerts, B., Craessaerts, G., De Baerdemaeker, J., 2009. Estimation of the crop density of small grains using LiDAR sensors. *Biosyst. Eng.* 102, 22–30. doi:10.1016/j.biosystemseng.2008.10.003
- Suomalainen, J., Anders, N., Iqbal, S., Roerink, G., Franke, J., Wenting, P., Hünninger, D., Bartholomeus, H., Becker, R., Kooistra, L., 2014. A Lightweight Hyperspectral Mapping System and Photogrammetric Processing Chain for Unmanned Aerial Vehicles. *Remote Sens.* 6, 11013–11030. doi:10.3390/rs60x000x
- Thenkabail, P.S., Mariotto, I., Gumma, M.K., Middleton, E.M., Landis, D.R., Huemmrich, K.F., 2013. Selection of hyperspectral narrowbands (HNBS) and composition of hyperspectral twoband vegetation indices (HVIs) for biophysical characterization and discrimination of crop types using field reflectance and Hyperion/EO-1 data. *IEEE J. Sel. Top. Appl. Earth Obs. Remote Sens.* 6, 427–439. doi:10.1109/JSTARS.2013.2252601
- Thenkabail, P.S., Smith, R.B., De Pauw, E., 2000. Hyperspectral Vegetation Indices and Their Relationships with Agricultural Crop Characteristics. *Remote Sens. Environ.* 71, 158–182. doi:10.1016/S0034-4257(99)00067-X
- Thenkabail, P.S., Smith, R.B., Pauw, E. De, De Pauw, E., 2002. Evaluation of Narrowband and Broadband Vegetation Indices for Determining Optimal Hyperspectral Wavebands for Agricultural Crop Characterization. *Photogramm. Eng. Remote Sensing* 68, 607–621. doi:0099-111210216806-60
- Tilly, N., Hoffmeister, D., Aasen, H., Brands, J., Bareth, G., 2014a. Multi-temporal Crop Surface Models derived from terrestrial laser scanning for accurate plant height measurement and biomass estimation of barley. *Kölner Geogr. Arb.* 94, 83–91. doi:10.5880/TR32DB.KGA94.12
- Tilly, N., Hoffmeister, D., Cao, Q., Huang, S., Lenz-Wiedemann, V., Miao, Y., Bareth, G., 2014b. Multitemporal crop surface models: accurate plant height measurement and biomass estimation with terrestrial laser scanning in paddy rice. *J. Appl. Remote Sens.* 8, 083671–1–22. doi:10.1117/1.JRS.8.083671
- Tilly, N., Hoffmeister, D., Cao, Q., Lenz-Wiedemann, V., Miao, Y., Bareth, G., 2015. Transferability of Models for Estimating Paddy Rice Biomass from Spatial Plant Height Data. *Agriculture* 5, 538–560. doi:10.3390/agriculture5030538
- Tilly, N., Hoffmeister, D., Schiedung, H., Brands, J., Bareth, G., 2014c. Terrestrial laser scanning for plant height measurement and biomass estimation of maize. *Int. Arch. Photogramm. Remote Sens. Spat. Inf. Sci.* XL-7. doi:10.5194/isprsarchives-XL-7-181-2014
- Topcon Positioning Systems, I., 2006. HiPer Pro Operator's Manual. http://www.top-survey.com/top-survey/downloads/HiPerPro_om.pdf
- Torabzadeh, H., Morsdorf, F., Schaepman, M.E., 2014. Fusion of imaging spectroscopy and airborne laser scanning data for characterization of forest ecosystems – A review. *ISPRS J. Photogramm. Remote Sens.* 97, 25–35. doi:10.1016/j.isprsjprs.2014.08.001
- UNFPA, 2010. State of world population 2010-from conflict and crisis to renewal: generations of change. http://www.unfpa.org/sites/default/files/pub-pdf/EN_SOWP10.pdf
- Uni Bonn, 2010a. Soil Campus Klein-Altendorf. http://www.cka.uni-bonn.de/standort/copy_of_boden
- Uni Bonn, 2010b. Climate Campus Klein-Altendorf. http://www.cka.uni-bonn.de/standort/copy_of_klima

- van Wart, J., Kersebaum, K.C., Peng, S., Milner, M., Cassman, K.G., 2013. Estimating crop yield potential at regional to national scales. *F. Crop. Res.* 143, 34–43. doi:10.1016/j.fcr.2012.11.018
- Vauhkonen, J., Hakala, T., Suomalainen, J., Kaasalainen, S., Nevalainen, O., Vastaranta, M., Holopainen, M., Hyyppä, J., 2013. Classification of Spruce and Pine Trees Using Active Hyperspectral LiDAR. *Geosci. Remote Sens. Lett. IEEE* 10, 1138–1141. doi:10.1109/LGRS.2012.2232278
- Velodyne, 2014. Velodyne HDL-64E User's Manual. http://www.velodynelidar.com/lidar/products/manual/63-HDL64E_S2_Manual_Rev_D_2011_web.pdf
- Wallace, L., Watson, C., Lucieer, A., 2014. Detecting pruning of individual stems using airborne laser scanning data captured from an Unmanned Aerial Vehicle. *Int. J. Appl. Earth Obs. Geoinf.* 30, 76–85. doi:10.1016/j.jag.2014.01.010
- Willmott, C.J., 1981. On the validation of models. *Phys. Geogr.* 2, 184–194. doi:10.1080/02723646.1981.10642213
- Willmott, C.J., Wicks, D.E., 1980. An Empirical Method for the Spatial Interpolation of Monthly Precipitation within California. *Phys. Geogr.* 1, 59–73. doi:10.1080/02723646.1980.10642189
- Zhang, L., Grift, T.E., 2012. A LIDAR-based crop height measurement system for *Miscanthus giganteus*. *Comput. Electron. Agric.* 85, 70–76. doi:10.1016/j.compag.2012.04.001
- © 2015 by the authors; licensee MDPI, Basel, Switzerland. This article is an open access article distributed under the terms and conditions of the Creative Commons Attribution license (<http://creativecommons.org/licenses/by/4.0/>).

7 Discussion

The overall aim of this study was to establish a robust method for the non-destructive estimation of crop biomass at field scale. A literature review reveals that numerous ground- or vehicle-based studies address biomass estimations with VIs based on passive spectrometer measurements. In contrast, an active TLS system was applied in this study. Beside the independence of solar radiation, the possibility to capture the entire crop surface of a field is thereby a main advantage. However, since the scanner operates only with one wavelength an obtained 3D point cloud is unsuitable for the derivation of VIs. Hence, another way to achieve plant parameter information was required. This was solved by interpolating the point cloud to a CSM, which allowed, in combination with a DTM, the calculation of spatially resolved plant heights. Although plant height is known as suitable estimator for biomass it is not very widely investigated so far. A further benefit of TLS is that the frequency of measurements and thus the temporal resolution could be easily adapted since it is as ground-based active system quite flexible to use. Limitations are, for example, continuous rain or heavy wind. In all case studies the intended biweekly rhythm for the TLS campaigns during the key vegetative phase was almost reached. This allowed to establish multi-temporal CSMs and hence to monitor temporal and spatial changes in plant height.

All case studies investigated cereals which are the most important group of crops regarding world nutrition. Moreover, examples of cereals were selected which cover different forms of the general appearance and growing characteristics. Paddy rice was chosen due to its cultivation on flooded fields, maize was used as example for large plant heights, and barley as representative for most of the other cereals, like wheat and rye. In order to ensure the comparability between the case studies, similar preconditions were intended. Common aspects were, for example, comparable sensor set-ups in the field, which included the use of similar TLS systems and the acquisition from the field edges with a certain sensor height above the canopy. In addition, the main post-processing steps were carried out in an equal manner. However, some differences between the sites must also be stated. This involves the different scales (plot or field) and platforms as well as the general environmental conditions.

From the comprehensive case studies the suitability of this approach and the important role of plant height as robust estimator for biomass with crop-specific BRMs can be suggested. Nevertheless, strengths and limitations of both the acquisition in the field and the gained data were observed. Issues for discussion are, for example, the influence of the scanning geometry on the results, the usability of the comparative measurements due to the different measuring process and dimensions of the resulting data, or the validity of the BRMs. According to this, the following sections address four main topics: (I) the impact of the sensor set-up on the measurements, (II) the performance of the platforms in the field, (III) the results of the plant height measurements, and (IV) the estimations with the BRMs, also considering the fusion with VIs. Finally future prospects for laser scanning applications in agriculture are given.

7.1 Sensor set-ups and scanning geometries

From the total number of 35 field campaigns, the Riegl LMS-Z420i scanner was used for all measurements in Germany and those in Jiansanjiang in 2012; for the six campaigns in

Jiansanjiang in 2011 the newer Riegl VZ-1000 was available. Irrespective of some minor differences the acquisition with both systems worked well and main advantages of TLS are the independency from an external light source and that the system is quite robust against poor weather. Both systems operate with the time-of-flight measuring principle and enable the fast acquisition of large areas with high measuring rates (**Table 2-1**). The VZ-1000 has some advantages such as a longer range of 1,400 m (LMS-Z420i: 1,000 m), a lower weight of 9.8 kg (LMS-Z420i: 16 kg), and the scanner captures the full waveform of the laser signal (Riegl LMS GmbH, 2013, 2010). However according to the manufacturers' specification the accuracy of the LMS-Z420i is still sufficiently exact to 10 mm (VZ-1000: 8 mm).

Apart from the different scanners, overall four platforms (**Figure 7-1**) were used which differ, inter alia, in the height of the sensor above ground and the transportability in the field; the latter aspect is addressed in the next section. The height of the sensor influences the scanning geometry and is thus likely to affect the measurements. At nearly all scan positions



Figure 7-1. Platforms for TLS with the approximate sensor height: (A) Tripod (1.5 m); (B) Tractor-trailer system (3 m); (C) Tractor with hydraulic platform (4 m); (D) Cherry picker (8 m).

in Jiansanjiang the scanner was mounted on a tripod, resulting in a sensor height of ~1.5 m above ground **(A)**. Where possible, the tripod was established on a small trailer behind a tractor, increasing the sensor height up to ~3 m **(B)**. At both sites in Germany vehicle-based platforms were available. For all campaigns at the Campus Klein-Altendorf, the scanner was attached to a hydraulic platform of a tractor, raising the sensor height up to ~4 m **(C)**. Due to the higher plant height of the maize plants, observed in Selhausen, also a higher position of the sensor above the ground was necessary. Therefore, the scanner was attached to the basket of a cherry picker, whereby a sensor height of ~8 m above ground was reached **(D)**.

It should be noted that a larger sensor height reduces the inclination angle between the laser beam and the theoretical vertical axis, which alters the incidence angle of the laser beam on the crop surface. This and the oblique perspective of the scanner have an impact on the measurements. In **Figure 7-2** the different theoretical laser paths depending on the sensor height are sketched for the used platforms; both tractor systems are summarized, since they have approximately equal heights. From the sketched paths it can be concluded that the steeper the angles, the deeper the vegetation may get penetrated. Consequently, beside the reflection points at the top of the canopy, obtained from all sensor heights, further points at lower plant layers are attained from larger heights. These values reduce the calculated mean plant height. Such angle-dependent effects on laser scanning data are also noted by Ehlert and Heisig (2013). They observed overestimations of the heights of reflection points, depending on the inclination and scanning angle, whereby the overestimations increased with increasing angles. Unfortunately, a general correction function could not be developed and the authors concluded that specific corrections are necessary for different sensors and crops. Furthermore, factors such as the density of the vegetation cover and the horizontal distance between sensor and position in the field are likely to influence the results. Since in none of

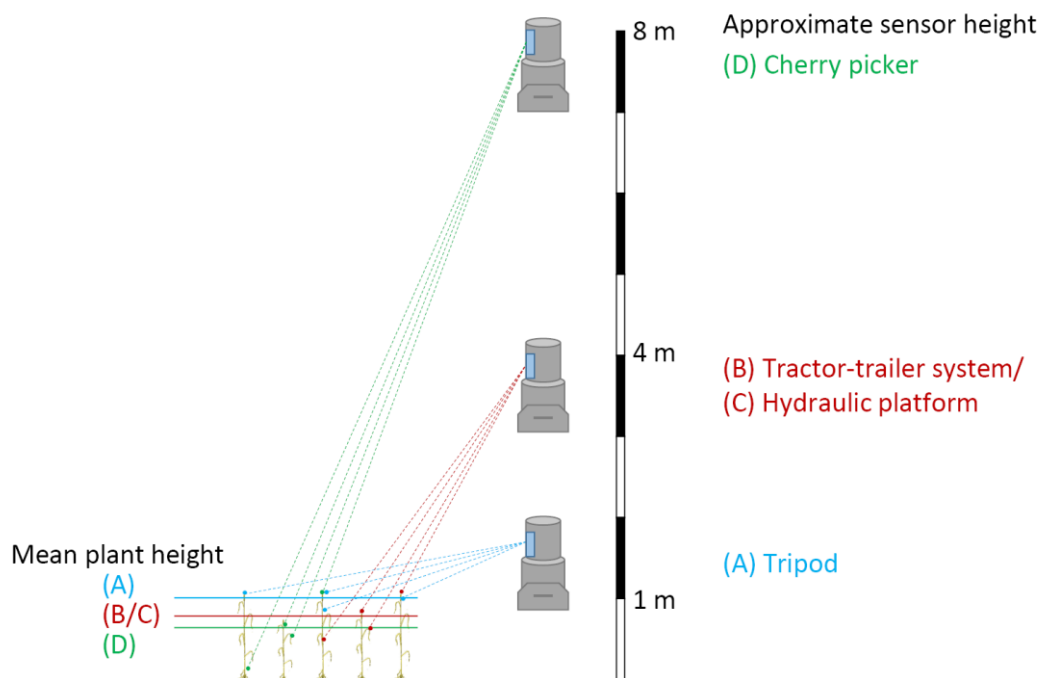


Figure 7-2. Influence of the sensor height and the resulting inclination angle on the incidence angle. This affects which plant parts are ascertainable, which in turn influences the calculated mean plant height. Single plants modified from Large (1954).

the case studies measurements from different heights at the same position were carried out, a comprehensive comparison was not possible, and further research is desirable.

Compared to other studies applying TLS for agriculture (Eitel et al., 2011; Hosoi and Omasa, 2012; Lumme et al., 2008), the presented approach shows major advantages. In these approaches in-field measurements were performed at plot level and have not been shown as being transferable to field level yet. In contrast, with the here presented approach the measurements are performed from the field edges which allows to capture the entire field and moreover the plant growth is kept undisturbed. Acquisitions from the edges are in particular useful for crops where an entering of the field is not possible, due to water in the field as in the case of paddy rice or if the plants are too large as in the case of maize.

Nevertheless, issues caused by this measuring process with a static scanner and an oblique perspective have to be noted. Firstly, heterogeneous point densities and occlusion effects have to be considered for static TLS measurements (Höfle, 2014). Secondly, the point density decreases with increasing distance from the scanner and as shown by Hämmerle and Höfle (2014) the scanning resolution has an influence on the results. They used dense point clouds of a high-end TLS system, with a resolution of 5 mm at 10 m distance, to establish CSMs. By thinning the point clouds they simulated data sets with a lower resolution and showed that with 25 % of the number of points, the CSM coverage, meaning at least one point per cell, is still above 90 %.

With regard to these aspects, in each campaign of the here presented case studies the field was scanned from at least four positions around the field. This set-up should help to compensate occlusion effects and to ensure an adequate number of reflection points for the entire field. A consistent selection of points for the CSM interpolation was intended by using a filtering scheme for selecting maximum points in the post-processing. Nevertheless, further research is necessary since, besides the scanning resolution, the crop variety and plant density have an influence on the results (Hämmerle and Höfle, 2014). This research should also address the definition of crop- and case-specific minimum point densities.

Beside these geometric effects, the scanning range and the incidence angle influence the measured signal (Kaasalainen et al., 2011). Hence, a radiometric calibration is advisable for static TLS if a qualitative analysis of the reflected signal is intended (Kaasalainen et al., 2011; Koenig et al., 2015). The captured intensity values may be used to detect single plants for example (Hoffmeister et al., 2012; Höfle, 2014). Unfortunately, a radiometric correction was not available in this study which made a consideration of the intensity value not meaningful. Further research should address the benefit of including these values in the analyses, since this might simplify the distinction between reflections on plants and ground.

7.2 Platforms

Besides the influence on the measurements, all platforms differ regarding their performance in the field. **Table 7-1** provides the discovered advantages and disadvantages of the used platform. Tripod-based setups are worthwhile if the scan position cannot be reached with vehicles, as shown for the dikes between the rice paddies (Section 3.2.2). However, steeper incidence angles are attained from larger heights, reachable with the vehicle-based

setups. In contrast to the easier transport of the scanner between the scan positions with the vehicles, the stability of the scanner during the measurements decreases.

Table 7-1. Advantages and disadvantages of the platforms used for field surveys.

Advantages	Disadvantages
Tripod	
<ul style="list-style-type: none"> · Flexible to be set up in the field · Almost each position, accessible by foot can be reached · Stable position during measurement 	<ul style="list-style-type: none"> · Laborious transport between scan positions · Low sensor height above ground
Tractor-trailer system	
<ul style="list-style-type: none"> · Higher sensor height above ground than reachable with the tripod · Easy and rapid transport between scan positions 	<ul style="list-style-type: none"> · Slightly unstable establishment on trailer, in particular during changes between scan positions · Not every position can be reached, e.g. due to small dikes between rice paddies
Tractor with hydraulic platform	
<ul style="list-style-type: none"> · Higher sensor height above ground than reachable with tripod · Very easy and rapid transport between scan positions 	<ul style="list-style-type: none"> · Slightly unstable platform, in particular during windy conditions · Assumable not every position can be reached, but other positions were not necessary in the case study
Cherry picker	
<ul style="list-style-type: none"> · Much higher sensor height above ground than reachable with tripod or smaller vehicle-based platforms · Easy transport between scan positions 	<ul style="list-style-type: none"> · Unstable platform, in particular during windy conditions · Assumable not every position can be reached, but other positions were not necessary in the case study · Aligning of vehicle can be slightly time-consuming depending on the ground (e.g. asphalt vs. field path)

The highest degree of instability was observable with the cherry picker, in particular during wind gusts. Although generally slight movements are captured and equalized by the scanner, stronger movements cause errors in the measurements. **Figure 7-3** shows the calculated plant heights for the maize field in Selhausen on two campaign dates. For the early campaign a radial pattern of varying plant heights is visible around each corner as center point. As the scan positions were established close to the corners and none of these patterns were observable in the other campaigns, it must be assumed that these ones are caused by movements of the cherry picker basket during the scans and do not really show varying plant heights. In contrast, in the later campaign, a smooth crop surface was obtained, allowing plant height differences to be detected, as shown in section 5.3.1.

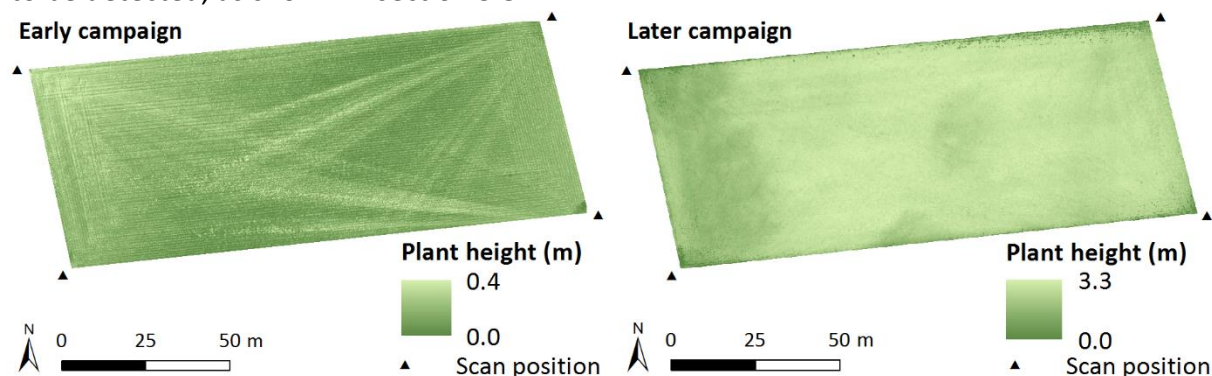


Figure 7-3. Influence of platform movements during the scans on the calculated maize plant heights. Scans were acquired from the basket of the cherry picker, placed close to the corners of the field.

In summary, each platform showed strengths and weaknesses in terms of their usability for crop monitoring approaches with TLS. The tractor with hydraulic platform might be the best compromise solution to enable an easy and rapid transport of the scanner between the scan positions, while maintaining a fairly stable platform in an adequate height above ground for crops with low plant heights such as barley. The cherry picker reveals potential for applications, where higher sensor heights above ground are required but improvements of the stability are necessary to ensure faultless measurements. Since such vehicle-based platforms might not be available at each location, other acquisition methods should be considered; the last section of this chapter provides some suggestions.

7.3 Plant height measurements

Based on the results of the case studies it can be assumed that TLS-derived point clouds are well suited for acquiring 3D data of plant height. Although Hoffmeister et al. (2010) showed that the general concept of CSMs is useful for obtaining 3D data of plant height from TLS-derived point clouds, no comparative measurements have been conducted to prove this. In contrast, manual measurements were carried out in all presented case studies to obtain comparative data sets. For this, several plants heights were measured with measuring tapes or rulers in each plot of the field experiments or at defined positions in the larger fields. Taking the measuring process and the resulting dimension of the acquired data into account, differences between the methods have to be regarded.

Assuming that the sketched plants in **Figure 7-4** represent the cross section through a common area, these differences are clearly visible. In the TLS data set almost the entire crop surface is captured in the 3D point cloud, which is interpolated to a CSM with a dimension of 2.5D and a resolution of 1 cm in the post-processing. In contrast, only a few plants are manually measured and the values are recorded per spatial unit, without assessing the precise 2D location. Hence, the CSM-derived values and the manual measurements have to be averaged for common spatial units, resulting in 1D data sets. Both measuring methods are suitable to capture the height of the largest plants, but the CSM also contains reflections on lower plants, which are mostly neglected in the manual measurements. As a result, the calculated mean heights are likely to differ, showing lower values for the CSM-derived values

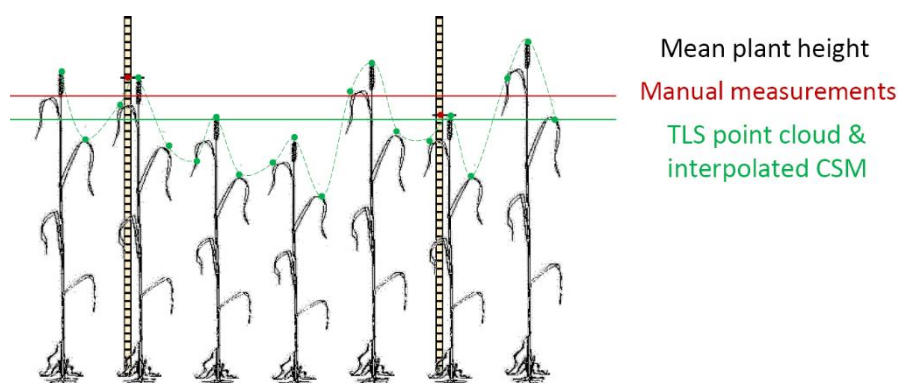


Figure 7-4. Plant heights ascertainable from the TLS-derived point clouds and the manual measurements. The measuring processes influence the calculated mean plant height. Single plants modified from Large (1954).

in most of the cases. Despite these clear differences, the manual measurements are worthwhile for validating whether the general tendency of the TLS measurements is correct.

For this validation analysis the linear regression of the averaged CSM-derived vs. manually measured plant heights was established in each case study and the related coefficient of determination (R^2) was used to quantify the relationship between both measurements. As a summary of the 35 campaigns, all averaged CSM-derived values are plotted against the manually measured plant heights in **Figure 7-5**. This includes 396, 60, and 508 values for paddy rice, maize, and barley, respectively. With regard to the higher values for the maize plant heights the values are plotted for all cereals (left) and only for paddy rice and barley (right). Both scatterplots clearly show the linear trend, supported by very high R^2 values of 0.95 and 0.89. As stated in Tilly et al. (2014b, Chapter 5), a high R^2 value of 0.93 was also achieved for maize alone, but a data gap is observable (**Figure 5-4**) and the period of main increase in plant height was not well covered. Hence further studies are required to confirm these results. Both regression lines in **Figure 7-5** show a slope of almost 1 with their intercepts close to the origin, meaning that they are close to the 1:1 line, which would reveal a perfect linear relationship between both variables. These slight displacements in the positive y-direction, confirm the higher values assumed for the manual measurements (**Figure 7-4**). However, regarding the scatterplot for paddy rice and barley (right) the regression line and the 1:1 line cross each other at a CSM-derived plant height of ~ 0.5 m. A possible explanation for this is that beyond this point such a dense vegetation cover might be assumed that fewer low plant layers are captured in the point cloud, which in turn increases the averaged CSM-derived plant height (**Figure 7-2**).

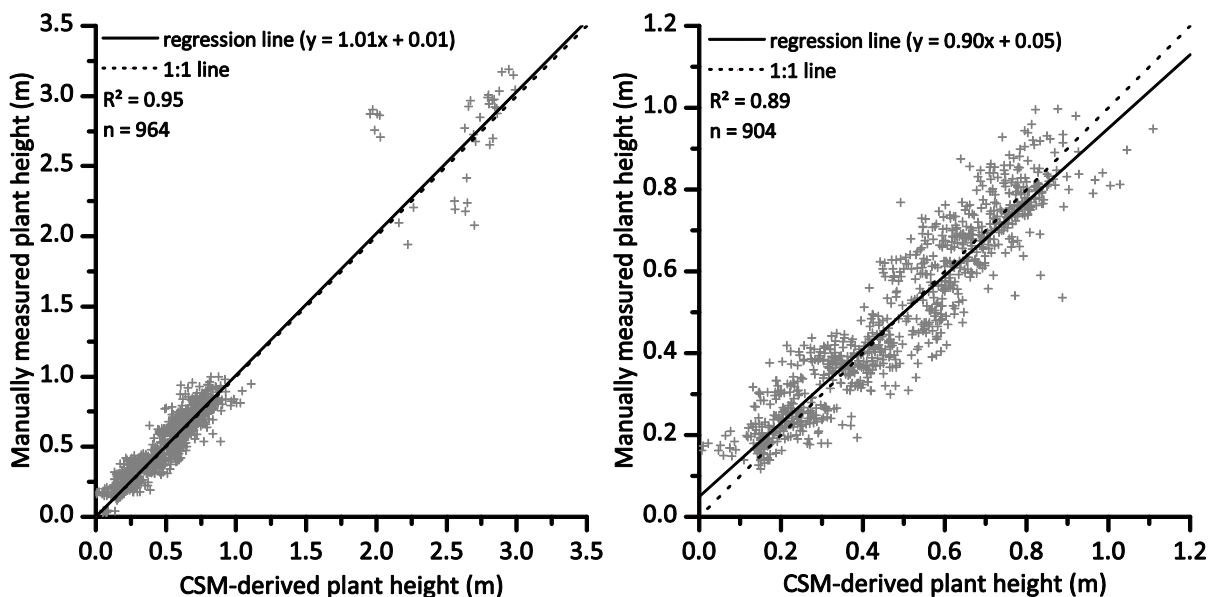


Figure 7-5. Averaged CSM-derived vs. manually measured plant heights of all campaigns on paddy rice, maize, and barley (left) and of all except maize (right).

In comparison to other studies applying ground-based measurements of plant height, the main benefits of the TLS approach are the objective detection and capturing of the entire crop surface. Recently, Marshall and Thenkabail (2015) used manual measurements of plant height to improve biomass estimations from spectral measurements. They showed that the

predictability of estimations from spectral data can be increased by additional non-spectral predictors and assigned plant height as most important one. However, as mentioned above, due to the laborious work, only a few plant heights can be manually measured and moreover such measurements are always prone to selection bias. Marshall and Thenkabail (2015) also complained about the difficult upscaling of manual measurements and proposed LiDAR approaches as promising remote sensing method to derive this metric. Other remote sensing methods, such as light curtains (Busemeyer et al., 2013; Montes et al., 2011) or ultrasonic sensor (Reddersen et al., 2014) can also be applied to avoid the selection bias, but they are limited to single measurements at discrete positions or across small areas. Thus they are not suitable for spatially resolved acquisitions of plant height at field scale.

Overall, the comparative data sets were useful for a general validation of the TLS data, but due to the absence of precise 2D information for each manually measured height, analyzing the accuracy or precision of the CSMs was not meaningful. These metrics are however worthwhile to evaluate the maximum attainable resolution which is important for site-specific crop management, as shown in **Figure 1-1**. Consequently, other measuring methods or improved processes should be considered in further research. An acquisition of the x, y coordinates for each discrete value of manual measurements might be a first step. This might be done with DGPS measurements which are however quite laborious.

Beyond that, the loss of information through the conversion of the TLS-derived 3D point clouds in 2.5D raster data sets should be considered. Typically a DTM is limited to this representation of one z value per x, y coordinate, but increasing interest is directed towards the direct analysis of point clouds. A promising approach therefore is the LAStools software suite which offers tools for the efficient post-processing of LiDAR data, primarily acquired with ALS (rapidlasso GmbH, 2015). The lascanopy tool, for example, can be used to derive common forestry metrics such as vegetation density or height, as shown in a study on the mapping of mangroves (Kamal et al., 2015). However, these developments are rather recent and such tools are less researched so far, in particular for TLS data. Consequently, they could not have been considered in this study, but further investigations are desirable.

7.4 Biomass estimations

A main incentive for determining plant height at field scale with TLS is the usability of plant height as non-destructive estimator for cereal or rather crop biomass. In all case studies the estimations were carried out based on the averaged 1D data sets of plant height and biomass, but the different spatial extents of the investigated areas still need to be considered. As stated in the beginning, the presented approach aims at the application at field scale. However, previously a sufficient knowledge about the development of both parameters across the growing season was required. For this purpose, two field experiments each with several plots of different crop cultivars and varying fertilizer treatments were monitored. The differences between the plots were worthwhile to capture several plant conditions at one growing stage and establish comprehensive BRMs according to the equations in **Table 2-3**. Moreover, the multi-annual surveys on these fields with similar preconditions allowed to investigate the temporal transferability of the BRMs. The paddy rice case studies were supplemented by

campaigns on two farmer's conventionally managed fields. Thereby in addition to the temporal, the spatial transferability of the BRMs to the larger field scale was examined. The application of the approach at a large field was also addressed in the maize case study.

Generally, it should be distinguished between the estimation of fresh and dry biomass. While fresh biomass is frequently used as an input parameter in crop growth models, the amount of dry biomass is important for the calculation of indices like the harvest index or the NNI. According to the case studies, this section mainly addresses dry biomass but some remarks on fresh biomass are given in conjunction with the discussion on the benefits through fusing plant height and VIs at the end of this section. According to the overall workflow the results of the field experiments are firstly regarded to examine whether the development of plant height and dry biomass across the growing season can be captured with the presented approach. Afterwards, the transferability to field scale is evaluated.

The results of all case studies reveal the strong correlation between CSM-derived plant height and dry biomass. As an example in **Table 7-2** the R^2 values for the linear and exponential regressions between CSM-derived plant height and dry biomass are listed for both field experiments. For the barley data sets of 2013 and 2014 the values are given for the whole observed period and the pre-anthesis, as the main increase in plant height occurs during this key vegetative phase of the growing season (**Table 2-2**); in 2012 and on the paddy rice experiment only the pre-anthesis was surveyed. Linear and exponential regressions were established to investigate how well they express the relation between plant height and dry biomass across the growing season and to derive the equations for the BRMs (**Table 2-3**). A better fit of exponential regressions can be concluded from the values achieved on the barley experiment 2013 and 2014, in particular when the whole observed period is regarded. This aligns well with other studies, which suggest exponential models (Aasen et al., 2014; Thenkabail et al., 2000). In contrast, almost similar values were attained with the linear and exponential models for the barley experiment 2012 and for the paddy rice experiment of both years. A possible reason for this is that only earlier growing stages were surveyed which will be discussed hereafter based on the results of the barley case study.

Table 7-2. R^2 values for linear and exponential regression between CSM-derived plant height and dry biomass for the field experiments.

Site and year	Linear	Exponential
Paddy rice experiment 2011	0.86	0.84
Paddy rice experiment 2012	0.66	0.65
Barley experiment 2012	0.85	0.83
Barley experiment 2013 (whole observed period)	0.68	0.79
Barley experiment 2013 (pre-anthesis)	0.65	0.74
Barley experiment 2014 (whole observed period)	0.66	0.87
Barley experiment 2014 (pre-anthesis)	0.84	0.88

For comparing the results with generally assumed growth patterns, **Figure 7-6** shows the observed development of plant height and dry biomass of barley across the growing season, based on the data derived from the barley field experiment presented in Tilly et al. (2015a, Chapter 6). For each data point all mean values of either CSM-derived plant height or destructively measured dry biomass, attained in one of the overall 14 campaigns are averaged.

Moreover, the general trend curve of each parameter is indicated as polynomial function of the 3rd degree. Since the campaigns were carried out across three growing seasons, the values are plotted against the day after seeding as comparable timescale. Although variations between the values of the different years are observable, the overall trend can be summarized to three phases: before day 50 after seeding a slight increase is detectable for plant height and dry biomass, then until day 80 after seeding both parameters rise strongly, and afterwards the plant height stays almost constant while the dry biomass further increases. Referring to **Table 6-1**, day 50 and day 80 after seeding are broadly assignable to the change from BBCH stage 2 (Tillering) to 3 (Stem elongation) and from 5 (Heading) to 6 (Anthesis), respectively. Taking now **Figure 2-4** into account, these plant heights fit well to the assumed plant growth across the growing season with slightly increasing plant heights during tillering, a strong rising during stem extension and heading, and almost constant plant heights afterwards.

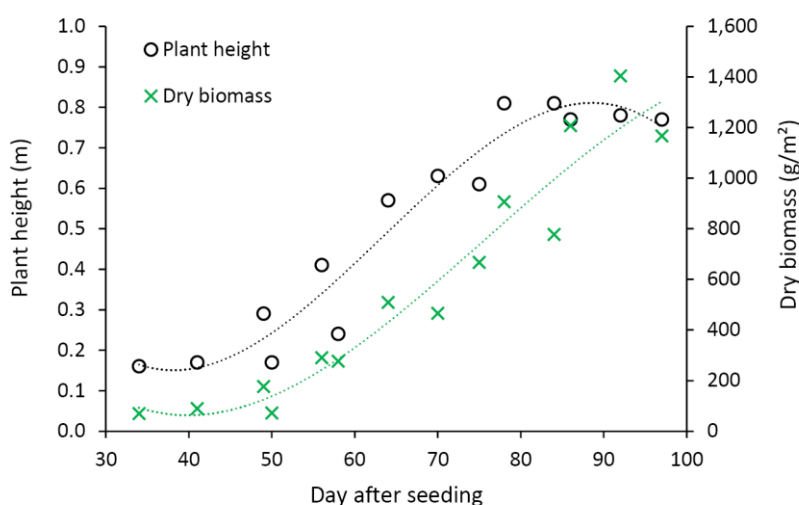


Figure 7-6. Mean trend of plant height and dry biomass of barley across the growing season with trend curves as polynomial functions of the 3rd degree.

Such general statements are more complicated for biomass. First of all, the development of the plants as qualitative change has to be regarded. As shown in **Figure 7-7** the increase of dry biomass across the growing season can be allocated to different plant parts, namely root, leaf, stem, spike, and grain. The root biomass stays almost constant across the growing season and is not considered in the following as only the aboveground biomass was regarded in the case studies. Approximately until day 50 after seeding leaves make up the greatest portion of the total dry biomass. Afterwards the leaf and stem biomass values increase and constitute mostly to the total amount. Around day 80 after seeding the spike and shortly afterwards the grain biomass start to contribute substantially to the increasing total dry biomass. This again fits well to the three phases observed for the barley biomass (**Figure 7-6**).

The general trend between both parameters can hence be summarized according to these three phases. During the early growing stages (< BBCH Stage 3; ~ day 50 after seeding) increasing dry biomass can be expected as being almost proportional to increasing plant height, with a slight increase of both parameters and a parallel course of the trend curves. In the middle phase (< BBCH Stage 6; ~ day 80 after seeding) the values strongly increase, but the relation is still almost linear and the trend curves are still almost parallel to each other.

However, after anthesis this tendency changes. Since the biomass further increases while the plant height stays constant, a non-linear relation must be assumed, which is also indicated by the different course of the trend curves. Overall, this fits well to the better performance of the exponential BRMs, in particular when the whole observed period, beyond anthesis, is regarded. (**Table 7-2**).

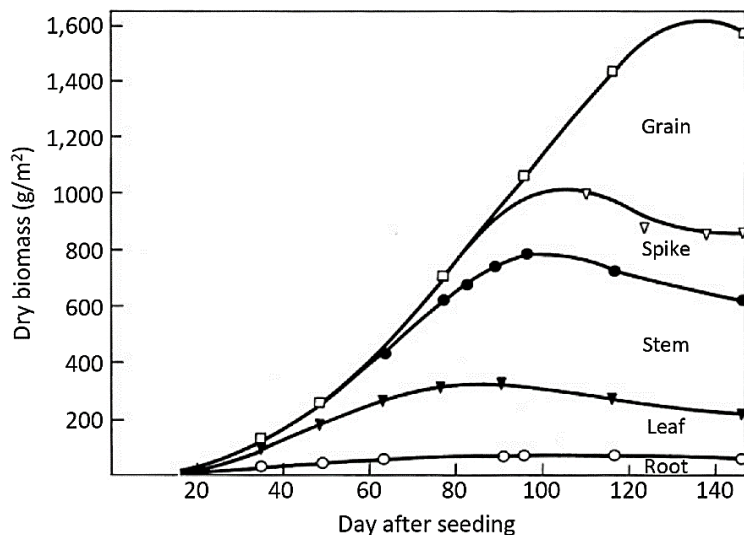


Figure 7-7. Dry biomass accumulation in crop parts. Modified from Fischer (1983).

Nevertheless, the validity of the linear and exponential models should be further investigated. It is shown that good results are achievable with the BRMs, but the question remains whether the dependency of biomass on other plant parameters can be expressed by such quite simple mathematical expressions or if more complex functions are necessary. Lemaire et al. (2007), for example, discovered an allometric relationship between LAI expansion and dry biomass accumulation for different crops. Further research should be carried out regarding the question if such allometric functions also better constitute the relationship between plant height and dry biomass. However, it has to be kept in mind that the approach is aimed to be simple to apply at field scale and it is questionable which model is the best compromise solution to keep the balance between effort and benefit.

Generally, the achieved results are comparable good as those stated in other studies on TLS-based estimations of biomass. Results for the estimations of dry biomass were shown by Eitel et al. (2014). In that study, high R^2 values of at least 0.72 were found for the relationship between observed dry biomass of wheat and TLS-derived vegetation volume. Lumme et al. (2008) estimated the grain yield of different crops and yielded correlation coefficient of up to 0.99 against reference values. Hosoi and Omasa (2012) demonstrated that the biomass of paddy rice can be estimated from lidar-derived plant area density (R^2 up to 0.99). The authors also presented similar results for estimations on wheat (Hosoi and Omasa, 2009). However, all of these studies were carried out at plot level and their applicability at field scale is not shown yet. On the contrary, along with the aim of finding a trustworthy estimator for biomass, a major aim of the herein presented study was that the approach should be suitable for a practical implementation at field scale. This usability of the

CSM approach for scales larger than plot level was shown by surveys on two paddy rice fields and one maize field.

In the paddy rice case study the BRMs were investigated whether they can be transferred to other sites (Tilly et al., 2015b, Chapter 4). Therefore, several BRMs were established with the field experiment data sets according to the equations stated in **Table 2-3**. Then, the independent plant height data sets from the farmer's fields, which were not considered in the model calibration, were used for estimating the biomass on these fields (Section 4.2.5). The validation against destructive samplings revealed moderate to good results ($R^2 = 0.56 - 0.90$; **Table 4-5**). These analyses were based on the spatially averaged 1D data sets, but such biomass estimations are possible for the entire field. This is exemplified in **Figure 7-8**, showing a dry biomass map for the paddy rice units investigated in village 36 (Field description given in section 4.2.1). Based on the 3D data of plant height, the dry biomass is estimated for the entire field with the linear BRM, established from the two year combined data set of the field experiment (**Table 4-5**). This BRM was chosen since it showed the best performance in the validation analysis. The map demonstrates that CSM-derived plant heights are worthwhile for a spatially resolved mapping of dry biomass. As shown in **Figure 4-2**, the plant development in these management units was very heterogeneous and must be taken into account as source of error for the estimations. Nevertheless, this heterogeneous plant status is clearly visible, in particular in the eastern unit, which shows overall lower values for the amount of dry biomass.

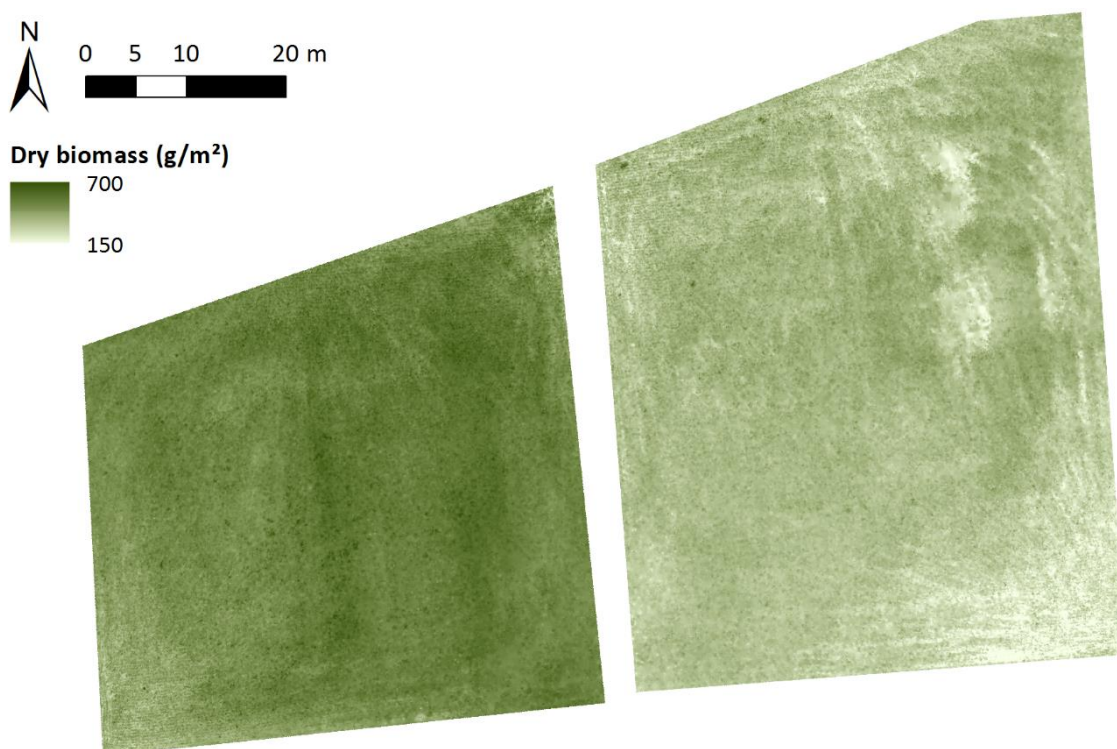


Figure 7-8. Dry biomass map of the paddy rice units in village 36 for the 16.07.2012. Estimated from the CSM-derived plant height with the BRM: $Biomass = 12.37 \cdot \text{plant height} - 273.19$ (Table 4-5).

Spatially resolved mapping of biomass at field scale is frequently performed with satellite remote sensing. Active systems with SAR sensors, for example, are useful to overcome problems of cloudiness and light dependency (Koppe et al., 2012; Ribbes and Le Toan, 1999; Zhang et al., 2014). Cloud-free conditions are necessary for observations with optical sensors,

which are further limited by the dependency on solar radiation. Nevertheless, acquisitions at multiple wavelengths allow the derivation of VIs which can be used for quantifying biomass (Claverie et al., 2012; Kross et al., 2015), but moreover they allow a qualitative assessment of parameters, such as the LAI or chlorophyll and nitrogen content (Clevers and Gitelson, 2013; Delegido et al., 2013). In-situ studies are widely performed since ground-based measurements are useful to evaluate satellite-derived data (Gnyp et al., 2014a; Koppe et al., 2010). Therefore, ground- or vehicle-based approaches with field spectrometers are investigated which aim at the derivation of VIs for estimating biomass (Casanova et al., 1998; Gnyp et al., 2014b; Montes et al., 2011; Thenkabail et al., 2000). In the meanwhile, the benefit of spectral measurements for evaluating the plant status during the growing season was also recognized in some areas of conventional agriculture. This use of optical sensors can be demonstrated by the number of available commercial devices, such as Crop Circle (Holland Scientific Inc., 2011), GreenSeeker (Nu-Tech International, 2015), ISARIA (Fritzmeier Umwelttechnik, 2015), or N-Sensor (Yara, 2015). These or similar sensors are extensively investigated in scientific studies (Cao et al., 2013; Erdle et al., 2011) and regularly used in practice (Gebbers et al., 2011; Thessler et al., 2011).

The spatial area covered by one spectrometer measurement is however small and hence the acquisition of an entire field is almost impossible and not intended with common sensors. Nevertheless, it is known that hyperspectral data are well suited for estimating plant parameters related to the canopy density and cover, such as the LAI (Broge and Leblanc, 2001; Haboudane et al., 2004) or for determining the water content (Clevers et al., 2008). Since qualitative statements are hardly possible with the TLS-derived plant heights, the fusion of spectral and non-spectral metrics is highly recommendable and targeted in the overall aim of this study (**Figure 1-2**). Moreover, reconsidering the assumed non-linear relation between plant height and biomass during the final growth stages (**Figure 7-6**), the information covered in the VIs might be valuable to improve biomass estimations. A literature search of existing research on the fusion of spectral and non-spectral estimators yielded only a few number of studies. Beside the already mentioned approach by Marshall and Thenkabail (2015), Reddersen et al. (2014) showed an approach for predicting grassland biomass from LAI, ultrasonic sward height, and VIs. Moreover, Bendig et al. (2015) presented first attempts of fusing UAV-based measurements of plant height with VIs.

A first step towards the fusion of TLS-derived plant height and spectral data is shown for the barley field experiment in Tilly et al. (2015a, Chapter 6). By establishing bivariate and multivariate BRMs based on plant height and six VIs, strengths and weaknesses of both parameters as individual estimators and the benefit of fusing plant height with each of the VIs were investigated. A main outcome of this study is that TLS-derived plant height is a robust individual estimator across all regarded cases (**Table 6-6**). For dry biomass R^2 values up to 0.85 (estimated vs. measured biomass) were reached with plant height as estimator, while the VIs showed highly differing results (R^2 : 0.07 - 0.87). It has to be noted that for the pre-anthesis some VIs (REIP, GnyLi, NRI) performed slightly better or equally good as plant height. In contrast, most of the VIs showed a better performance for the estimation of fresh biomass (R^2 : 0.21 - 0.82), while plant height performed slightly worse (R^2 up to 0.73). In order to assess

this, the activities in ripening cereals should be examined by considering in which plant parts assimilation occurs, meaning that exogenous substances are converted to endogenous compounds (Munzert and Frahm, 2005). **Figure 7-9** shows this for cereals after heading (BBCH stage 5, **Table 2-2**). It is clearly visible that assimilation processes take place almost entirely in the upper parts of the plants and that while plant height stays constant, the biomass increases, in particular due to the growing ears. Supported by the better performance of the VIs for the estimation of fresh biomass, it can be assumed that this increase in living plant material might be better determinable by qualitative aspects such as LAI or water content.

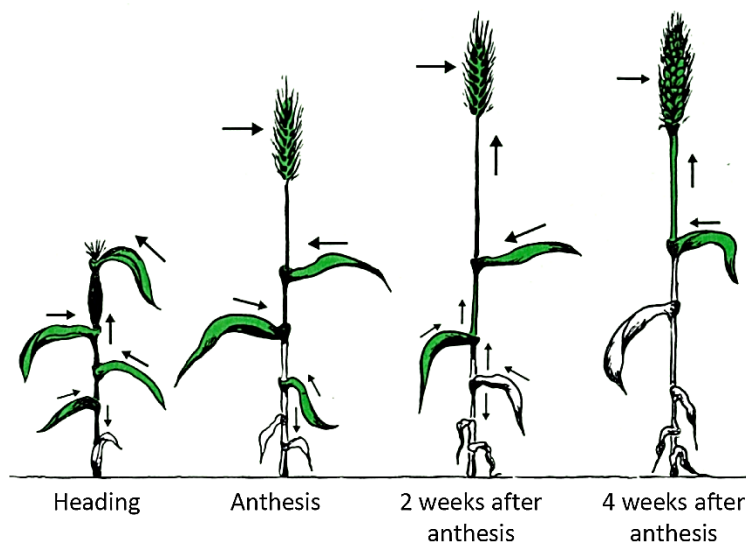


Figure 7-9. Assimilation in ripening cereal. Green color marks active plant parts. Modified from Munzert and Frahm (2005).

Although the multivariate BRMs could improve the estimations in some cases (R^2 up to 0.89), a major benefit could not be concluded. Nonetheless, the idea of such improved biomass estimations should not be rejected. This case studies was a first attempt and certain criticisms have to be stated, such as that VIs were used which are known for estimating biomass from hyperspectral data and further studies are necessary to investigate if other parts of the spectral range or other combinations of bands are better suitable. Moreover, six spectrometer measurements were carried out per plot but without assessing the x, y coordinates of each position. These measurements were averaged, resulting in 1D data sets with one spectrum per plot. Hence, possible in-plot variations in plant height could not be directly linked to variations of the density, LAI, or water. Recent studies show attempts of directly acquiring spatial and spectral data with one system, whereby errors related to different sensors can be prevented. Aasen et al. (2015), for example, introduced a method to obtain 3D hyperspectral information from a UAV-based snapshot camera. Based on the data of one campaign, they attained good results for the calculation of plant height ($R^2 = 0.70$) and moderate values for biomass ($R^2 = 0.29$). Compared to estimations across the growing season, analyses based on measurements of a single date are known to show a weaker performance. Thus it can be concluded that this approach should be further regarded with a more extensive data set.

Overall, the results of all case studies demonstrate the advantages of the presented approach. The major outcomes are that (I) TLS-derived plant heights show a strong

relationship to biomass, allowing the derivation of BRMs, (II) these BRMs enable non-destructive estimations based on independent plant height data sets, (III) spatially resolved biomass estimations at field scale are possible with a CSM, and (IV) an improvement of the BRMs through the fusion with spectral data cannot be concluded, but should be further targeted.

Nevertheless, some issues remain, which could not have been regarded in the framework of the case studies. This includes, for example, the variations between the cultivars of one cereal or the influence of the different fertilizer treatments. Further research is necessary, also bearing in mind whether very case-specific approaches and more complex models, such as the above mentioned allometric functions (Lemaire et al., 2007), are required or if rather general BRMs can be established by enlarging the data set.

7.5 Future prospects for laser scanning in agriculture

The used TLS systems and platforms performed satisfactorily in all case studies and demonstrated their usability for monitoring plant height. Furthermore, the developed approach offers potential for the realization in agricultural applications. Nevertheless, with regard to the stated issues of scanning geometry (**Figure 7-2**) or transportability (**Table 7-1**), consideration has to be given to the ongoing technical advances in the field of laser scanning. In connection with this, the overall availability of new platforms for remote sensing should also be considered.

In general, laser scanning systems are developing in two directions. The number of available high-end sensors increases constantly, with the focus on longer scanning ranges and/or higher measuring rates, such as the Riegl VZ-2000 (Riegl LMS GmbH, 2015a) or the Leica Scan Station P40 (Leica Geosystems, 2015). On the contrary, cost-effective systems come up, such as the Velodyne HDL-64E LiDAR sensor (Velodyne, 2014), enabling only acquisitions with lower resolutions but having the main advantage of being available for a broader audience. The decreasing prices and widespread availability can be shown by the variety of applications for which LiDAR sensors are already used. Several car manufacturer attempt to integrate them into self-driving cars, such as the Google Car (Boyko and Zhu, 2014). Moreover, LiDAR sensors are part of robots, like the rough-terrain robot BigDog (Boston Dynamics, 2013). Even though higher measuring rates and faster acquisitions are favorable, for price-oriented matters, as in the agricultural sector, approaches are required which are realizable in practical applications. Regarding this practicability three categories of systems should be considered, distinguishable through their position in relation to the regarded field. These are ground- or vehicle-based static systems, mobile systems which are mostly vehicle-based, and low-altitude airborne systems.

Maintaining the static position of TLS during the measurement, one opportunity is the establishment of monitoring stations at the field edges or in the center of a field. Permanently installed systems might be used for an almost continuous gathering of data across the growing season, without or with less human assistance. However, some issues have to be addressed first, such as the development of affordable systems with regard to the cost-benefit ratio, solutions for a weather-resistant and theft-proof installation, or the definition of the required

number of stations, taking into account the measuring range and point density. Moreover, monitoring approaches – as presented in the case studies – with static scanners, but which are movable between different locations are still meaningful. Based on such measurements with a proven method, the reliable knowledge about the behavior of crops across the growing season and their responds to changing environmental factors can be enlarged. Beyond that, the obtained data can be used as trustworthy reference source for the evaluation of newly developed methods.

Mobile mapping systems based on TLS, also known as mobile laser scanning (MLS), are already applied in some cases and should be further considered. Such systems emerged in the last two decades and are characterized by their kinematic measuring procedure, meaning the position and orientation of the scanner is variable during the scan (Kutterer, 2010). A main difference between static and kinematic systems is how the geometric relationship between the reflection points is obtained. Static systems capture point clouds with a good internal geometric quality and point clouds from different positions can be easily matched based on accurate DGPS data. In contrast, in the kinematic mode, each reflection point is captured in an own coordinate system due to the motion of the scanner. Consequently, for each reflection point the exact position and orientation of the system have to be derived from an inertial measurement unit (IMU) and a GNSS. Although the synchronization between these devices requires additional effort, the acquisition process can be accelerated, in particular in urban environments (Kutterer, 2010). Several systems are already available and benchmark analysis revealed elevation accuracies of up to 3.5 cm for road mapping (Kaartinen et al., 2012).

Such accuracy tests are hardly possible in agricultural applications, because the vegetation is very likely to move in contrast to the stable position of roads, building façades, or other objects in urban environments. A further challenge for the application of MLS in more rural environments is the choice of an appropriate platform, as field paths might be hardly accessible with conventional cars. In the last few years, different approaches focused on the development of other small vehicle-based MLS systems (Kukko et al., 2012). Moreover, some multi-sensor platforms exist, like the Phenomobile, which carries three LiDAR sensors, four RGB stereo cameras, a spectrometer or hyperspectral camera, and an infra-red thermometer or infra-red thermal camera (**Figure 7-10 (A)**; Deery et al., 2014). The achieved data is matched

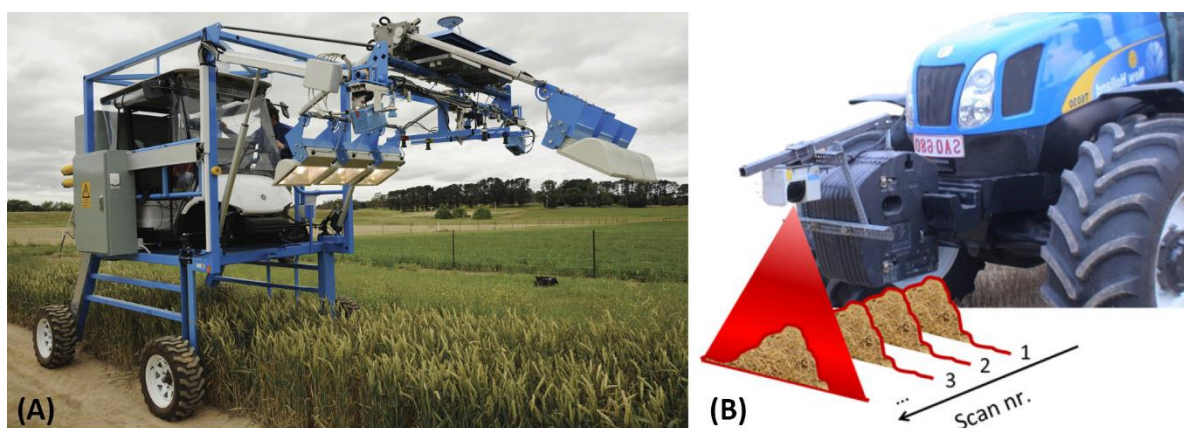


Figure 7-10. MLS systems for crop monitoring: (A) Phenomobile (Deery et al., 2014); (B) LiDAR sensor, attached to a combined harvester (Lenaerts et al., 2012).

based on the accurate GPS information. Hence, such platforms might greatly contribute to the simultaneous acquisition of spectral and non-spectral metrics. In general, MLS systems are frequently designed for the application at plot level and hence they are useful for monitoring field experiments, which are common practice in crop science, but hardly usable at field scale. However, for the practical application in conventional agriculture, MLS systems can also be worthwhile since, supposing that affordable systems are available, they might get attached to tractors or other vehicles and capture data during the regular field management. One potential application therefore is already shown with a LiDAR sensor, attached to a combined harvester for measuring the swath height of cereals (**Figure 7-10 (B)**; Lenaerts et al., 2012). The authors expect that with this knowledge machine settings can be optimized to prevent damages of straws, which would lower the quality and thus reduce the price. Beside the use of vehicles as platform, applications with humans as source of motion, also referred to as personal laser scanning (PLS) (Liang et al., 2013), should be considered. So far only used in pioneering studies on the detection of trees, backpack systems like the AKHKA R2 (Liang et al., 2013) or hand-held mobile laser scanner such as the ZEB1 (Ryding et al., 2015) might be useful for crop monitoring.

Low-altitude airborne systems are also conceivable platforms for laser scanning. A distinction has to be drawn between manned and unmanned systems. As an example for the latter, the recently introduced Riegl RiCOPTER (Riegl LMS GmbH, 2015b) should be mentioned as a promising system. In addition to the LiDAR sensor, this system already includes an IMU/GNSS unit and according to the manufacturer's specification the performance is also very good with a measuring rate of up to 350,000 points/sec, a maximal range of 550 m, and a range accuracy of 10 mm. The accuracy is however influenced by the position accuracy of the IMU/GNSS unit being specified to range from 0.05 m to 0.3 m. Unfortunately, studies on the application of the RiCOPTER are not available yet. Another promising UAV LiDAR system is the cost-effective alternative YellowScan (YellowScan, 2015). Even though the performance of the scanner is much lower (maximal measuring rate 40,000 points/sec; maximal range 150 m; range accuracy 10 cm), such low-cost systems should be considered for the price-oriented agricultural sector. Up to now, other UAV-based laser scanning systems were successfully used for detecting pruning of individual stems (Wallace et al., 2014) and determining tree heights (Jaakkola et al., 2010), but crop monitoring approaches have not been conducted yet. The usability of UAVs for crop monitoring has been demonstrated with RGB imaging (Bendig et al., 2014) and spectral measurements (**Figure 7-11 (A)**; Aasen et al., 2015; Honkavaara et al., 2013). Main benefits are the easy acquisition of large areas and the very flexible usage, but a weak point of this small systems is the vulnerability to wind and rain (Colomina and Molina, 2014).

In contrast, manned systems, like the gyrocopter shown in **Figure 7-11 (B)**, should be more resistant against poor weather, due to their size and general construction. Although less research has been done on these platforms yet, gyrocopters reveal potential as laser scanning platform due to their flexible usage, high maximum payload and assumable stable position. Unfortunately, this system is only equipped with a conventional RGB-, a thermal-, and a hyperspectral snapshot camera so far (Weber et al., 2015). However, a few commercial

companies already offer LiDAR-based mapping services with gyrocopters (LiDAR USA, 2015; WekuFly, 2015). A major issue for both types of airborne systems is that flight permissions have to be regarded for all systems depending on the national laws. Moreover, the different viewing perspectives have to be regarded, considering the comparability with measurements from ground- or vehicle-based platforms.

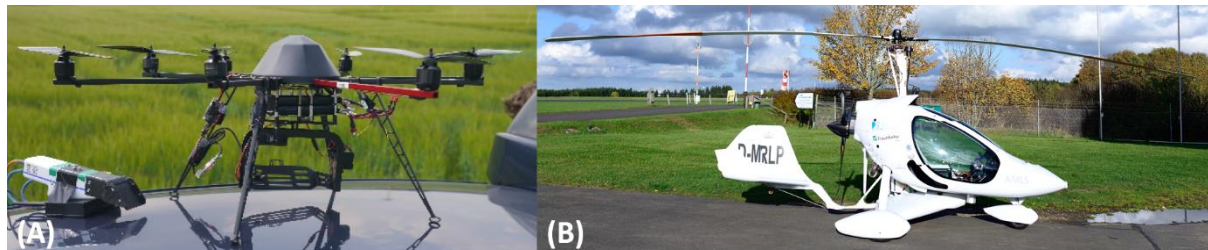


Figure 7-11. Low-altitude airborne platforms: (A) MikroCopter Okto XL with hyperspectral snapshot camera (modified from Aasen et al., 2015); (B) Gyrocopter (Weber et al., 2015).

As already shown for the different sensor heights of the TLS platforms (**Figure 7-2**), the inclination angle and scanning geometry are likely to influence the results. Taking now into account that the perspective of airborne measurements is commonly nadir or almost nadir, acquired data and ground- or vehicle- based measurements from an oblique perspective cannot be compared without further ado. Nevertheless, a combination of both methods is advisable as also shown in a comparative study on modeling peatland surface structures from TLS and common plane-based ALS (Luscombe et al., 2014). Based on the request for improving ALS-based digital surface models, the authors emphasize the consideration of TLS to attain canopy structure in a finer spatial resolution and with greater precision. However, considering the issues arising from different perspective, low-altitude ALS systems might be more suitable since they allow a similar nadir perspective. Conversely to the downscaling of plane-based ALS, the use of low-altitude ALS systems might enable to upscale the CSM-based approach for crop monitoring across larger areas. A first attempt of estimating biomass from plane-based ALS data was presented by Li et al. (2015). Based on the data set of a single campaign, they achieved good results for estimating canopy height, LAI, and biomass of maize. The validation analysis against field-measured aboveground biomass revealed high R^2 values of 0.82.

Finally, reconsidering the simultaneous acquisition of 3D data of plant height and spectral data, the development of hyperspectral scanners (Suomalainen et al., 2011) has to be regarded as promising solution. First laboratory studies showed the usability for capturing spectral data and visualizing the gained spectral indices as a 3D point cloud for a Norway spruce (Hakala et al., 2012) or for classifying spruce and pine trees (Vauhkonen et al., 2014). Similar attempts in forestry applications were also performed with multispectral systems. Gaulton et al. (2013), for example, presented an approach with a dual-wavelength laser scanner for measuring the 3D distribution of vegetation biochemical properties. Another multi-wavelength system with four lasers was introduced by Wei et al. (2012) as promising system for acquiring the physiology of a canopy. Even though the applicability under field conditions and usability for crop monitoring is not shown yet, a high potential can be assumed for such systems.

The application of other wavelengths than the typically used near-infrared light is also findable in other research fields. Arising from the limited applicability of these conventional systems under wet conditions a demand for systems operating with other wavelengths emerged. In airborne laser bathymetry a green laser beam can be used to detect submerged structures (Doneus et al., 2013). Very recently a few systems were introduced which operate with more than one wavelength (Doneus et al., 2015), like the HawkEye III (AHAB, 2015), the Optech Titan (Teledyne Optech Inc., 2015), or the RIEGL VQ-880-G (Riegl LMS GmbH, 2015c). Generally, the application of such airborne systems in agricultural applications is conceivable, but prior an appropriate platform has to be found. Commonly used planes are not flexible enough and the payload of UAVs would be widely exceeded. Hence, the above portrayed gyrocopter might be a suitable platform.

Overall, the range of possible applications for laser scanning in agriculture is very large and depending on the purpose, different platforms and systems appear to be best suitable. With regard to the general increasing focus on site-specific crop management, a growing request for non-destructive monitoring approaches can be prognosticated. Beside the general advantages of laser scanning as reliable measuring system, the accomplished results demonstrate the usability for crop monitoring. Consequently, further research on the realization in practical approaches is desirable.

8 Conclusion

Terrestrial laser scanning (TLS) is a promising system for monitoring the plant height of crops. The greatest strength of this approach is the possibility to easily acquire 3D data of plant height at field level with a very high spatial resolution. Moreover, the ground-based active sensor allows a flexible use and the frequency of measurements can be adapted to the required temporal resolution. This overall evaluation shall address both the field surveys and the achieved data.

In the field, each platform showed advantages and disadvantages, but overall vehicle-based set-ups are preferable. They have major benefits such as an easier transport of the scanner in the field but the stability of the platform in particular during the measurements has to be regarded. The larger sensor height seems to be useful for an exact detection of the crop surface even if a comprehensive analysis was not possible in this study. Hence, further research on the influence of the sensor height and scanning geometry on the results is necessary. In this context, the oblique perspective of the scanner, due to the acquisition from the field edges, has to be regarded. The herein regarded crops paddy rice, maize, and barley all belong to the group of cereals which is the most important group for world nutrition. Most of the other representatives of this group, such as wheat, rye, or oat are cultivated on easily accessible fields. For these crops measuring methods might be better implementable, which can be carried out directly from vehicles used for the regular field management, such as approaches with mobile laser scanning. However, a transferability of the presented approach to other crops, such as tea, sunflower, or sorghum is conceivable. Since an entering of these fields during the growing season is not possible or difficult due to the large plant heights or flooded fields, acquisitions from the field edges are unavoidable.

Regarding the achieved data, the major outcomes can be concluded according to the working process, portrayed at the beginning of this thesis:

- I. TLS is well suitable for acquiring 3D point clouds at plot and field level.
- II. The point clouds can be interpolated to CSM, which represent the entire crop canopy of a field as a 2.5D data set in a very high resolution.
- III. By subtracting a DTM of the bare ground from each CSM, plant heights can be calculated pixel-wise.
- IV. Reliable BRMs can be established based on the 1D data sets, in which plant height and biomass are spatially averaged across common areas.
- V. A major benefit from the fusion of plant height and VIs in multivariate BRMs cannot be concluded, whereby plant height outperforms most of the used VIs.
- VI. The validation against comparative data underlines the correctness of the TLS-derived data and demonstrates the advantages and robustness of this approach.

Considering now the demand for such measurements, it should be recalled that the plant status depends on variable factors, such as weather and soil conditions or field management practices. Biomass-related indices, such as the harvest index and NNI, are widely used to quantify this plant status, but the direct non-destructive determination of biomass is not possible. Hence, it can be concluded that the main benefits of this TLS-based approach, such

as the very high spatial resolution, the temporal flexibility, and the acquisition of the entire crop surface are worthwhile for a spatially resolved evaluation of the plant status and based on that optimize site-specific crop management. The comparison of plant height and VIs as individual estimators in the barley case study showed that plant height is a recommendable and robust plant parameter for estimating biomass. Nevertheless, it has to be noted that VIs are important for capturing parameters of the vegetation cover, like density or leaf area index and biochemical or biophysical parameters, such as nitrogen, chlorophyll, or water content. Consequently, research should further focus on a useful simultaneous acquisition of plant height and spectral data.

The rising trend towards precision agriculture or rather site-specific crop management since the late 20th century and the generally increasing recognition of the interaction between food security and sustainability caused a growing research focus on non-contact surveys with remote sensing sensors for agricultural applications. A diversity of approaches for different purposes is already available, each of which has certain advantages and disadvantages. Looking at the future, even though promising systems exist, the realization in practical applications for farmers is still insufficient. In this context, the above discussed conceivable approaches based on laser scanning offer promising solutions due to their flexible and quite independent applicability. Overall, the implementation of crop monitoring in conventional agriculture is urgently required to enable site-specific crop management and secure the food supply for almost 10 billion world citizens by the middle of this century.

References

Chapter 1, 2, and 7

- Aasen, H., Burkart, A., Bolten, A., Bareth, G., 2015. Generating 3D Hyperspectral Information with Lightweight UAV Snapshot Cameras for Vegetation Monitoring: From Camera Calibration to Quality Assurance. *ISPRS J. Photogramm. Remote Sens.* 108, 245–259. doi:10.1016/j.isprsjprs.2015.08.002
- Aasen, H., Gnyp, M.L., Miao, Y., Bareth, G., 2014. Automated hyperspectral vegetation index retrieval from multiple correlation matrices with HyperCor. *Photogramm. Eng. Remote Sens.* 80, 785–796. doi:10.14358/PERS.80.8.785
- Adamchuk, V.I., Hummel, J.W., Morgan, M.T., Upadhyaya, S.K., 2004. On-the-go soil sensors for precision agriculture. *Comput. Electron. Agric.* 44, 71–91. doi:10.1016/j.compag.2004.03.002
- AHAB, 2015. Datasheet Leica HawkEye-III. [http://www.airbornehydro.com/sites/default/files/Leica HawkEye-III. http://www.airbornehydro.com/sites/default/files/Leica AHAB HawkEye DS.pdf](http://www.airbornehydro.com/sites/default/files/Leica%20AHAB%20HawkEye%20DS.pdf)
- Allan, J.A., 1990. Sensors, Platforms and Applications; acquiring and managing remotely sensed data, in: Steven, M.D., Clark, J.A. (Eds.), *Applications of Remote Sensing in Agriculture*. Butterworths, London.
- Arendt, E., Zannini, E., 2013. *Cereal Grains for the Food and Beverage Industries, Food Science, Technology and Nutrition: Number 248*. Woodhead Publishing Limited, Oxford.
- Atzberger, C., 2013. Advances in Remote Sensing of Agriculture: Context Description, Existing Operational Monitoring Systems and Major Information Needs. *Remote Sens.* 5, 949–981. doi:10.3390/rs5020949
- Auernhammer, H., 2001. Precision farming - The environmental challenge. *Comput. Electron. Agric.* 30, 31–43. doi:10.1016/S0168-1699(00)00153-8
- Bendig, J., Bolten, A., Bennertz, S., Broscheit, J., Eichfuss, S., Bareth, G., 2014. Estimating Biomass of Barley Using Crop Surface Models (CSMs) Derived from UAV-Based RGB Imaging. *Remote Sens.* 6, 10395–10412. doi:10.3390/rs61110395
- Bendig, J., Yu, K., Aasen, H., Bolten, A., Bennertz, S., Broscheit, J., Gnyp, M.L., Bareth, G., 2015. Combining UAV-based plant height from crop surface models, visible, and near infrared vegetation indices for biomass monitoring in barley. *Int. J. Appl. Earth Obs. Geoinf.* 39, 79–87. doi:10.1016/j.jag.2015.02.012
- Beraldin, J.-A., Blais, F., Lohr, U., 2010. Laser Scanning Technology, in: Vosselman, G., Maas, H.G. (Eds.), *Airborne and Terrestrial Laser Scanning*. CRC Press Taylor & Francis Group, Boca Raton, pp. 1–39.
- Bidinger, F., Musgrave, R.B., Fischer, R.A., 1977. Contribution of stored pre-anthesis assimilate to grain yield in wheat and barley. *Nature* 270, 431–433. doi:10.1038/270431a0
- Boston Dynamics, 2013. BigDog - The Most Advanced Rough-Terrain Robot on Earth. http://www.bostondynamics.com/robot_bigdog.html
- Boukerrou, L., Rasmusson, D.D., 1990. Breeding for High Biomass Yield in Spring Barley. *Crop Sci.* 30, 31–35. doi:10.2135/cropsci1990.0011183X003000010007x
- Boyko, A.S., Zhu, J., 2014. Using geometric features and history information to detect features such as car exhaust in point maps. <https://www.google.com/patents/US8818609>
- Briese, C., 2010. Extraction of Digital Terrain Models, in: Vosselman, G., Maas, H.G. (Eds.), *Airborne and Terrestrial Laser Scanning*. CRC Press Taylor & Francis Group, Boca Raton, pp. 135–167.

- Broge, N.H., Leblanc, E., 2001. Comparing prediction power and stability of broadband and hyperspectral vegetation indices for estimation of green leaf area index and canopy chlorophyll density. *Remote Sens. Environ.* 76, 156–172. doi:10.1016/S0034-4257(00)00197-8
- Buckley, S.J., Howell, J.A., Enge, H.D., Kurz, T.H., 2008. Terrestrial laser scanning in geology: data acquisition, processing and accuracy considerations. *J. Geol. Soc. London.* 165, 625–638. doi:10.1144/0016-76492007-100
- Busemeyer, L., Mentrup, D., Möller, K., Wunder, E., Alheit, K., Hahn, V., Maurer, H.P., Reif, J.C., Würschum, T., Müller, J., Rahe, F., Ruckelshausen, A., 2013. Breedvision - A multi-sensor platform for non-destructive field-based phenotyping in plant breeding. *Sensors* 13, 2830–2847. doi:10.3390/s130302830
- Campbell, J.B., Wynne, R.H., 2011. *Introduction to Remote Sensing*, 5th ed. The Guilford Press, New York.
- Cao, Q., Miao, Y., Wang, H., Huang, S., Cheng, S., Khosla, R., Jiang, R., 2013. Non-destructive estimation of rice plant nitrogen status with Crop Circle multispectral active canopy sensor. *F. Crop. Res.* 154, 133–144. doi:10.1016/j.fcr.2013.08.005
- Casanova, D., Epema, G.F., Goudriaan, J., 1998. Monitoring rice reflectance at field level for estimating biomass and LAI. *F. Crop. Res.* 55, 83–92. doi:10.1016/S0378-4290(97)00064-6
- Claverie, M., Demarez, V., Duchemin, B., Hagolle, O., Ducrot, D., Marais-Sicre, C., Dejoux, J.-F., Huc, M., Keravec, P., Béziat, P., Fieuzal, R., Ceschia, E., Dedieu, G., 2012. Maize and sunflower biomass estimation in southwest France using high spatial and temporal resolution remote sensing data. *Remote Sens. Environ.* 124, 844–857. doi:10.1016/j.rse.2012.04.005
- Clevers, J.G.P.W., Gitelson, A.A., 2013. Remote estimation of crop and grass chlorophyll and nitrogen content using red-edge bands on Sentinel-2 and -3. *Int. J. Appl. Earth Obs. Geoinf.* 23, 344–351. doi:10.1016/j.jag.2012.10.008
- Clevers, J.G.P.W., Kooistra, L., Schaepman, M.E., 2008. Using spectral information from the NIR water absorption features for the retrieval of canopy water content. *Int. J. Appl. Earth Obs. Geoinf.* 10, 388–397. doi:10.1016/j.jag.2008.03.003
- Colomina, I., Molina, P., 2014. Unmanned aerial systems for photogrammetry and remote sensing: A review. *ISPRS J. Photogramm. Remote Sens.* 92, 79–97. doi:10.1016/j.isprsjprs.2014.02.013
- Deery, D., Jimenez-Berni, J., Jones, H., Sirault, X., Furbank, R., 2014. Proximal Remote Sensing Buggies and Potential Applications for Field-Based Phenotyping, *Agronomy*. doi:10.3390/agronomy4030349
- Delegido, J., Verrelst, J., Meza, C.M., Rivera, J.P., Alonso, L., Moreno, J., 2013. A red-edge spectral index for remote sensing estimation of green LAI over agroecosystems. *Eur. J. Agron.* 46, 42–52. doi:10.1016/j.eja.2012.12.001
- DigitalGlobe, 2014. Datasheet WorldView-3. https://www.digitalglobe.com/sites/default/files/DG_WorldView3_DS_forWeb_0.pdf
- Ding, Y., Chan, J.C.L., 2005. The East Asian summer monsoon: an overview. *Meteorol. Atmos. Phys.* 89, 117–142. doi:10.1007/s00703-005-0125-z
- Doneus, M., Doneus, N., Briese, C., Pregesbauer, M., Mandlbürger, G., Verhoeven, G., 2013. Airborne laser bathymetry – detecting and recording submerged archaeological sites from the air. *J. Archaeol. Sci.* 40, 2136–2151. doi:10.1016/j.jas.2012.12.021

- Doneus, M., Miholjek, I., Mandlbürger, G., Doneus, N., Verhoeven, G., Briese, C., Pregesbauer, M., 2015. Airborne Laser Bathymetry for Documentation of Submerged Archaeological Sites in Shallow Water. *ISPRS - Int. Arch. Photogramm. Remote Sens. Spat. Inf. Sci.* XL-5/W5, 99–107. doi:10.5194/isprsarchives-XL-5-W5-99-2015
- Edney, M.J., 2010. Barley: characteristics and quality requirements, in: Wrigley, C., Batey, I. (Eds.), *Cereal Grains: Assessing and Managing Quality*. Woodhead Publishing Limited, Oxford, pp. 141–162. doi:10.1533/978-1-84569-563-7.2.141
- Ehlert, D., Heisig, M., 2013. Sources of angle-dependent errors in terrestrial laser scanner-based crop stand measurement. *Comput. Electron. Agric.* 93, 10–16. doi:10.1016/j.compag.2013.01.002
- Ehlert, D., Heisig, M., Adamek, R., 2010. Suitability of a laser rangefinder to characterize winter wheat. *Precis. Agric.* 11, 650–663. doi:10.1007/s11119-010-9191-4
- Eitel, J.U.H., Magney, T.S., Vierling, L.A., Brown, T.T., Huggins, D.R., 2014. LiDAR based biomass and crop nitrogen estimates for rapid, non-destructive assessment of wheat nitrogen status. *F. Crop. Res.* 159, 21–32. doi:10.1016/j.fcr.2014.01.008
- Eitel, J.U.H., Vierling, L.A., Long, D.S., Raymond Hunt, E., 2011. Early season remote sensing of wheat nitrogen status using a green scanning laser. *Agric. For. Meteorol.* 151, 1338–1345. doi:10.1016/j.agrformet.2011.05.015
- Erdle, K., Mistele, B., Schmidhalter, U., 2011. Comparison of active and passive spectral sensors in discriminating biomass parameters and nitrogen status in wheat cultivars. *F. Crop. Res.* 124, 74–84. doi:10.1016/j.fcr.2011.06.007
- FAO, 2014. FAOSTAT. <http://faostat3.fao.org/faostat-gateway/go/to/home/E>
- FAO, 2011. Crops statistics - concepts, definitions and classifications. <http://www.fao.org/economic/the-statistics-division-ess/methodology/methodology-systems/crops-statistics-concepts-definitions-and-classifications/en/>
- FAO, 1994. Definition and classification of commodities. <http://www.fao.org/es/faodef/fdef01e.htm>
- Feekes, W., 1941. De Tarwe en haar milieu. *Versl. van Tech. Tarwe Comm.* 17, 560–561.
- Fischer, R.A., 1993. Irrigated spring wheat and timing and amount of nitrogen fertilizer. II. Physiology of grain yield response. *F. Crop. Res.* 33, 57–80. doi:10.1016/0378-4290(93)90094-4
- Fischer, R.A., 1983. Wheat, in: International Rice Research Institute (Ed.), *Potential Productivity of Field Crops Under Different Environments*. Los Baños Laguna, Philippines, pp. 129–154.
- Fritzmeier Umwelttechnik, 2015. ISARIA. <http://fritzmeier-umwelttechnik.com/index.php/isaria/>
- Gao, J., Liu, Y., 2011. Climate warming and land use change in Heilongjiang Province, Northeast China. *Appl. Geogr.* 31, 476–482. doi:10.1016/j.apgeog.2010.11.005
- Gaulton, R., Danson, F.M., Ramirez, F.A., Gunawan, O., 2013. The potential of dual-wavelength laser scanning for estimating vegetation moisture content. *Remote Sens. Environ.* 132, 32–39. doi:10.1016/j.rse.2013.01.001
- Gebbers, R., Ehlert, D., Adamek, R., 2011. Rapid Mapping of the Leaf Area Index in Agricultural Crops. *Agron. J.* 103, 1532–1541. doi:10.2134/agronj2011.0201
- Gnyp, M., 2014. Evaluating and Developing Methods for Non-Destructive Monitoring of Biomass and Nitrogen in Wheat and Rice Using Hyperspectral Remote Sensing. Dissertation, University of Cologne.

- Gnyp, M.L., Bareth, G., Li, F., Lenz-Wiedemann, V.I.S., Koppe, W., Miao, Y., Hennig, S.D., Jia, L., Laudien, R., Chen, X., Zhang, F., 2014a. Development and implementation of a multiscale biomass model using hyperspectral vegetation indices for winter wheat in the North China Plain. *Int. J. Appl. Earth Obs. Geoinf.* 33, 232–242. doi:10.1016/j.jag.2014.05.006
- Gnyp, M.L., Miao, Y., Yuan, F., Ustin, S.L., Yu, K., Yao, Y., Huang, S., Bareth, G., 2014b. Hyperspectral canopy sensing of paddy rice aboveground biomass at different growth stages. *F. Crop. Res.* 155, 42–55. doi:10.1016/j.fcr.2013.09.023
- Guyot, G., Baret, F., Jacquemoud, S., 1992. Imaging spectroscopy for vegetation studies, in: Toselli, F., Bodechtel, J. (Eds.), *Imaging Spectroscopy for Vegetation Studies*. Kluwer, Dordrecht, Netherlands, pp. 145–165.
- Haboudane, D., Miller, J.R., Pattey, E., Zarco-Tejada, P.J., Strachan, I.B., 2004. Hyperspectral vegetation indices and novel algorithms for predicting green LAI of crop canopies: Modeling and validation in the context of precision agriculture. *Remote Sens. Environ.* 90, 337–352. doi:10.1016/j.rse.2003.12.013
- Hakala, T., Suomalainen, J., Kaasalainen, S., Chen, Y., 2012. Full waveform hyperspectral LiDAR for terrestrial laser scanning. *Opt. Express* 20, 7119–7127. doi:10.1364/OE.20.007119
- Hämmerle, M., Höfle, B., 2014. Effects of Reduced Terrestrial LiDAR Point Density on High-Resolution Grain Crop Surface Models in Precision Agriculture. *Sensors* 14, 24212–24230. doi:10.3390/s141224212
- Hoffmeister, D., 2014. Feasibility studies of terrestrial laser scanning in Coastal Geomorphology, Agronomy, and Geoarchaeology. Dissertation, University of Cologne.
- Hoffmeister, D., Bolten, A., Curdt, C., Waldhoff, G., Bareth, G., 2010. High resolution Crop Surface Models (CSM) and Crop Volume Models (CVM) on field level by terrestrial laser scanning, in: Guo, H., Wang, C. (Eds.), *Proc. of SPIE, 6th International Symposium on Digital Earth*. Beijing, China. doi:10.1117/12.872315
- Hoffmeister, D., Tilly, N., Bendig, J., Curdt, C., Bareth, G., 2012. Detektion von Wachstumsvariabilität in vier Zuckerrübensorten, in: Clasen, M., Fröhlich, G., Bernhardt, H., Hildebrand, K., Theuvsen, B. (Eds.), *Informationstechnologie Für Eine Nachhaltige Landwirtschaft*, Proc. 32. GIL-Jahrestagung. Köllen Verlag, Bonn, Germany, Freising, pp. 135–138.
- Höfle, B., 2014. Radiometric Correction of Terrestrial LiDAR Point Cloud Data for Individual Maize Plant Detection. *Geosci. Remote Sens. Lett. IEEE* 11, 94–98. doi:10.1109/LGRS.2013.2247022
- Holland Scientific Inc., 2011. Crop Circle ACS-470. <http://hollandscientific.com/crop-circle-acs-470-multi-spectral-crop-canopy-sensor/>
- Honkavaara, E., Saari, H., Kaivosoja, J., Pölönen, I., Hakala, T., Litkey, P., Mäkynen, J., Pesonen, L., 2013. Processing and assessment of spectrometric, stereoscopic imagery collected using a lightweight UAV spectral camera for precision agriculture. *Remote Sens.* 5, 5006–5039. doi:10.3390/rs5105006
- Hosoi, F., Omasa, K., 2012. Estimation of vertical plant area density profiles in a rice canopy at different growth stages by high-resolution portable scanning lidar with a lightweight mirror. *ISPRS J. Photogramm. Remote Sens.* 74, 11–19. doi:10.1016/j.isprsjprs.2012.08.001
- Hosoi, F., Omasa, K., 2009. Estimating vertical plant area density profile and growth parameters of a wheat canopy at different growth stages using three-dimensional portable lidar imaging. *ISPRS J. Photogramm. Remote Sens.* 64, 151–158. doi:10.1016/j.isprsjprs.2008.09.003

- Jaakkola, A., Hyypä, J., Kukko, A., Yu, X., Kaartinen, H., Lehtomäki, M., Lin, Y., 2010. A low-cost multi-sensoral mobile mapping system and its feasibility for tree measurements. *ISPRS J. Photogramm. Remote Sens.* 65, 514–522. doi:10.1016/j.isprsjprs.2010.08.002
- Jensen, J.R., 2007. *Remote Sensing of the Environment*, 2nd ed. Prentice Hall, Upper Saddle River, NJ.
- Juliano, B.O., 2004. Rice/Overview, in: Wrigley, C., Corke, H., Walker, C.E. (Eds.), *Encyclopedia of Grain Science*. Elsevier, pp. 41–48.
- Kaartinen, H., Hyypä, J., Kukko, A., Jaakkola, A., Hyypä, H., 2012. Benchmarking Mobile Laser Scanning Systems Using a Permanent Test Field. *Sensors* 12, 12814–12835. doi:10.3390/s120912814
- Kaasalainen, S., Jaakkola, A., Kaasalainen, M., Krooks, A., Kukko, A., 2011. Analysis of Incidence Angle and Distance Effects on Terrestrial Laser Scanner Intensity: Search for Correction Methods. *Remote Sens.* 3, 2207–2221. doi:10.3390/rs3102207
- Kamal, M., Phinn, S., Johansen, K., 2015. Object-Based Approach for Multi-Scale Mangrove Composition Mapping Using Multi-Resolution Image Datasets. *Remote Sens.* 7, 4753–4783. doi:10.3390/rs70404753
- Kim, Y., Lee, H., Hong, S., 2013. Continuous Monitoring of Rice Growth With a Stable Ground-Based Scatterometer System. *Geosci. Remote Sens. Lett. IEEE* 10, 831–835. doi:10.1109/LGRS.2012.2225595
- Kling, J.G., Hayes, P.M., Ullrich, S.E., 2004. Barley/Genetics and Breeding, in: Wrigley, C., Corke, H., Walker, C.E. (Eds.), *Encyclopedia of Grain Science*. Elsevier, pp. 27–38.
- Koenig, K., Höfle, B., Hämmerle, M., Jarmer, T., Siegmann, B., 2015. Comparative classification analysis of post-harvest growth detection from terrestrial LiDAR point clouds in precision agriculture. *ISPRS J. Photogramm. Remote Sens.* 104, 112–125. doi:10.1016/j.isprsjprs.2015.03.003
- Koppe, W., Gnyp, M.L., Hennig, S.D., Li, F., Miao, Y., Chen, X., Jia, L., Bareth, G., 2012. Multi-Temporal Hyperspectral and Radar Remote Sensing for Estimating Winter Wheat Biomass in the North China Plain. *Photogramm. - Fernerkundung - Geoinf.* 3, 281–298. doi:10.1127/1432-8364/2012/0117
- Koppe, W., Li, F., Gnyp, M.L., Miao, Y., Jia, L., Chen, X., Zhang, F., Bareth, G., 2010. Evaluating Multispectral and Hyperspectral Satellite Remote Sensing Data for Estimating Winter Wheat Growth Parameters at Regional Scale in the North China Plain. *Photogramm. - Fernerkundung - Geoinf.* 3, 167–178. doi:10.1127/1432-8364/2010/0047
- Kross, A., McNairn, H., Lapen, D., Sunohara, M., Champagne, C., 2015. Assessment of RapidEye vegetation indices for estimation of leaf area index and biomass in corn and soybean crops. *Int. J. Appl. Earth Obs. Geoinf.* 34, 235–248. doi:10.1016/j.jag.2014.08.002
- Kukko, A., Kaartinen, H., Hyypä, J., Chen, Y., 2012. Multiplatform Mobile Laser Scanning: Usability and Performance. *Sensors* 12, 11712–11733. doi:10.3390/s120911712
- Kutterer, H., 2010. Mobile Mapping, in: Vosselman, G., Maas, H.G. (Eds.), *Airborne and Terrestrial Laser Scanning*. CRC Press Taylor & Francis Group, Boca Raton, pp. 293–311.
- Lambers, K., Eisenbeiss, H., Sauerbier, M., Kupferschmidt, D., Gaisecker, T., Sotoodeh, S., Hanusch, T., 2007. Combining photogrammetry and laser scanning for the recording and modelling of the Late Intermediate Period site of Pinchango Alto, Palpa, Peru. *J. Archaeol. Sci.* 34, 1702–1712. doi:10.1016/j.jas.2006.12.008
- Larcher, W., 2003. *Physiological Plant Ecology*, 4th ed. Springer-Verlag Berlin Heidelberg.

- Large, A.R.G., Heritage, G.L., 2009. Laser Scanning – Evolution of the Discipline, in: Heritage, G.L., Large, A.R.G. (Eds.), *Laser Scanning for the Environmental Sciences*. Wiley-Blackwell, West Sussex, UK, pp. 1–20.
- Large, E.C., 1954. Growth stages in cereals - Illustration of the Feekes scale. *Plant Pathol.* 3, 128–129. doi:10.1111/j.1365-3059.1954.tb00716.x
- Lee, E.A., 2004. Maize/Genetics, in: Wrigley, C., Corke, H., Walker, C.E. (Eds.), *Encyclopedia of Grain Science*. Elsevier, pp. 191–204.
- Lee, W.S., Alchanatis, V., Yang, C., Hirafuji, M., Moshou, D., Li, C., 2010. Sensing technologies for precision specialty crop production. *Comput. Electron. Agric.* 74, 2–33. doi:10.1016/j.compag.2010.08.005
- Leica Geosystems, 2015. Datasheet Leica ScanStation P40. http://www.leica-geosystems.com/downloads123/hds/hds/general/brochures-datasheet/Leica_ScanStation_P30-P40_Plant_DS_en.pdf
- Lemaire, G., Jeuffroy, M.-H., Gastal, F., 2008. Diagnosis tool for plant and crop N status in vegetative stage. *Eur. J. Agron.* 28, 614–624. doi:10.1016/j.eja.2008.01.005
- Lemaire, G., Oosterom, E. Van, Sheehy, J., Jeuffroy, M.H., Massignam, A., Rossato, L., 2007. Is crop N demand more closely related to dry matter accumulation or leaf area expansion during vegetative growth? *F. Crop. Res.* 100, 91–106. doi:10.1016/j.fcr.2006.05.009
- Lenaerts, B., Missotten, B., De Baerdemaeker, J., Saeys, W., 2012. LiDaR sensing to monitor straw output quality of a combine harvester. *Comput. Electron. Agric.* 85, 40–44. doi:10.1016/j.compag.2012.03.011
- Li, W., Niu, Z., Huang, N., Wang, C., Gao, S., Wu, C., 2015. Airborne LiDAR technique for estimating biomass components of maize : A case study in Zhangye City, Northwest China. *Ecol. Indic.* 57, 486–496. doi:10.1016/j.ecolind.2015.04.016
- Liaghat, S., Balasundram, S.K., 2010. A Review : The role of remote sensing in precision agriculture. *Am. Soc. Agric. Biol. Eng.* 5, 50–55. doi:10.3844/ajabssp.2010.50.55
- Liang, X., Kukko, A., Kaartinen, H., Hyyppä, J., Yu, X., Jaakkola, A., Wang, Y., 2013. Possibilities of a personal laser scanning system for forest mapping and ecosystem services. *Sensors* 14, 1228–1248. doi:10.3390/s140101228
- LiDAR USA, 2015. SkyLook. <http://www.lidarusa.com/gyrosolutions.php>
- Lillesand, T.M., Kiefer, R.W., Chipman, J.W., 2004. *Remote Sensing and Image Interpretation*, 5th ed. Wiley, Danvers, MA.
- Liu, X., Dong, G., Wang, X., Xue, Z., Jiang, M., Lu, X., Zhang, Y., 2013. Characterizing the spatial pattern of marshlands in the Sanjiang Plain, Northeast China. *Ecol. Eng.* 53, 335–342. doi:10.1016/j.ecoleng.2012.12.071
- Löffler, E., 1985. *Geographie und Fernerkundung*. Springer, Wiesbaden.
- Lumme, J., Karjalainen, M., Kaartinen, H., Kukko, A., Hyyppä, J., Hyyppä, H., Jaakkola, A., Kleemola, J., 2008. Terrestrial laser scanning of agricultural crops. *Int. Arch. Photogramm. Remote Sens. Spat. Inf. Sci.* 37 (Part B5) 563–566.
- Luscombe, D.J., Anderson, K., Gatis, N., Wetherelt, A., Grand-Clement, E., Brazier, R.E., 2014. What does airborne LiDAR really measure in upland ecosystems? *Ecohydrology* 8, 584–594. doi:10.1002/eco.1527
- Marsden, T., Morley, A., 2014. Current food questions and their scholarly challenges, in: Marsden, T., Morley, A. (Eds.), *Sustainable Food Systems*. Routledge, Abingdon, Oxon, pp. 1–29.

- Marshall, M., Thenkabail, P., 2015. Developing in situ Non-Destructive Estimates of Crop Biomass to Address Issues of Scale in Remote Sensing. *Remote Sens.* 7, 808–835. doi:10.3390/rs70100808
- Michell, P., Large, R. V., 1983. The estimation of herbage mass of perennial ryegrass swards: a comparative evaluation of a rising-plate meter and a single-probe capacitance meter calibrated at and above ground level. *Grass Forage Sci.* 38, 295–299. doi:10.1111/j.1365-2494.1983.tb01652.x
- Montes, J.M., Technow, F., Dhillon, B.S., Mauch, F., Melchinger, A.E., 2011. High-throughput non-destructive biomass determination during early plant development in maize under field conditions. *F. Crop. Res.* 121, 268–273. doi:10.1016/j.fcr.2010.12.017
- Mulla, D.J., 2012. Twenty five years of remote sensing in precision agriculture: Key advances and remaining knowledge gaps. *Biosyst. Eng.* 114, 358–371. doi:10.1016/j.biosystemseng.2012.08.009
- Munzert, M., Frahm, J., 2005. *Pflanzliche Erzeugung*, 12th ed. BLV Buchverlag, München.
- Nemoto, K., Morita, S., Baba, T., 1995. Shoot and Root Development in Rice Related to the Phyllochron. *Crop Sci.* 35, 24–29. doi:10.2135/cropsci1995.0011183X003500010005x
- Nu-Tech International, 2015. GreenSeeker. <http://www.nutechinternational.com/nutech-green-seeker.htm>
- Oliver, M., 2013. An overview of precision agriculture, in: Oliver, M., Bishop, T., Marchant, B. (Eds.), *Precision Agriculture for Sustainability and Environmental Protection*. Springer, USA, pp. 3–19.
- Peel, M.C., Finlayson, B.L., McMahon, T.A., 2007. Updated world map of the Köppen-Geiger climate classification. *Hydrol. Earth Syst. Sci.* 11, 1633–1644. doi:hal-00298818
- Petrie, G., Toth, C.K., 2008. Introduction to Laser Ranging, Profiling, and Scanning, in: Shan, J., Toth, C.K. (Eds.), *Topographic Laser Ranging and Scanning*. CRC Press Taylor & Francis Group, Boca Raton.
- Price, C., Munns, R., 2010. Growth analysis: a quantitative approach, in: Munns, R., Schmidt, S., Beveridge, C. (Eds.), *Plants in Action*. Australia.
- Psomas, A., Kneubühler, M., Huber, S., Itten, K., 2011. Hyperspectral remote sensing for estimating aboveground biomass. *Int. J. Remote Sens.* 32, 9007–9031. doi:10.1080/01431161.2010.532172
- rapidlasso GmbH, 2015. LAStools. <http://rapidlasso.com/lastools/>
- Reddersen, B., Fricke, T., Wachendorf, M., 2014. A multi-sensor approach for predicting biomass of extensively managed grassland. *Comput. Electron. Agric.* 109, 247–260. doi:10.1016/j.compag.2014.10.011
- Research Centre Jülich, 2015. Climate statistics. http://www.fz-juelich.de/gs/DE/UEberUns/Organisation/S-U/Meteorologie/klima/statistik_tabelle.html?nn=1223380
- Ribbes, F., Le Toan, T., 1999. Rice field mapping and monitoring with RADARSAT data. *Int. J. Remote Sens.* 20, 745–765. doi:10.1080/014311699213172
- Riegl LMS GmbH, 2015a. Datasheet Riegl VZ-2000. http://www.riegl.com/uploads/tx_pxpriegldownloads/DataSheet_VZ-2000_2015-03-24.pdf
- Riegl LMS GmbH, 2015b. Infosheet RiCOPTER. http://www.riegl.com/uploads/tx_pxpriegldownloads/RiCOPTER_at_a_glance_2015-03-31.pdf
- Riegl LMS GmbH, 2015c. Datasheet Riegl VQ-880-G. http://www.riegl.com/uploads/tx_pxpriegldownloads/VQ-880-G_at_a_glance_2015-09-01.pdf

- Riegl LMS GmbH, 2013. Datasheet Riegl VZ-1000. http://www.riegl.com/uploads/tx_pxpriegldownloads/DataSheet_VZ-1000_18-09-2013.pdf
- Riegl LMS GmbH, 2010. Datasheet Riegl LMS-Z420i. http://www.riegl.com/uploads/tx_pxpriegldownloads/10_DataSheet_Z420i_03-05-2010.pdf
- Rudolph, S., van der Kruk, J., von Hebel, C., Ali, M., Herbst, M., Montzka, C., Pätzold, S., Robinson, D.A., Vereecken, H., Weihermüller, L., 2015. Linking satellite derived LAI patterns with subsoil heterogeneity using large-scale ground-based electromagnetic induction measurements. *Geoderma* 241-242, 262–271. doi:10.1016/j.geoderma.2014.11.015
- Ryding, J., Williams, E., Smith, M., Eichhorn, M., 2015. Assessing Handheld Mobile Laser Scanners for Forest Surveys. *Remote Sens.* 7, 1095–1111. doi:10.3390/rs70101095
- Schaefer, M., Inkpen, R., 2010. Towards a protocol for laser scanning of rock surfaces. *Earth Surf. Process. Landforms* 35, 417–423. doi:10.1002/esp.1938
- Schultz, J., 2005. *The Ecozones of the World*, 2nd ed. Springer, Berlin Heidelberg New York.
- Suomalainen, J., Hakala, T., Kaartinen, H., Räikkönen, E., Kaasalainen, S., 2011. Demonstration of a virtual active hyperspectral LiDAR in automated point cloud classification. *ISPRS J. Photogramm. Remote Sens.* 66, 637–641. doi:10.1016/j.isprsjprs.2011.04.002
- Teledyne Optech Inc., 2015. Datasheet Optech Titan. <http://www.teledyneoptech.com/wp-content/uploads/Titan-Specsheet-150515-WEB.pdf>
- Thenkabail, P.S., Smith, R.B., De Pauw, E., 2000. Hyperspectral Vegetation Indices and Their Relationships with Agricultural Crop Characteristics. *Remote Sens. Environ.* 71, 158–182. doi:10.1016/S0034-4257(99)00067-X
- Thessler, S., Kooistra, L., Teye, F., Huitu, H., Bregt, A., 2011. Geosensors to Support Crop Production: Current Applications and User Requirements. *Sensors* 11, 6656–6684. doi:10.3390/s110706656
- Tilly, N., Aasen, H., Bareth, G., 2015a. Fusion of Plant Height and Vegetation Indices for the Estimation of Barley Biomass. *Remote Sens.* 7, 11449–11480. doi:10.3390/rs70911449
- Tilly, N., Hoffmeister, D., Cao, Q., Huang, S., Lenz-Wiedemann, V., Miao, Y., Bareth, G., 2014a. Multitemporal crop surface models: accurate plant height measurement and biomass estimation with terrestrial laser scanning in paddy rice. *J. Appl. Remote Sens.* 8, 083671–1–2. doi:10.1117/1.JRS.8.083671
- Tilly, N., Hoffmeister, D., Cao, Q., Lenz-Wiedemann, V., Miao, Y., Bareth, G., 2015b. Transferability of Models for Estimating Paddy Rice Biomass from Spatial Plant Height Data. *Agriculture* 5, 538–560. doi:10.3390/agriculture5030538
- Tilly, N., Hoffmeister, D., Schiedung, H., Brands, J., Bareth, G., 2014b. Terrestrial laser scanning for plant height measurement and biomass estimation of maize. *Int. Arch. Photogramm. Remote Sens. Spat. Inf. Sci.* XL-7. doi:10.5194/isprsarchives-XL-7-181-2014
- Uni Bonn, 2010a. Soil Campus Klein-Altendorf. http://www.cka.uni-bonn.de/standort/copy_of_boden
- Uni Bonn, 2010b. Climate Campus Klein-Altendorf. http://www.cka.uni-bonn.de/standort/copy_of_klima
- US House of Representatives, 1997. Bill No. H.R.2534. An Act to reform, extend and repeal certain agricultural research, extension and education programs and for other purposes. Title IV - New research, extension and education initiatives. Subtitle B - Precision Agriculture.

- van Leeuwen, M., Hilker, T., Coops, N.C., Frazer, G., Wulder, M.A., Newnham, G.J., Culvenor, D.S., 2011. Assessment of standing wood and fiber quality using ground and airborne laser scanning: A review. *For. Ecol. Manage.* 261, 1467–1478. doi:10.1016/j.foreco.2011.01.032
- Vauhkonen, J., Næsset, E., Gobakken, T., 2014. Deriving airborne laser scanning based computational canopy volume for forest biomass and allometry studies. *ISPRS J. Photogramm. Remote Sens.* 96, 57–66. doi:10.1016/j.isprsjprs.2014.07.001
- Velodyne, 2014. Velodyne HDL-64E User's Manual. [http://www.velodynelidar.com/lidar/products/manual/63-HDL64E S2 Manual_Rev D_2011_web.pdf](http://www.velodynelidar.com/lidar/products/manual/63-HDL64E%20Manual_Rev%20D_2011_web.pdf)
- Wallace, L., Watson, C., Lucieer, A., 2014. Detecting pruning of individual stems using airborne laser scanning data captured from an Unmanned Aerial Vehicle. *Int. J. Appl. Earth Obs. Geoinf.* 30, 76–85. doi:10.1016/j.jag.2014.01.010
- Wang, Y., Yang, Y., 2001. Effects of agriculture reclamation on hydrologic characteristics in the Sanjiang Plain. *Chinese Geogr. Sci.* 11, 163–167. doi:10.1007/s11769-001-0037-x
- Wang, Z., Zhang, B., Zhang, S., Li, X., Liu, D., Song, K., Li, J., Li, F., Duan, H., 2006. Changes of land use and of ecosystem service values in Sanjiang Plain, Northeast China. *Environ. Monit. Assess.* 112, 69–91. doi:10.1007/s10661-006-0312-5
- Weber, I., Jenal, A., Kneer, C., Bongartz, J., 2015. Gyrocopter-Based Remote Sensing Platform. *ISPRS - Int. Arch. Photogramm. Remote Sens. Spat. Inf. Sci.* XL-7/W3, 1333–1337. doi:10.5194/isprarchives-XL-7-W3-1333-2015
- Wei, G., Shalei, S., Bo, Z., Shuo, S., Faquan, L., Xuewu, C., 2012. Multi-wavelength canopy LiDAR for remote sensing of vegetation: Design and system performance. *ISPRS J. Photogramm. Remote Sens.* 69, 1–9. doi:10.1016/j.isprsjprs.2012.02.001
- WekuFly, 2015. airborne view service. <http://www.weku-fly.de/index.php/de/leistung>
- Whelan, B., Taylor, J., 2013. Precision Agriculture for Grain Production Systems. CSIRO PUBLISHING, Collingwood VIC.
- Xu, X., He, P., Qiu, S., Pampolino, M.F., Zhao, S., Johnston, A.M., Zhou, W., 2014. Estimating a new approach of fertilizer recommendation across small-holder farms in China. *F. Crop. Res.* doi:10.1016/j.fcr.2014.04.014
- Yara, 2015. N-Sensor. <http://www.yara.de/pflanzenernaehrung/tools-und-services/n-sensor/>
- YellowScan, 2015. Datasheet YellowScan. <http://yellowscan.lavionjaune.com/data/leafletYS.pdf>
- Zhang, Y., Liu, X., Su, S., Wang, C., 2014. Retrieving canopy height and density of paddy rice from Radarsat-2 images with a canopy scattering model. *Int. J. Appl. Earth Obs. Geoinf.* 28, 170–180. doi:10.1016/j.jag.2013.12.005

Appendix A: Eigenanteil

Kapitel 3

Titel	Multitemporal crop surface models: accurate plant height measurement and biomass estimation with terrestrial laser scanning in paddy rice
Autoren	Tilly, Nora Hoffmeister, Dirk Cao, Qiang Huang, Shanyu Lenz-Wiedemann, Victoria Miao, Yuxin Bareth, Georg
Status	Veröffentlicht
Journal	Journal of Applied Remote Sensing
Jahr	2014
Ausgabe/ Seite	8/ 083671-1-22
DOI	10.1117/1.JRS.8.083671
Beitrag	<ul style="list-style-type: none"> • Durchführung der Feldarbeiten in China 2011 (TLS und manuelle Messungen) • Datenanalyse • Verfassen des Manuskripts und Überarbeitung zur Veröffentlichung

Kapitel 4

Titel	Transferability of Models for Estimating Paddy Rice Biomass from Spatial Plant Height Data
Autoren	Tilly, Nora Hoffmeister, Dirk Cao, Qiang Lenz-Wiedemann, Victoria Miao, Yuxin Bareth, Georg
Status	Veröffentlicht
Journal	Agriculture: special issue: "Remote sensing for crop production and management"
Jahr	2015
Ausgabe/ Seite	5/ 538-560
DOI	10.3390/agriculture5030538
Beitrag	<ul style="list-style-type: none"> • Durchführung der Feldarbeiten in China 2011 und 2012 (TLS und manuelle Messungen) • Datenanalyse • Verfassen des Manuskripts und Überarbeitung zur Veröffentlichung

Kapitel 5

Titel	Terrestrial laser scanning for plant height measurement and biomass estimation of maize
Autoren	Tilly, Nora Hoffmeister, Dirk Schiedung, Henning Brands, Jonas Bareth, George
Status	Veröffentlicht
Journal	The International Archives of the Photogrammetry, Remote Sensing and Spatial Information Sciences
Jahr	2014
Ausgabe/ Seite	XL-7/ 7
Beitrag	<ul style="list-style-type: none">• Durchführung der Feldarbeiten in Deutschland 2013 (TLS Messungen)• Datenanalyse• Verfassen des Manuskripts und Überarbeitung zur Veröffentlichung

Kapitel 6

Titel	Fusion of plant height and vegetation indices for the estimation of barley biomass
Autoren	Tilly, Nora Aasen, Helge Bareth, Georg
Status	Veröffentlicht
Journal	Remote sensing: special issue "Remote Sensing in Precision Agriculture"
Jahr	2015
Ausgabe/ Seite	7/ 11449-11480
DOI	10.3390/rs70911449
Beitrag	<ul style="list-style-type: none">• Durchführung der Feldarbeiten in Deutschland 2012, 2013 und 2014 (TLS Messungen)• Datenanalyse• Verfassen des Manuskripts und Überarbeitung zur Veröffentlichung

Appendix B: Erklärung

Ich versichere, dass ich die von mir vorgelegte Dissertation selbständig angefertigt, die benutzten Quellen und Hilfsmittel vollständig angegeben und die Stellen der Arbeit – einschließlich Tabellen, Karten und Abbildungen –, die anderen Werken im Wortlaut oder dem Sinn nach entnommen sind, in jedem Einzelfall als Entlehnung kenntlich gemacht habe; dass diese Dissertation noch keiner anderen Fakultät oder Universität zur Prüfung vorgelegen hat; dass sie – abgesehen von unten angegebenen Teilpublikationen – noch nicht veröffentlicht worden ist, sowie, dass ich eine solche Veröffentlichung vor Abschluss des Promotionsverfahrens nicht vornehmen werde.

Die Bestimmungen der Promotionsordnung sind mir bekannt. Die von mir vorgelegte Dissertation ist von Prof. Dr. Georg Bareth betreut worden.

Köln, den

Appendix C: Curriculum vitae

Nora Isabelle Tilly

Date of birth: 22 March 1986
Place of birth: Cologne
Nationality: German
Place of residence: Cologne
Email: nora.tilly@uni-koeln.de

EDUCATION

1992 - 1996 Elementary school: KGS Lohrbergstraße, Cologne
1996 - 2005 Secondary school: Hildegard-von-Bingen Gymnasium, Cologne
2005 - 2010 Study of Geography, University of Cologne
Degree: Diploma
2007 Semester abroad, University College Dublin
2011 - 2016 Doctoral studies, University of Cologne

EMPLOYMENT

2008 - 2010 Student assistant, GIS & RS group, Institute of Geography, University of Cologne
2010 - 2011 Academic assistant, GIS & RS group, Institute of Geography, University of Cologne
2011 - present Lecturer, Institute of Geography, University of Cologne